2013

Surface-supported Ag islands stabilized by a quantum size effect: their interaction with small molecules relevant to ethylene epoxidation

Dahai Shao
Iowa State University

Surface-supported Ag islands stabilized by a quantum size effect: Their interaction with small molecules relevant to ethylene epoxidation

by

Dahai Shao

A dissertation submitted to the graduate faculty

in partial fulfillment of the requirements for the degree of

DOCTOR OF PHILOSOPHY

Major: Chemistry

Program of Study Committee:
Patricia A. Thiel, Major Professor
James W. Evans
Gordon J. Miller
Michael C. Tringides
Theresa Windus

Iowa State University
Ames, Iowa
2013

Dedicated to my wonderful family, friends, and everybody who has played a crucial role in my life.

TABLE OF CONTENTS

CHAPTER 1

INTRODUCTION

Growth of nanometer-scale metal thin films on substrates where intermixing is negligible has been a widely studied subject [1-11]. On a nanometer scale, which is usually a comparable dimension to the electron Fermi wavelength, many properties of thin films may be different from those of their bulk phase counterparts, such as electrical resistivity [1,12], surface adsorption energy [7,13], work function [14], and superconducting critical temperature [15, 16].

Many such differences are ascribed to the confinement of electrons in thin films. Electrons are confined between the electronic boundary with the vacuum on one side and the electronic boundary with the substrate on the other. So to some extent this confinement resembles the particle-in-a-box model, wherein specific half-wavelengths match the length of the box (in this case, the thickness of the film). Besides the properties mentioned above, electron confinement may also affect the growth of thin films, by preferentially stabilizing certain heights of thin films [1-3,6-8,10]. Such an effect is called a quantum size effect (QSE).

Theoretical studies have been dedicated to illustrating the conditions that need to be satisfied for the quantum size effect to occur [17-22]. Generally the height that satisfies Equation 1 is preferentially favored.

$$h = m \bullet \lambda_F / 2 \qquad (1)$$

where h is the height of thin films, λ_F is the Fermi wavelength of electrons, and m is an integer.

Ag/Si(111)-7x7 is a prototypical system where the QSE is well established [1,2,8,23,24]. After being deposited on the Si(111)-7x7 substrate at 150 K and subsequently annealed to room temperature (RT), Ag forms islands with a uniform height of 2 layer

thickness [1]. Other studies report that such preference for 2-layer islands is also observed after deposition at RT directly [8,23]. However, there is no consensus whether the preference of even-layer islands is preserved for islands higher than the first bilayer [2,8,23,24]. Miyazaki *et al* report that islands higher than 6-layers are not favored by the two-step deposition [24], while Goswami *et al* report such preference is preserved for islands up to 20-layer thick [23].

Ag/NiAl(110) is another system where QSE manifests significantly [6,7,25,26]. NiAl is a binary intermetallic compound with a stoichiometric ratio of 1:1. The lattice of NiAl adopts the CsCl structure. Due to its immiscibility with Ag, it serves as a substrate for growing Ag thin films. Studies [6,7,25] show that following deposition from 200 to 300 K, Ag grows on NiAl(110) via a bilayer mode. Islands of even layers are strongly stabilized.

Ag is a very effective catalyst for catalyzing the reaction of ethylene epoxidation, which is a selective oxidation of ethylene to a partially-oxidized form, ethylene oxide (EO) [27,42,43]. EO serves as a versatile industrial intermediate in the production of ethylene glycols, nonionic surfactants [27]. The mechanism that is responsible for the unique selectivity of Ag for ethylene epoxidation attracts much research interest [28-31].These studies show one important step in the epoxidation reaction is the formation of an intermediate called surface oxametallacycle (OMA) [28-31]. Figure 1 shows a schematic diagram of this intermediate. However, most of the mechanistic studies [28,29] focusing on OMAs tackle the reverse pathway, i.e. starting from the product of this reaction, ethylene oxide. The remainder of the reaction pathway, especially how ethylene and oxygen react on the catalyst surface and form the OMA, is still under study. Therefore, it is of great importance to understand the mechanism of surface adsorption of ethylene and oxygen on Ag surfaces, since surface adsorption is usually an important step toward surface reaction.

Adsorption of ethylene on low Miller-index Ag surfaces [32-41] or on oxygen pre-

covered Ag surfaces [31,44,46,47] serves as a prototype system to help further understand such processes on more complicated Ag surfaces.

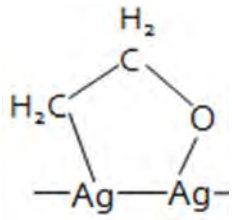

Fig. 1.A schematic diagram of surface oxametallacycles.

Ethylene molecularly adsorbs on Ag(111) [32,33,38], Ag(110) [32,34,35,37,39], and Ag(100) surfaces [36, 40]. The ethylene molecule remains intact until desorption with a peak desorption temperature ranging from 128 K to 155 K for all these surfaces [32,37,38,40]. Ethylene π-bonds with Ag (111) [32,33], Ag(110) [34,35,39], and Ag(100) [36,40] with its molecular plane parallel to the surface.

The adsorption of ethylene on oxygen pre-covered Ag surfaces has been studied for the oxygen-induced p(n×1) Ag(110) [44]. The stability of adsorbed ethylene (in terms of peak desorption temperature) increases with the surface coverage of atomic oxygen. On the other hand, adsorption of oxygen on ethylene pre-covered Ag(110) has been studied by Ho *et al* [41,45]. The vibrational motion of molecularly adsorbed oxygen is coupled with ethylene. Further studies [45] by Ho *et al* show that oxygen binds to ethylene through hydrogen bonds even at 13 K. However, the mechanism of forming the OMA through the co-adsorption of ethylene and oxygen is still under study. So far only theoretical calculations [31,46,47] have made progress on this subject.

This dissertation focuses on how QSE-stabilized, surface-supported Ag nanoclusters will interact with ethylene or oxygen. Experiments are performed to determine whether the QSE-mediated Ag islands react differently toward adsorption of ethylene or oxygen, or

whether the adsorption of these small molecules will affect the QSE-mediated stability of Ag islands.

Studies of the interaction of oxygen with Ag/Si(111)-7×7 were previously reported [48,49], but these studies were performed at a low Ag coverage where 3D Ag islands were not formed. So the study of such a system at a higher Ag coverage will be a subject of this work. The interaction of ethylene with Ag/Si(111)-7×7, as well as the interaction of oxygen with Ag/NiAl(110) are also important parts of this study.

References

[1] L. Gavioli, K.R. Kimberlin, M.C. Triniges, J.F. Wendelken, Z. Zhang. Phys. Rev. Lett.82 (1999), 129.

[2] M. Miyazaki, H. Hirayama, Surf. Sci. 602 (2008), 276.

[3] K. Budde, E. Abram, V. Yeh, M.C. Tringides, Phys. Rev. B. 61 (2000), R10602.

[4] J. Braun, J.P. Toennies, Surf. Sci. 384 (1997), L858.

[5] D.A. Luh, T. Miller, J.J. Paggel, M.Y. Chou, T.C. Chiang, Science, 292 (2001), 1131.

[6] B.Unal, F. Qin, Y. Han, D.-J. Liu, D. Jing, A.R. Layson, C.J. Jenks, J.W. Evans, P.A. Thiel, Phys. Rev. B. 76 (2007), 195410.

[7] Y. Han, B.Unal, F. Qin, D. Jing, C.J. Jenks, D.-J.Liu, P.A. Thiel, J.W. Evans, Phys. Rev. Lett, 100 (2008), 116105.

[8] B. Unal, A. Belianinov, P.A. thiel, M.C. Tringides, Phys. Rev. B. 81 (2010), 085411.

[9] V. Fournee, H.R. Sharma, M. Shimoda, A.P. Tsai, B. Unal, A.R. Ross, T.A. Lograsso, P.A. Thiel, Phys. Rev. Lett. 95 (2005), 155504.

[10] M. Hupalo, V. Yeh, L. Berbil-Bautista, S. Kremmer, E. Abram, and M.C. Tringides, Phys. Rev. B. 64 (2001), 1556307.

[11] T.-C. Chiang, Surf. Sci. Rep. 39 (2000), 181.

[12] M. Jalochowski, E. Bauer, Phys. Rev. B. 38 (1988), 42.

[13] D. Shao, X. Liu, N. Lu, C.-Z. Wang, K.-M. Ho, M.C. Tringides, P.A. Thiel, Surf. Sci. 606 (2012), 1871.

[14] Y. Qi, X. Ma, P. Jiang, S. Ji, Y. Fu, J.-F.Jia, Q.-K. Xue, and S.B. Zhang, Appl. Phys. Lett. 90 (2007), 013109.

[15] A.A. Shanenko, M.D. Croitoru , F.M. Peeters, Europhys. Lett.76 (2006), 498.

[16] B. Chen, Z. Zhu, X.C. Xie, Phys. Rev. B 74 (2006), 132504.

[17] F.K. Schulte, Surf. Sci. 55 (1976), 427.

[18] Y. Han, D.-J. Liu, Phys. Rev. B. 80 (2009), 155404.

[19] P. J. Feibelman, Phys. Rev. B. 27 (1983), 1991.

[20] I.P. Batra, S. Ciraci, G.P. Srivastava, Phys. Rev. B 34 (1986), 8246.

[21] N. Trivedi, N.W. Ashcroft, Phys. Rev. B. 38 (1988), 12298.

[22]J.M. Pitarke, A.G. Eguiluz, Phys. Rev. B. 63 (2001), 045116.

[23] D.K. Goswami, K. Bhattacharjee, B. Satpati, S. Roy, P.V. Satyam, B.N. Dev, Surf.Sci. 601 (2007), 603.

[24] L. Huang, S. Jay Chey, J.H. Weaver, Surf. Sci. 416 (1998), L1101.

[25] Y. Han, B. Unal, D. Jing, F. Qin, C.J. Jenks, D.-J. Liu, P.A. Thiel, J.W. Evans, Phys. Rev. B. 81 (2010), 115462.

[26] Y. Han, J.W. Evans, D.-J. Liu, Surf. Sci. 602 (2008), 2532.

[27] K. Weisssermel, H.-J. Arpe, Industrial Organic Chemistry. Weinheim: VCH, 1997.

[28] S. Linic, M.A. Barteau, J. Am. Chem. Soc. 124 (2002), 310.

[29] S. Linic, M.A. Barteau, J. Am. Chem. Soc. 125 (2003), 4034.

[30] M.-L. Bocquet, A. Michaelides, D. Loffreda, P. Sautet, A. Alavi, D.A. King, J. Am. Chem. Soc. 125 (2003), 5620.

[31] A. Kokalj, P. Gava, S. de Gironcoli, S. Baroni, J. Phys. Chem. C. 112 (2008), 1019.

[32] D. Stacchiola, G. Wu, M. Kaltchev, and W.T. Tysoe, Surf.Sci.486(2001), 9.

[33] T.E. Felter, W.H. Weinberg, P.A. Zhdan, and G.K. Boreskov, Surf. Sci. 97(1980), L313.

[34] C. Backx, C.P.M. de Groot, and P. Biloen, Appl. Surf.Sci. 6(1980), 256.

[35] B. Kruger and C. Benndorf, Surf. Sci. 178(1986), 704.

[36] D.A. Slater, P. Hollins, and M.A. Chesters, J. Electron. Spectrosc. Relat. Phenom. 64/65(1993), 95.

[37] C.T. Campbell and M.T. Paffett, Appl. Surf. Sci. 19(1984), 28

[38] X.-L. Zhou and J. M. White, J. Phys. Chem, 96(1992), 7703.

[39] M. Akita, N. Osaka, S. Hiramoto, and K, Itoh, Surf. Sci. 427(1999), 374.

[40] D. Arvantis, K. Baberschke, L. Wenzel, U. Dobler, Phys, Rev. Lett, 57(1986), 3175.

[41] J.R. Hahn, W. Ho. Phys. Rev. B. 80(2009), 165428.

[42] M.O. Ozbek, R. A. van Santen, Catal. Lett.143 (2013), 131–141.

[43] P.A. Kilty, W.M.H. Sachtler, Catal. Rev. – Sci. and Engr. 10 (1974), 1.

[44] M. Akita, S. Hiramoto, N. Osaka, K. Itoh, J. Phys. Chem. B. 103 (1999), 10189.

[45] J.R. Hahn, W. Ho. Phys. J. Phys. Chem. B. 109 (2005), 20350.

[46] V. I. Avdeev, G.M. Zhidomirov. Surf. Sci. 492 (2001), 137.

[47] A. Kokalj, A.D. Corso, S. de Gironcoli, S. Baroni, J. Phys. Chem, B. 110 (2006), 367.

[48] J. Jiao, M. Pan, Q. Xue, X, Bao, Chn, J. Catal.24 (2003), 433.

[49] Z. Zhang, J. Jiao, Z. Jiang, D. Tan, Q. Fu, X. Bao, J. Vac. Sci. Technol. A. 26(2008), 1.

CHAPTER 2

EFFECT OF OXYGEN ON THE STABILITY OF AG ISLANDS ON SI(111)-7×7

A paper published in Surface Science. 606(23-24), 1871 (2012).

Dahai Shao[1,2], Xiaojie Liu[1,3], Ning Lu[1,3], C.-Z. Wang[1,3], Kai-Ming Ho[1,3], M.C. Tringides[1,3] and P.A. Thiel[1,2,4]

[1]Ames Laboratory, [2]Department of Chemistry, [3]Department of Physics and Astronomy, and [4]Department of Materials Science and Engineering

Iowa State University, Ames Iowa 50011 USA

Abstract

We have used scanning tunneling microscopy to probe the effect of oxygen exposure on an ensemble of Ag islands separated by a Ag wetting layer on Si(111)-7×7. Starting from a distribution dominated by islands that are 1 layer high (measured with respect to the wetting layer), coarsening in ultrahigh vacuum at room temperature leads to growth of 2-layer islands at the expense of 1-layer islands, which is expected. If the sample is exposed to oxygen, 3-layer islands are favored, which is unexpected. There is no evidence for oxygen adsorption on top of Ag islands, but there is clear evidence for adsorption in the wetting layer. Several possible explanations are considered.

Keywords: film growth, surface structure and morphology, scanning tunneling microscopy, semiconductor surfaces, density functional theory.

1. Introduction.

Nanoparticles of silver are technologically important for many reasons. They are used as sensors and tags because of the surface-enhanced Raman effect.[1, 2] Silver is the best-known catalyst for production of ethylene oxide from oxygen and ethylene, a chemical reaction of major economic importance.[3, 4] The optical properties of silver nanoparticles or films, in or on Si, are attracting attention for possible applications inphotovoltaics,[5] fiber optics,[6] and photonic band gap devices.[7] In addition to its optical properties, silver is attractive in such technologies because it is immiscible with silicon, a feature that is unusual among transition metals.

The goal of the present work is to determine the effect of oxygen on the stability of Ag islands supported on Si(111), and specifically whether Ag islands on Si(111) react differently to oxygen exposure, depending on their height. For Ag on Si(111)-7×7, it is believed that a quantum size effect (QSE) preferentially stabilizes Ag islands that are two layers high.[8-10] However, there have been no studies to determine how these Ag islands may respond to an oxygen-rich environment.

The Ag/Si(111)-7×7 system (without oxygen) has been studied extensively.[9-15] Up to a coverage of 0.5-0.6 monolayers (ML), Ag forms an irregular wetting layer (WL) in which the Ag is nonmetallic, and remnants of the original Si(111)-7×7 are exposed.[9, 16, 17] After the WL saturates at 0.5-0.6 ML, excess Ag aggregates as taller islands. Fig. 1 is a schematic that defines the various structures on this surface, and the nomenclature used in this paper.

The Ag island height distribution depends on deposition conditions.[9, 18] Two-layer islands are favored most strongly when Ag is deposited below 300 K and annealed. Amore heterogeneous distribution is obtained (presumably because of kinetic limitations)by deposition of Ag at 300 K, and this is desirable for the present purpose because it allows in

situ comparison of islands with different heights.

There have been two previous studies of the interaction of oxygen with Ag/Si(111)-7×7.[17, 19] Unlike the present work, they did not focus on Ag coverages high enough to produce QSE-stabilized islands, but rather on low Ag coverages corresponding to a partially-filled WL. The most extensive report was from Zhang *et al*.[17] who used scanning tunneling microscopy (STM), photoelectron spectroscopy, and vibrational spectroscopy. They found that oxygen adsorbs selectively on Si. However, even a very low coverage of Ag (0.06 ML) alters the surface electronic states of Si, and suppresses oxygen adsorption beyond that expected from simple site-blocking. Furthermore, they reported that co-adsorbed Ag changes the binding mode of atomic oxygen pairs. On clean Si(111)-7×7, it had been established that oxygen adsorbs dissociatively, forming localized pairs of atoms that can bind to Si in two distinct configurations.[17 20-22]In one configuration, both oxygen atoms insert into Si-Si pi bonds ("ins-ins" configuration), and in the other, less-stable configuration, one oxygen atom adsorbs atop a single a Si atom while the other inserts into a Si-Si bond ("ad-ins" configuration). Zhang *et al*.[17] found that co-adsorbed Ag promotes the ad-ins configuration, and suggested that the driving force is stronger Ag interaction with the adsorbed form of atomic oxygen.

2. Experimental and Computational Details.

Experiments were performed in an Omicron variable-temperature STM system described elsewhere.[23] Chamber base pressure did not exceed 1.5×10^{-8} Pa throughout the procedures, including Ag evaporation. The Si sample was p-type, boron-doped, with resistivity of 0.02 Ohm*cm. We prepared the Si(111)-7×7 surface according to standardprocedures.[24-26] Ag was deposited at 300 K. The sample was exposed to oxygen, also at 300 K, by back-filling the chamber through a leak valve. Oxygen pressures were in the

range 2×10^{-8} to 4×10^{-7} Pa. Exposures are given in Langmuirs (L) where $1L = 1.3 \times 10^{-4}$ Pa-s. During oxygen exposure the STM tip was usually withdrawn to avoid possible shadowing effects, and so the same region was not imaged before and after oxygen exposure. The total Ag coverage, θ_{Ag}, was calculated from STM images on the basis of the areas of different types of features. For this purpose, it was assumed that the Ag coverage in the WL was θ_{WL} = 0.5 ML, and in the interfacial layer and in each upper layer of a Ag island, local coverage was assumed to be 1.0 ML. Using this calibration, islands emerged (by definition) above 0.5 ML. Islands were identified and analyzed in the STM images, using WSxM software.[27] Typically, acquired image sizes were 250×250 nm^2, because this afforded a good compromise between statistics(capturing many islands in a single image) and accuracy (being able to identify individual islands and measure their areas). Positive tip bias, V_b, corresponds to a filled-states image.

We found that Ag island density can be measurably different close to step edges than in the middle of terraces, so the present discussion and analysis is restricted to areas that were at least 250 nm away from a step edge.

Two main types of experiments were performed: A control experiment, and an oxygen exposure experiment. In both cases, Ag was first deposited on the surface. At a time 1.3 to 1.7 hours after the start of Ag deposition, an initial set of STM images was captured. Next, the sample was either allowed to age in UHV (the control experiment) or was exposed to oxygen during the equivalent period. A final set of images was then acquired, such that the total time elapsed between the start of deposition and the second set of images was 2.7 to 3.0 hours. Every effort was made to ensure that the control and oxygen-exposure experiments were identical except for the way the sample was treated between the two imaging phases.

First-principles calculations were performed using the generalized gradient approximation (GGA) in the formulation by Perdew-Burke-Ernzerhof (PBE)[28] implemented

in the Vienna ab initio simulation package (VASP).[29-31] Valence electrons were treated explicitly and their interactions with ionic cores were described by Projector Augmented Wave (PAW) pseudopotentials.[32, 33] Lattice constants obtained from these calculation were 0.547 nm for Si and 0.416 nm for Ag, using the PAW-PBE under density functional theory (DFT). Supercells of a 4×4 Ag(111) film on a 3×3 Si(111)substrate, consisting of two bi-layers of Si passivated by hydrogen at the bottom (Fig. 2),were used in the calculations. The lateral dimension of the (3×3) Si(111) substrate (1.160nm) was close to the lateral dimension (1.176 nm) of a (4×4) Ag cell. Therefore, the lattice mismatch effects due to the use of periodic boundary conditions in the calculations should be small. The dimension of the supercell in the z direction was 3.5 nm, which allowed a vacuum region of about 2 nm to separate the atoms in the supercell and their replicas. The wave functions were expanded in a plane wave basis set with an energy cut-off of 250 eV. A k-point grid of 3 x 3 Monkhorst-Pack type was used for the surface Brillouin zone. All atoms in the supercell were allowed to relax until the forces on each atom were smaller than 0.02 eV/ nm.

3. Experimental Results.

First consider the effect of oxygen on the WL, which is shown in Fig. 3. In Fig. 3(A), the large bright feature is a 2-layer Ag island, surrounded by WL. Before oxygen exposure, the Si(111)-7×7 unit cell can be resolved in the WL, as shown in Fig. 3(B),where its unit cell (somewhat distorted) is outlined. The brighter, more amorphous regions are Ag in the WL. Fig. 3(C-D) shows similar images after oxygen exposure. The 7×7 is no longer visible, and the features in the WL are less well-defined.

Oxygen exposure affects not only the qualitative appearance of features in the WL, but also the quantitative vertical roughness. We measure WL roughness using images with areas of at least 25 nm^2 (without Ag islands), since below this size threshold, roughness

depends on image size and hence is not a robust parameter. The root-mean-square (RMS) roughness of the WL consistently increases after oxygen exposure, by~0.02 nm (by ~30 to 50%), whereas it does not change significantly when the clean surface is simply aged over the same time period. This is quantitatively true for both positive and negative values of E_b.

Consider next the Ag islands. Fig. 4 shows representative STM images from a pair of experiments consisting of a control, and 100 *L* oxygen exposure. In both experiments, θ_{Ag}~0.6 ML. Fig. 5 shows similar data but here θ_{Ag} is higher, ~ 1.4 ML.

Because of the higher θ_{Ag}, islands in Fig. 5 have larger area than in Fig. 4, but their number density is about the same. Another consequence of the higher θ_{Ag} is that almost all the islands in Fig. 5 are initially 2-layer, whereas in Fig. 4 the majority are initially 1-layer. In both figures, the final images from the control experiment are visually similar to those from the oxygen exposure experiment. Clearly, many Ag islands survive oxygen exposure.

There is no evidence for oxygen adsorption on the tops of Ag islands. Fig. 6 compares high-resolution images of Ag islands before and after oxygen exposure. The roughness can be attributed to the underlying Si(111)-7×7 interface. On some island tops, the 7×7 can even be resolved.[8] There is essentially no difference between the two sets of images. The island tops are too small for quantitative roughness analysis, like that done for the WL. The conclusion that oxygen does not adsorb on top of Ag islands is incomplete agreement with the expectations from DFT presented in Section 4 below.

The Ag island height distribution is also of interest. Island heights are determined from individual island profiles. Several examples are shown in Fig. 7. We typically take the reference point to be the qualitative average of the wetting layer, as shown in the figure. On the clean surface, this yields the Ag island heights shown in Table 1 in the rows labeled with 0 *L* oxygen exposure. These values are physically-reasonable for 1-, 2-, and 3-layer islands.[8]

After oxygen exposure, we choose again the average-WL as baseline. This choice of baseline yields the island heights shown in Table 1 in the rows labeled with 100*L* oxygen exposure. Islands can be classified as 1-, 2-, 3-, and 4-layershigh, and their heights compare very well with clean surface values.

Fig. 8 and DENSITIES2 show N_L, the number density of Ag islands of various heights, corresponding to Fig. 4 and Fig. 5, respectively. In the control experiment of Fig. 8(A-B), all island densities decrease with time, but the relative population of 2-layerislands increases at the expense of 1-layer islands. These observations indicate that the Ag island ensemble coarsens significantly on a timescale of hours, at 300 K and in UHV. Furthermore, these observations are consistent with the 2-layer islands being moststable.[9, 18] By contrast, in the corresponding oxygen exposure experiment of Fig. 8(C-D), the density of apparent 3-layer islands grows at the expense of both 1- and 2-layer islands.

The effect of oxygen is even more pronounced at the higher Ag coverage, as illustrated in Fig. 9. Initially, 78% of the islands are 2-layer islands. In the control experiment of Fig. 9(A-B), there is a slight degree of coarsening, manifest in the loss of 1-layer islands and increase of 2-layer islands. The change due to coarsening is smaller than in Fig. 8(A-B), since at higher θ_{Ag} the initial distribution is closer to ideal (initially, there are fewer 1-layer islands). The effect of oxygen exposure in Fig. 9(C-D) is to shift the island distribution almost entirely from 2-layer to apparent 3-layer islands. Additionally, a few 4-layer islands appear.

In summary, our main experimental observations are:

(1) Oxygen adsorbs in the WL. This causes a qualitative change in the appearance of the WL and a quantitative increase in roughness. Specifically, the 7×7 disappears, the WL features become amorphous, and the RMS roughness increases by 0.2 nm.

(2) Ag islands survive oxygen exposure, but the predominant island height—

measured relative to the average WL—is 3-layers after exposure.

4. Computational Results.

As described in Section 1 and shown in Fig. 1, this surface presents regions of exposed Ag and exposed Si. The configurations shown in Fig. 2 were analyzed to delineate trends in this system, both with and without oxygen.

We take a single Ag layer as a model for Ag in the WL, and higher Ag layers to represent Ag in the protruding islands. To make this clear, the first layer of Ag in the model is labeled as WL. Thicker films are indexed by an integer L, starting with L=1, i.e. L is the number of layers above the WL. For the clean surface, there is evidence that Ag, both in the WL and in the islands, resembles (111) layers of the bulk metal lying parallel to the Si(111) substrate.[11,12, 16] Geometries in Fig. 2 were constructed accordingly. There is, however, some uncertainty about the atomic structure of Ag in the interfacial layer at the base of the Ag islands.[11, 12] Our model treats it as a layer of Ag(111).

Using DFT, we examine trends in two quantities: The adsorption energy of atomic oxygen, E_a, at different Ag layer thicknesses; and the stabilities of Ag layers with different thicknesses. Consider first the former. E_a is the difference between the total energy of the O/Ag(111)/Si(111) system, and the sum of the energy of the substrate which includes any Ag layers plus the energy of an isolated oxygen atom. There is one oxygen atom per (3x3) Si unit cell or (4×4) Ag unit cell, corresponding to a coverage of 1/9 ML relative to Si, or 1/16 ML relative to Ag. Each value of E_a reported here is the most favorable one found using several different initial geometries. The configurations shown in Fig. 2 all represent oxygen atoms on top of the Si or Ag surface, but we also consider configurations where the oxygen atoms intercalate at the Si-Ag interface.

Fig. 10 shows the variation in E_a when oxygen interacts with Ag layers of increasing

thickness. The value "0" on the abscissa represents the Ag-free Si surface. For values to the right of L =0, the top and bottom curves show E_a for oxygen adsorbed on top of Ag and sub-surface, respectively.

There are three main trends. First, E_a is far lower (at least 2.8 eV more favorable) on bare Si than at any other site. Second, E_a is always significantly lower for oxygen sandwiched between Ag and Si, than for oxygen on top of Ag. Third, among the Ag layers, E_a for oxygen interacting with the WL is lower than for the other exposed Ag layers. From DFT, then, one expects oxygen to adsorb predominantly at exposed Si regions. If adsorption on exposed Si is not possible, e.g. due to saturation of Si sites, one expects oxygen to intercalate between Ag and Si before adsorbing on top of Ag (if kinetics allows).

The stability of a Ag island with a specific height L is given by the surface energy per (1×1) unit cell, E_S, which is defined as $E_s=(E_{total}-(E_{SiH}+nE_{Ag}))/A$. Here, E_{total} is the total energy of the whole system, E_{SiH} is the energy of the Si(111) substrate, E_{Ag} is the bulk energy of silver, n is the number of Ag atoms in the system, and A is the area of the 4 × 4 Ag(111) surface. Fig. 11(A) shows E_S for the clean surface, with a minimum at L=1, and L=2 close by. The energy minimum (and also the negative surface energy values) around L=1 and 2 indicate that 1 and 2 layers of Ag(111) films on Si(111) are energetically favorable. While this is not perfect agreement with experiment (which shows a minimum at L=2), the existence of a minimum at small L is in qualitative agreement. The discrepancy may indicate that a 4×4 Ag(111) supercell is not a perfect model for the Ag film.

The effect of a single atom of oxygen in an optimized geometry *on top* of Ag and toward the middle of the supercell (Fig. 2) is shown in Fig. 11(B). The definition of the surface energy is similar to that for the clean surface, i.e., $E_s=(E_{total}-(E_{SiH}+E_O+n-E_{Ag}))/A$, where E_O is one half the binding energy of the oxygen molecule with spin polarization corrections.[34] In contrast to the clean surface, here E_S increases steadily with L. Note that the dashed line

drawn between the values of E_S at WL and at L=4 undercuts the values at L=1-3. Therefore Ag islands with L=1-3 are not stable against separation into WL and L=3 islands, if a trace of oxygen is present.

Fig. 11(C) shows the effect of a single atom of oxygen at an *interfacial* site. Here, the surface energy exhibits a minimum at layer 1, similar to the clean surface, and has another metastable minimum at layer 4. The dashed line again indicates that there would be disproportionation, this time between 2- and 4-layer islands.

DFT does not indicate a specific stabilization of 3-layer Ag islands, as shown by experiment. However, DFT does indicate that a trace of oxygen can change the relative stabilities of different-height Ag islands. Such a low level of oxygen on the Ag islands would almost certainly go undetected with STM.

5. Discussion.

There is no evidence that oxygen adsorbs on top of Ag islands. This is based on our data (Fig. 6) and is reasonable in light of our DFT calculations (Fig. 10). However, a trace of adsorbed oxygen on Ag would probably go unnoticed in our STM images.

Oxygen does adsorb in the WL. Within the WL, it almost certainly adsorbs on the exposed Si, based both on kinetic and thermodynamic evidence. Kinetically, the initial sticking coefficient of oxygen at 300 K is 0.13 on pure Si(111)-7×7,[35] and only 10^{-5} - 10^{-6} on pure Ag(111).[36] Thermodynamically, DFT shows that the adsorption energy of atomic oxygen on Si is 2.8 eV more favorable than at any site involving Ag (Fig. 10).

Furthermore, as noted in Sec. 1, Zhang *et al*.[17] studied the interaction of oxygen with Ag/Si(111)-7×7, focusing on low θ_{Ag} corresponding to a partially- or completely-filled WL. They interpreted all of their data—from photoelectron spectroscopies and from STM - in terms of oxygen adsorption on Si, not on Ag. They also showed that the presence of

Ag on Si(111) at low coverage served to reduce subsequent adsorption of oxygen on Si, which they attributed to modification of the electronic surface states of Si by the Ag. A similar effect has been reported for oxygen adsorption in the presence of Au/Si(111).[37] However, the difference between the binding energy of oxygen on Si and Ag is so high that any perturbation probably still leaves Si as the strongly favored adsorbent in this system.

We have considered several possible mechanisms by which oxygen exposure could change the Ag island height distribution. One is that the average level of the WL changes, hence shifting the baseline for measuring island heights. However, this is incompatible with the fact that a large fraction of 1-layer islands survive oxygen exposure, at the lower θ_{Ag}. Another is that oxygen displaces Ag from the WL into the Ag islands, although this does not explain the preference for 3-layer islands at both coverages. It also is incompatible with the previous work of Zhang *et al*.[17] described above, which showed no evidence for displacement of Ag from Si(111) by oxygen, at low θ_{Ag}. We regard the most viable hypothesis to be one in which traces of oxygen, on or below the Ag islands, change the relative stability of the islands. The DFT results in Section 4 and Fig. 11 show that even1/16 ML of oxygen can indeed change the stability of islands as a function of their height.

This model would require facile equilibration and hence easy exchange of Ag between islands. Exchange would have to be more facile than that which occurs without oxygen, since in the control experiments, coarsening is far from complete on the timescale of the observations [Fig. 8(A, B) or Fig. 9(A, B)]. However, oxygen is known to accelerate mass transport phenomena—including coarsening—on silver surfaces, presumably by forming mobile oxygen-silver complexes.[38-41] Furthermore, at low Ag coverages (far below saturation of the WL) on Si(111)-7×7, Jiao *et al*.[19] reported that adsorbed oxygen promotes migration of Ag atoms and small clusters at room temperature. Thus, there is support for possible accelerated equilibration between Ag islands in the presence of oxygen.

In summary, we regard the most plausible explanation to be an oxygen-induced shift in island stability. Further experiments with photoelectron spectroscopy could been lightening, although issues of species identification and detection limit could be challenging in this system.

Conclusions.

The purpose of this study was to determine the effect of oxygen on the stability of Ag islands supported on Si(111). Experimentally, we found that the Ag islands survive exposure to oxygen. There is no evidence that oxygen adsorbs on top of the Ag islands, but it does adsorb in the wetting layer. Furthermore, oxygen exposure changes the height distribution of the Ag islands. DFT calculations show that even traces of atomic oxygen adsorbed on top of, or beneath, Ag islands can change the equilibrium height distribution.

Acknowledgements. This work was supported by the U.S. Department of Energy, Office of Basic Energy Science, Division of Materials Sciences and Engineering. Ames Laboratory is operated for the U.S. Department of Energy by Iowa State University under Contract No. DE-AC02-07CH11358. We thank J. Evans for a careful reading and helpful suggestions.

References

[1] P. L. Stiles, J. A. Dieringer, N. C. Shah, and R. P. Van Duyne, Annual Rev. Analyt. Chem. 1, 601 (2008).

[2] K. A. Willets and R. P. Van Duyne, Annual Rev. Phys. Chem. 58, 267 (2007).

[3] J. G. Serafin, A. C. Liu, and S. R. Seyedmonir, J. Mol. Cat.A 131, 157 (1998).

[4] R. A. van Santen and H. Kuipers, Adv. Catal. 35, 265 (1987).

[5] S. Pillai, K. R. Catchpole, T. Trupke, and M. A. Green, J. Appl. Phys. 101, 93105 (2007).

[6] S. Naczas, P. Akhter, and M. Huang, Appl. Phys. Lett.98, 113101 (2011).

[7] V. Poborchii, T. Tada, T. Kanayama, and A. Moroz, Appl. Phys. Lett. 82, 508 (2003).

[8] B. Ünal, A. Belianinov, P. A. Thiel, and M. C. Tringides, Phys. Rev. B 81, 085411 (2010).

[9] L. Gavioli, K. R. Kimberlin, M. C. Tringides, J. F. Wendelken, and Z. Zhang, Phys. Rev. Lett. 82, 129 (1999).

[10] D. K. Goswami, K. Bhattacharjee, B. Satpati, S. Roy, P. V. Satyam, and B. N. Dev, Surf. Sci. 601, 603 (2007).

[11] E. J. van Loenen, M. Iwami, R. M. Tromp, and J. F. van der Veen, Surf. Sci. 137, 1 (1984).

[12] R. D. Aburano, H. Hong, J. M. Roesler, K. Chung, D. S. Lin, P. Zeschack, H. Chen, and T. C. Chiang, Phys. Rev. B 52, 1839 (1995).

[13] L. Huang, S. J. Chey, and J. H. Weaver, Surf. Sci. 416, L1101 (1998).

[14] P. Sobotik, I. Ostadal, J. Myslivecek, T. Jarolimek, and F. Lavicky, Surf. Sci. 482-485, 797 (2001).

[15] H. Hirayama, Surf. Sci. 603, 1492 (2009).

[16] S. Tosch and H. Neddermeyer, Phys. Rev. Lett.61 (1988).

[17] S. Zhang, J. Jiao, Z. Jiang, D. Tan, Q. Fu, X. Bao, X. Liu, J. Jia, and Q. Xue, J. Vac. Sci. Technol. A 26, 62 (2008).

[18] K. R. Kimberlin, G. M. Rutter, L. M. Nagle, K. R. Roos, and M. Tringides, Surf. Interf. Analysis 35, 1069 (2003).

[19] J. Jiao, M. Pan, Q. Xue, and X. Bao, Chin. J. Catal. 24, 433 (2003).

[20] S.-H. Lee and M.-H. Kang, Phys. Rev. Lett. 82, 968 (1999).

[21] H. Okuyama, Y. Ohtsuka, and T. Aruga, J. Chem. Phys. 122, 234709 (2005).

[22] H. Okuyama, T. Yamada, and T. Aruga, Jpn. J. App. Phys. 44, 5362 (2005).

[23] B. Ünal, F. Qin, Y. Han, D. J. Liu, D. Jing, A. R. Layson, C. Jenks, J. W. Evans, and P. A. Thiel, Phys. Rev. B 76, 195410 (2007).

[24] R. J. Phaneuf, N. C. Bartelt, E. D. Williams, W. Swiech, and E. Bauer, Phys. Rev. Lett. 71, 2284 (1993).

[25] B. Z. Olshanetsky, A. E. Solovyov, A. E. Dolbak, and A. A. Maslov, Surf. Sci. 306, 327

(1994).

[26] V. Tsai, X.-S. Wang, E. D. Williams, J. Schneir, and R. Dixson, Appl. Phys. Lett. 71, 495 (1997).

[27] I. Horcas, R. Fernandez, J. M. Gomez-Rodriguez, J. Colchero, J. Gomez-Herrero, and A. M. Baro, Rev. Sci. Instr. 78, 013705 (2007).

[28] J. P. Perdew, K. Burke, and M. Ernzerhof, Phys. Rev. Lett. 77, 3865 (1996).

[29] G. Kresse and J. Hafner, Phys. Rev. B 47, 558 (1993).

[30] G. Kresse and J. Furthmüller, Comput. Mater. Sci. 6, 15 (1996).

[31] G. Kresse and J. Furthmüller, Phys. Rev. B 54, 11169 (1996).

[32] P. E. Blöchl, Phys. Rev. B 50, 17953 (1994).

[33] G. Kresse and D. Joubert, Phys. Rev. B 59, 1758 (1999).

[34] G. Makov and M. C. Payne, Phys. Rev. B 51, 4014 (1995).

[35] P. Gupta, C. H. Mak, P. A. Coon, and S. M. George, Phys. Rev. B 40, 7739 (1989).

[36] C. T. Campbell, Surf. Sci. 157, 43 (1985).

[37] K. Kishi, M. Daté, and M. Haruta, Surf. Sci. 486, L475 (2001).

[38] J. S. Ozcomert, W. W. Pai, N. C. Bartelt, and J. E. Reutt-Robey, Phys. Rev. Lett. 72, 258 (1994).

[39] A. R. Layson, J. W. Evans, V. Fournée, and P. A. Thiel, J. Chem. Phys. 118, 6467 (2003).

[40] A. R. Layson, J. W. Evans, and P.A. Thiel, Phys. Rev. B 65, 193409 (2002).

[41] A. R. Layson and P. A. Thiel, Surf. Sci. 472, L151 (2001).

Table 1

Heights of Ag islands above the average WL. Columns labeled 1L, 2L, 3L, and 4L show the average and range of heights of apparent 1, 2, 3, and 4-layer islands, respectively. In these columns, uncertainties in the average values are + 1 standard deviation, complete ranges are given in parentheses, and all values are in units of nm. At least 15 islands were analyzed for each average.

Ag coverage, ML	Oxygen exposure, ℒ	1L	2L	3L	4L
0.6	0	0.33 ± 0.03 (0.24 - 0.37)	0.58 ± 0.02 (0.53 - 0.62)	n.a.	
0.6	100	0.30 ± 0.02 (0.24 - 0.36)	0.56 ± 0.02 (0.48 - 0.54)	0.78 ± 0.01 (0.73 - 0.86)	
1.4	0	0.32 ± 0.03 (0.27 - 0.35)	0. 58 ± 0.01 (0.57 - 0.58)	0.81 ± 0.02 (0.79 - 0.83)	
1.4	100	n.a.	0.56 ± 0.02 (0.54 - 0.59)	0.78 ± 0.02 (0.76 - 0. 80)	1.01 ± 0.03 (0.99 - 1.07)

Figures

Fig. 1. Schematic showing the different types of surfaces and Ag layers in this system. WL stands for the wetting layer, and the height of a Ag island above the WL is indexed by L.

Fig. 2. Different types of structures analyzed with DFT. Left panels show top views, and right panels show side views. Large gray circles are Si atoms, medium-size red circles are oxygen atoms, and small blue circles are H atoms. (Color on-line.)

Fig. 3. STM images that illustrate the WL at θ_{Ag}~1.4 ML. Left images (A and B) are taken before oxygen exposure, and right images (C and D) after 100*L* oxygen exposure. Top images (A and C) are 50 × 50 nm^2, while bottom images (B and D) are 15 × 15 nm^2. Arrows in images (B) and (D) indicate location of associated line profiles. All images are acquired at +1.0 V tip bias, 0.5 nA.

Fig. 4. Representative STM images at θ_{Ag}~0.6 ML from a control experiment (A and B), and an oxygen exposure experiment (C and D). As described in Section 2, the time interval between the top and bottom image in each experiment is the same. The difference is that between A and B the sample is exposed to vacuum. Between C and D the sample is exposed to 100*L* oxygen. Image parameters are 250 × 250 nm^2, -1.0 V tip bias, 0.5 nA.

Fig. 5.Representative STM images from a control experiment (A and B), and an oxygen exposure experiment (C and D). Conditions and parameters are identical to Fig. 4, except that at θ_{Ag} ~ 1.4 ML and V_b = +1.0 V.

Fig. 6. STM images of Ag island tops for the clean surface (A-C) and after 100 *L* oxygen exposure (D-F). Tunneling current is 0.5 nA in all cases. V_b = +1.0 V in A, B, D, and E; V_b = -1.0 V in C and F. Image size is about 10 × 10 nm^2 in each panel. Island heights are 3-layer in A, E, and F; 4-layer in D; and 2-layer in B and C. Images have been Fourier filtered.

Fig. 7. Sample profiles of 1-layer, 2-layer, and 3-layer islands at +1.0 V tip bias,

0.5 nA.

Fig. 8. Histograms of Ag island number densities for the experiment represented in Fig. 4. The total analyzed area is 0.31 μm^2, corresponding to at least 300 islands, in each case.

Fig. 9. Histograms of Ag island number densities for the experiment represented in Fig. 5. The total analyzed area is 0.20 μm^2, corresponding to at least 200 islands in each case.

Fig. 10. Adsorption energy of oxygen on Ag and Si surfaces, and at the Ag-Si interface.

Fig. 11. DFT-derived surface energy, E_s, as a function of Ag layer thickness, L, above the WL. Energies in (A) are for the oxygen-free surface, and in (B) for the surfaces with oxygen adsorbed on top of Ag, according to the configurations in Fig. 2. Panel (C) shows results for oxygen at the Ag-Si interface.

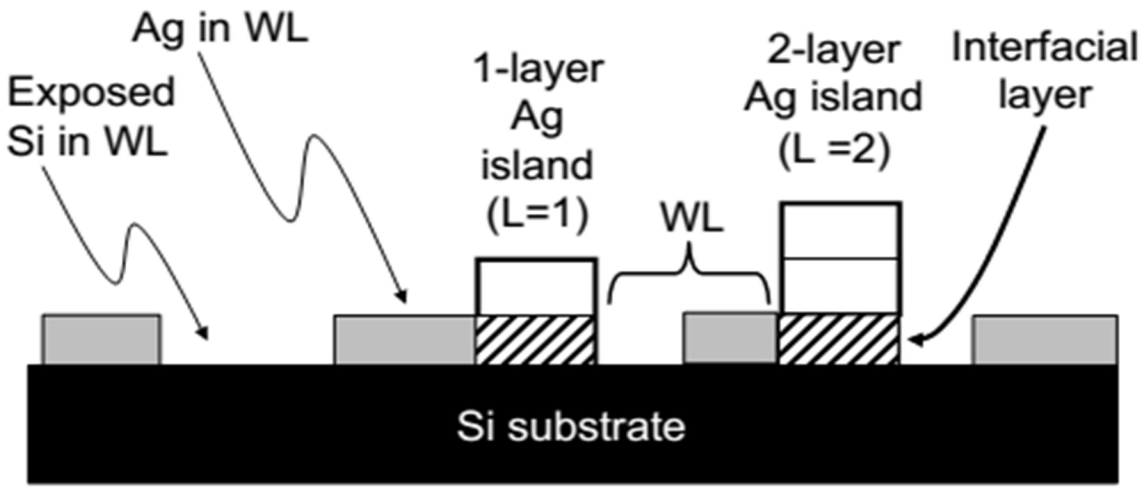

Fig. 1

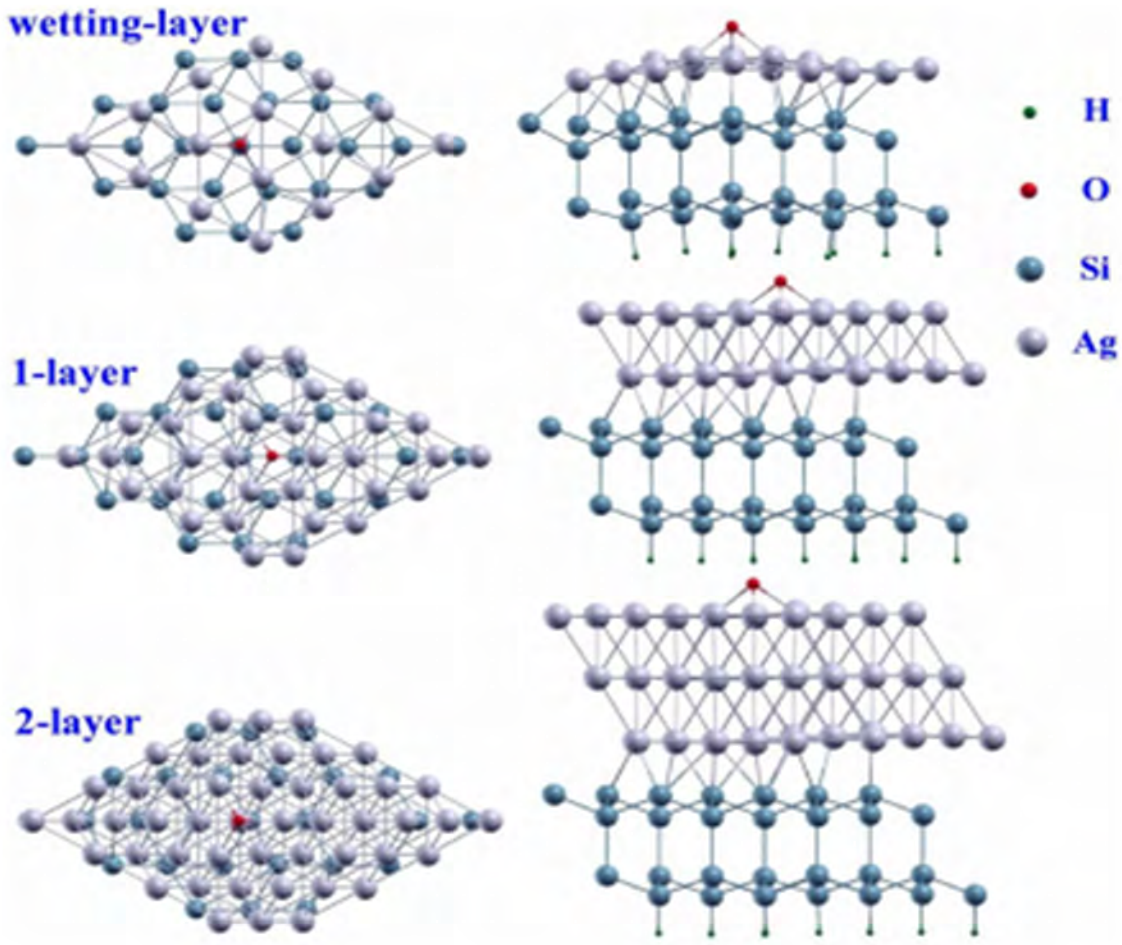

Fig. 2

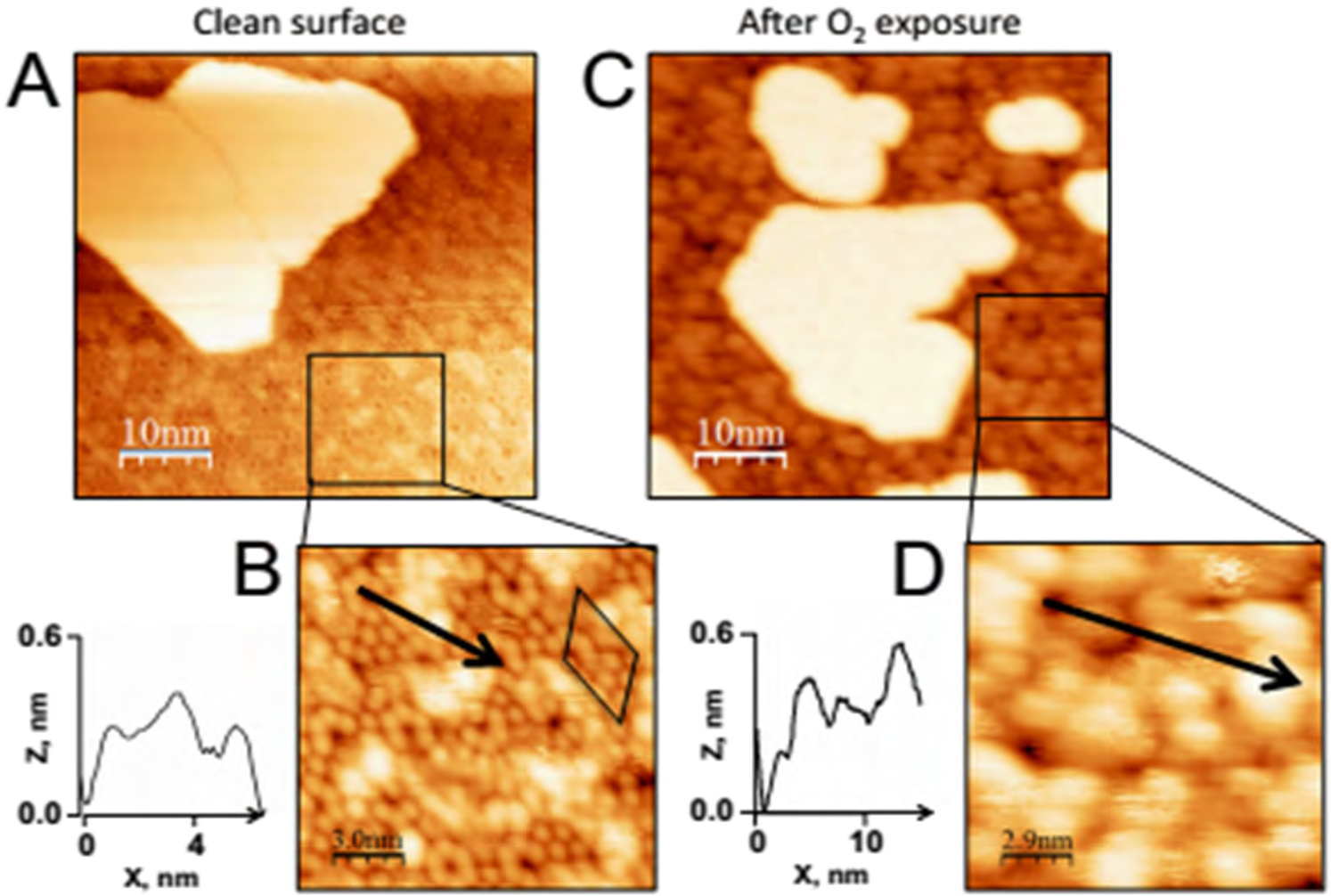

Fig. 3

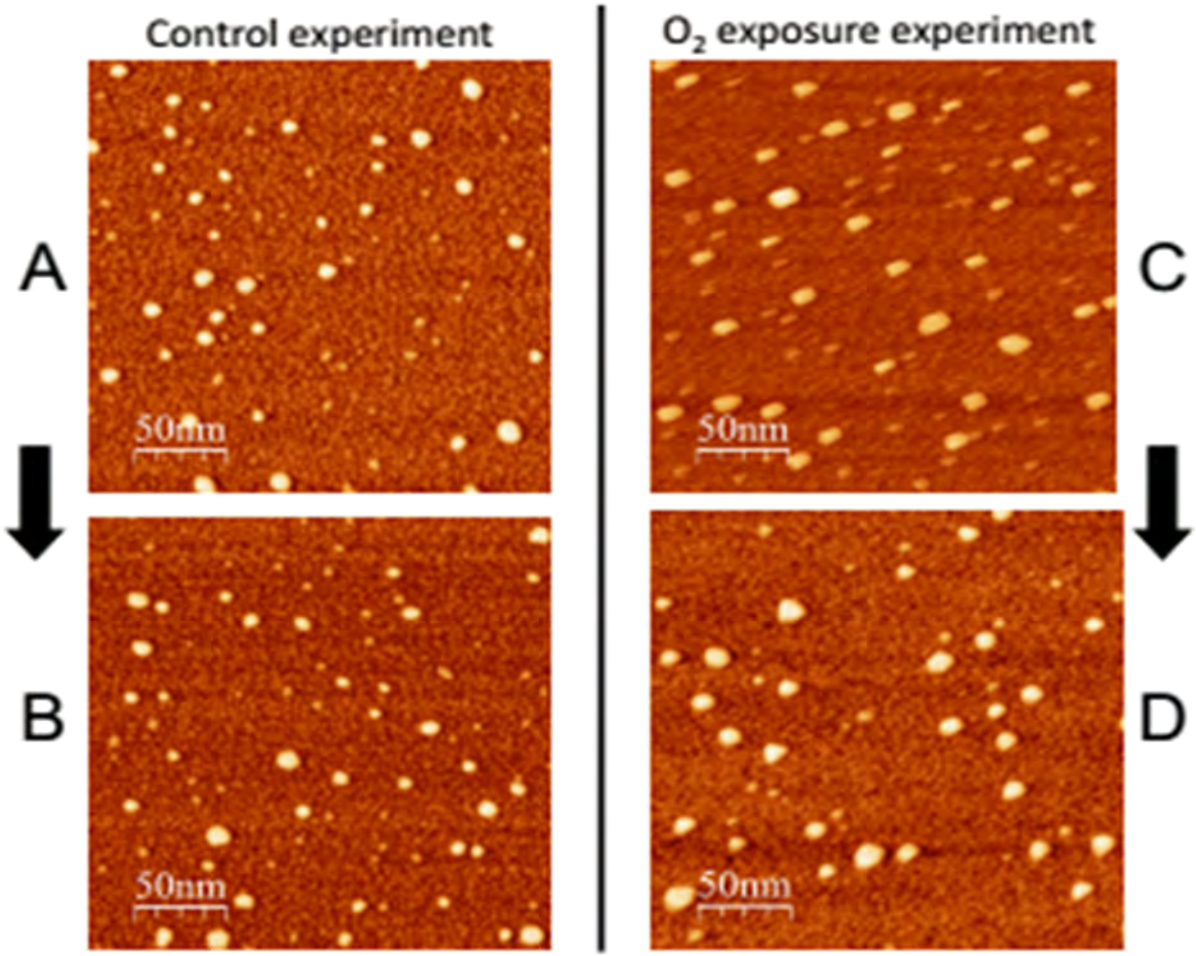

Fig. 4

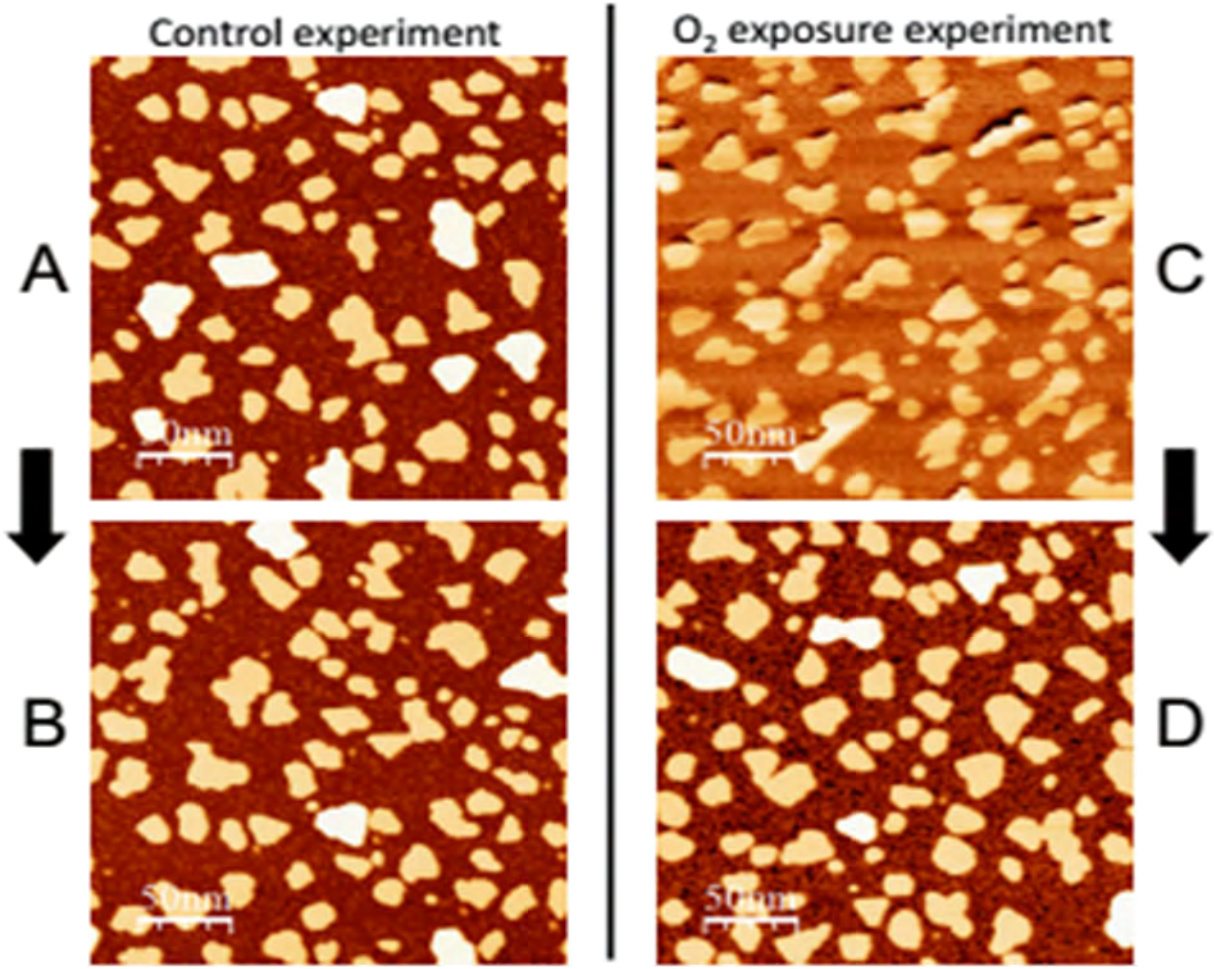

Fig. 5

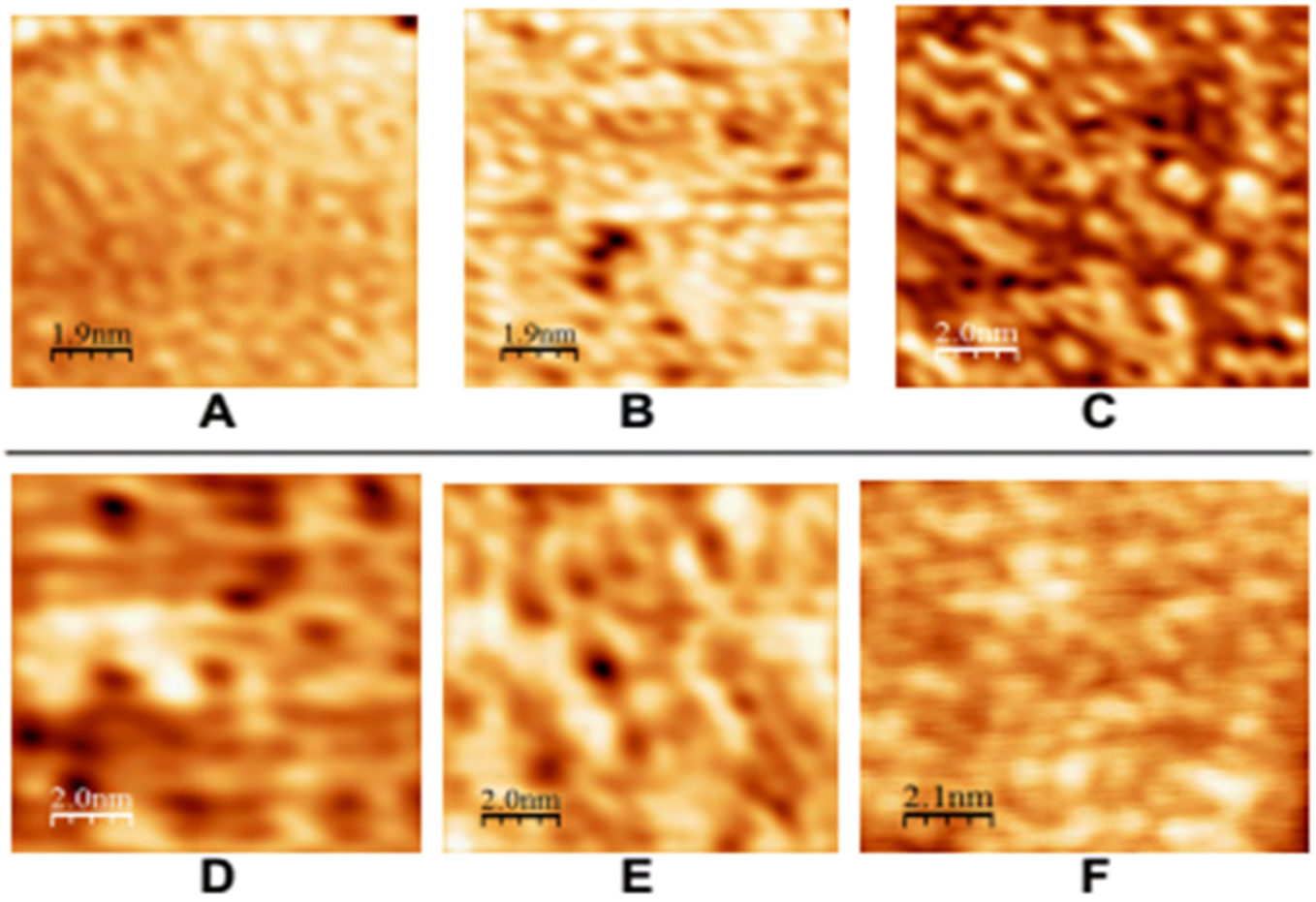

Fig. 6

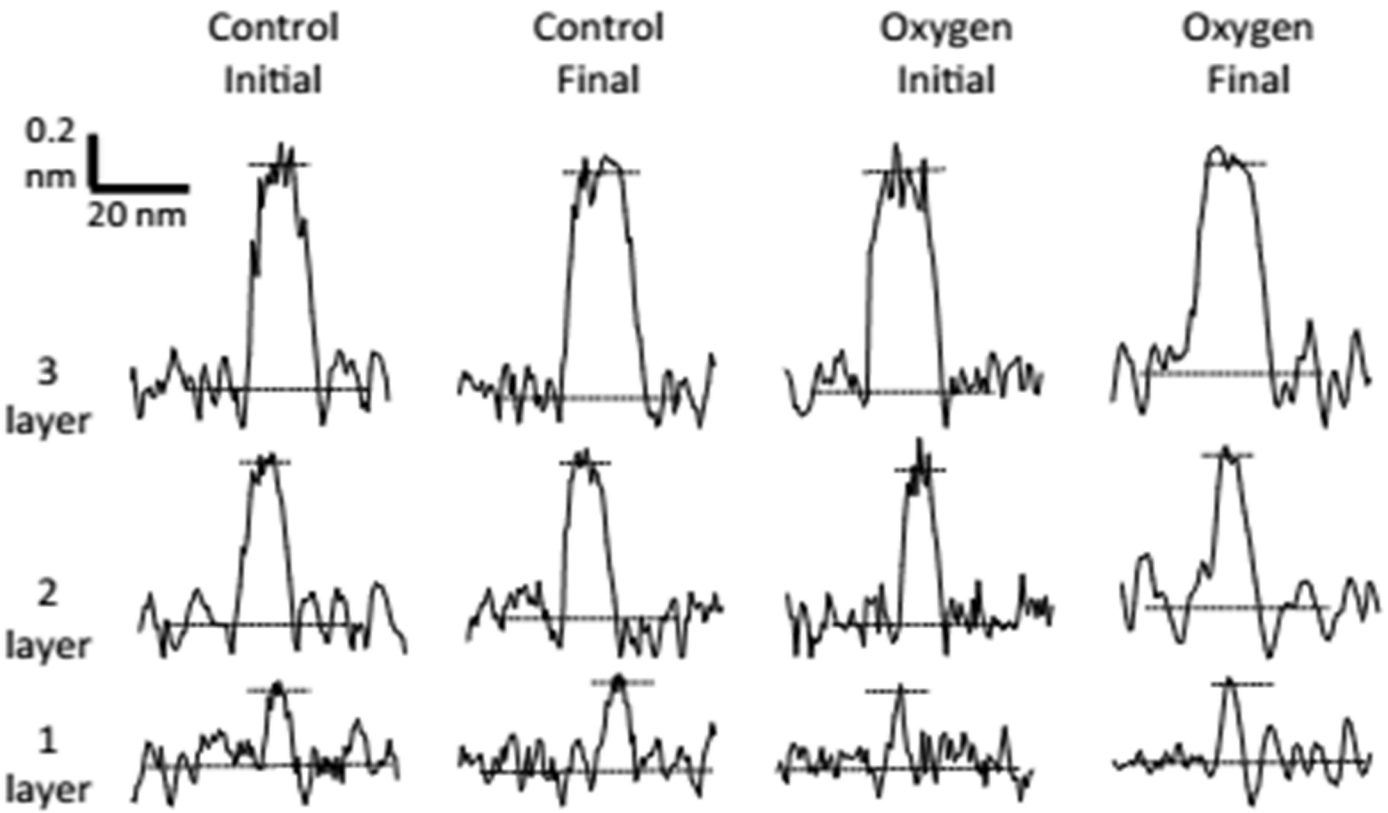

Fig. 7

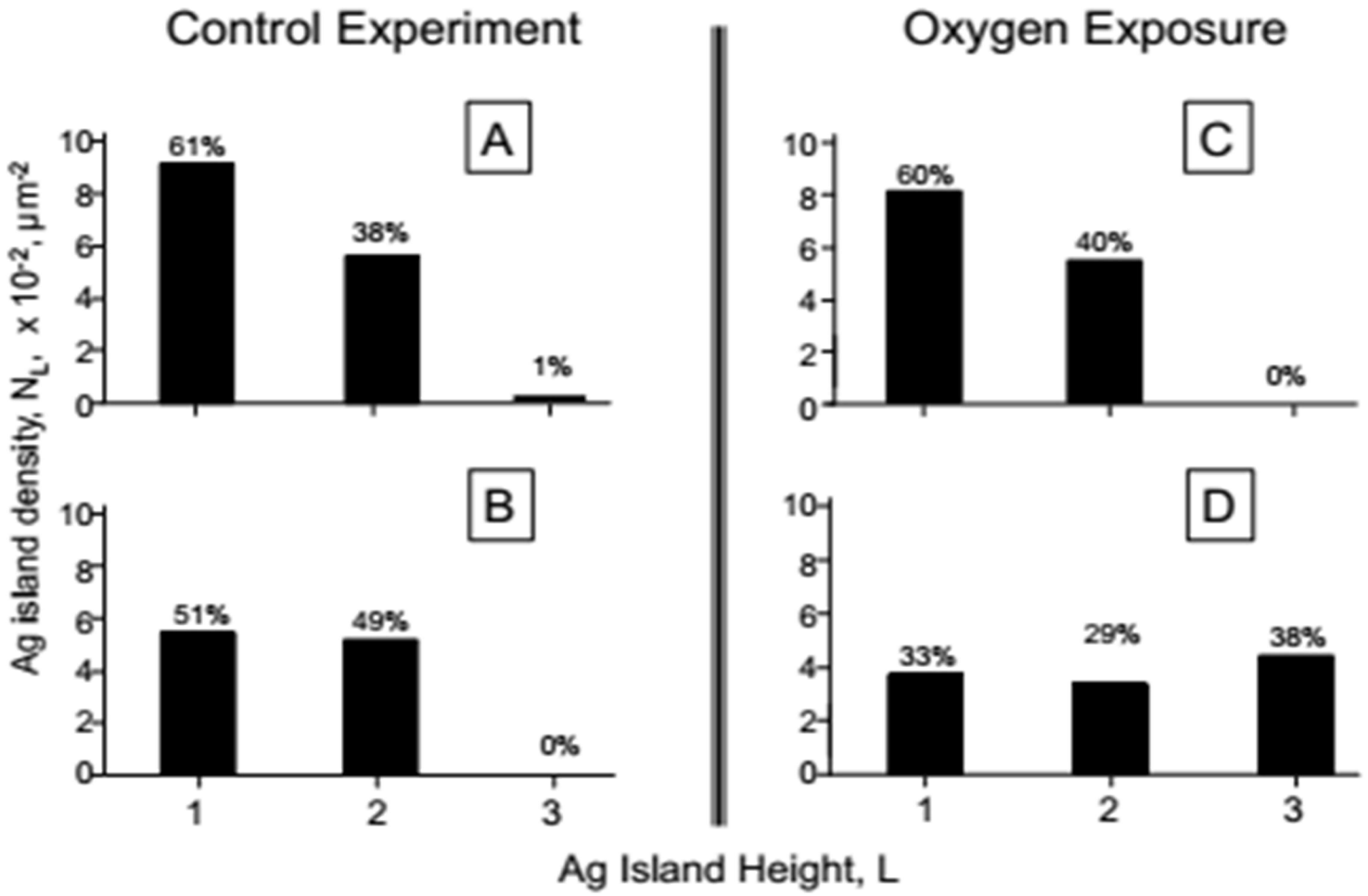

Fig. 8

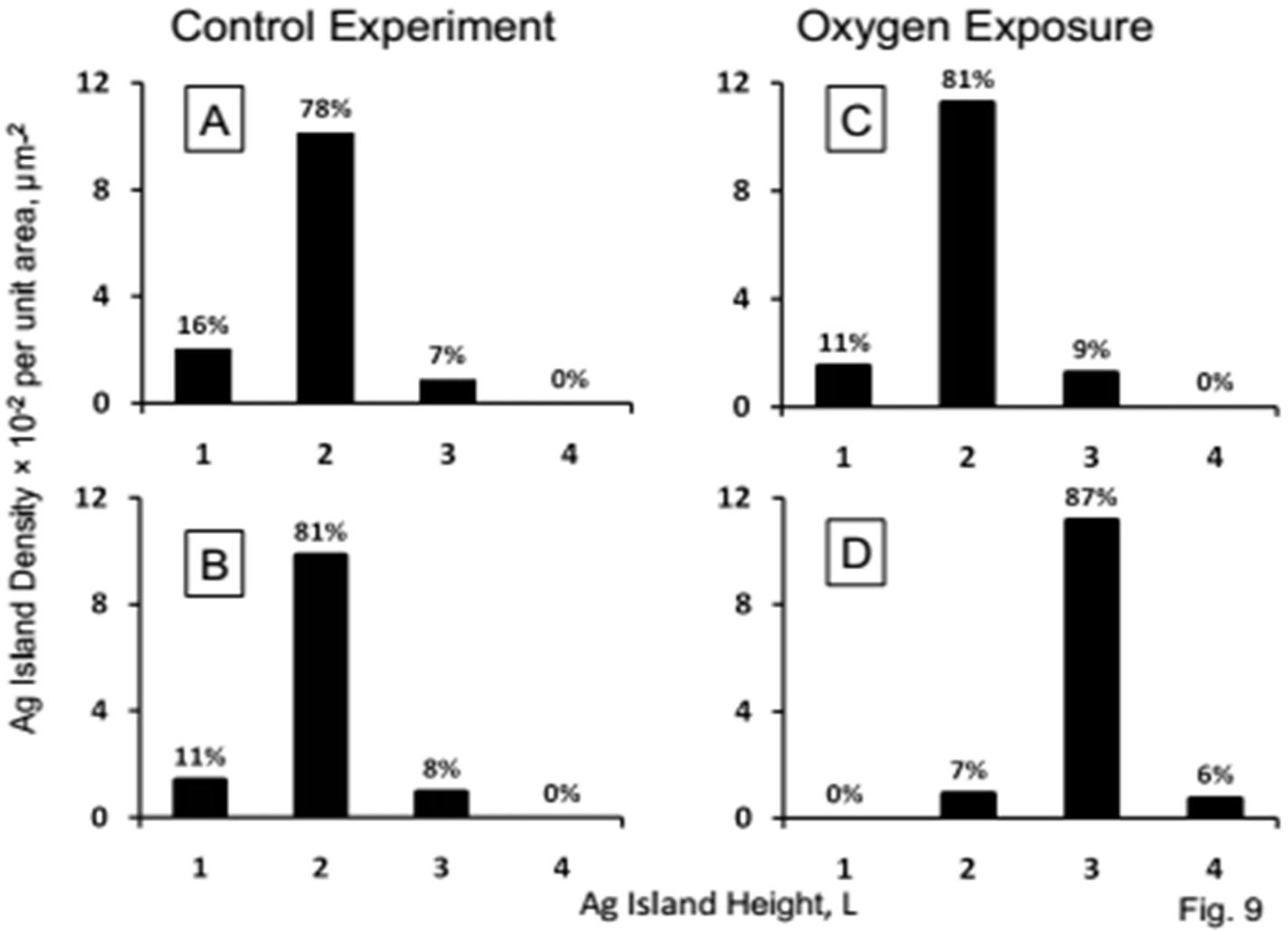

Fig. 9

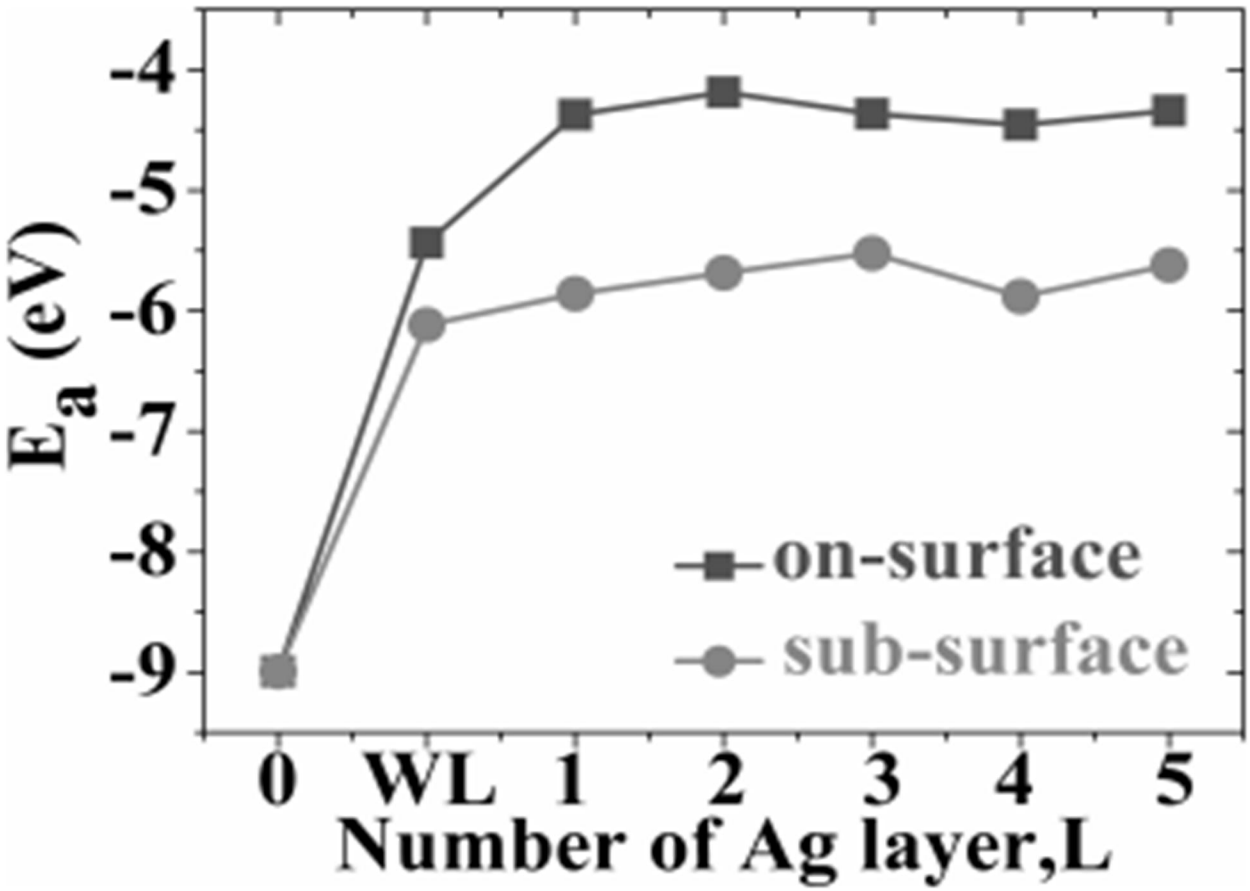

Fig. 10

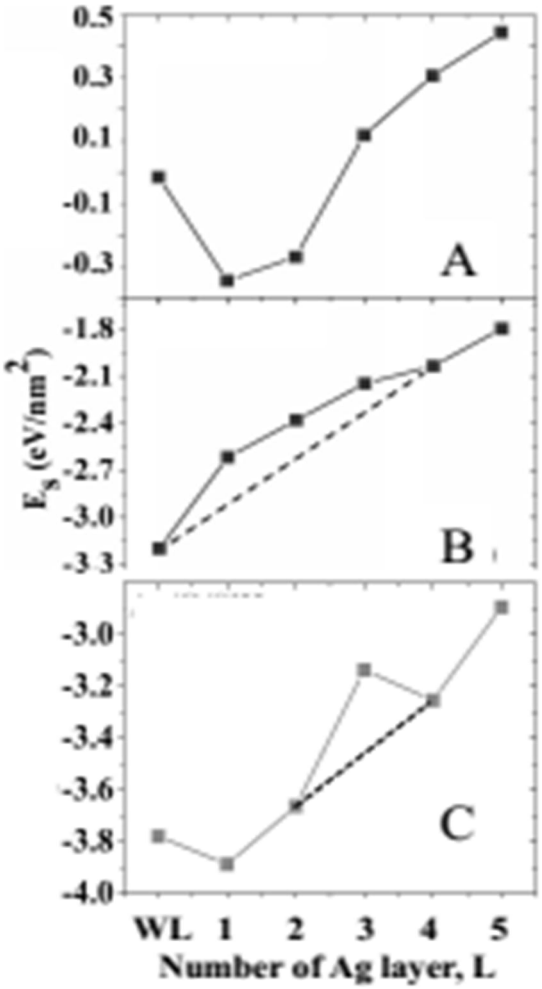

Fig. 11

CHAPTER 3

ADDITIONAL INFORMATION ABOUT THE EFFECT OF OXYGEN ON THE STABILITY OF AG ISLANDS ON SI(111)-7×7

This chapter provides additional results of data analysis for Chapter 2. The results consist of basic experimental information, representative STM images, timeline of data acquisition, island height distribution, island height line profiles, Root-Mean-Square (RMS) roughness of wetting layers, and average island area. The methods of performing these analyses are also included in this chapter. The following content is sorted chronologically.

1. Run 1

This section covers detailed analysis of data acquired in February 2011, which is labeled as Run 1.

1.1. Basic information

Table 1.1shows the experimental conditions for each experiment in this run. And as shown previously, Ag is always deposited at room temperature. Fig. 1.1 - 1.5 show representative Scanning Tunneling Microscopy (STM) data. As shown in Fig. 1.1, the images of the 120 K experiment basically experience a higher level of noise (characterized by the horizontal bright stripes) than other experiments of this run. This is probably caused by the flow of liquid nitrogen used as the coolant. The images from the experiment of 300K, 10 Langmuir (*L*) oxygen exposure have a lower level of noise, but most images have a a multiple-tip effect, as shown in Fig. 1.2. The images taken for the clean Ag/Si(111)-7×7 surface, as a control group are distorted, as shown in Fig. 1.3. Fig 1.4 show one image from the experiment of 300 K, 100 *L*

oxygen exposure. Images of this experiment generally have a better resolution than other experiments. However, the noise level is still not ideal, as shown in the line profile of Fig.1.5, where a typical 3-layer island has higher corrugation than it should have on the island top.

1.2. STM images and timeline for data acquisition

For most of the experiments mentioned in this section, a control group is usually available to offset the possible coarsening effect in the time scale of a typical experiment. Representative STM images and the timeline for experiment of 120 K and 10 *L* O_2 exposure, 300 K and 10 *L* O_2 exposure, and 300 K and 100 *L* O_2 exposure are shown in Fig. 1.6, 1.7, and 1.8, respectively. All experiments of Run 1 are performed at an initial Ag island height distribution of 1+2 layer. There are usually four groups in each experiment, i.e. "control initial", "control final", "oxygen initial", and "oxygen final". One typical image is shown for each group. The time interval between an initial group and final group is the same for the control experiment and the oxygen experiment.

Specifically for the experiment performed at 120 K, there is no control experiment due to the difficulty of cooling to 120 K at that time. Please also note that the images of this experiment are only of 100×100 nm^2, since it is difficult finding terraces big enough (250×250 nm^2) during this experiment.

1.3. Island height distribution

The island height histograms of the 120 K and two 300 K (10 *L* and 100 *L*) experiments are shown in Fig. 1.9 to 1.11 respectively. The percentage numbers above each column are the relative populations for an island of each layer thickness. N_{TOT} denotes the total island density of all islands, in units of μm^{-2}. "Initial" denotes the images taken before oxygen exposure (for the oxygen experiment), or at approximately the same time (for the control group), and "final"

denotes the images taken after oxygen exposure (for the oxygen experiment), or at approximately the same time (for the control group).The control experiment of the 120 K experiment is not available. The approach used for measuring island density is described in Section 4, Data Analysis Methods.

1.4. Island height line profiles

The typical line profiles of the 120 K and two 300 K experiments are shown in Fig. 1.12 to 1.14 respectively. One line profile is shown for an island of each layer thickness. “Clean in” denotes the initial stage of the control group, “Clean fin” denotes the final stage of the control group, “Ox in” denotes the initial stage of the oxygen experiment, and “Ox fin” denotes the final stage of the oxygen experiment.

1.5. Wetting layer images and roughness

Table 1.2 shows the average RMS roughness of the wetting layer before and after oxygen exposure. Each value is shown in the format “average value +/- standard deviation”. The approach used for measuring wetting layer roughness is described in Section 4, Data Analysis Methods.

Due to lack of images at higher magnification (for example, 50x50 nm^2), it is difficult to resolve the wetting layer very well. Fig. 1.15 shows a zoomed-in part (10x10 nm^2) of a 250×250 nm^2 image of the wetting layer after oxygen exposure (100 *L*) at 300 K. The pixels in this image are too big to resolve any atomic-size features. And it is the same situation for wetting layer images of other experiments in this run.

1.6. Average island area

Average island area for 300 K, 100 *L* experiment is shown in Table 1.3. The approach used for measuring average island area is described in Section 4, Data Analysis Methods.

2. Run 2

This section covers detailed analysis of data acquired in May - June 2011, which is labeled as Run 2.

2.1. Basic information

Table 2.1shows the experimental conditions for each experiment in this run. The image quality for 1-layer experiment is better than that of experiments in Run 1, as shown in Fig. 2.1. The images of 1+2-layer and 2-layer experiment, however, suffer from a severe a multiple-tip effect, as shown in Fig. 2.2 - 2.5.

Despite the multiple-tip effect, the wetting layer is much better resolved that that of Run 1 (Fig. 1.15), as shown in Fig. 2.6.

2.2. STM images and timeline of data acquisition

Representative STM images for experiment of 1-layer, 1+2-layer, and2-layer are shown in Fig. 2.7, 2.8, and 2.9, respectively. All experiments of Run 2 are performed at 300 K, and all oxygen exposure experiments of Run 2 are performed at oxygen exposure of 100 *L*, as shown in Table 2.1. There are usually four groups in each experiment, i.e. “control initial”, “control final”, “oxygen initial”, and “oxygen final”. One typical image is shown for each group. The time interval between an initial group and final group is the same for the control experiment and the oxygen experiment.

2.3. Island height distribution

The island height histograms of the 1-layer, 1+2-layer, and 2-layerexperiments are shown in Fig. 2.10, 2.11, and 2.12 respectively. The percentage numbers above each column are the relative populations for an island of each layer thickness. N_{TOT} denotes the total island density of

all islands, in units of μm^{-2}. "Initial" denotes the images taken before oxygen exposure (for the oxygen experiment), or at approximately the same time (for the control group), and "final" denotes the images taken after oxygen exposure (for the oxygen experiment), or at approximately the same time (for the control group). The approach used for measuring island density is described in Section 4, Data Analysis Methods.

2.4. Island height line profiles

Fig. 2.13-15 shows the line profiles for island heights in the 1-layer, 1+2-layer, and 2-layer experiments, respectively. One line profile is shown for an island of each layer thickness. "Clean in" denotes the initial stage of the control group, "Clean fin" denotes the final stage of the control group, "Ox in" denotes the initial stage of the oxygen experiment, and "Ox fin" denotes the final stage of the oxygen experiment. All these experiments suffer from a a multiple-tip effect at one or more stages in the experiment. So only the line profiles from stages that are free from a multiple-tip effects are shown.

2.5. Wetting layer images and roughness

Table 2.2 shows the average RMS roughness of the wetting layer before and after oxygen exposure. Each number is shown in the format "average value +/- standard deviation". The approach used for measuring wetting layer roughness is described in Section 4, Data Analysis Methods. Fig. 2.16 shows typical wetting layer images before and after oxygen exposure.

2.6. Average island area

All Run 2 experiments suffer from a a multiple-tip effect, so the average area information is not accurate for reference.

3. Run 3

This section covers detailed analysis of data acquired in February 2012, which is labeled as Run 3.

3.1. Basic information

Table 3.1 shows the experimental conditions for each experiment in this run. Most of the images in this run show good resolution. Both Ag islands and wetting layers are well resolved, as shown in Fig. 3.1, 3.2, and 3.3, respectively.

3.2. STM images and timeline of data acquisition

Representative STM images for the 2-layer experiment are shown in Fig. 3.5. There are four groups in this experiment, i.e. “control initial”, “control final”, “oxygen initial”, and “oxygen final”. One typical image is shown for each group. The time interval between an initial group and final group is the same for the control experiment and the oxygen experiment.

3.3. Island height distribution

The island height histogram of the experiment is shown in Fig. 3.6. The percentage numbers above each column are the relative populations for an island of each layer thickness. “Initial” denotes the images taken before oxygen exposure (for the oxygen experiment), or approximately the same time (for the control group), and “final” denotes the images taken after oxygen exposure (for the oxygen experiment), or approximately the same time (for the control group). The approach used for measuring island density is described in Section 4, Data Analysis Methods.

3.4. Island height line profiles

Fig. 3.7 shows the line profiles for island heights in the experiment of Run 3. One line profile is shown for an island of each layer thickness. “Clean in” denotes the initial stage of the control group, “Clean fin” denotes the final stage of the control group, “Ox in” denotes the initial

stage of the oxygen experiment, and "Ox fin" denotes the final stage of the oxygen experiment.

3.5. Wetting layer images and roughness

Table 3.2 shows the average RMS roughness of the wetting layer before and after oxygen exposure. Each number is shown in the format "average value +/- standard deviation". The approach used for measuring wetting layer roughness is described in Section 4, Data Analysis Methods. Fig. 3.8 shows typical wetting layer images before and after oxygen exposure.

3.6. Average island area

Average island area for 2-layer, 300 K, 100 *L* experiment is shown in Table 3.3.

4. Data Analysis Methods

4.1. Island density

Island density is defined as the number of islands per unit area, in units of μm^{-2}. For each group ("oxygen initial", "oxygen final", "control initial", "control final", etc.), the total analysis area is usually 0.25 to 0.31 μm^2(equivalent to the sum of the area of 4 to 5 images with the size of 250×250 nm^2). There is no general rule for choosing the number of images. However, 4 to 5 such 250×250 nm^2 images are generally considered statistically reliable in STM studies, since most dimensions used in STM analysis are much less then this size.

After islands are divided by layer thickness based on height line profiles, the corresponding numbers of these islands are counted manually. Manual counting usually helps eliminate the counting of "false" islands that are actually just spikes in the substrate, which would occur with automatic counting by WSxM software. In order to minimize the human error during the counting, each image is counted three times for an island of each layer thickness. The average value is used in the density analysis if the difference between maximum and minimum

does not exceed 2. If there is a significant difference between these countings (>2), more counting will be included.

Islands that straddle different images are included in the counting if more than half of the island is in the image, and excluded if less than half is in the image, although sometimes islands are in irregular in shape, so it could be difficult to determine the size of half islands.

4.2. Wetting layer roughness

The room-mean-square (RMS) roughness of the wetting layer is measured by WSxM software, through a function called "Roughness Analysis", in units of nm. In order to analyze roughness, images are cropped into small regions where there is only the wetting layer included. These small images are cropped carefully to make sure the image area does not have an effect on roughness, since it is shown from Fig. 4.1 that roughness is a function of image area until after a certain value, 29 nm^2, where the curve reaches the asymptotic region.

For each experiment group (for example, "oxygen initial", "oxygen final", "control initial", "control final"), 15 to 20 images are analyzed to ensure the statistical reliability. The result is reported in the format "average value ± standard deviation", in units of nm.

4.3. Coverage

Ag coverage is determined by Equation 4.1, in units of monolayer (ML). As shown in Fig. 4.2, there are different features on the Si(111)-7×7 surface after Ag deposition, and these features include the wetting layer (the inhomogeneous layer that is first formed when Ag is deposited on Si(111)-7×7), Ag islands (1-layer, 2-layer, 3-layer, …), and interfacial layer (the layer that is between Ag islands and Si substrate).

In Equation 4.1, n is the number of different kinds of features in total, A_i is the fractional area of Feature i, θ_i is the coverage of Ag of Feature i (for the wetting layer, θ=0.5, for all other

features θ=1), and δ_i is the height coefficient of Feature i (for the wetting layer, δ=1, for 1-layer island, δ=2, for 2-layer island, δ=3, for 3-layer island, δ=4,…).

$$\theta = \sum_{i=1}^{n} \delta_i A_i \theta_i \qquad (4.1)$$

For example, for the experiment that has only 1-, and 2-layer islands, $\theta = 0.5 \times A_{\text{wetting layer}} + 2 \times A_{\text{1-layer}} + 3 \times A_{\text{2-layer}}$.

The fractional area, A, is measured by WSxM software, through a function called "flooding". In this function, a height is first set up as the reference level, and then only features higher than this reference level will be analyzed in terms of area, making "flooding" similar to its normal meaning that only structures higher than the flood level are not covered by water and registered.

The selection of reference level is of great importance. Ideally, the half maximum should be the reference level. However, during the analysis, as shown in Fig.4.3, at half maximum, there is a great chance that islands of lower heights or the wetting layer can contribute to the area because of the corrugation caused by noise. In order to minimize the contribution from lower features, the reference level is set as high as possible, usually right below island tops, as shown in Fig. 4.3.

To ensure statistically reliability, 4 to 5 such 250 × 250 nm^2 images are used to analyze coverage. The average value is taken as the reported results. These images are selected from early stage in order to avoid interference from coarsening or oxygen exposure.

4.4. Average island area

For an island of each layer thickness, average island area is defined as the total island area divided by the number of islands, in units of nm^2.

The total island area is also determined through "flooding" of WSxM, but in a more

accurate manner. As shown in Fig. 4.4, interference from lower features could contribute to the area analysis if the half maximum is chosen as the reference level for flooding. In order to minimize the interference, each island is cropped individually into a very small image where there is only this island in the image, and then the half maximum is used as the reference level for flooding to determine the area. As in the previous section, 4 to 5 images are used to make sure the data is statistically reliable. This procedure is shown in Fig. 4.4.

4.5. Island volume density

For an island of each layer thickness, the volume density is defined as the total volume per unit area, in units of $nm^3/\mu m^2$.

The island volume is determined in a very similar way to the method of determining average island area mentioned in the previous section. In order to minimize the interference, each island is cropped individually into a very small image where there is only this island in the image. The island volume is determined also through the "flooding" function where any part above the reference level is measured in terms of volume. The reference level, however, is not the half maximum, but the one as low as possible. As in the previous section, 4 to 5 images with the size of 250×250 nm^2 are used to make sure the data is statistically reliable. This procedure is shown in Fig. 4.

4.6. Island height

Island heights are measured based on line profiles by WSxM software, in units of nm. For an island, a line is drawn across it and extended on both sides to include part of the wetting layer that surrounds the island as the baseline, as shown in Fig. 1. Due to the mechanism of the piezo-scanner, the wetting layer is not always the same height across the entire image, especially if the image extends over many features, so it is more accurate to use the adjacent wetting layer

as the baseline instead of the average height of the wetting layer of the entire image. There is no clear cut-off for the range in which the wetting layer can be used as the baseline.

Please note that the direction of the arrow of the line in the image corresponds to the direction of x+ in the line profile.

The island height is calculated as the pixel height difference between the two height extremes. The maximum is the average height of the island tops. Due to the corrugation on the islands, this value is taken empirically. The minimum is the average height of the wetting layer, which is also taken empirically, as shown in Fig. 4.6.

The average height is calculated based on 10 to 20 islands for an island of each layer thickness. The results are reported in the format "average value ± standard deviation", in units of nm.

Table 1.1. Experimental conditions for experiments of Run 1.

Experiment date	02/03/2011	02/09/2011	02/21/2011
Ag coverage[(1)],monolayer (ML)	1.03	0.66	0.66
Initial Ag island height distribution	1+2 layer	1+2 layer	1+2 layer
O_2 exposure, Langmuir (*L*)	10	10	100
O_2 exposure temperature[(2)], K	120	300	300
Annealing experiment	No	No	No
Relevant control experiment available?	No	Yes	Yes

(1) The approach used for measuring Ag coverage is in Section 4, Data Analysis Methods.

(2) The surface is exposed to oxygen and imaged by STM at the same temperature. So in the following sections, "oxygen exposure temperature" is used to represent both temperatures.

Table 1.2. RMS roughness of the wetting layer before and after oxygen exposure for all Run 1 experiments, taken at -1.0 V tip bias, 0.5 nA tunneling current.

Oxygen exposure temperature, K	Run: Experiment	Oxygen exposure, *L*	RMS roughness, nm, before O_2 exposure	RMS roughness, nm, after O_2 exposure
120	Control for 1+2-layer	0	n.a.	n.a.
	1+2-layer	10	0.050 ± 0.002	0.076 ± 0.003
300	Control for 1+2-layer	0	0.079 ± 0.003	0.080 ± 0.003
	1+2-layer	10	0.067 ± 0.003	0.084 ± 0.003
		100	0.070 ± 0.004	0.092 ± 0.004

Table 1.3. Average island area for Run 1: 1+2-layer, 300 K, 100 *L* experiment.

Ag island height, layer thickness		1	2	3
Average island area, nm^2	Control, initial	17.6	45.9	49.3
	Control, final	7.52	56.0	106.6
	O_2 exposure, initial	26.3	44.4	87.6
	O_2 exposure, final	10.8	21.5	68.3

Table 2.1. Experimental conditions for experiments of Run 2.

Experiment date	06/02/2011	06/25/2011	06/30/2011
Ag coverage[(1)], ML	0.51	0.69[(2)]	1.96[(3)]
Initial Ag island height distribution	1 layer	1+2 layer	2 layer
O_2 exposure, *L*	100	100	100
O_2 exposure temperature[(4)], K	300	300	300
Annealing experiment	Yes[(5)]	Yes	Yes
Relevant control available	Yes	Yes	Yes
Comments on data		A multiple-tip effects for "before-oxygen-exposure"	A multiple-tip effects for "before and after-oxygen-exposure"

(1) The approach used for measuring Ag coverage is described in Section 4, Data Analysis Methods.

(2) There is a multiple-tip effect in this experiment, so the Ag coverage is not reliable. Instead of measuring coverage from this experiment, coverage is measured from the control experiment which has the identical deposition conditions.

(3) This coverage is severely affected by a multiple-tip effect.

(4) The surface is exposed to oxygen and imaged by STM at the same temperature. So in the following sections, "oxygen exposure temperature" is used to represent both temperatures.

(5) Annealing is only available to control experiment due to electronics failure for the oxygen exposure experiment.

Table 2.2. RMS roughness of the wetting layer before and after oxygen exposure for all Run 2 experiments, taken at -1.0 V tip bias, 0.5 nA tunneling current.

Run: Experiment	Oxygen exposure, *L*	Oxygen exposure temperature, K	RMS roughness, nm, before O_2 exposure	RMS roughness, nm, after O_2 exposure
Run 2: Control for 1-layer	0	300	0.054 ± 0.003	0.055 ± 0.003
Run 2: 1-layer	100	300	0.051 ± 0.002	0.078 ± 0.003
Run 2: Control for 1+2-layer	0	300	0.051 ± 0.003	0.052 ± 0.002
Run 2: 1+2-layer	100	300	0.059 ± 0.004	0.080 ± 0.002
Run 2: Control for 2-layer	0	300	0.040 ± 0.007	0.040 ± 0.011
Run 2: 2-layer	100	300	0.038 ± 0.006	0.073 ± 0.003

Table 3.1. Experimental conditions of the experiment in Run 3.

Experiment date	02/06/2012
Ag coverage(1), ML	1.36
Initial Ag island height distribution	2 layer
O_2 exposure, *L*	100
O_2 exposure temperature(2), K	300
Annealing experiment	No
Relevant control available	Yes
Notes in data	Good resolution

(1) The approach used for measuring Ag coverage is described in Section 4, Data Analysis Methods.

(2) The surface is exposed to oxygen and imaged by scanning tunneling microscopy at the same temperature. So in the following sections, "oxygen exposure temperature" is used to represent both temperatures.

Table 3.2. RMS roughness of the wetting layer before and after oxygen exposure for all Run 3 experiments, taken at -1.0 V tip bias, 0.5 nA tunneling current.

Run: Experiment	Oxygen exposure, *L*	Oxygen exposure temperature, K	RMS roughness, nm, before O_2 exposure	RMS roughness, nm, after O_2 exposure
Run 3: Control for 2-layer	0	300	0.058 ± 0.003	0.060 ± 0.004
Run 3: 2-layer	100	300	0.065 ± 0.010	0.077 ± 0.003

Table 3.3. Average island area for Run 3: 2-layer, 300 K, 100 *L* experiment.

Ag island Height, layer thickness		1	2	3	4
Average island area, nm^2	Control, initial	15	260	426	n.a.
	Control, final	17	248	449	n.a.
	O_2 exposure, initial	n.a. due to double-tip effect			
	O_2 exposure, final	none	19	248	518

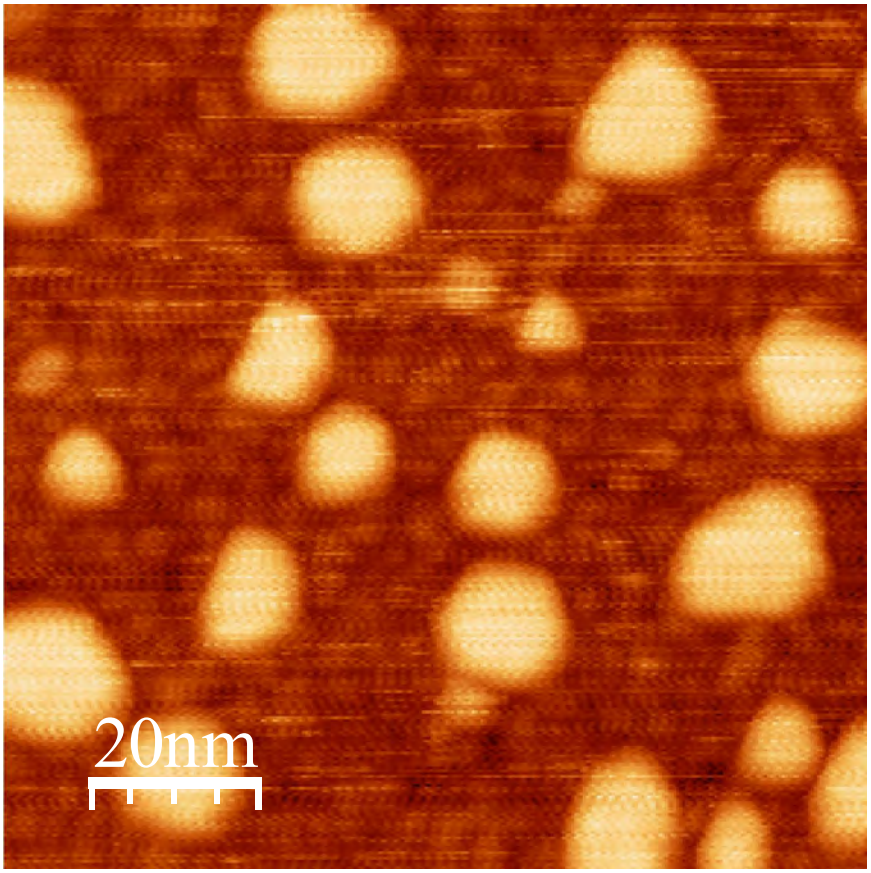

Figure 1.1

Run 1: 1+2-layer, 120 K, the control experiment (for 10 *L* oxygen exposure). An image of clean Ag/Si(111)-7×7 at 120 K,-1.0 V tip bias, 0.5 nA, 100×100 nm^2.

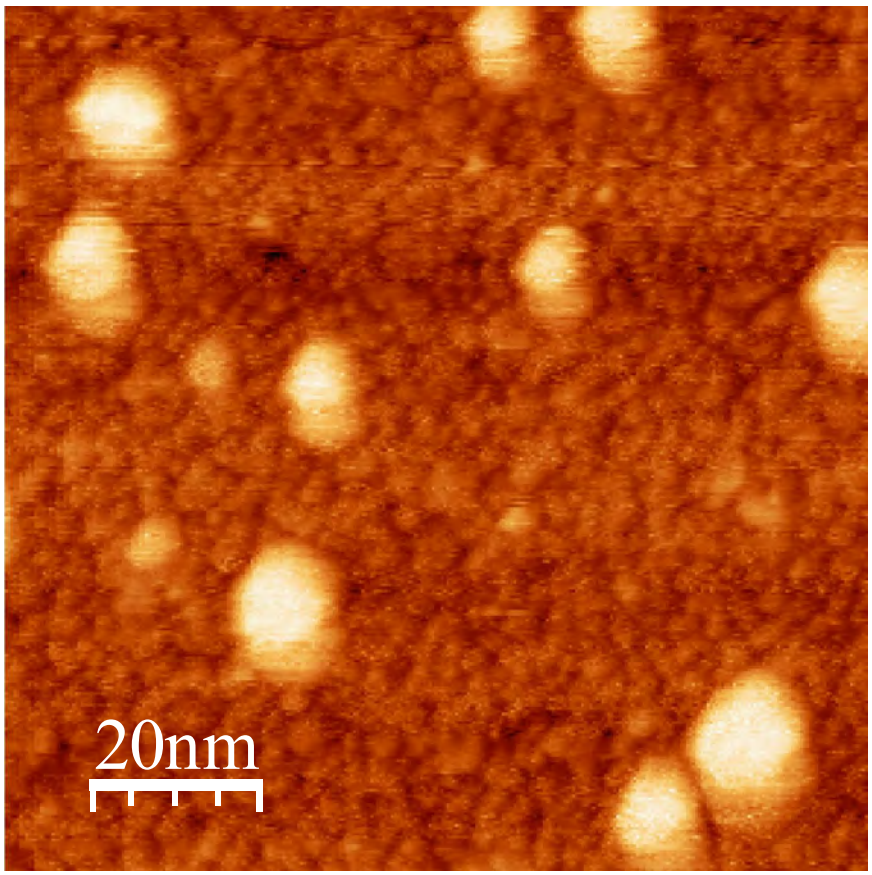

Figure 1.2

Run 1: 1+2-layer, 300 K, the control experiment (for 10 *L* oxygen exposure).An image of clean Ag/Si(111)-7×7, -1.0 V tip bias, 0.5 nA, 100×100 nm^2.

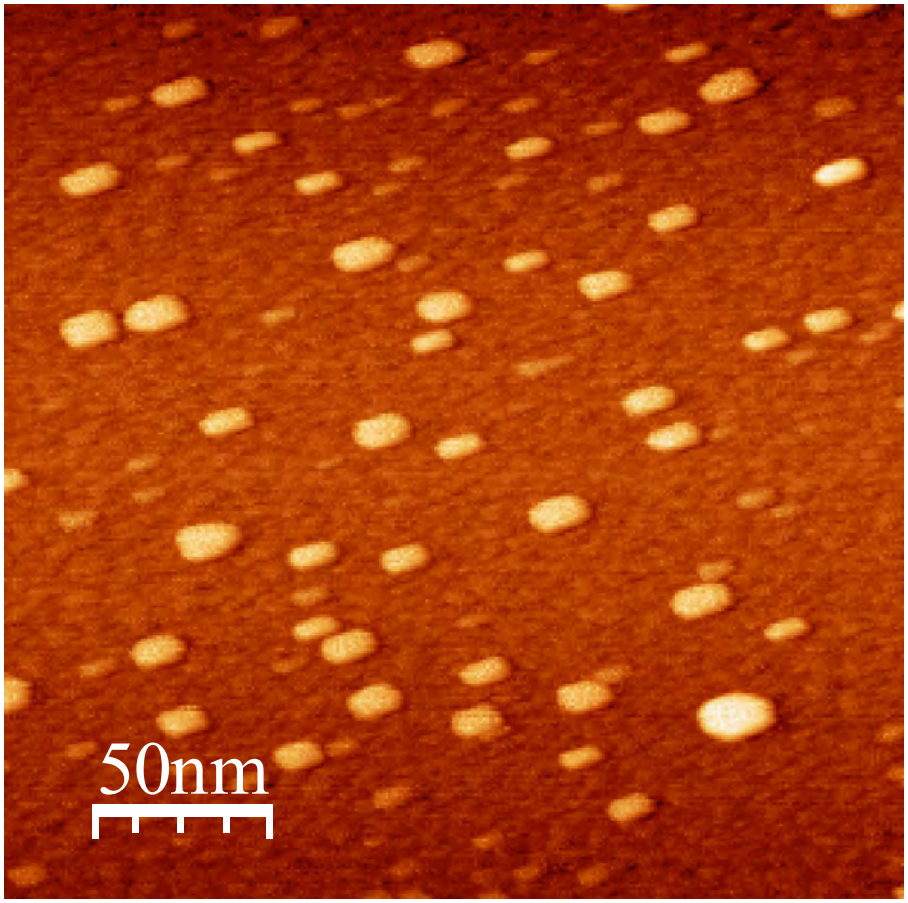

Figure 1.3

Run 1: 1+2-layer, 300 K, the control experiment (for 100 *L* oxygen exposure).An image of clean Ag/Si(111)-7×7, -1.0 V tip bias, 0.5 nA, 250×250 nm^2.

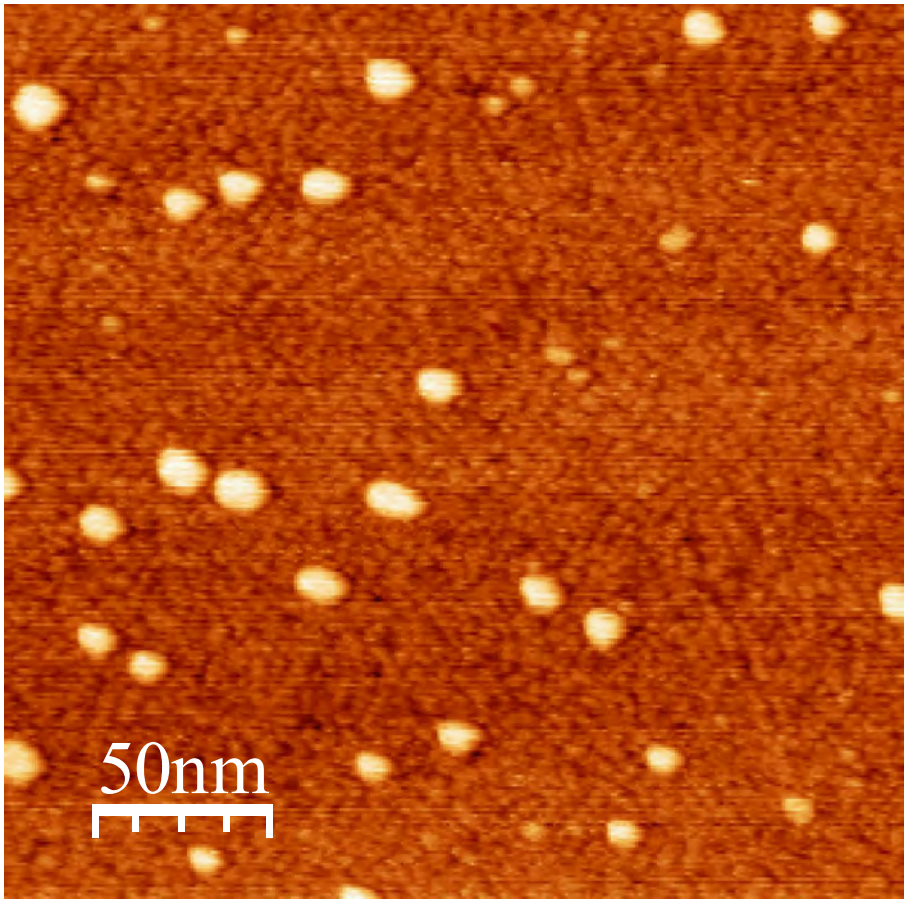

Figure 1.4

Run 1: 1+2-layer, 300 K, 100 *L* oxygen exposure. An image of oxygen-exposed Ag/Si(111)-7×7, -1.0 V tip bias, 0.5 nA, 250×250 nm^2.

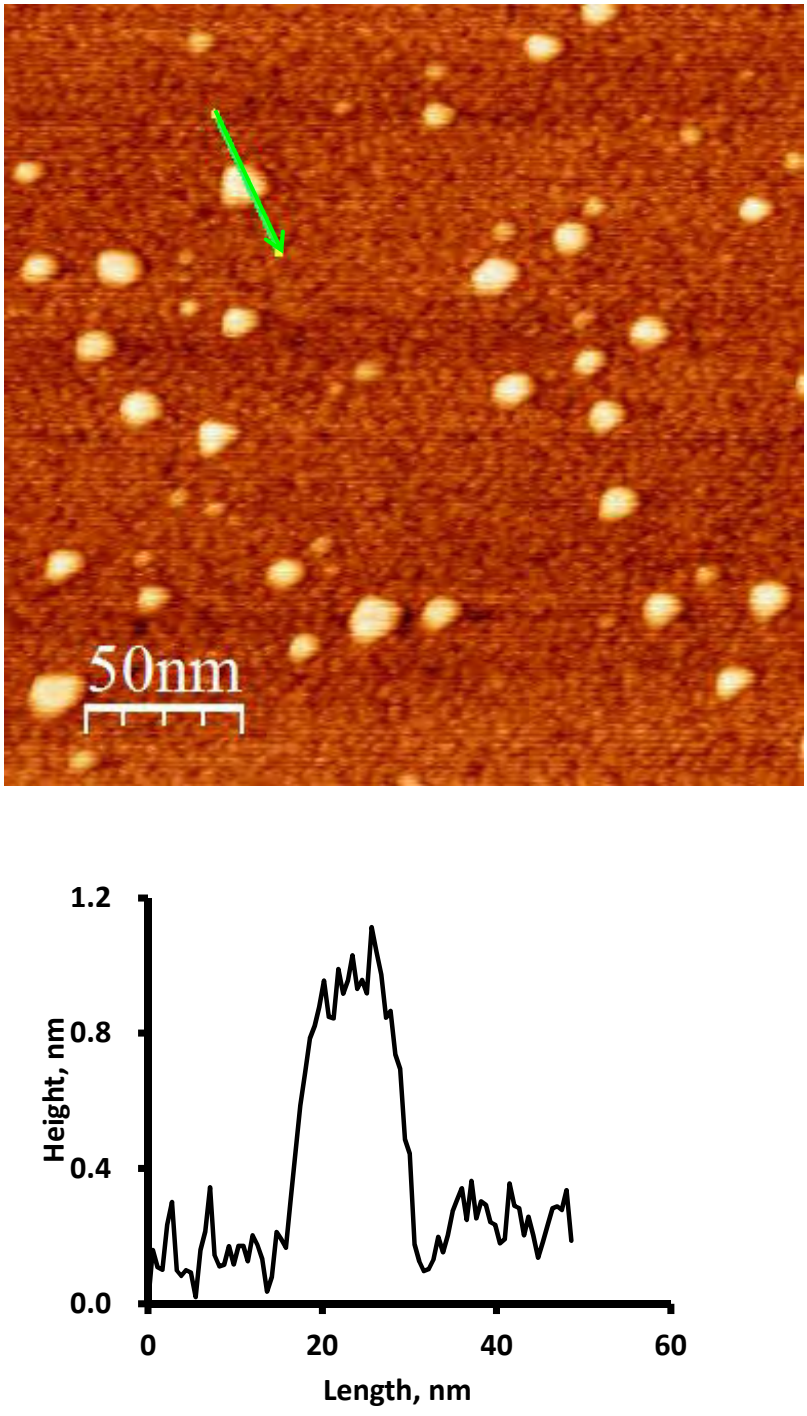

Figure 1.5 Run 1: 1+2-layer, 300 K, 100 *L* oxygen exposure, A line profile (lower panel) of a 3-layer Ag island (the island crossed by the green line from the upper panel) from the Ag/Si(111)-7×7 surface after oxygen exposure (100 *L*) at 300 K, taken at -1.0 V tip bias, 0.5 nA. The upper image size is 250×250 nm^2.

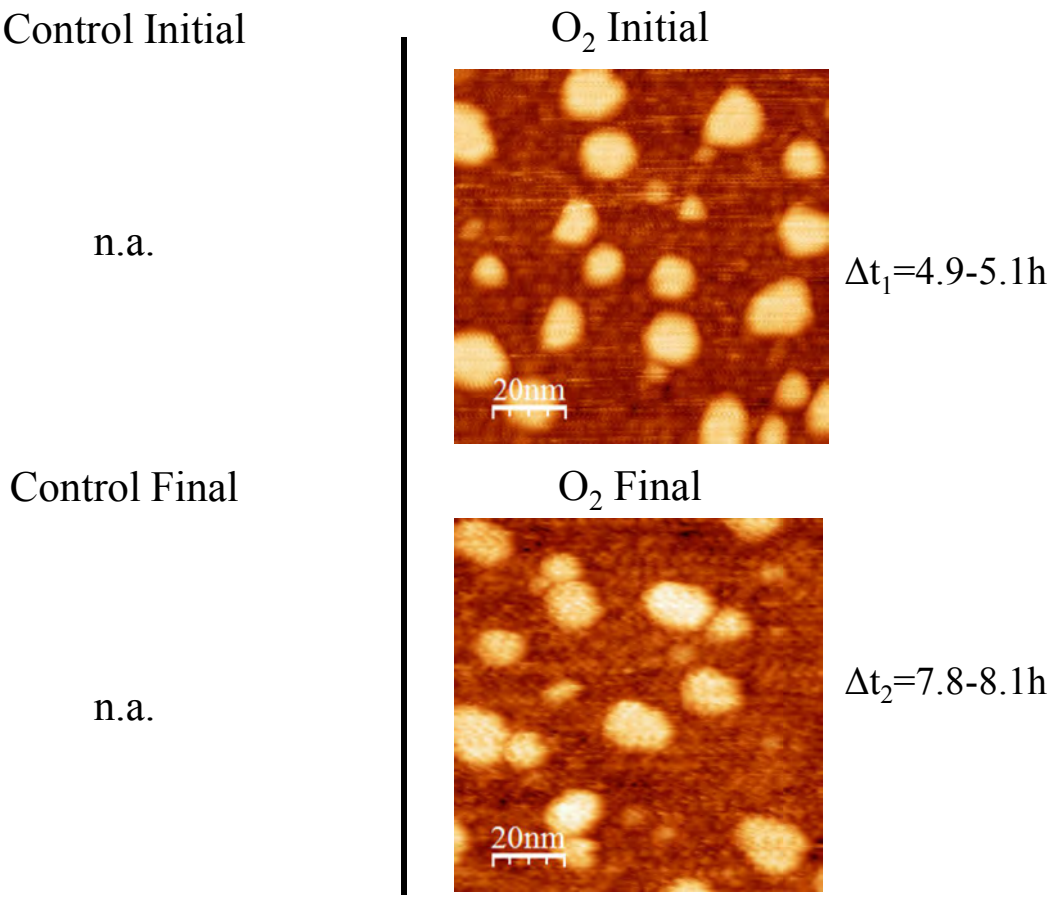

Figure 1.6

Representative images for Run 1: 1+2-layer, 120 K, 10 *L* oxygen exposure , taken at -1.0 V tip bias, 0.5 nA. The images are of 100×100 nm^2. Δt_1 is denoted as the time interval from the point of Ag deposition to that of acquisition of "initial" group images, and Δt_2 is denoted as the time interval from the point of Ag deposition to that of acquisition of "final" group images. There is no control experiment due to the difficulty of cooling to 120 K at that time.

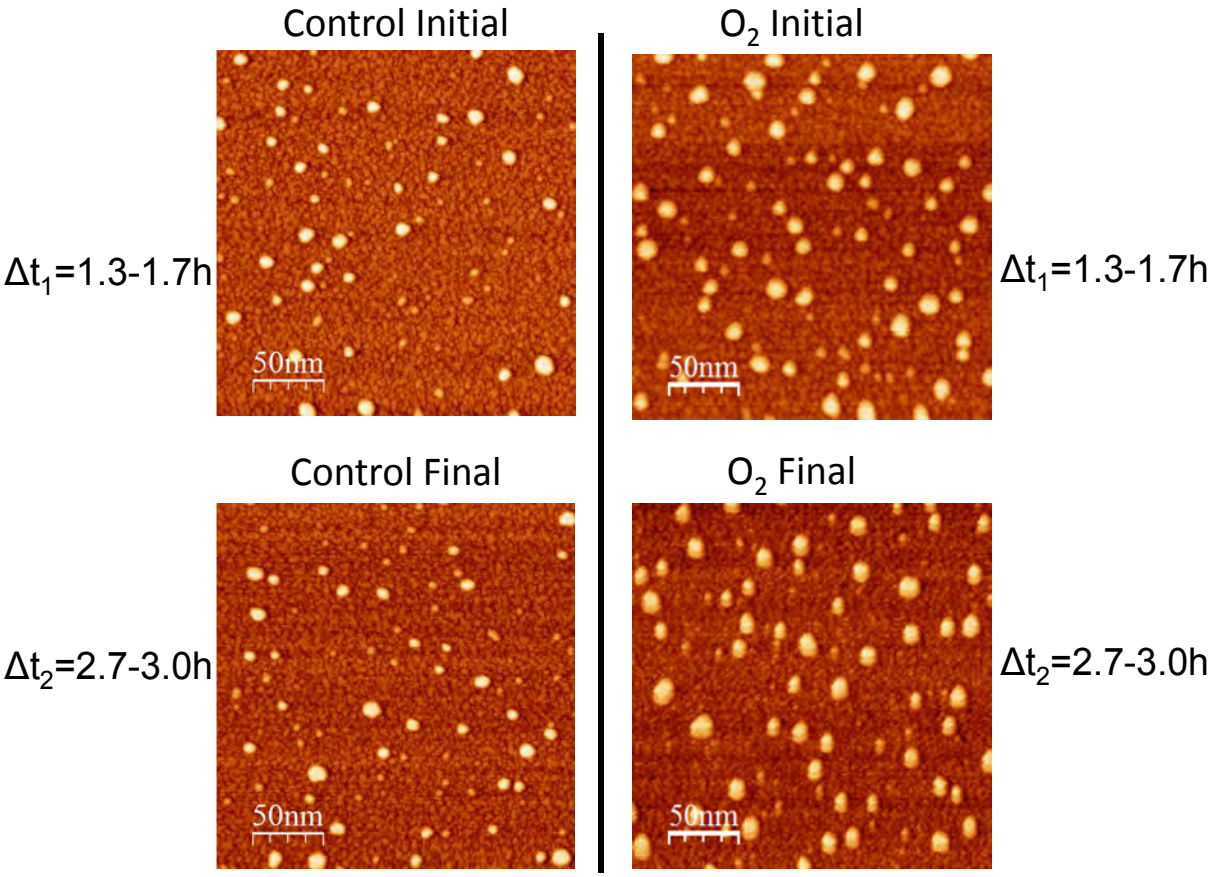

Figure 1.7

Representative images for Run 1: 1+2-layer, 300 K, 10 *L* oxygen exposure, taken at -1.0 V tip bias, 0.5 nA. The images are of 250×250 nm^2. Δt_1 is denoted as the time interval from the point of Ag deposition to that of acquisition of "initial" group images, and Δt_2 is denoted as the time interval from the point of Ag deposition to that of acquisition of "final" group images.

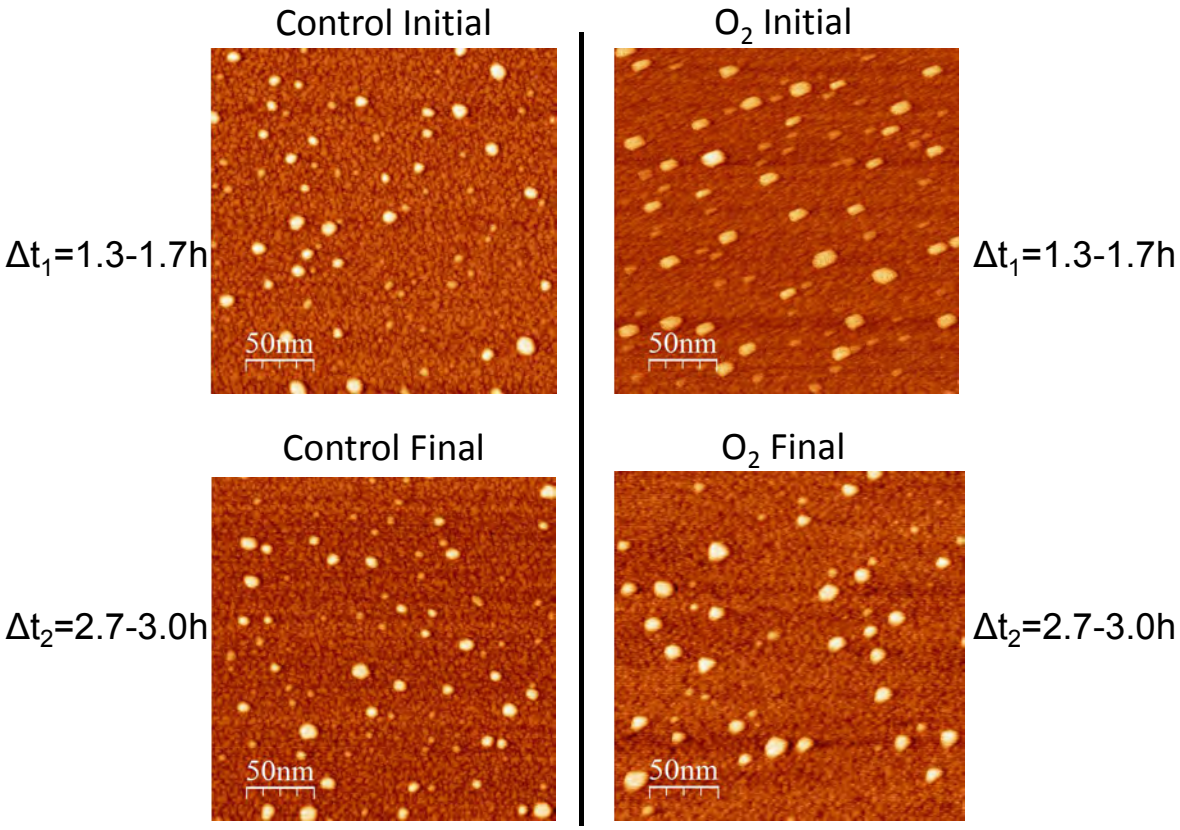

Figure 1.8

Representative images for Run 1: 1+2-layer, 300 K, 100 *L* oxygen exposure, taken at -1.0 V tip bias, 0.5 nA. The images are of 250×250 nm^2. Δt_1 is denoted as the time interval from the point of Ag deposition to that of acquisition of "initial" group images, and Δt_2 is denoted as the time interval from the point of Ag deposition to that of acquisition of "final" group images.

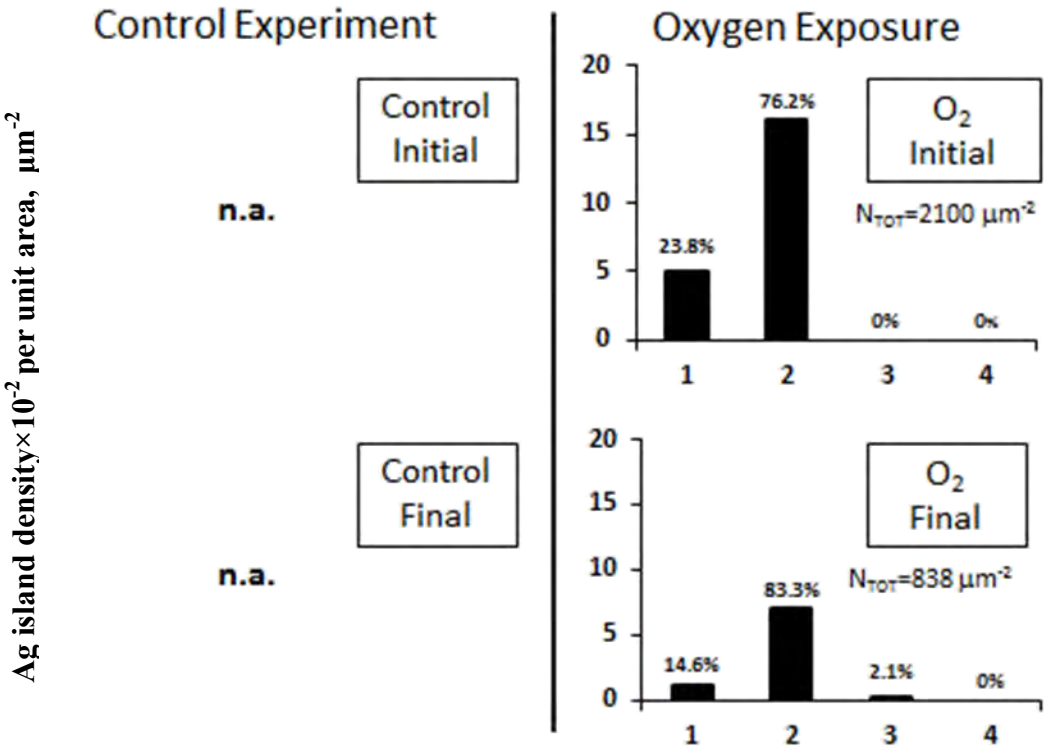

Figure 1.9

Island height histogram for Run 1: 1+2-layer, 10 *L* oxygen exposure, 120 K, taken at -1.0 V tip bias, 0.5 nA. The percentage numbers above each column are the relative populations for an island of each layer thickness. N_{TOT} denotes the total island density of all islands, in units of μm^{-2}. "Initial" denotes the images taken before oxygen exposure (for the oxygen experiment), or at approximately the same time (for the control group), and "final" denotes the images taken after oxygen exposure (for the oxygen experiment), or at approximately the same time (for the control group).

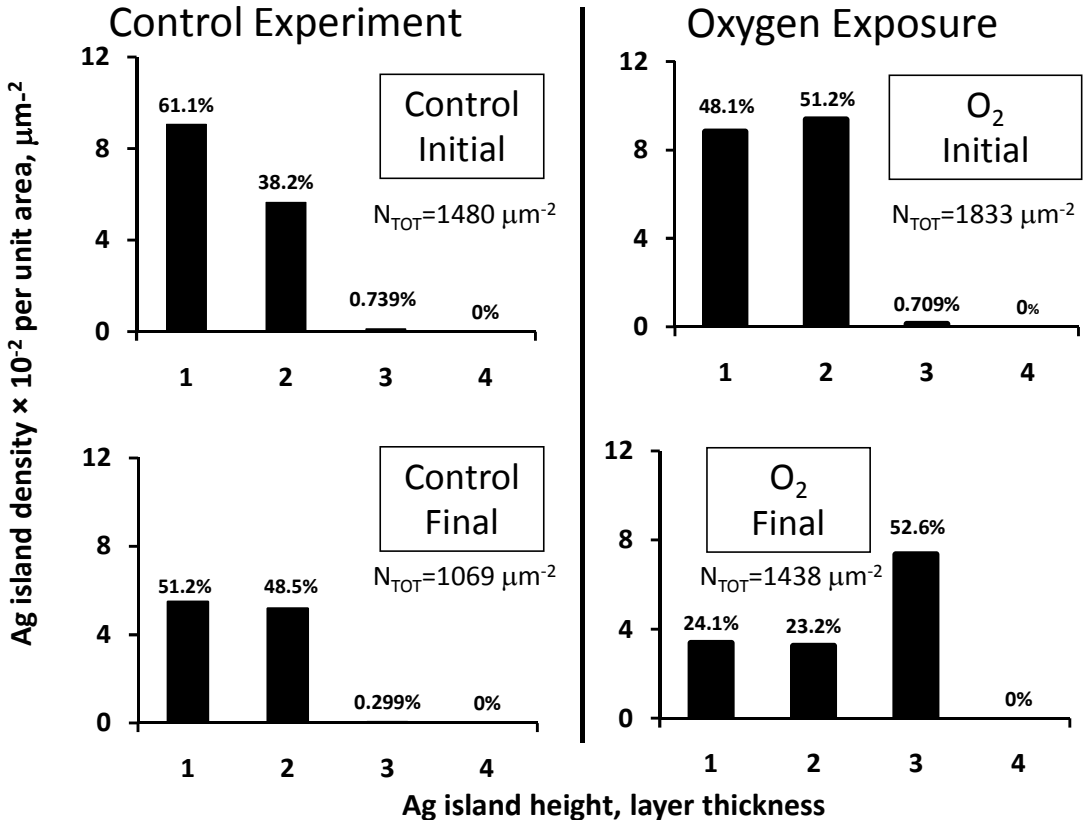

Figure 1.10

Island height histogram for Run 1: 1+2-layer, 10 *L* oxygen exposure, 300 K, taken at -1.0 V tip bias, 0.5 nA. The percentage numbers above each column are the relative populations for an island of each layer thickness. N_{TOT} denotes the total island density of all islands, in units of μm^{-2}. "Initial" denotes the images taken before oxygen exposure (for the oxygen experiment), or at approximately the same time (for the control group), and "final" denotes the images taken after oxygen exposure (for the oxygen experiment), or at approximately the same time (for the control group).

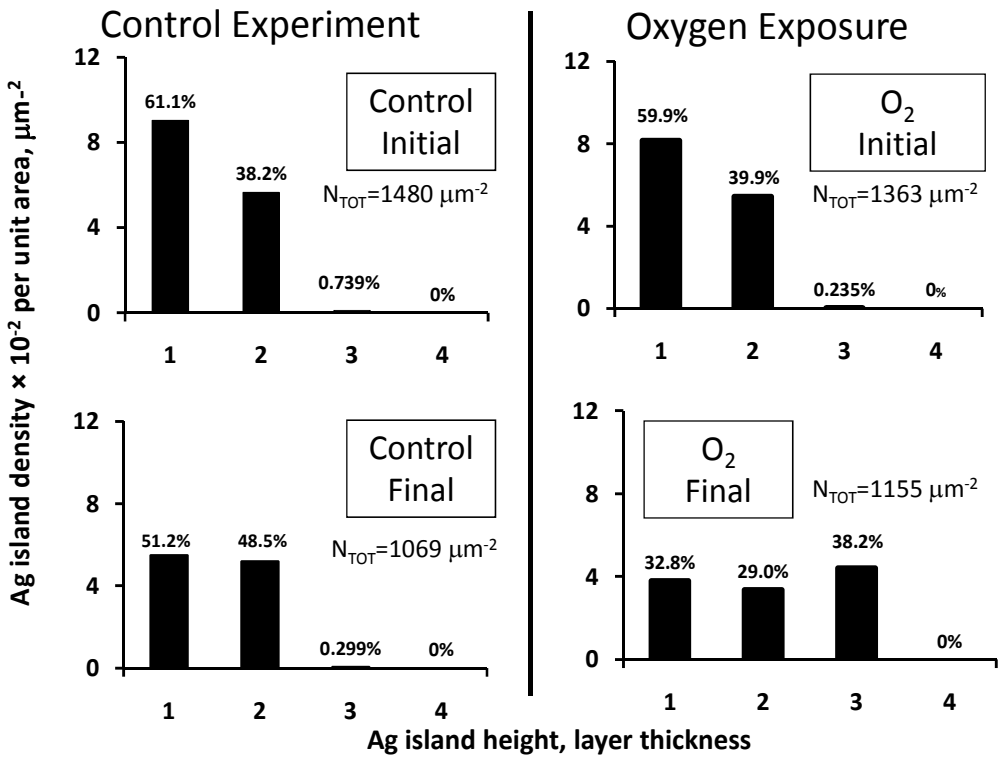

Figure 1.11

Island height histogram for Run 1: 1+2-layer, 100 *L* oxygen exposure, 300 K, taken at -1.0 V tip bias, 0.5 nA. The percentage numbers above each column are the relative population for islands of each kind. N_{TOT} denotes the total island density of all islands, in units of μm^{-2}. "Initial" denotes the images taken before oxygen exposure (for the oxygen experiment), or at approximately the same time (for the control group), and "final" denotes the images taken after oxygen exposure (for the oxygen experiment), or at approximately the same time (for the control group).

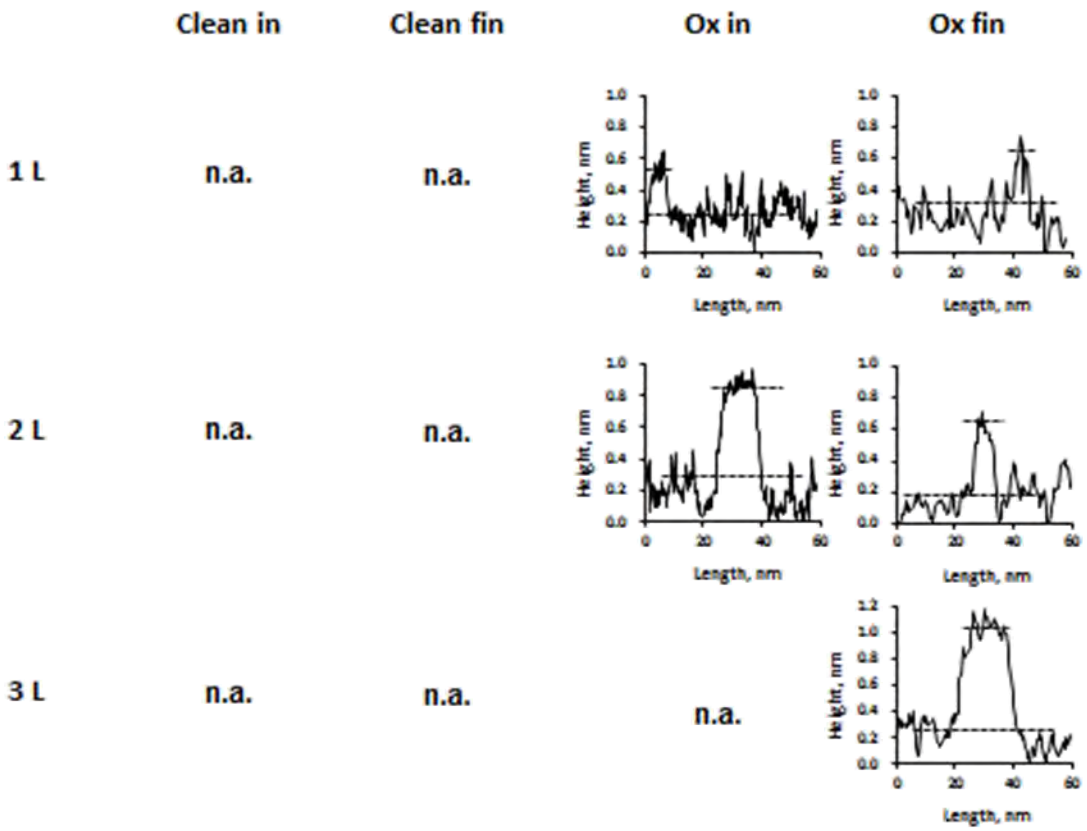

Figure 1.12

Island height line profiles for Run 1: 1+2-layer, 120 K, 10 *L* oxygen exposure, taken at -1.0 V tip bias, 0.5 nA. One line profile is shown for an island of each layer thickness. "Clean in" denotes the initial stage of the control group, "Clean fin" denotes the final stage of the control group, "Ox in" denotes the initial stage of the oxygen experiment, and "Ox fin" denotes the final stage of the oxygen experiment.

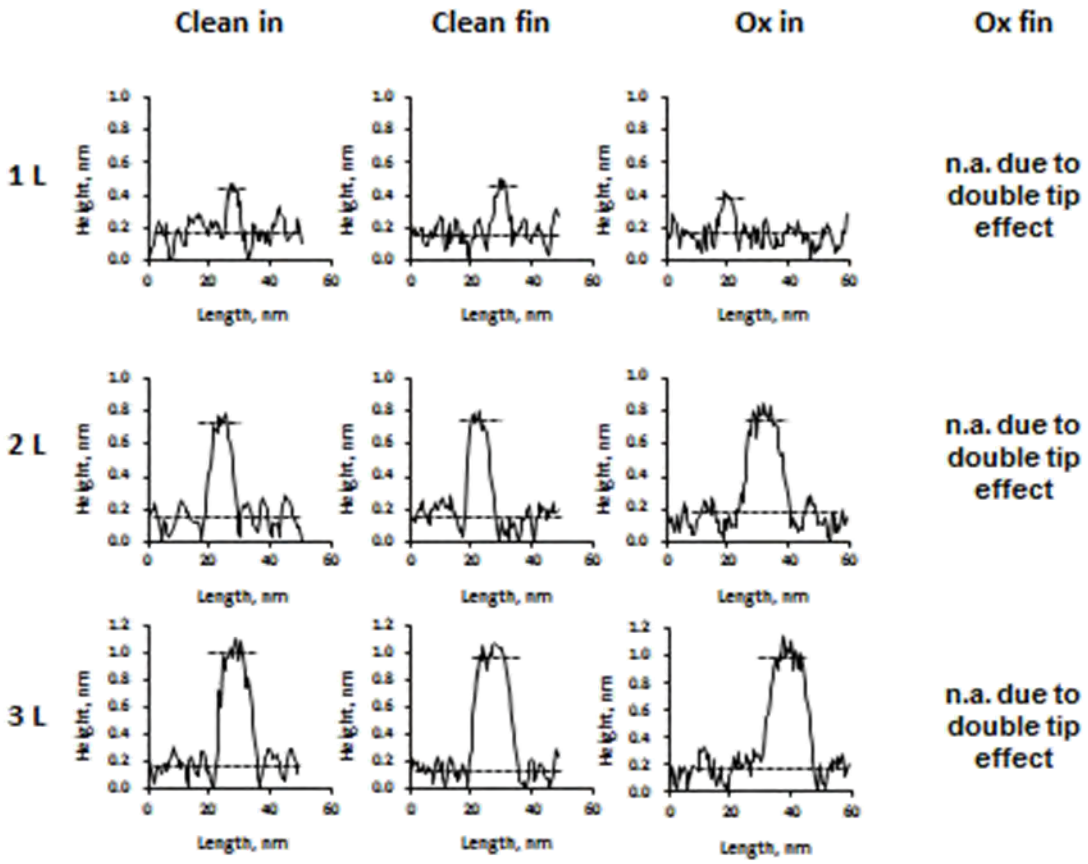

Figure 1.13

Island height line profiles for Run 1: 1+2-layer, 300 K, 10 *L* oxygen exposure, taken at -1.0 V tip bias, 0.5 nA. One line profile is shown for and island of each layer thickness. "Clean in" denotes the initial stage of the control group, "Clean fin" denotes the final stage of the control group, "Ox in" denotes the initial stage of the oxygen experiment, and "Ox fin" denotes the final stage of the oxygen experiment.

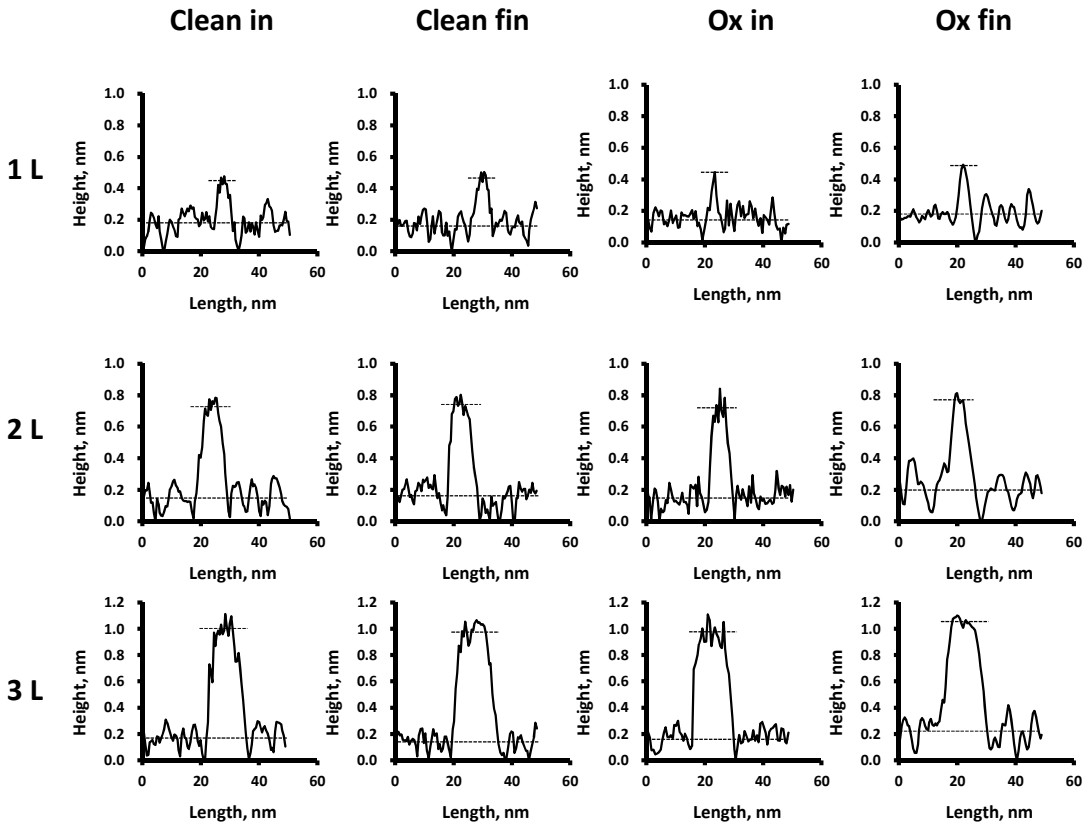

Figure 1.14

Island height line profiles for Run 1: 1+2-layer, 300 K, 100 *L* oxygen exposure, taken at -1.0 V tip bias, 0.5 nA. One line profile is shown for an island of each layer thickness. "Clean in" denotes the initial stage of the control group, "Clean fin" denotes the final stage of the control group, "Ox in" denotes the initial stage of the oxygen experiment, and "Ox fin" denotes the final stage of the oxygen experiment.

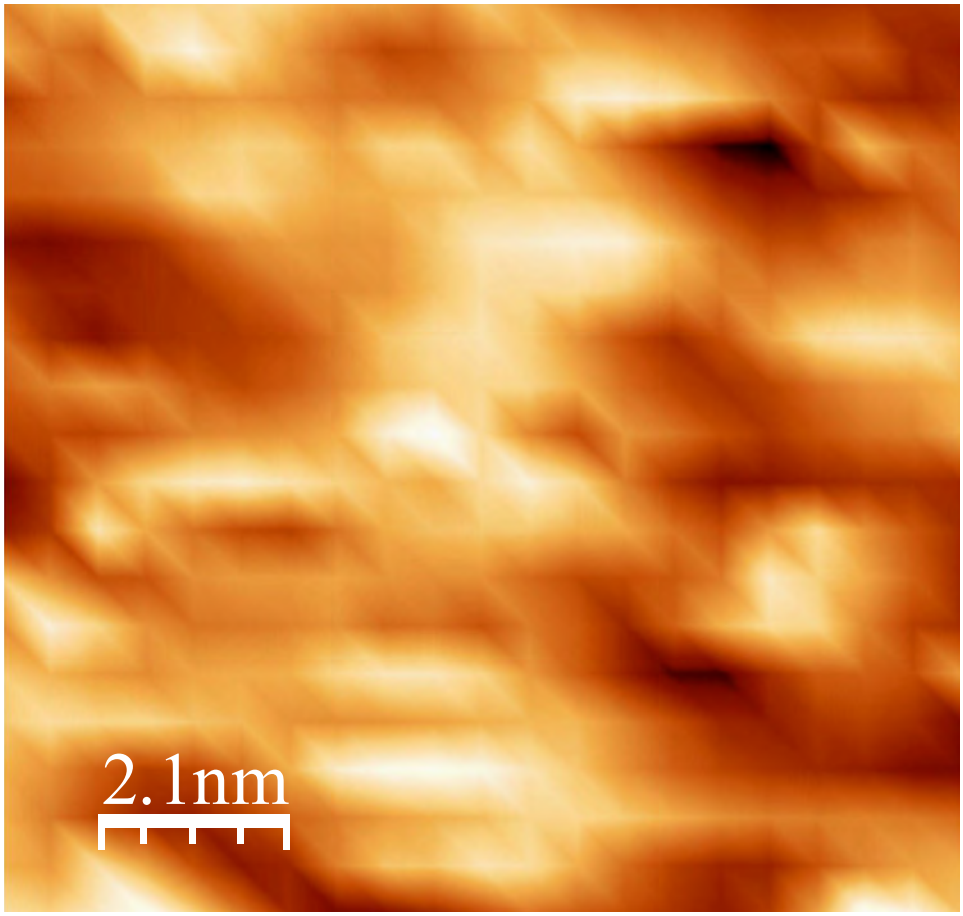

Figure 1.15

Run 1: 1+2-layer, 300 K, 100 *L* oxygen exposure, an image of wetting layer of the surface after oxygen exposure, taken at -1.0 V tip bias, and 0.5 nA tunneling current, 10×10 nm^2.

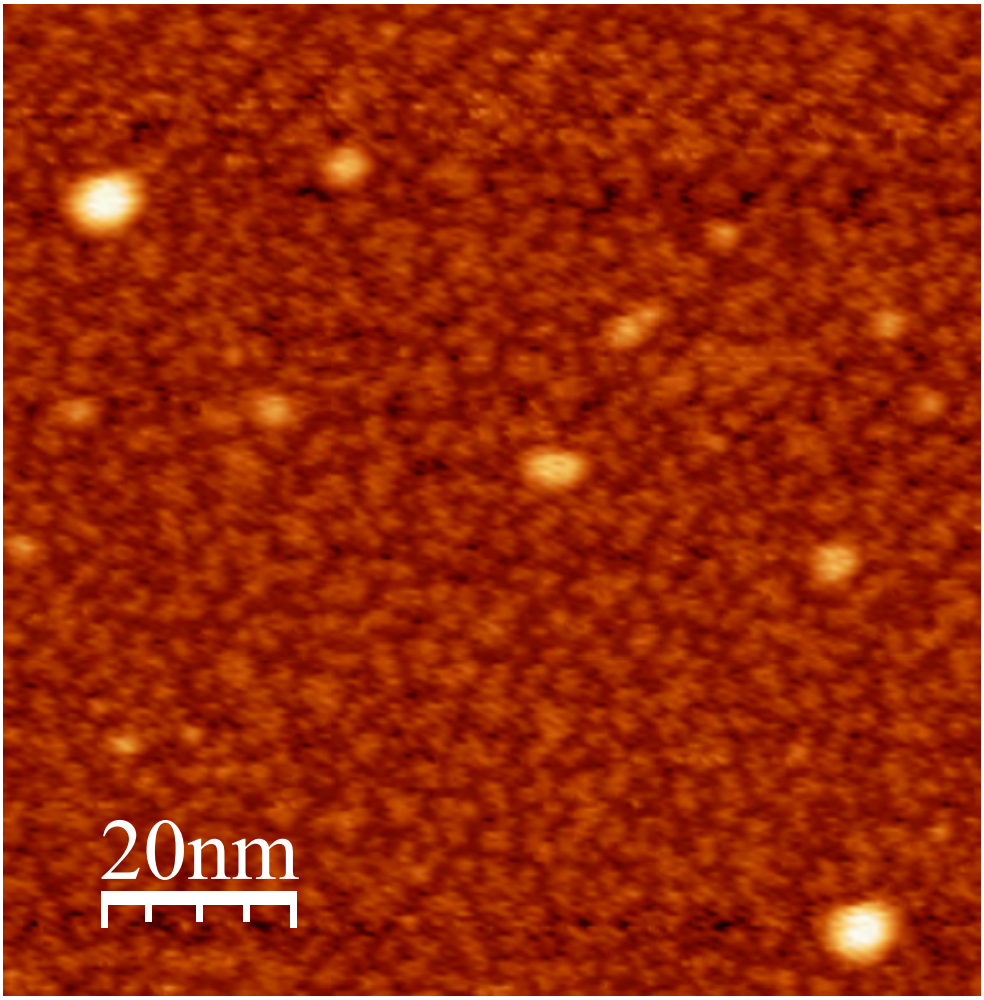

Figure 2.1

Run 2: 1-layer, 300 K, the control experiment (for 100 *L* oxygen exposure). An STM image of clean Ag/Si(111)-7×7 surface, taken at -1.0 V tip bias and 0.5 nA tunneling current, 100×100 nm^2.

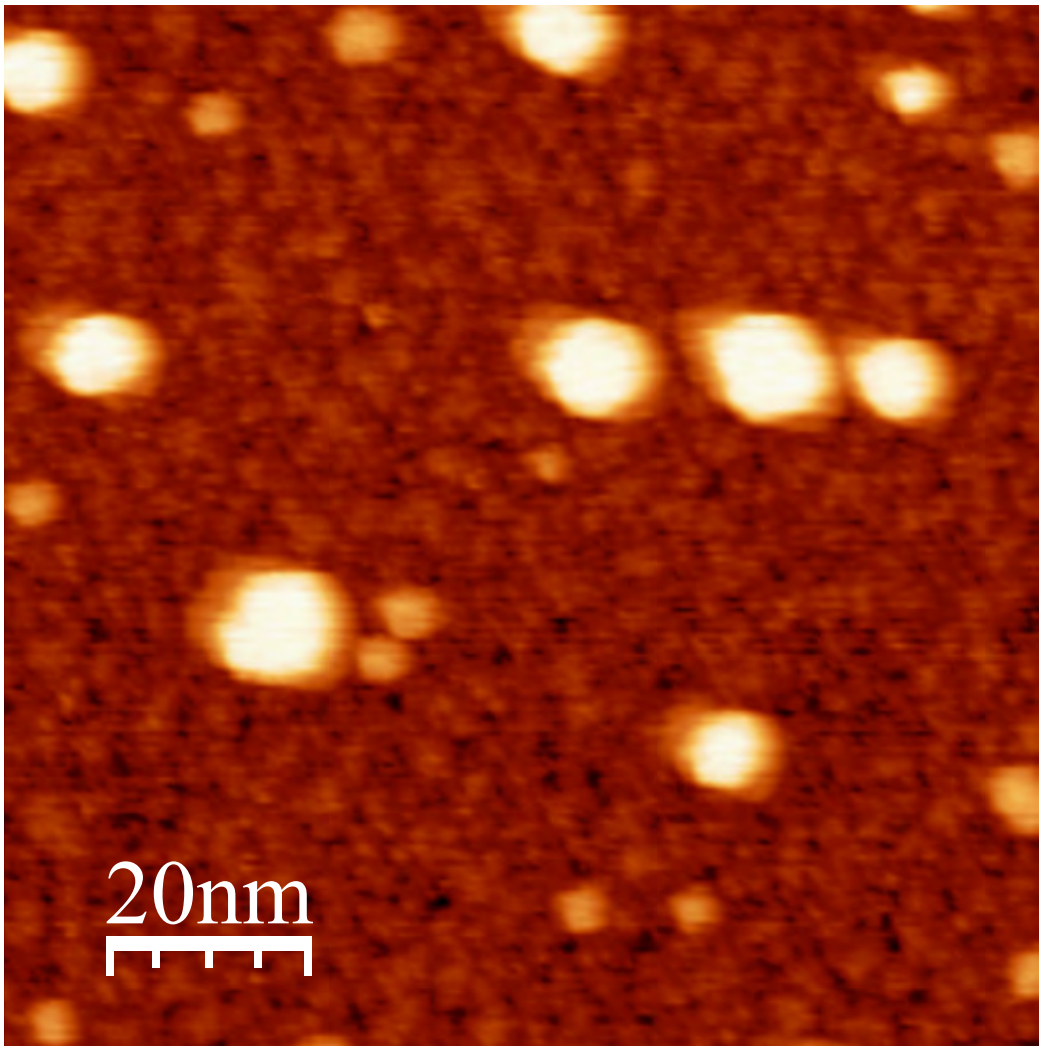

Figure 2.2

Run 2: 1+2-layer, 300 K, the control experiment (for 100 *L* oxygen exposure).An STM image of clean Ag/Si(111)-7×7 surface, taken at -1.0 V tip bias and 0.5 nA tunneling current, 100×100 nm^2.

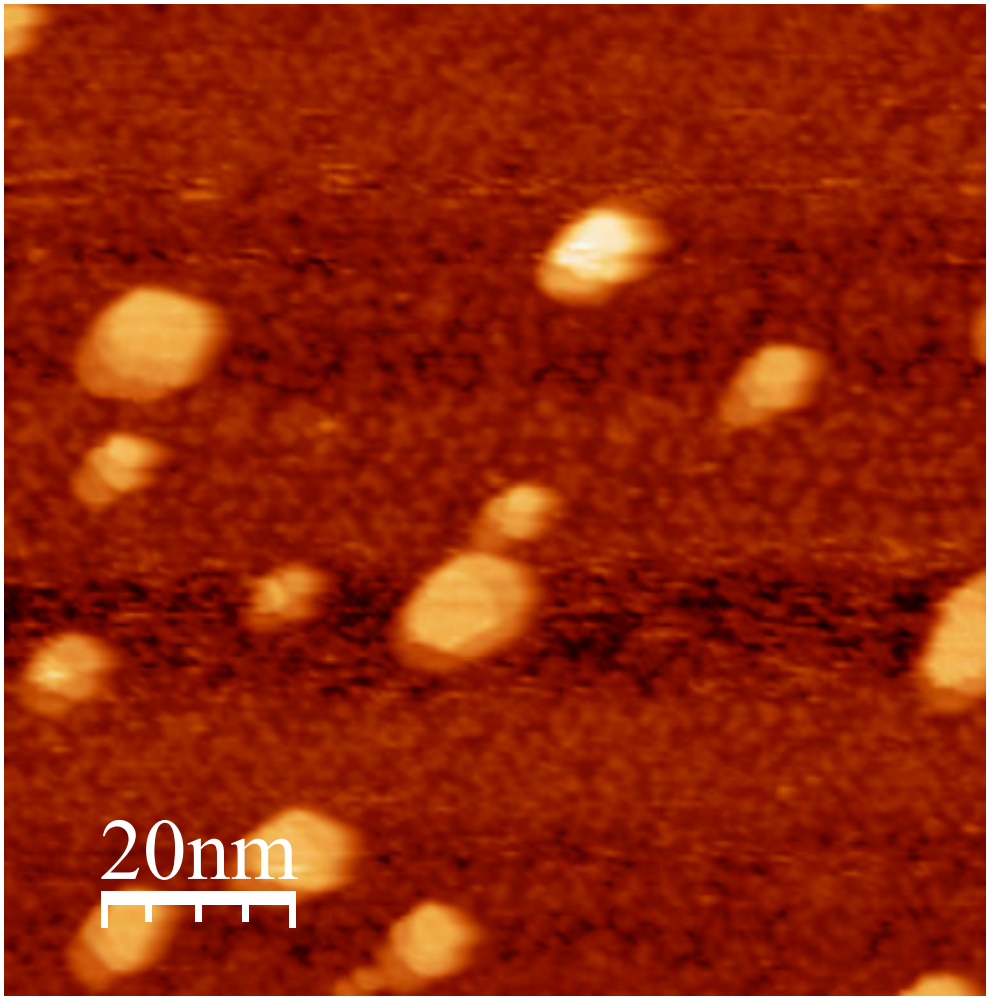

Figure 2.3

Run 2: 1+2-layer, 300 K, 100 *L* oxygen exposure experiment. An STM image of Ag/Si(111)-7×7 surface, taken at -1.0 V tip bias and 0.5 nA tunneling current, 100×100 nm^2.

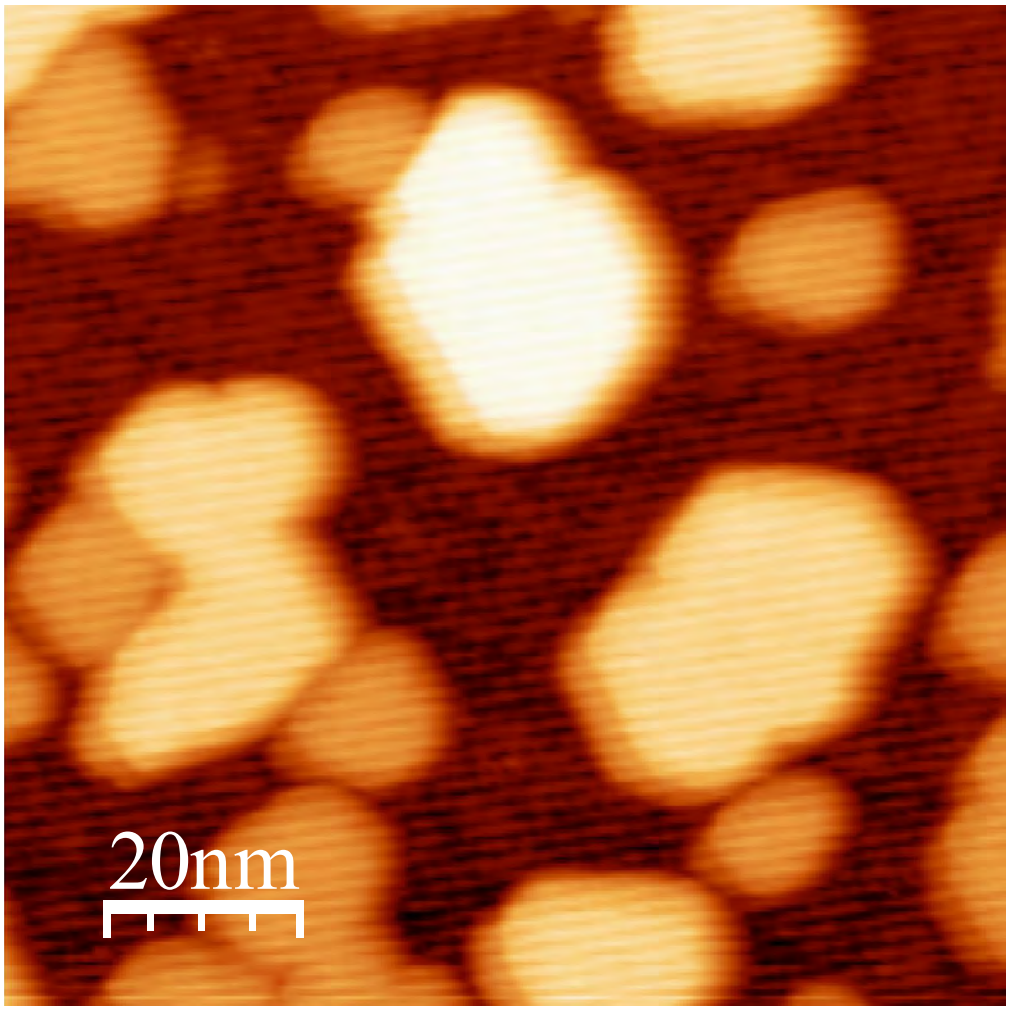

Figure 2.4

Run 2: 2-layer, 300 K, the control experiment (for 100 *L* oxygen exposure). An STM image of Ag/Si(111)-7×7 surface, taken at -1.0 V tip bias and 0.5 nA tunneling current, 100×100 nm^2.

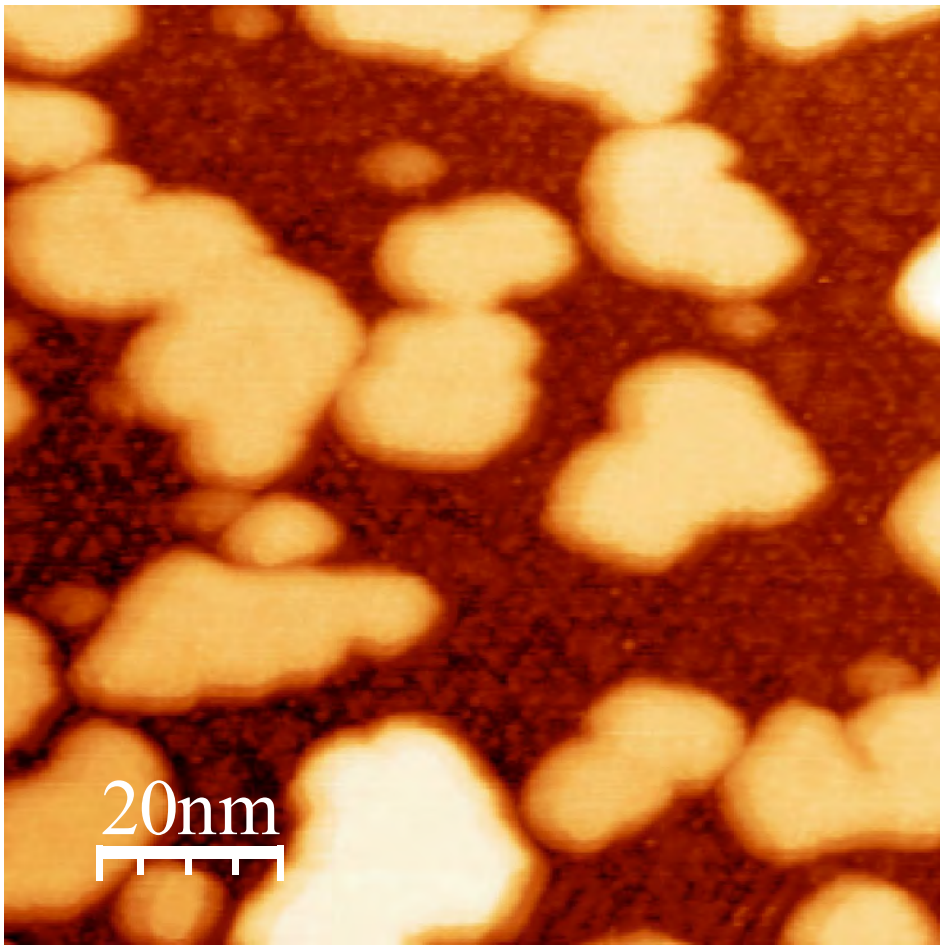

Figure 2.5

Run 2: 2-layer, 300 K, 100 *L* oxygen exposure experiment. An STM image of Ag/Si(111)-7×7 surface, taken at -1.0 V tip bias and 0.5 nA tunneling current, 100×100 nm^2.

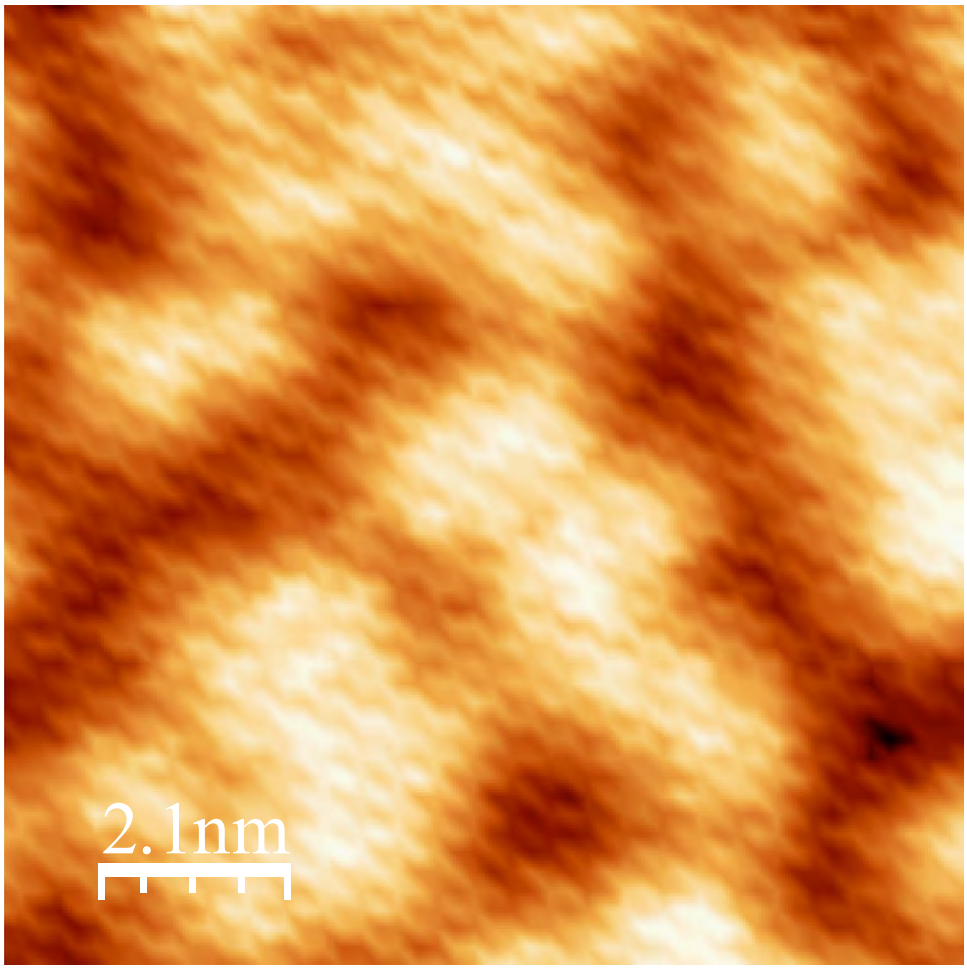

Figure 2.6

Run 2: 1-layer, 300 K, 100 *L* oxygen exposure experiment. An STM image of the wetting layer, taken at -1.0 V tip bias and 0.5 nA tunneling current, 10×10 nm^2.

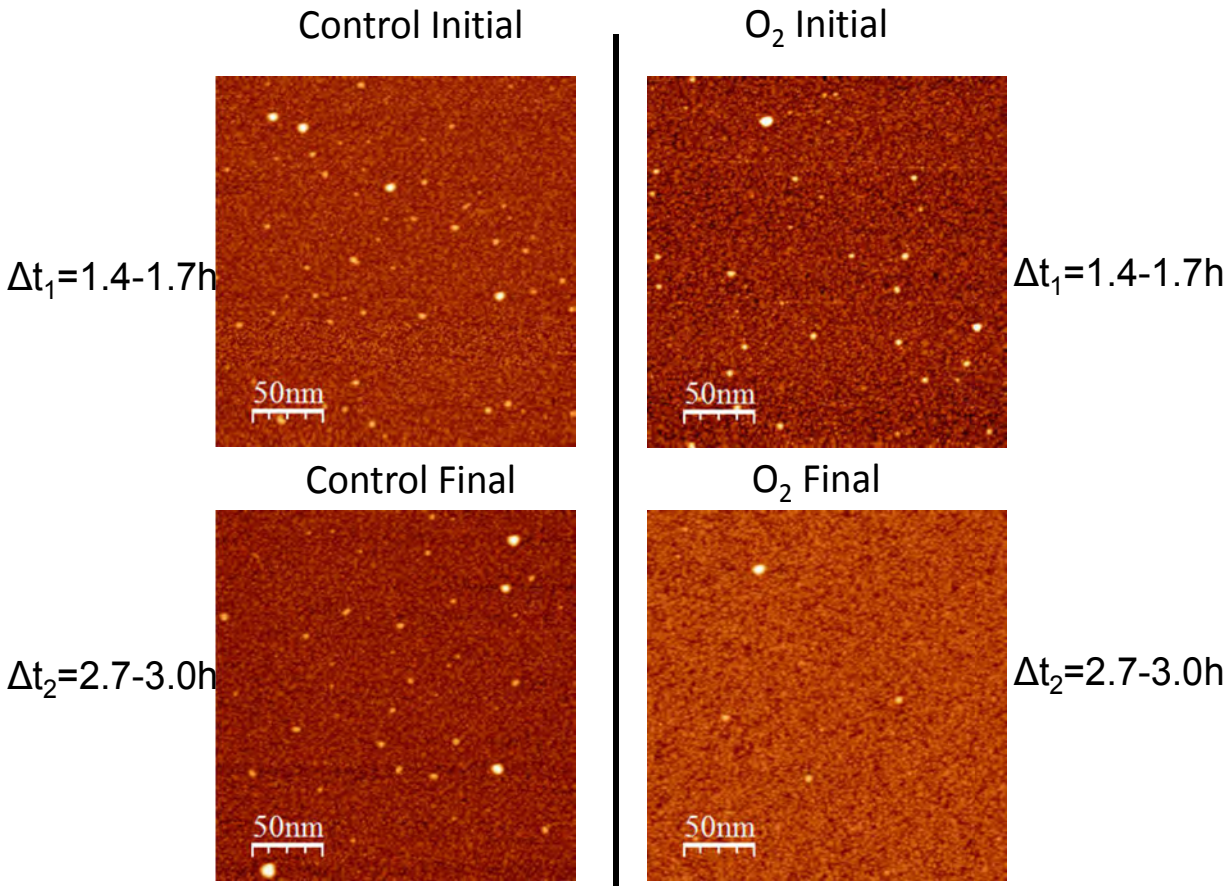

Figure 2.7

Representative images for Run 2: 1-layer, 300 K, 100 *L* oxygen exposure, taken at -1.0 V tip bias, 0.5 nA. The images are of 100×100 nm^2.Δt_1 is denoted as the time interval from the point of Ag deposition to that of acquisition of "initial" group images, and Δt_2 is denoted as the time interval from the point of Ag deposition to that of acquisition of "final" group images.

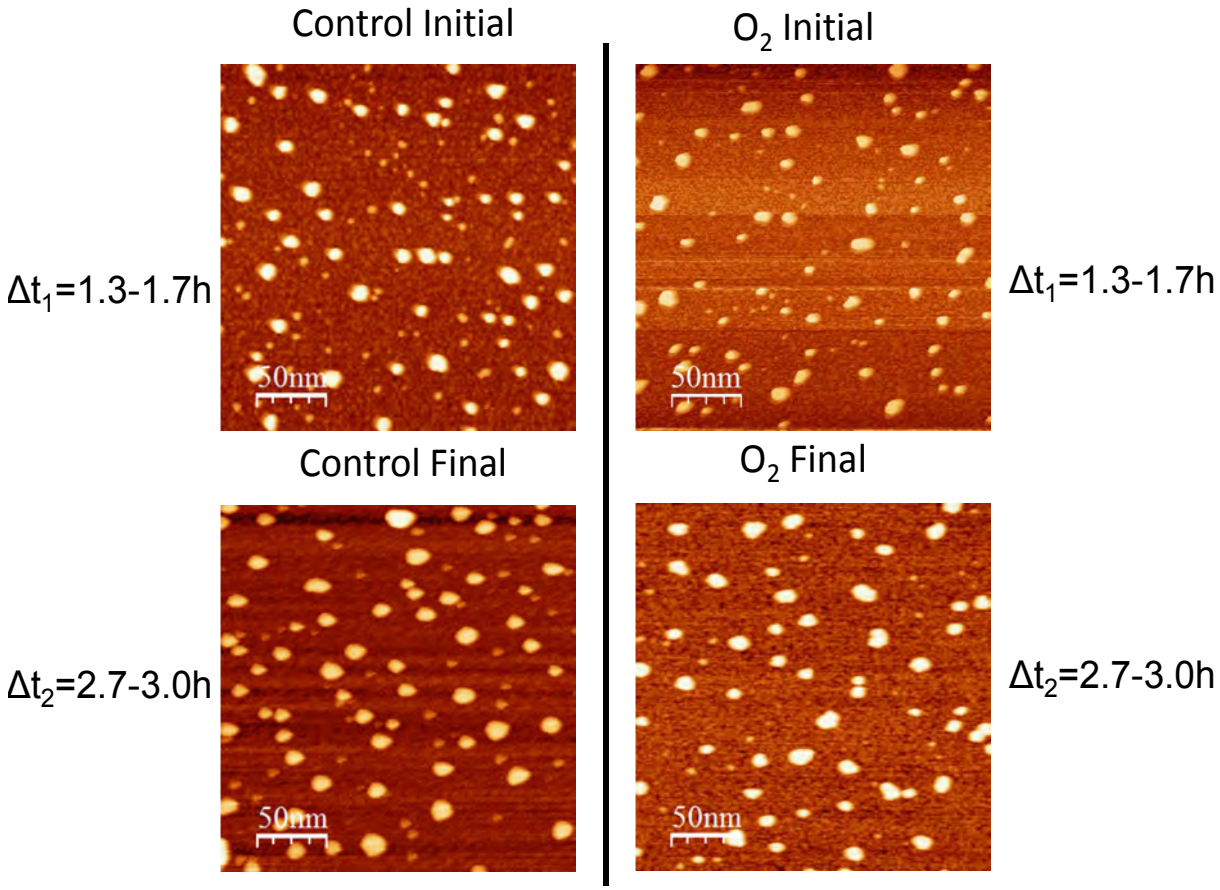

Figure 2.8

Representative images for Run 2: 1+2-layer, 300 K, 100 *L* oxygen exposure, taken at -1.0 V tip bias, 0.5 nA. The images are of 100×100 nm^2.Δt_1 is denoted as the time interval from the point of Ag deposition to that of acquisition of "initial" group images, and Δt_2 is denoted as the time interval from the point of Ag deposition to that of acquisition of "final" group images.

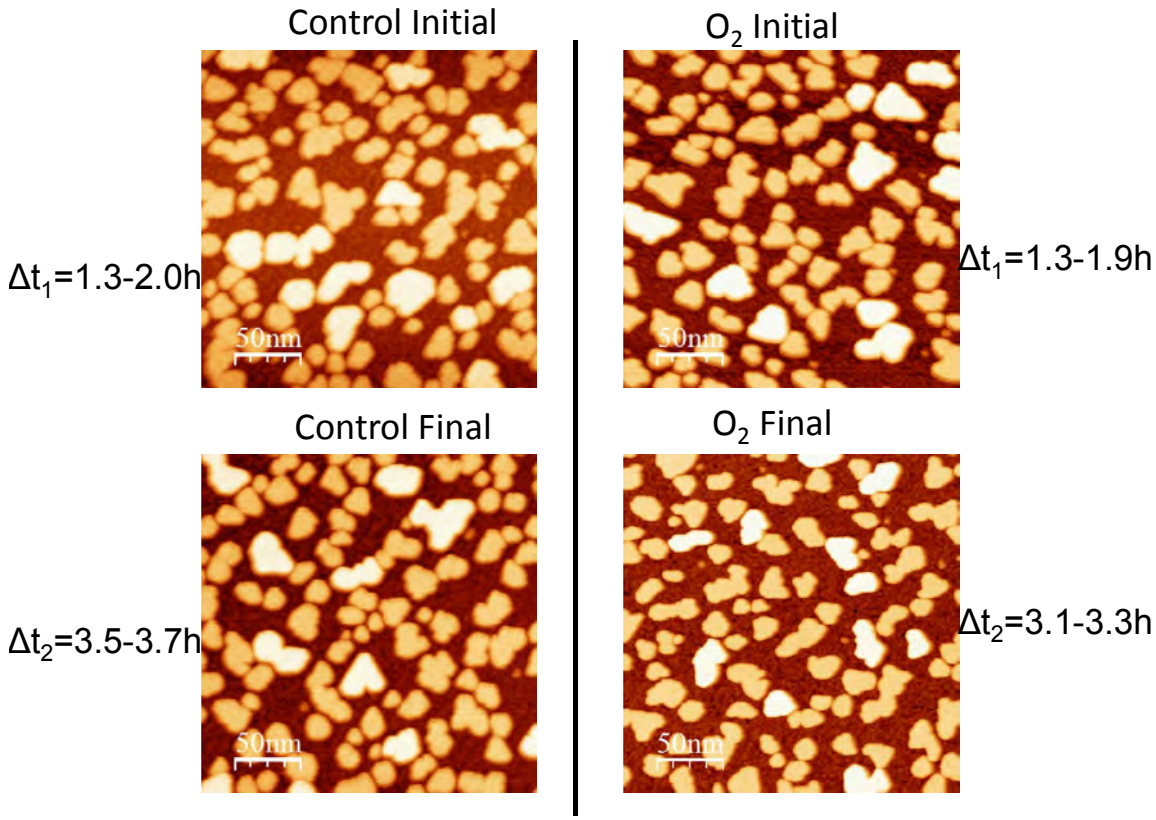

Figure 2.9

Representative images for Run 2: 2-layer, 300 K, 100 *L* oxygen exposure, taken at -1.0 V tip bias, 0.5 nA. The images are of 100×100 nm^2.Δt_1 is denoted as the time interval from the point of Ag deposition to that of acquisition of "initial" group images, and Δt_2 is denoted as the time interval from the point of Ag deposition to that of acquisition of "final" group images.

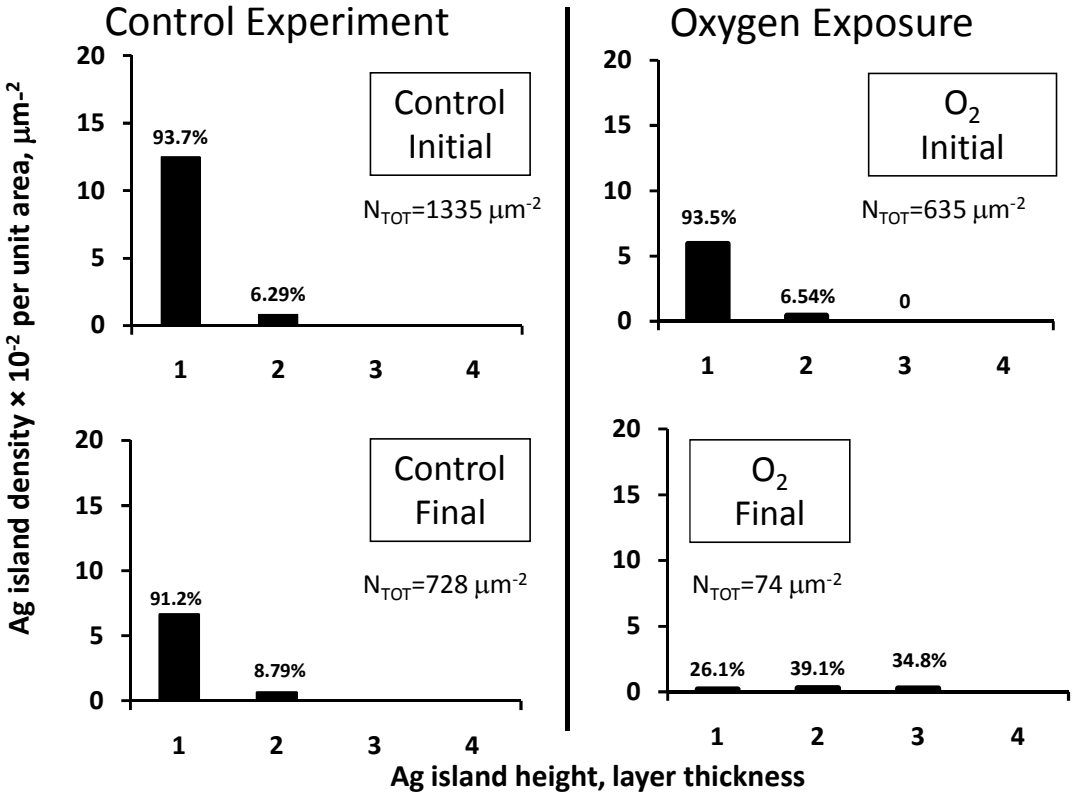

Figure 2.10

Island height histogram for Run 2: 1-layer, 100 *L* oxygen exposure, 300 K, taken at -1.0 V tip bias, 0.5 nA. The percentage numbers above each column are the relative populations for an island of each layer thickness. N_{TOT} denotes the total island density of all islands, in units of μm^{-2}. "Initial" denotes the images taken before oxygen exposure (for the oxygen experiment), or at approximately the same time (for the control group), and "final" denotes the images taken after oxygen exposure (for the oxygen experiment), or at approximately the same time (for the control group).

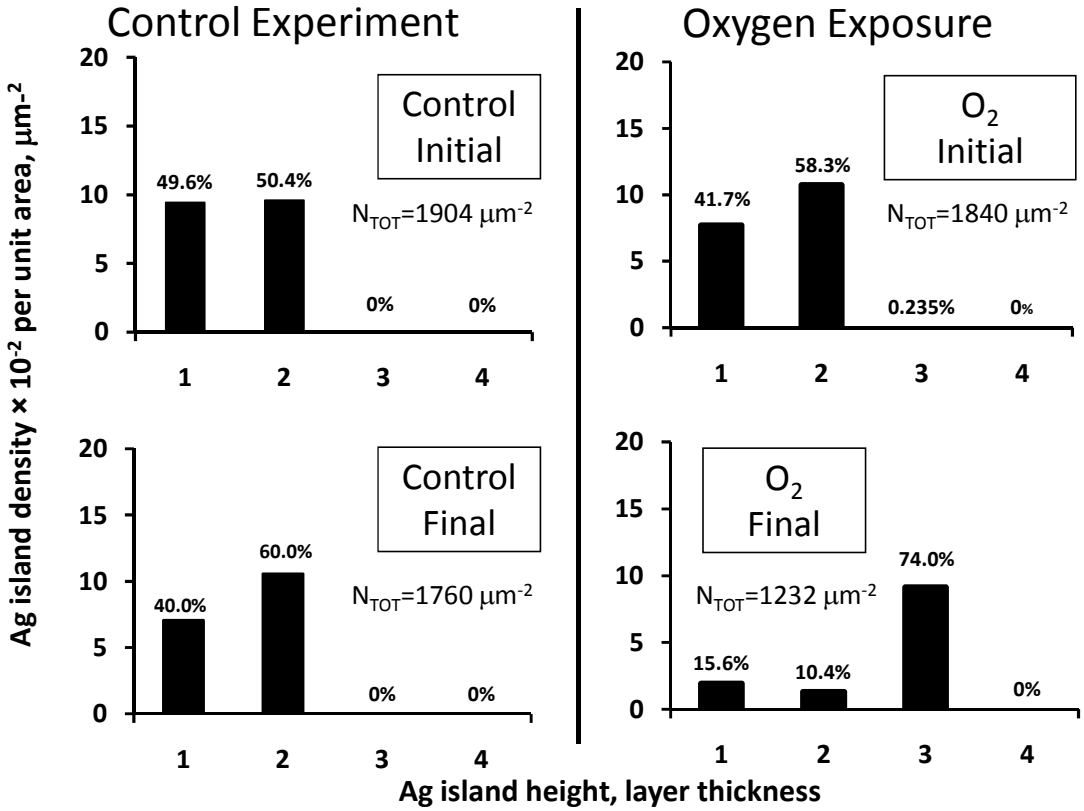

Figure 2.11

Island height histogram for Run 2: 1+2-layer, 100 *L* oxygen exposure, 300 K, taken at -1.0 V tip bias, 0.5 nA. The percentage numbers above each column are the relative populations for an island of each layer thickness. N_{TOT} denotes the total island density of all islands, in units of μm^{-2}. "Initial" denotes the images taken before oxygen exposure (for the oxygen experiment), or at approximately the same time (for the control group), and "final" denotes the images taken after oxygen exposure (for the oxygen experiment), or at approximately the same time (for the control group).

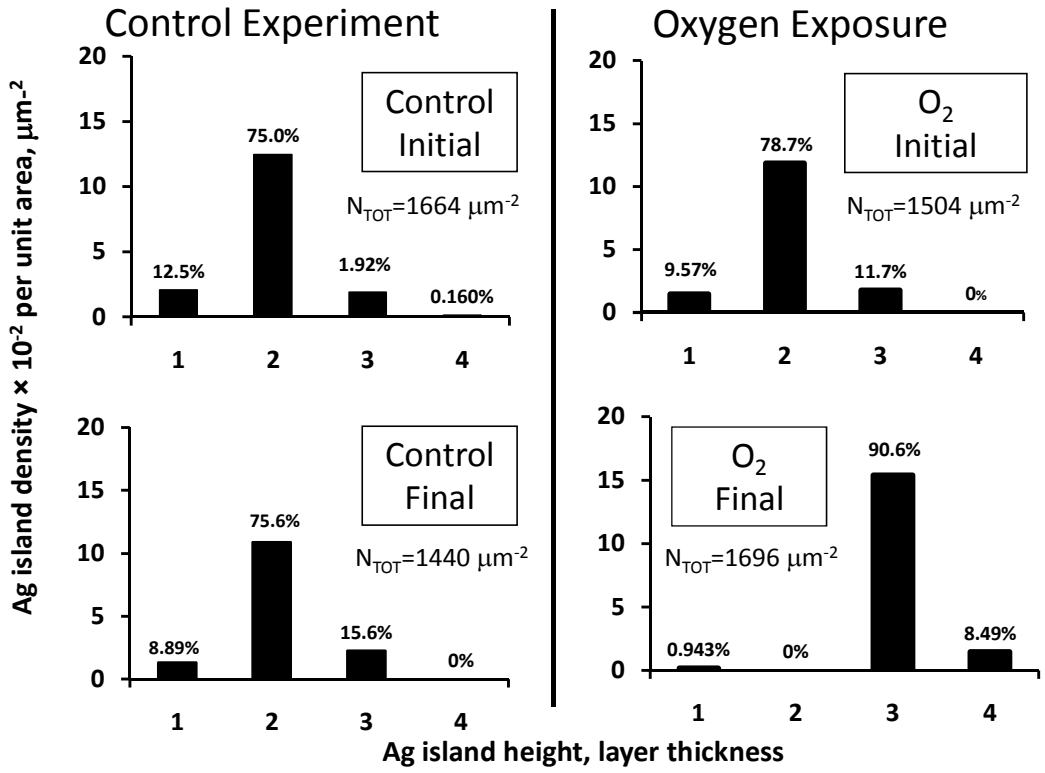

Figure 2.12

Island height histogram for Run 2: 2-layer, 100 *L* oxygen exposure, 300 K, taken at -1.0 V tip bias, 0.5 nA. The percentage numbers above each column are the relative populations for an island of each layer thickness. N_{TOT} denotes the total island density of all islands, in units of μm^{-2}. "Initial" denotes the images taken before oxygen exposure (for the oxygen experiment), or at approximately the same time (for the control group), and "final" denotes the images taken after oxygen exposure (for the oxygen experiment), or at approximately the same time (for the control group).

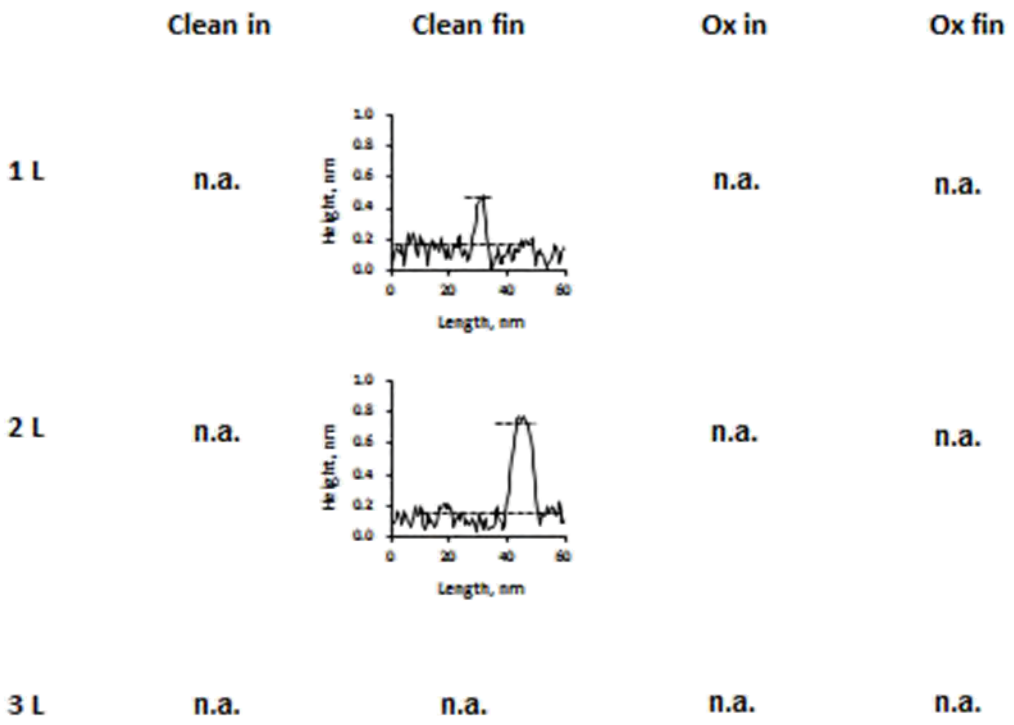

Figure 2.13

Island height line profiles for Run 2: 1-layer, 300 K, 100 *L* oxygen exposure, taken at -1.0 V tip bias, 0.5 nA. One line profile is shown for an island of each layer thickness. "Clean in" denotes the initial stage of the control group, "Clean fin" denotes the final stage of the control group, "Ox in" denotes the initial stage of the oxygen experiment, and "Ox fin" denotes the final stage of the oxygen experiment.

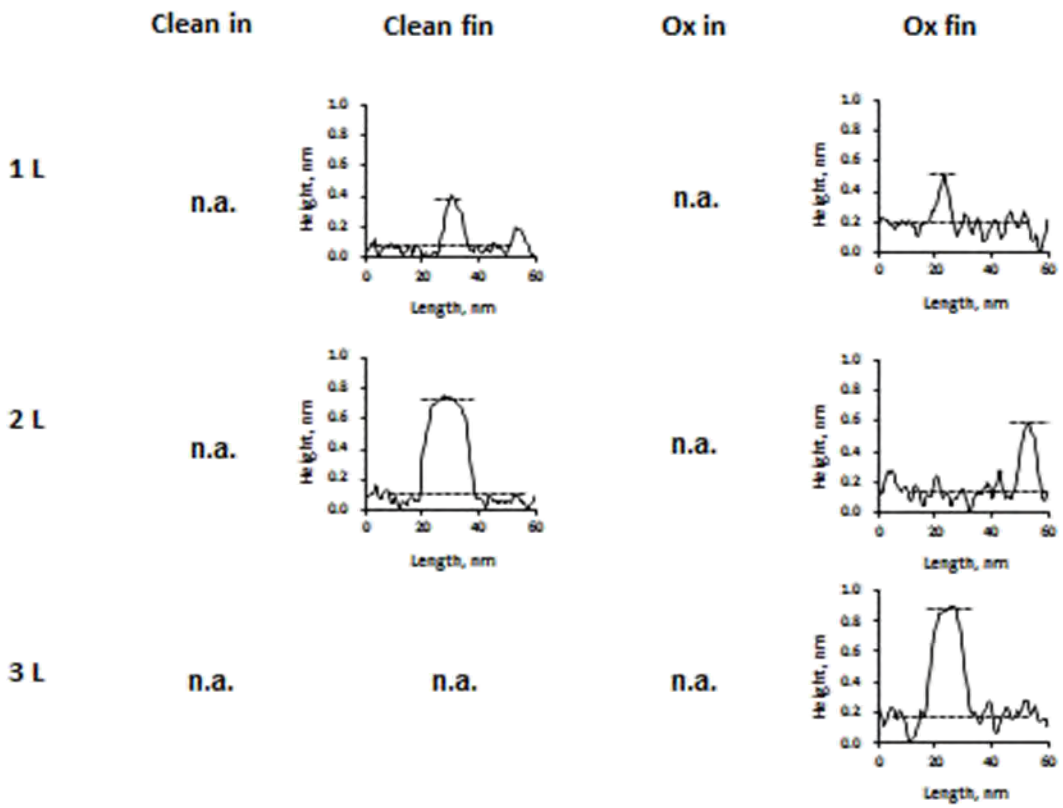

Figure 2.14

Island height line profiles for Run 2: 1+2-layer, 300 K, 100 *L* oxygen exposure, taken at -1.0 V tip bias, 0.5 nA. One line profile is shown for an island of each layer thickness. "Clean in" denotes the initial stage of the control group, "Clean fin" denotes the final stage of the control group, "Ox in" denotes the initial stage of the oxygen experiment, and "Ox fin" denotes the final stage of the oxygen experiment.

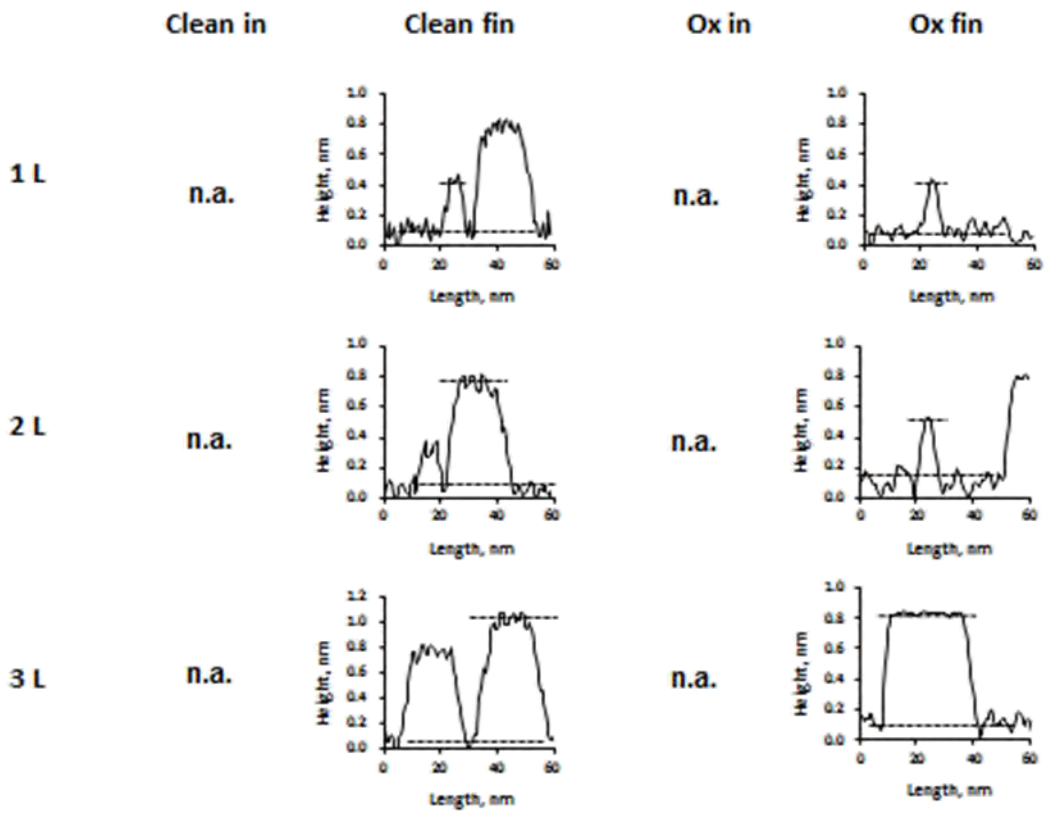

Figure 2.15

Island height line profiles for Run 2: 2-layer, 300 K, 100 *L* oxygen exposure, taken at -1.0 V tip bias, 0.5 nA. One line profile is shown for an island of each layer thickness. "Clean in" denotes the initial stage of the control group, "Clean fin" denotes the final stage of the control group, "Ox in" denotes the initial stage of the oxygen experiment, and "Ox fin" denotes the final stage of the oxygen experiment.

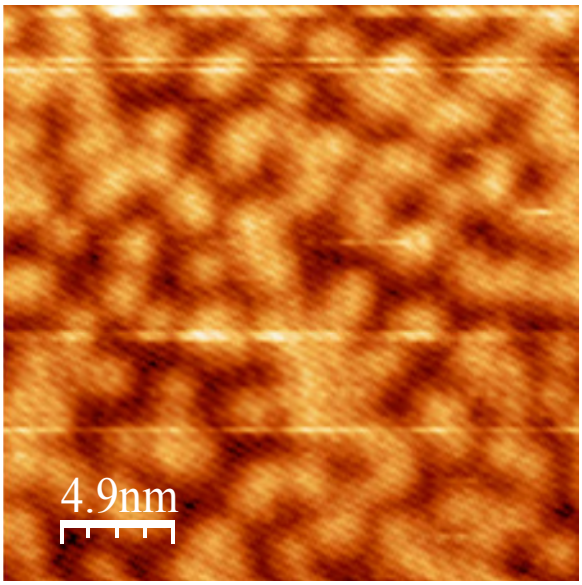

(a)

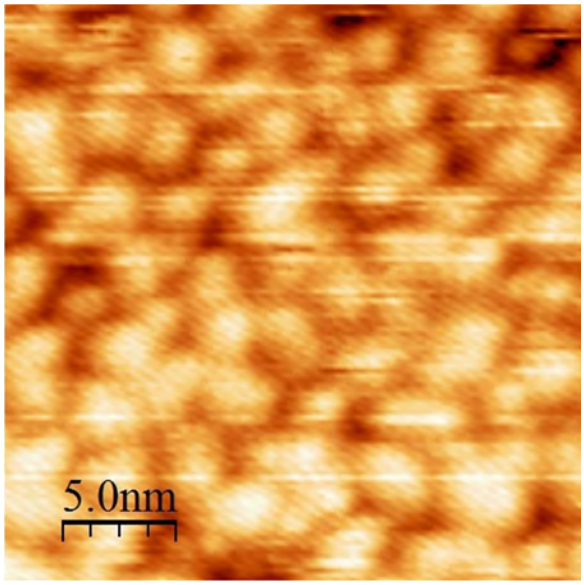

(b)

Figure 2.16

Typical wetting layer images before (a) and after (b) oxygen exposure, from Run 2: 1-layer experiment, taken at -1.0 V tip bias and 0.5 nA tunneling current, images are of 25×25 nm^2.

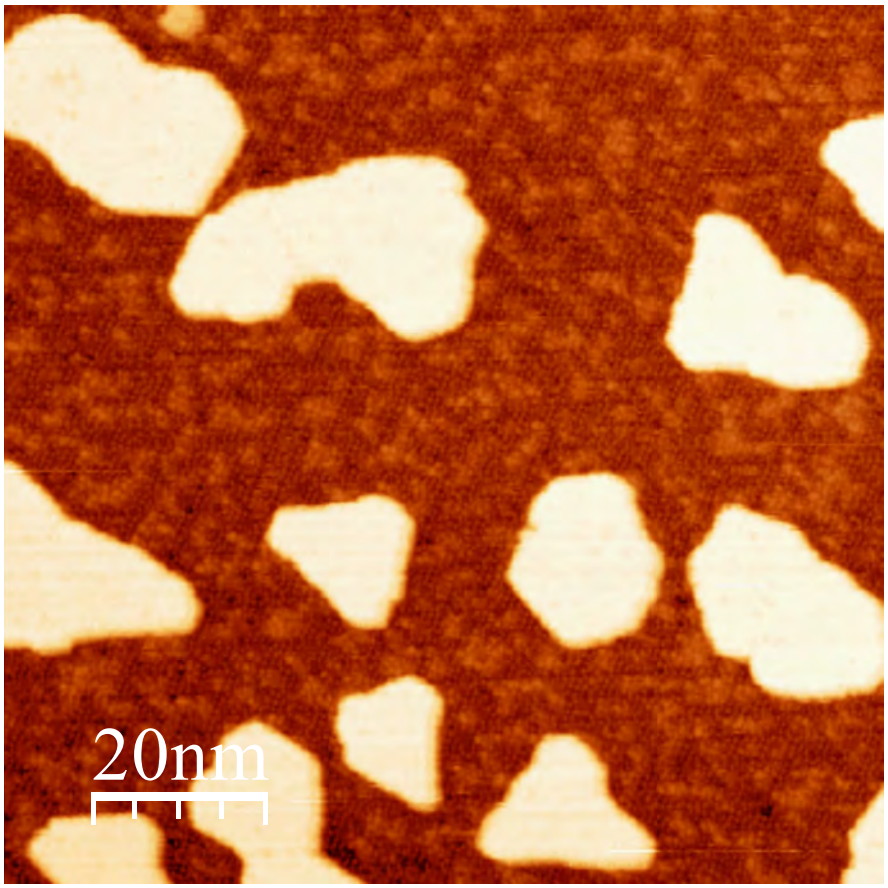

Figure 3.1

Run 3: 2-layer, 300 K, the control experiment (for 100 *L* oxygen exposure). An STM image of Ag/Si(111)-7×7 surface, taken at -1.0 V tip bias and 0.5 nA tunneling current, 100×100 nm^2.

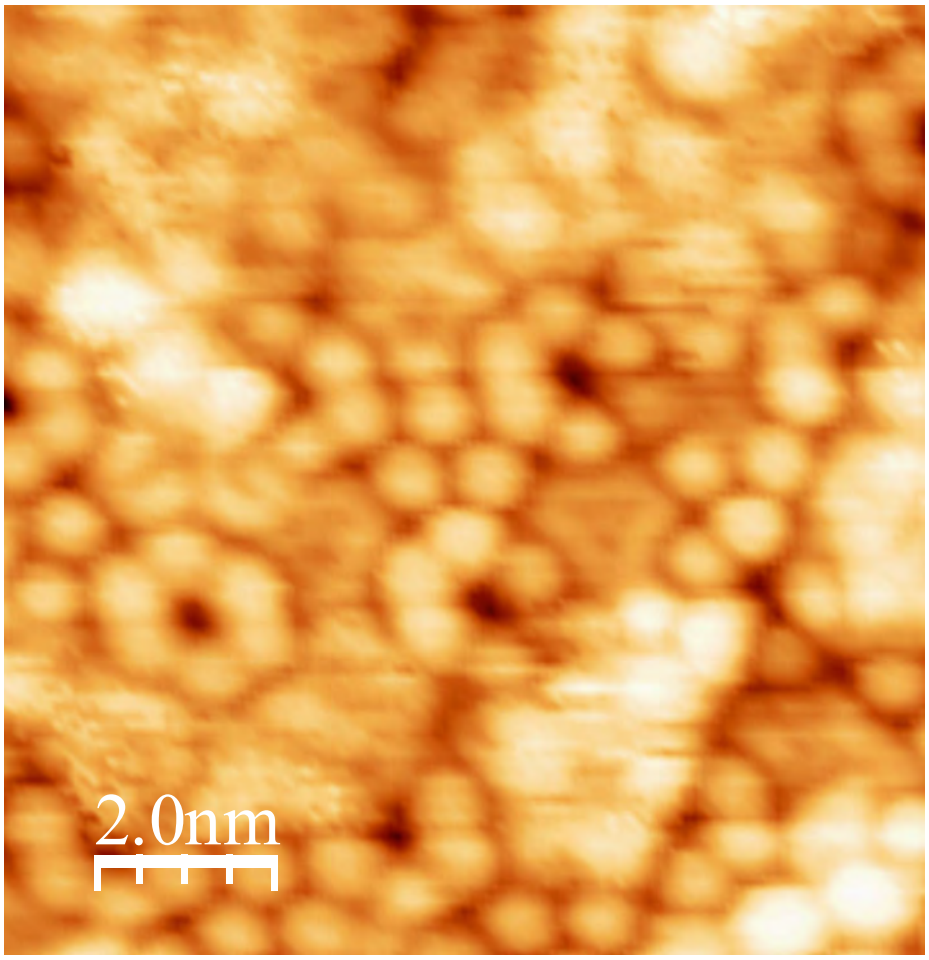

Figure 3.2

Run 3: 2-layer, 300 K, the control experiment (for 100 *L* oxygen exposure). An STM image of the wetting layer of Ag/Si(111)-7×7 surface, taken at +1.0 V tip bias and 0.5 nA tunneling current, 10×10 nm^2.

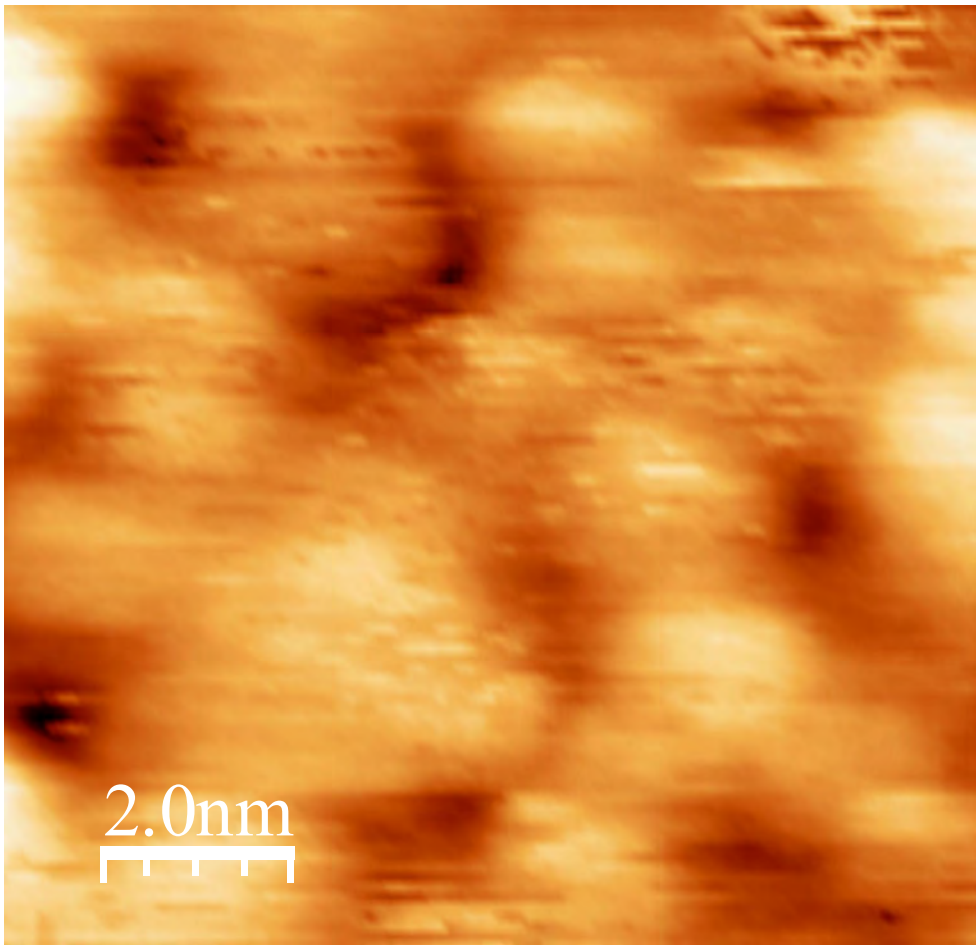

Figure 3.3

Run 3: 2-layer, 300 K, 100 *L* oxygen exposure experiment. An STM image of the wetting layer of Ag/Si(111)-7×7 surface, taken at +1.0 V tip bias and 0.5 nA tunneling current, 10×10 nm^2.

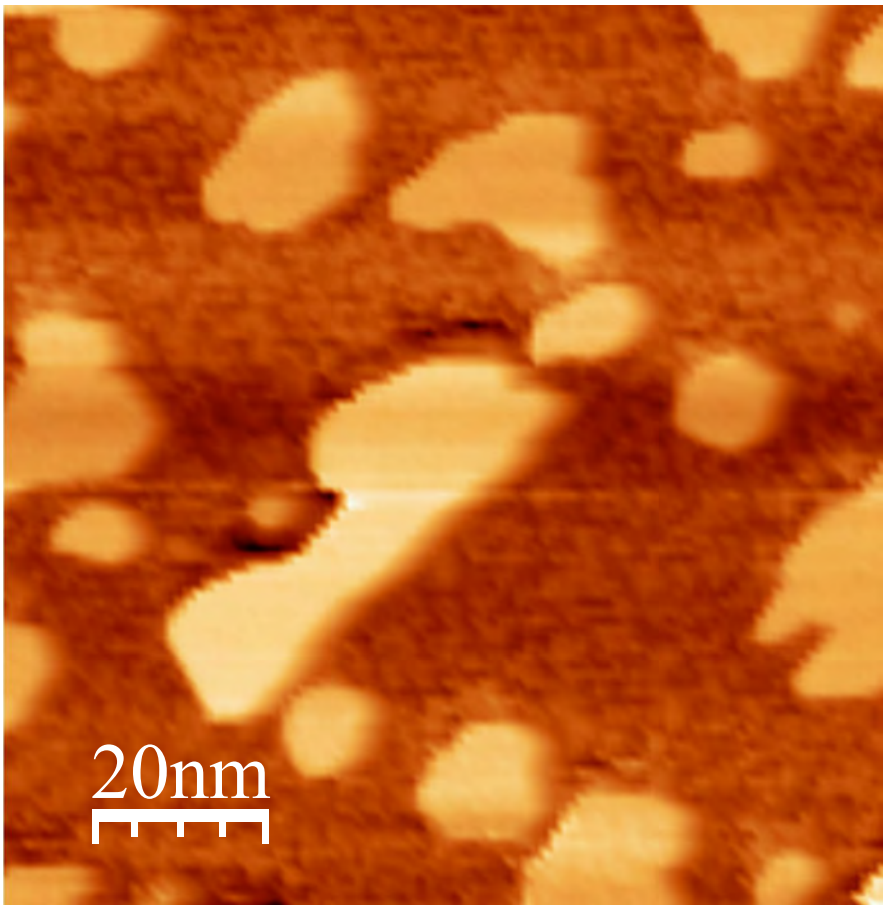

Figure 3.4

Run 3: 2-layer, 300 K, 100 *L* oxygen exposure experiment. An STM image of Ag/Si(111)-7×7 surface, taken at +1.0 V tip bias and 0.5 nA tunneling current, 100×100 nm^2.

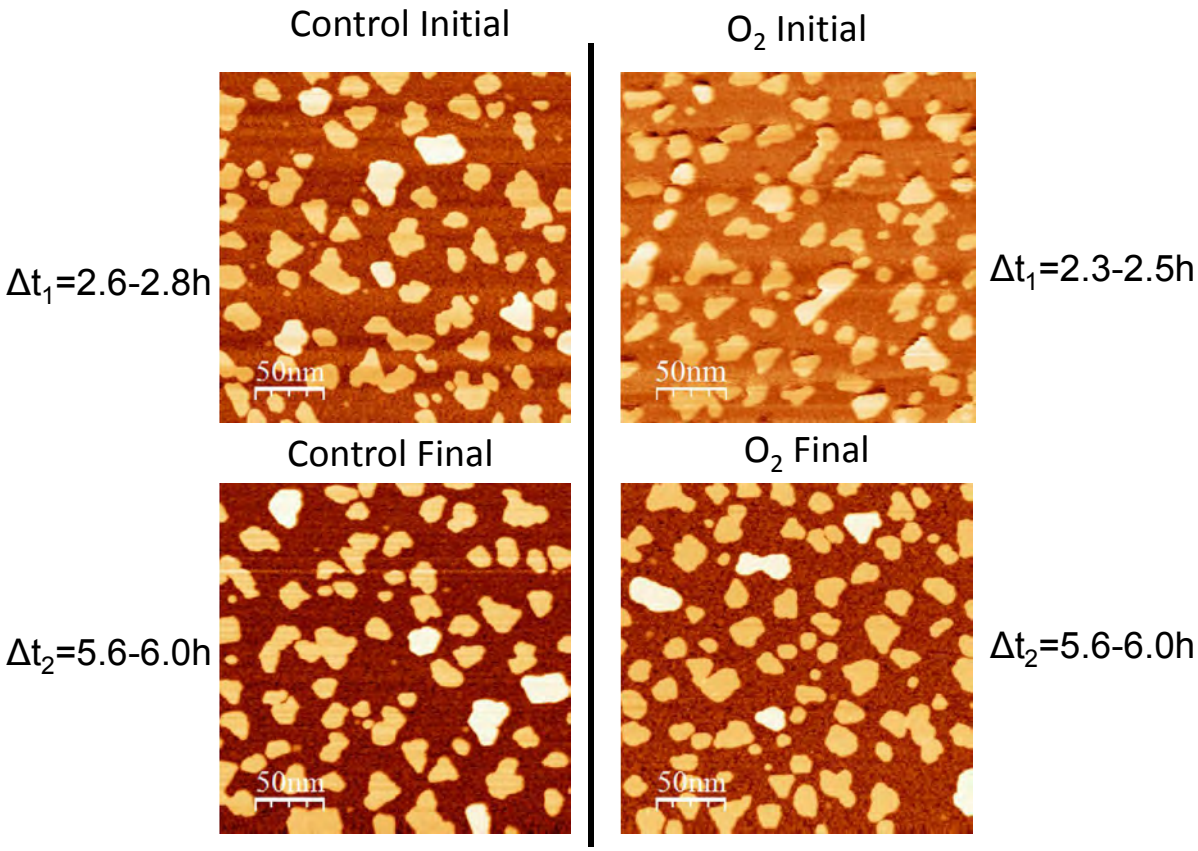

Figure 3.5

Representative images for Run 3: 2-layer, 300 K, 100 *L* oxygen exposure, taken at +1.0 V tip bias, 0.5 nA. The images are of 100×100 nm^2.Δt_1 is denoted as the time interval from the point of Ag deposition to that of acquisition of "initial" group images, and Δt_2 is denoted as the time interval from the point of Ag deposition to that of acquisition of "final" group images.

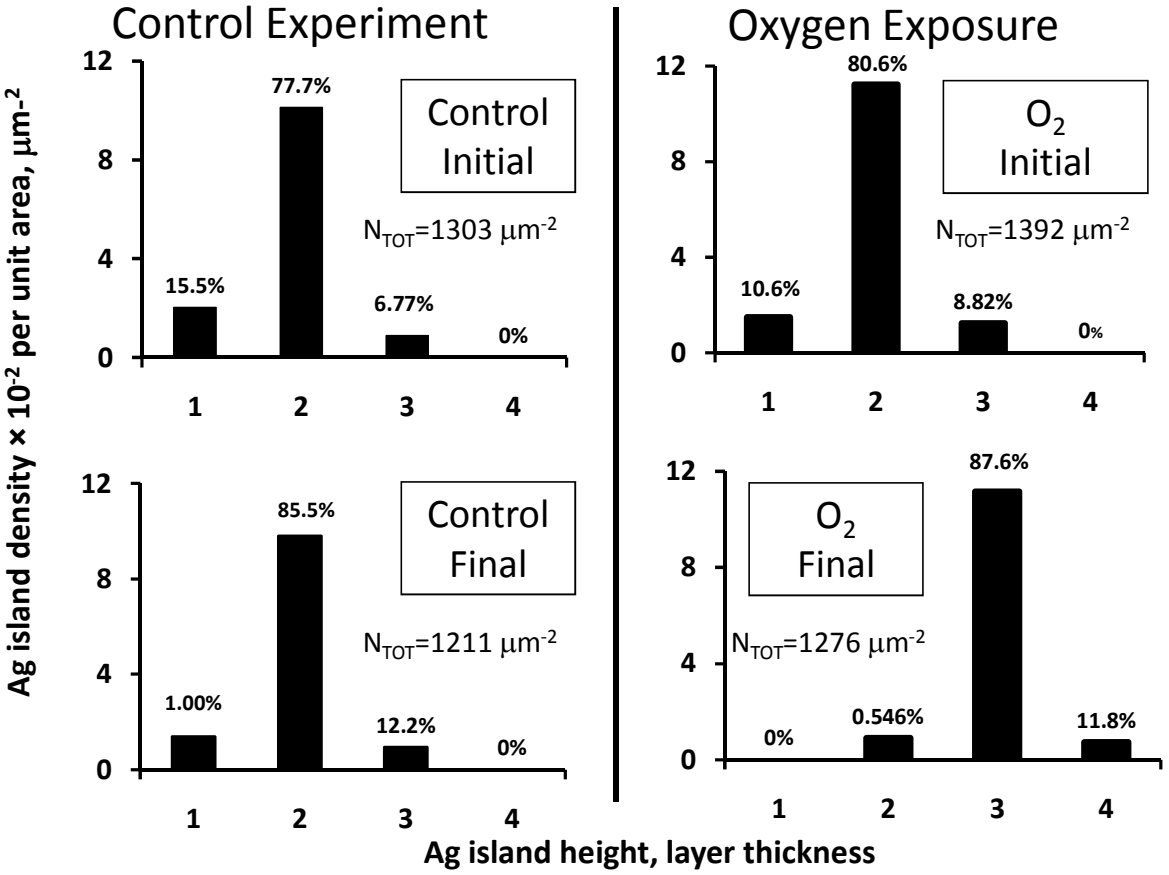

Figure 3.6

Island height histogram for Run 3: 2-layer, 100 *L* oxygen exposure, 300 K, taken at +1.0 V tip bias, 0.5 nA. The percentage numbers above each column are the relative populations for an island of each layer thickness. N_{TOT} denotes the total island density of all islands, in units of μm^{-2}. "Initial" denotes the images taken before oxygen exposure (for the oxygen experiment), or approximately the same time (for the control group), and "final" denotes the images taken after oxygen exposure (for the oxygen experiment), or approximately the same time (for the control group).

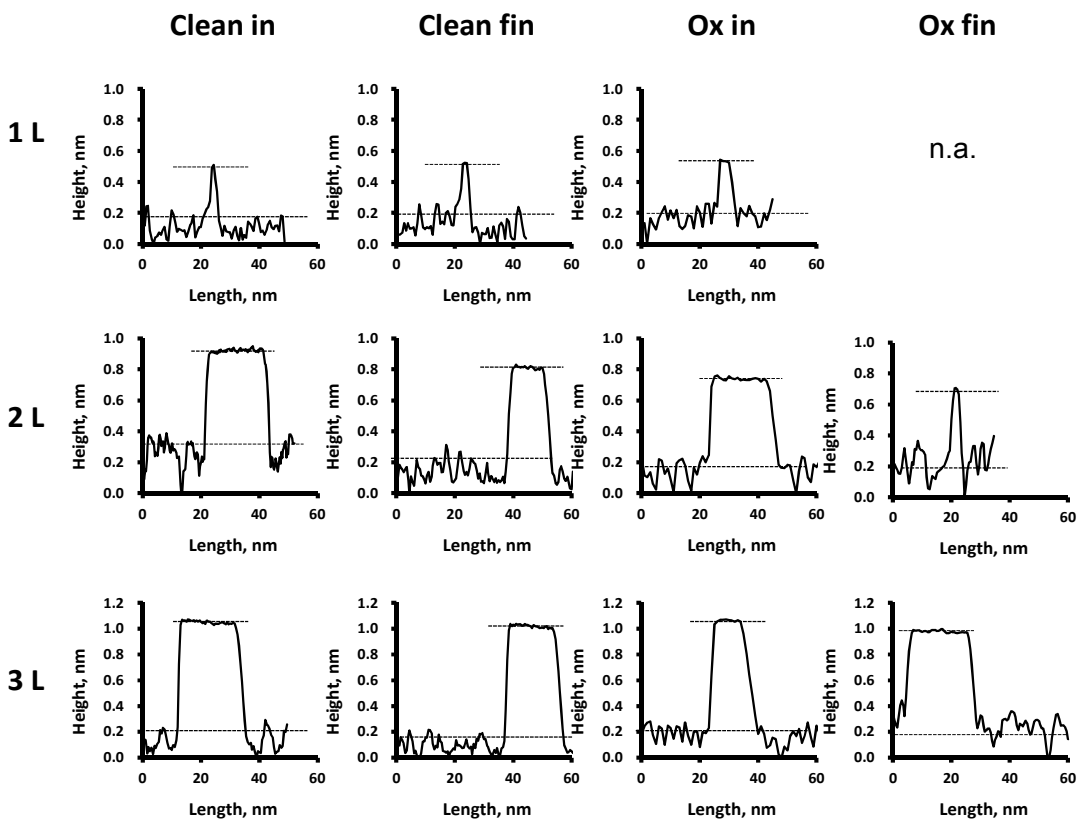

Figure 3.7

Island height line profiles for Run 3: 2-layer, 300 K, 100 *L* oxygen exposure, taken at -1.0 V tip bias, 0.5 nA. One line profile is shown for an island of each layer thickness. "Clean in" denotes the initial stage of the control group, "Clean fin" denotes the final stage of the control group, "Ox in" denotes the initial stage of the oxygen experiment, and "Ox fin" denotes the final stage of the oxygen experiment.

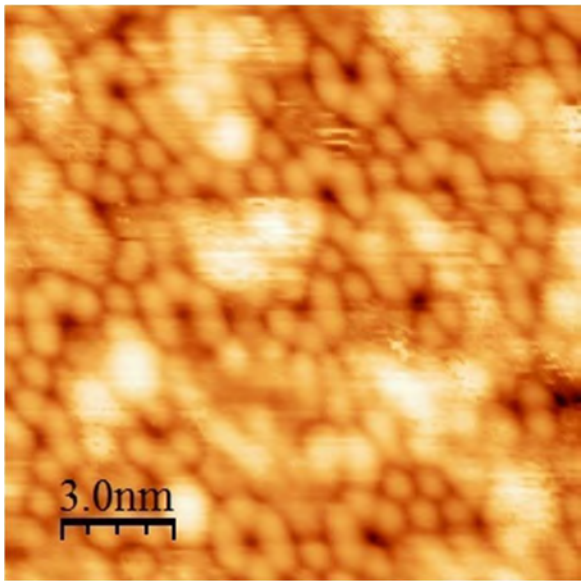

(a)

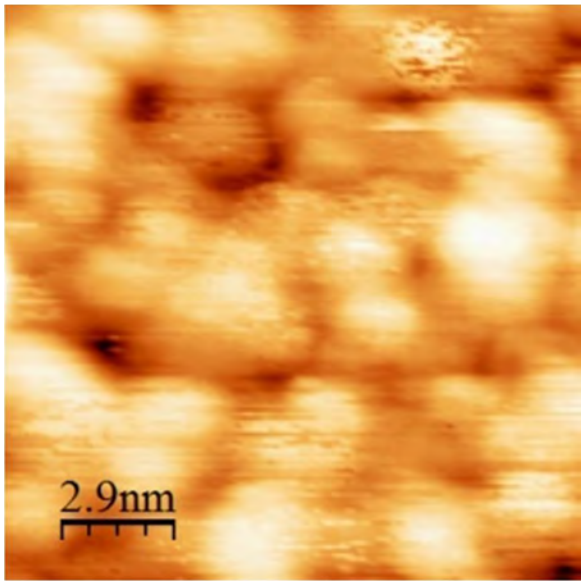

(b)

Figure 3.8

Typical wetting layer images before (a) and after (b) oxygen exposure, from Run 3: 2-layer experiment, taken at +1.0 V tip bias and 0.5 nA tunneling current, images are of 15×15 nm^2.

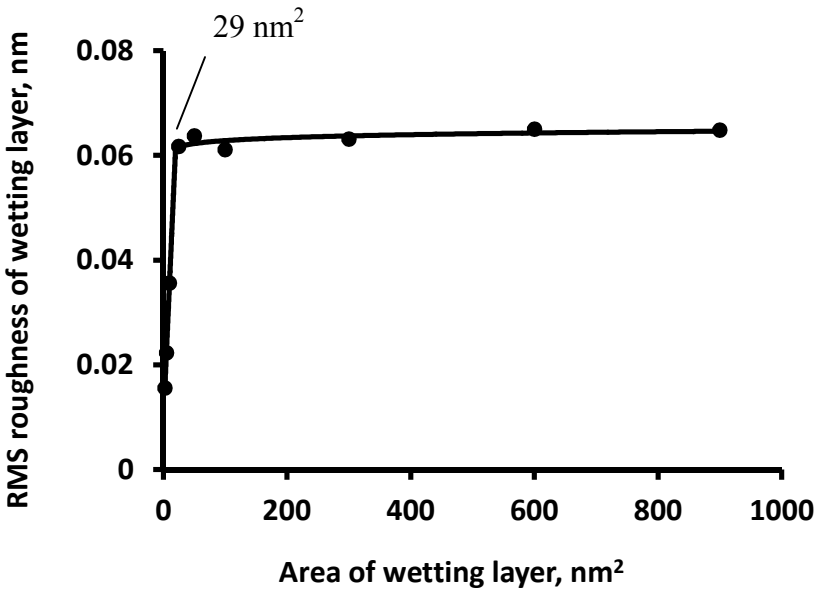

Figure 4.1

RMS roughness of wetting layer as a function of area, data from Run 3: 1+2-layer control experiment (for ethylene exposure experiment).

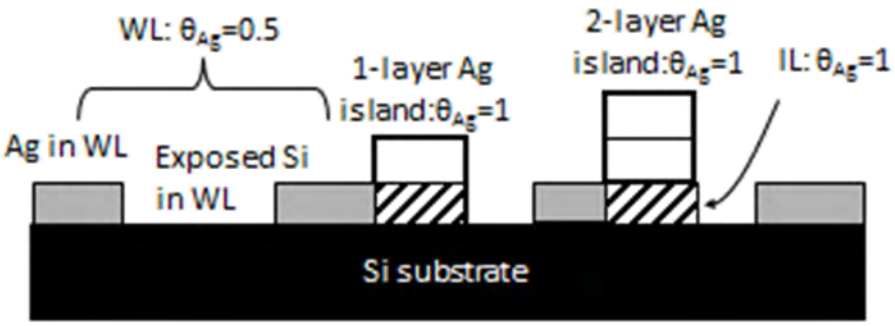

(a)

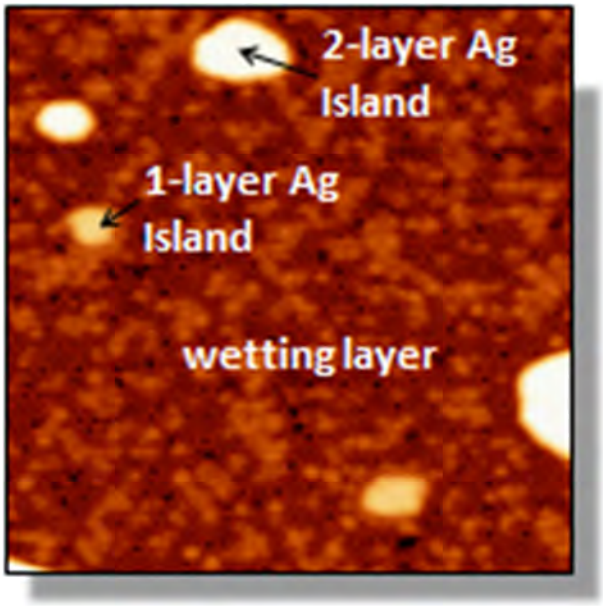

(b)

Figure 4.2

(a) Schematic diagram of Si(111)-7×7 surface after Ag deposition. WL denotes the wetting layer, IL denotes interfacial layer, and θ_{Ag} denotes the Ag coverage. (b) Real-space STM image of a representative Si(111)-7×7 surface after Ag deposition, from Run 3: 1+2-layer control experiment (for ethylene exposure), taken at +1.0 V tip bias, 0.5 nA tunneling current, 50×50 nm^2.

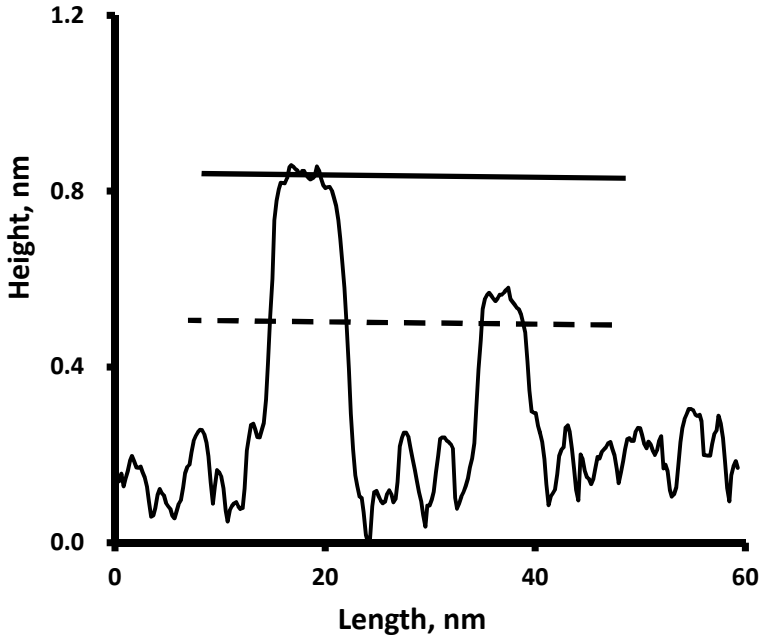

Figure 4.3

Schematic diagram of selecting reference level in terms of measuring fractional area for coverage. Dashed line denotes the level of half maximum and solid line denotes the reference level that is finally selected. Data from Run 2: 1+2-layer control experiment (for 100 *L* oxygen exposure), taken at -1.0 V tip bias, and 0.5 nA tunneling current.

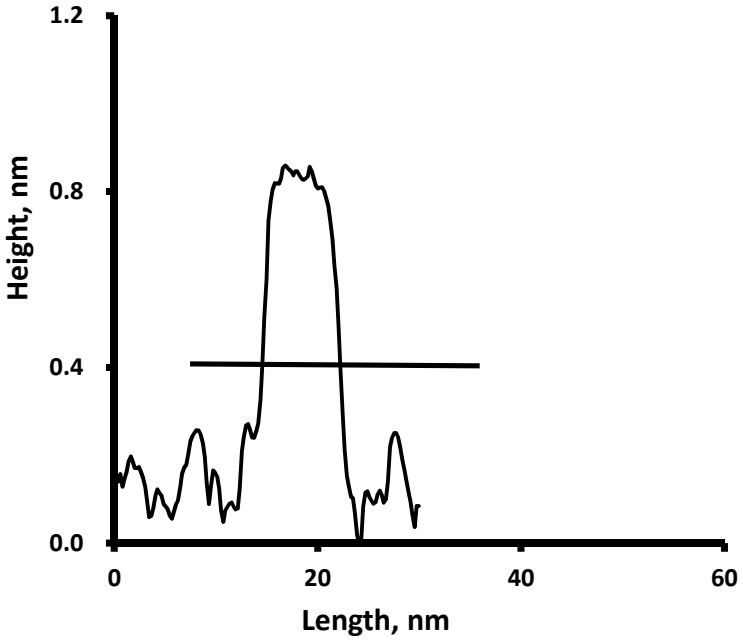

(a)

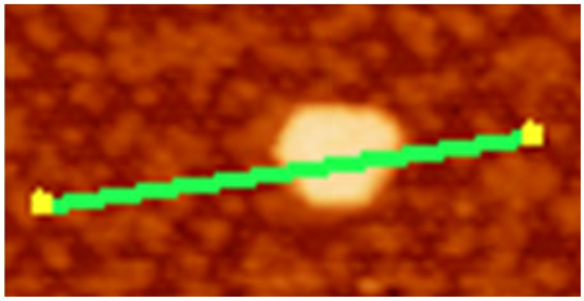

(b)

Figure 4.4

Schematic diagram of selecting reference level in terms of measuring average island area, (a) the line profile shows the half maximum as the reference level for "flooding" in WSxM, (b) the STM image of the island corresponding to the line profile in (a).17×34 nm^2, taken at -1.0 V tip bias, and 0.5 nA tunneling current. The direction of the arrow corresponds to the direction of x+ in the line profile of (a). Data from Run 2: 1+2-layer control experiment (for 100 *L* oxygen exposure).

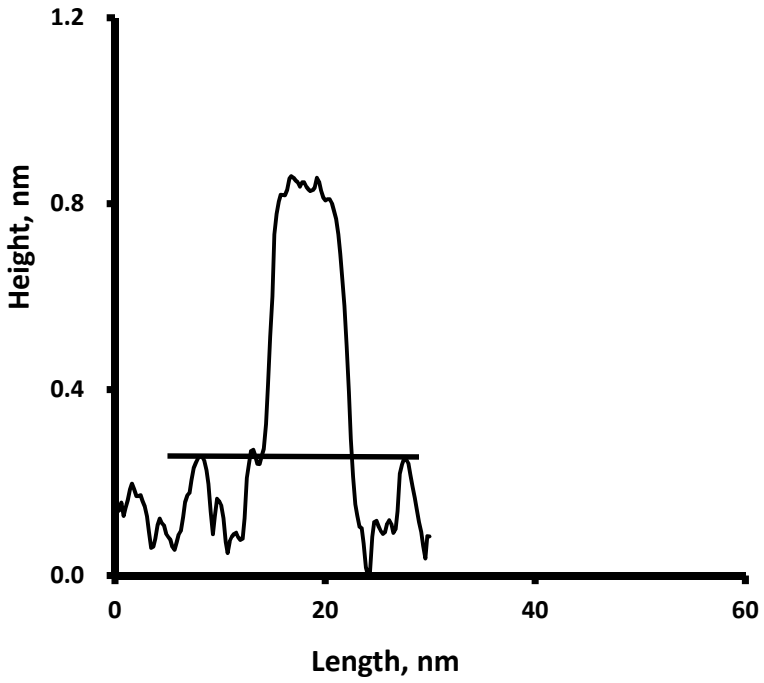

Figure 4.5

Schematic diagram of selecting reference level in terms of measuring island volume density. The line profile shows the lowest possible level as the reference level for "flooding" in WSxM, taken at -1.0 V tip bias, and 0.5 nA tunneling current. Data from Run 2: 1+2-layer control experiment (for 100 *L* oxygen exposure).

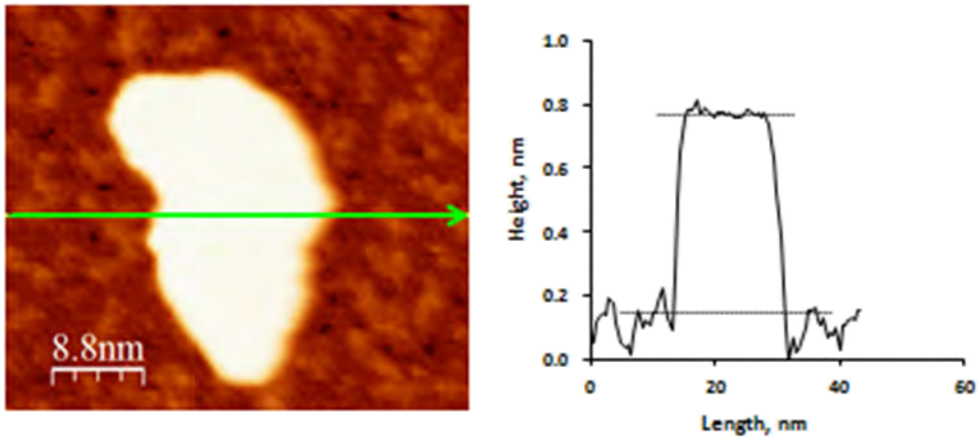

(a) (b)

Figure 4.6

(a)An STM image and (b) a line profile of a 2-layer island of Ag/Si(111)-7×7 surface, taken at +1.0 tip bias, 0.5 nA tunneling current. The image size is 44×37 nm^2. The height of this island is 0.58 nm. The two solid lines in (b) indicate the maximum and minimum vertical location of the island, respectively. Data from Run 3: 2-layer control experiment (for 100 *L* oxygen exposure).

CHAPTER 4

ADSORPTION OF ETHYLENE ON AG/SI(111)-7×7

A paper to be submitted

Dahai Shao[1,2], C.-Z. Wang[1,3], Kai-Ming Ho[1,3], M.C. Tringides[1,3] and P.A. Thiel[1,2,4]

[1]Ames Laboratory, [2]Department of Chemistry, [3]Department of Physics and Astronomy, and [4]Department of Materials Science and Engineering

Iowa State University, Ames Iowa 50011 USA

Abstract

The adsorption of ethylene on supported Ag nanoparticles is studied. Protrusions are observed when the surface is exposed with ethylene at 120 K. The protrusions disappear after annealing to 150 K. Such facts coincide with the desorption temperature of ethylene on low Miller index surfaces of Ag from Temperature-Programmed Desorption (TPD) studies. So the protrusions are likely to be ethylene-related species. Island edges are also decorated by ethylene exposure at 120 K. A possible explanation is that island edges are less coordinated thus more preferable for ethylene adsorption. Island height distribution is studied for ethylene adsorption and no significant change is observed for relative population of islands of different layer thicknesses.

1. Introduction

Ag has proven to be a very unique catalyst for ethylene epoxidation, which is the conversion of ethylene to a partially-oxidized form, ethylene oxide [1-3]. The role that Ag plays in preventing ethylene from undergoing complete combustion attracts a lot of interest.

Many surface studies tackle the issue by first looking into the surface adsorption of ethylene on single-crystal samples of Ag [4-12]. The surface desorption temperature is determined by many temperature-programmed-desorption (TPD) studies [4,9,10,12]. The peak temperature ranges from 125 K to 155 K for all three low-index Ag surfaces based on references of various sources, as seen in Table 1. And it decreases as the ethylene exposure increases, which is attributed to a repulsive lateral interaction [4,10]. The desorption energy has been also estimated based on TPD results, ranging from 37 to 40 kcal/mol for Ag(111) [4] and (110) [6,9]. This shows the interaction is quite weak between ethylene and Ag. The adsorption configuration is also of interest to many surface science groups and has been studied by various techniques [4-8,11,12]. Most studies show that ethylene adopts a uniform configuration for all low-index surfaces in which the molecular plane is parallel to the surface. However, whether ethylene adopts a specific site on these low-index surfaces has not been clarified yet through experiments. Theoretical calculations may provide some insight into this question. DFT calculations predict ethylene slightly preferentially adsorbs on the atop site of the close packed row for Ag(110) [13,14].

The growth of Ag nanoparticles on semiconductor substrates, such as Si(111)-7×7 attracts much attention, due to the fact that a quantum size effect mediates the growth process [15-18], which makes Ag nanoparticles quite different from Ag atoms on single crystal surfaces. For example, as mentioned in previous chapters, Ag/Si(111)-7×7 responds to oxygen exposure remarkably and shows a drastic change of the relative population of islands with different heights. This chapter intends to investigate how the same system will respond to ethylene exposure, or whether ethylene will adsorb differently than on Ag single crystals.

Table 1. Experimental data about ethylene adsorption and desorption on low-index Ag surfaces, from the literature.

Ethylene adsorption at	**Ag(111)**	**Ag(110)**	**Ag(100)**
Desorption temperature	T_p(peak temperature)= 142 K at 0.025 L C_2H_4 exposure, Decreasing to 128 K at 0.6 L [10] T_p=138 K at 3 L [4]	T_p=148 K at 0.04 L, Decreasing to 125 K at 1.5 L, [4] T_p=155 K at 0.75 L [9]	T_p=143 K at 1 L [12]
Desorption activation energy	39 kJ/mol, by Redhead analysis [4]	40 kJ/mol[6], 37 kJ/mol[9]	
Saturation coverage	0.33 ML by XPS [5] 0.5 ML [10]	0.5 ML by LEED [7]	
Adsorption geometry	Molecular plane parallel to the surface plane, by RAIRS [4] , XPS and UPS [5]	Molecular plane parallel to the surface plane, by HREELS [6], UPS [7], and RAIRS [11]	Molecular plane parallel to the surface plane, by RAIRS [8], and NEXAFS [12]
Average sticking coefficient at 100 K	>0.03 [5]	1 [7]	

2. Experimental details

Experiments were performed in an Omicron variable-temperature STM system. Chamber base pressure did not exceed 1.5 x 10^{-8} Pa throughout the experiments, including Ag evaporation, except during ethylene exposure. The Si sample was p-type, boron-doped, with

resistivity of 0.02 Ohm cm. The Si(111)-7x7 surface was prepared by flashing the Si sample to 1200 K and cooling down to room temperature in a stepwise manner. Ag was deposited via a Mantis electron-beam evaporator, with the sample at 300 K. The flux was 0.083 ML/min. The coverage used to calibrate the flux was based on the area of different Ag features, calculated by WSxM software, as described in Section 4, Chapter 3. The sample was exposed to ethylene (Matheson, lecture bottle, 99.95%) by either back-filling the chamber or direct dosing the sample from a tube doser just a few centimeters away from the sample, through a leak valve, for the appropriate time. Ethylene pressures measured at the ion gauge were in the range 1.3×10^{-6} to 1.3×10^{-5} Pa. Exposures were given in Langmuirs (L), where 1 $L = 1.3 \times 10^{-4}$Pa s. The pressure used for exposure measurement was based on the uncalibrated ionization gauge reading, although it should be noted that the pressure is higher at the crystal surface when the directional doser is used. C_2H_4 (Matheson, lecture bottle, 99.95%) was used without further purification, and its purity was checked with a mass spectrometer in the STM chamber. During data acquisition, the STM tip (W, electrochemically etched) was biased -3.0 V to +3.0 V with respect to the sample. The tunneling current was 0.5 nA. Data analysis was performed using WSxM software [20].

A series of experiments were performed at different ethylene exposures and exposure temperatures. Some experiments were followed by an annealing treatment. A detailed description of these experiments was listed in Table 2. For most of the experiments, a control group was also conducted. The conditions and time frame of data acquisition of the control group were the same as the ones in ethylene experiments except that for the control experiments, where the sample was simply allowed to age in the ultrahigh vacuum instead of

being exposed to ethylene.

The approach used for determining Ag coverage is the same as mentioned in Section 4.3, Chapter 3. And as mentioned previously, Ag is always deposited at room temperature.

The detailed time frame for the experiments is listed in Table 3. All the times are calibrated with respect to the point when Ag deposition begins. The experiment with 30 *L* ethylene exposure (backfilling) is not included since there is no control experiment for reference.

The approach used for measuring Ag island density is very similar to Section 4.6, Chapter 3. If conditions allow, a sampling area of 0.25 to 0.31 μm^2 (equivalent to 4 to 5 images with the size of 250 × 250 nm^2) is used. For some sections where imaging conditions are not very ideal, fewer images are used for analysis due to the limited availability. However, a sampling area equivalent to at least 2 images with the size of 250 × 250 nm^2 can be found, even for these sections. A detailed version of area analyzed for island density is shown in Table 4. The experiment with 30 *L* ethylene exposure (backfilling) is not included since there is no control experiment for reference.

Table 2.Information about different ethylene experiments.

Experiment date	01/14/2011	01/20/2011	02/03/2012	02/09/2012	02/12/2012
Ag coverage,monolayer (ML)	0.91	0.88	0.58	1.40	1.41
Initial Ag island height distribution	1+2 layer	1+2 layer	1+2 layer	2 layer	2 layer
Ethylene exposure, Langmuir (*L)* based on ion gauge pressure reading	2.5, tube dosing	25, tube dosing	3, backfilling	30, backfilling	30, tube-dosing
Ethylene exposure temperature, K	150	150	120	120	120
Annealing experiment	No	No	No	No	Yes
Relevant control experiment available?	Yes	Yes	Yes	No	Yes

Table 3.Time frame for control and ethylene experiments.

Ethylene exposure, *L*	Experiment	Ethylene exposure temperature, K	Annealing temperature, K	Time when the initial surface is imaged, h	Time when the surface after ethylene exposure is imaged, h	Time when the surface after annealing is imaged, h
30, tube dosing	control	120	150	6.6 - 6.7	8.4 - 8.5	12.8 - 13.1
	ethylene	120	150	6.6 - 6.7	7.7 - 8.1	10.9 - 11.2
3, backfilling	control	120	n.a.	6.8 - 7.5	8.5 - 9.3	n.a.
	ethylene	120	n.a.	6.1 - 6.4	8.2 - 9.6	n.a.
25, tube dosing	control	150	n.a.	3.9 - 4.2	6.3 - 6.6	n.a.
	ethylene	150	n.a.	3.9 - 4.2	6.3 - 6.7	n.a.
2.5, tube dosing	control	150	n.a.	4.9 - 5.3	6.4 - 6.7	n.a.
	ethylene	150	n.a.	4.7 - 5.2	6.4 - 6.7	n.a.

Table 4. Area sampled for island density analysis

Ethylene exposure, *L*	Experiment	Ethylene exposure temperature, K	Annealing temperature, K	Area sampled for clean surface, nm^2	Area for "after ethylene exposure", nm^2	Area for "after annealing", nm^2
30, tube dosing	control	120	150	1.3×10^5	1.9×10^5	1.3×10^5
	ethylene	120	150	1.3×10^5	1.9×10^5	1.3×10^5
3, backfilling	control	120	n.a.	3.8×10^5	1.2×10^5	n.a.
	ethylene	120	n.a.	1.0×10^5	2.3×10^5	n.a.
25, tube dosing	control	150	n.a.	3.1×10^5	3.1×10^5	n.a.
	ethylene	150	n.a.	3.1×10^5	3.1×10^5	n.a.
2.5 , tube dosing	control	150	n.a.	3.1×10^5	3.1×10^5	n.a.
	ethylene	150	n.a.	3.1×10^5	3.1×10^5	n.a.

3. Experimental Results

Fig. 1 shows STM images for the clean Ag/Si(111)-7×7 surface (Fig. 1(a) and 1(b)), the surface after ethylene exposure (30 *L*, backfilling) at 120 K (Fig. 1(c) and 1(d)), and the surface after being annealed to 150 K (Fig. 1(e) and 1(f)), respectively. Ag coverage is 1.40 ML, with the initial island distribution dominated by 2-layer islands. The distribution is in consistent with the fact that 2-layer thickness is preferred due to a quantum size effect [16]. This is the case in Fig. 1(a) and 1(b), for instance. After ethylene exposure, however, small protrusions are observed on islands (Fig. 1(c)), which are even more visible in differentiated images, as in Fig. 1(d). And similar protrusions are also seen in the second experiment where tube dosing is used, as shown in Fig. 1(e) and 1(f). After the sample is annealed to 150 K, the protrusions disappear (Fig. 1(g) and 1(h)). There is a multiple-tip effect in these images, but it is not severe enough to block the visibility of protrusions. We identify the protrusions as ethylene molecules or fragments of ethylene molecules, based on prior temperature programmed desorption (TPD) studies of ethylene [4,9,10,12], which showed that ethylene desorbs from Ag single crystal surfaces at a peak temperature of 140 K to 150 K, for all low Miller-index orientations. From this point of view, the protrusions are very likely to be ethylene-related features.

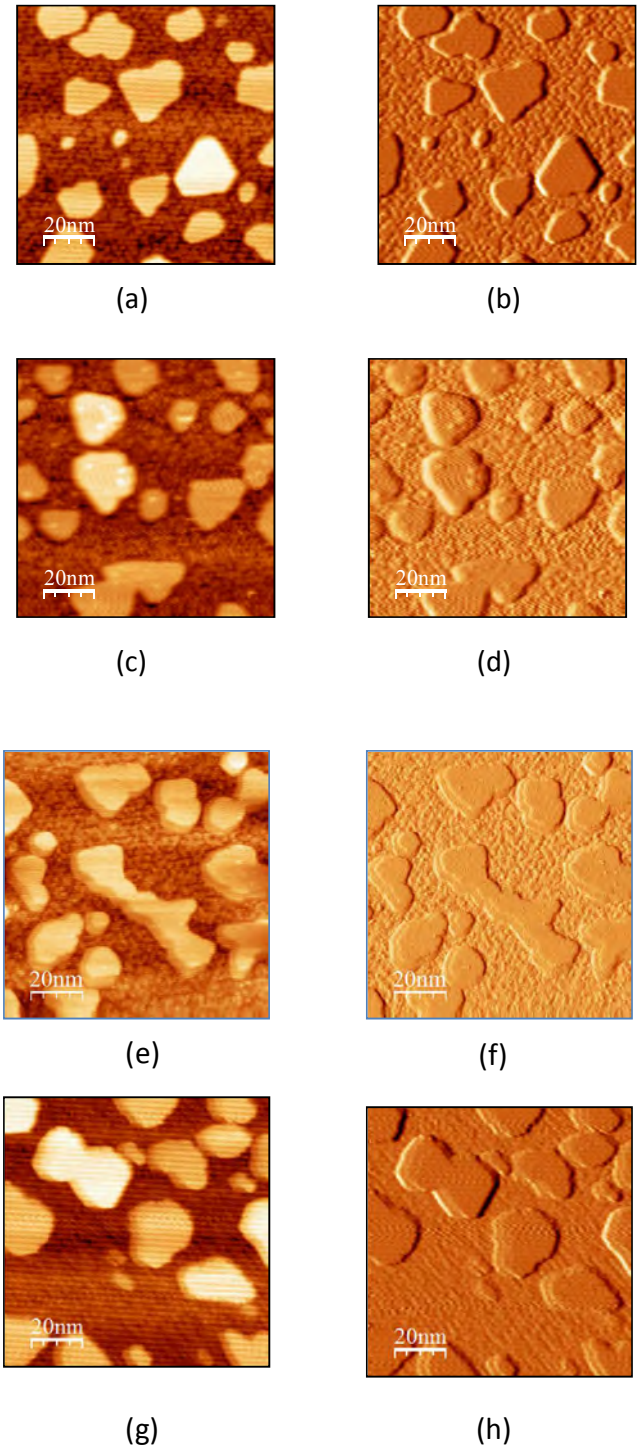

Fig. 1. STM images of Ag islands on Si(111)-7×7 substrate. Left panel shows images at constant current mode, while right panel shows images that have been differentiated. (a) and (b): clean Ag/Si(111)-7×7, at 120 K, (c) and (d): after 30 *L* ethylene exposure (back filling),

at 120 K, (e) and (f): after 30 *L* ethylene exposure (tube dosing), at 120 K. (g) and (h): after 30 *L* ethylene exposure (tube dosing), at 120 K, then annealed to 150 K. All image sizes are 100×100 nm^2, taken at tip bias of 3.0 V, tunneling current of 0.5 nA.

Fig. 2(a) shows the upper surface of islands at higher magnification (12×12 nm^2), which further illustrates the structure and dimensions of the protrusions. Fig. 2 (b) shows an expansion of Fig. 2(a) highlighting the rectangular area, where two protrusions are included. The protrusions are elliptical. The line profile across the long axis is shown in Fig. 2(c). Based on the line profiles of 15 protrusions, the average dimension along the long axis at half maximum height is 0.55 ± 0.03 nm (This value is reported in the format "average value ± 1 standard deviation", and so are the following values with similar expressions). This value is consistent with other ethylene STM studies, which identify the protrusions as ethylene molecules with a full width at half maximum (FWHM) of 0.5 to 0.6 nm [21-25]. Please note that such studies use a much lower tunneling bias, around 0.05 to 0.1 V. So the value from these references may not be useful if the protrusions are sensitive to tunneling bias.

An STM simulation study also shows a comparable value of 0.54 nm [26], based on a π-bonding configuration.

Based on the consistency of the protrusion width mentioned above, the adsorption configuration of ethylene is also likely to be similar to those from these published studies [4-8,11,12], which show a non-dissociative π-bonding adsorption with its molecular plane parallel to the surface. The similarity indicates the d-band of Ag islands is still not energetic enough to hybridize with the π-orbital of ethylene to form a stronger bond, say a di-σ bond.

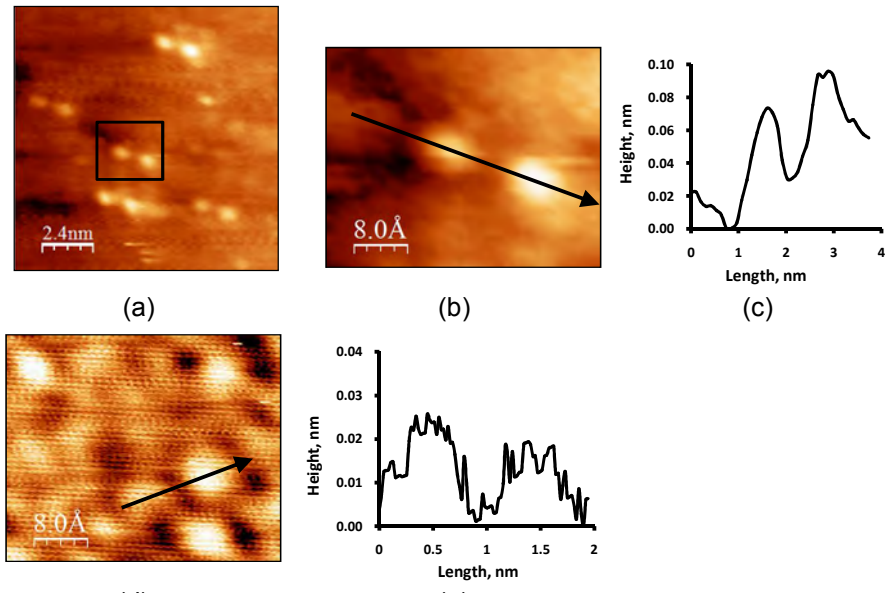

Fig. 2. (a) An example of protrusions on Ag islands after ethylene exposure at higher magnification, 12 × 12 nm^2. (b) An inset of (a) that corresponds to the highlighted area, 4.0 × 3.3 nm^2. (c) A line profile that corresponds to the line with the arrow in (b). (c) An STM image of the upper surface of Ag islands before ethylene exposure, 4.0 × 3.3 nm^2. (e) A line profile that corresponds to the line with the arrow in (d). All images are taken at tip bias of 3.0 V, tunneling current of 0.5 nA.

Besides the protrusions on island tops, there are other features that decorate island edges, making the edges brighter in contrast than the inner island terraces. Figure 3 shows details of such decoration. Fig. 3(b) and 3(c) shows the STM image for the surface after ethylene exposure (30 *L*, backfilling). The island edges are decorated with bright features. At 150 K, these features disappear as shown in Fig. 3(f). Similar features are also observed on the tube-dosing ethylene experiment, as shown in Fig. 3(d) and 3(e). Although we cannot resolve these features at higher magnification, the temperature where these features disappear is consistent with the desorption temperature of ethylene on Ag single crystals, making ethylene very likely to be the candidate for such features.

Theoretical calculations show ethylene adsorbs more stably on steps, adatoms, and kink sites other than close-packed surfaces, due to a stronger hybridization between Ag d-electrons and ethylene π-orbitals on these more open sites [28]. If the same trend applies to the Ag/Si(111)-7×7 system, then island edges are definitely a better candidate to accommodate ethylene than inner surfaces of islands, since Ag atoms are less coordinated on edges, making them more open than inner island terraces.

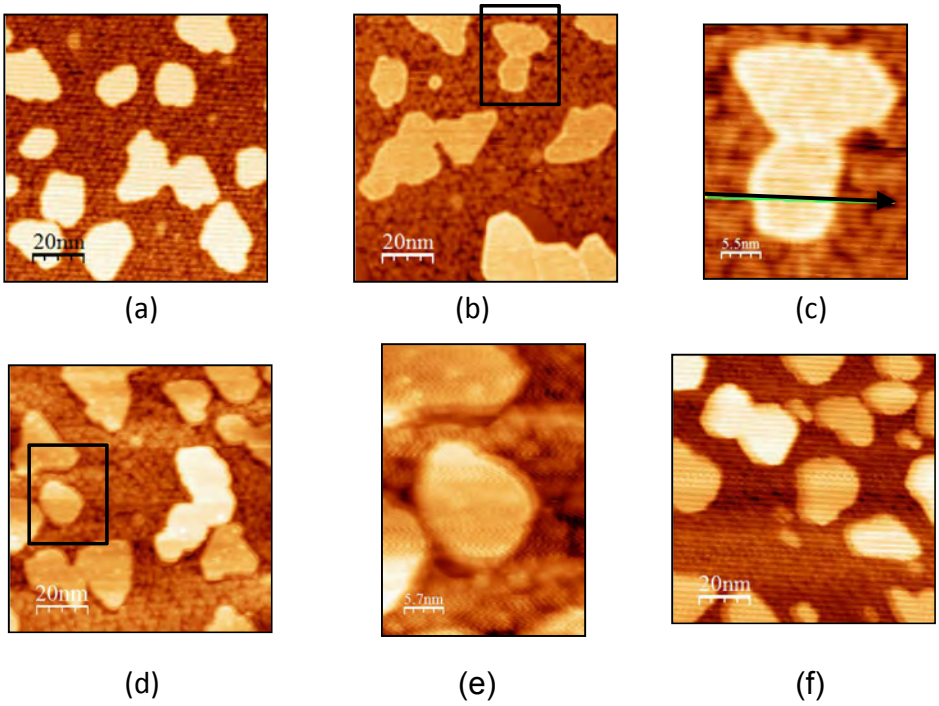

Fig. 3. (a) An STM images of Ag islands on Si(111)-7×7 substrate before ethylene exposure, 100× 100 nm^2. (b) An STM images of Ag islands on Si(111)-7×7 substrate after ethylene exposure (30 *L*, backfilling), 100 × 100 nm^2. (c) An expansion of the boxed area in (b), 27× 33 nm^2. (d) An STM images of Ag islands on Si(111)-7×7 substrate after ethylene exposure (30 *L*, tube dosing), 100 × 100 nm^2. (e) An expansion of the boxed area in (d), 28× 40 nm^2. (f) An STM images of Ag islands on Si(111)-7×7 substrate, annealed to 150 K after ethylene exposure (30 *L*, tube dosing), 100 × 100 nm^2. All images are taken at tip bias of 3.0 V,

tunneling current of 0.5 nA.

The average height of these protrusive rims that decorate island edges is 0.11 ± 0.02 nm, slightly higher than the height of the protrusions on island centers (0.07 nm). Fig. 4(a) is a high magnification STM image of a typical island with decorated edge. And Fig. 4(b) is a line profile across this island corresponding to the arrow line in Fig. 4(a). Fig. 4(c) shows a possible configuration of adsorbed ethylene on island edges.

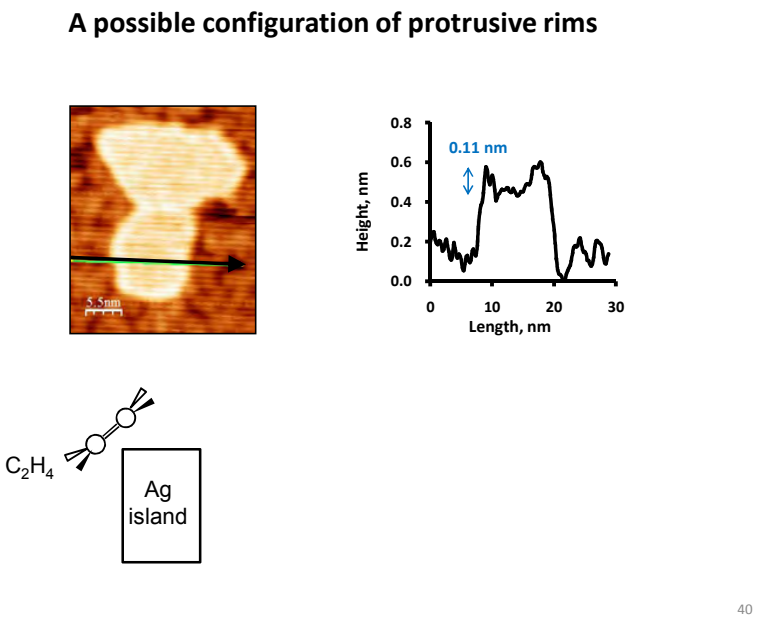

Fig. 4. A schematic diagram of possible configuration of ethylene adsorbing on island edges. (a) A high magnification image of a Ag island with edge decorated, 27 × 33 nm^2. (b) A line profile corresponds to the solid line in (a). (c) A schematic diagram of a possible configuration of adsorbed ethylene.

Island height distribution

Like studies for oxygen adsorption on Ag/Si(111)-7×7, island height distribution is

also studied for the ethylene experiment (30 *L*, tube dosing), as shown in Fig. 5. We must consider the possibility that coarsening could occur even without ethylene, and so a control experiment must be incorporated. (One might anticipate that coarsening would be very slow at these low temperatures, 120-150 K, but STM experiments with liquid nitrogen cooling are usually more time-consuming than experiments at room-temperature, and so a slower rate could be offset by a longer time.) The design of the control experiment in this ethylene study is analogous to the design of the control experiments in the oxygen study (Section 2, Chapter 2). That is to say, the control in the ethylene experiment has almost identical time line as in the ethylene exposure experiments, except that during the period allotted for ethylene exposure, the sample is simply resting in vacuum for the control experiment.

Determination of island height plays an important role in identifying the layer thickness of islands, therefore in the analysis of island height distribution.

The approach used for measuring island heights is the same as in Section 4.6, Chapter 3. The detailed island height information is listed in Table 5. The numbers are reported in the format "average value ± 1 standard deviation", in units of nm.

For the initial surface, 2-layer islands dominate the total island density, accounting for 78% (ethylene) or 83% (control) of the islands, with the remainder mostly being 1-layer islands. There are also a very small percentage of 3-layer islands, as shown in Fig. 5(d).

After ethylene exposure at 120 K, the relative population of 2-layer islands increases from 78% to 83%, indicating ethylene does not impose a significant effect on relative population of Ag islands at this temperature. The absolute density for 1-, and 2-layer islands decrease by 96 and 67 μm^{-2}, respectively, accounting for 32% and 5% of the initial

density, as shown in Fig. 5(e). This could be attributed to either a real but minor coarsening effect, or a random difference from insufficient sampling.

For the control group, there is no significant change of relative stability from "before ethylene exposure" to "after" either, as shown in Fig. 5(a) and (b). The percentage of 2-layer islands only changes from 83% to 81%, indicating that, at this low temperature, the coarsening effect is quite inhibited, even over the time scale of the experiment (~ 8 hours).

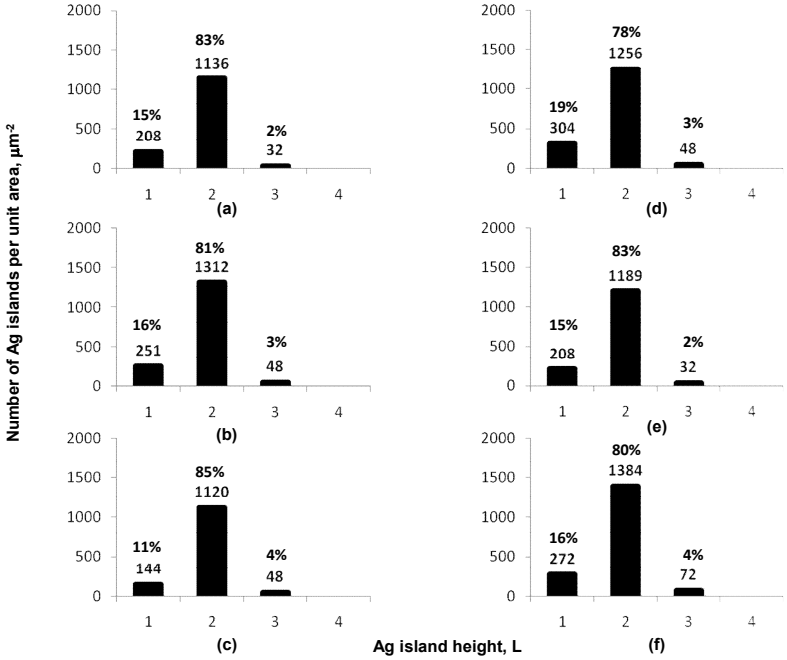

Fig. 5. Island height distribution for the control experiment (a, b, c) and the experiment with ethylene exposure (30 *L*, tube dosing, d, e, f). Data in (a) is taken at similar lapse of time as in (d). Data in (b) is taken at similar lapse of time as in (e). Data in (c) is taken at similar lapse of time as in (f). (d) Initial island height distribution at 120 K, (e) after 30 *L* ethylene exposure (tube dosing) at 120 K, (f) annealed to 150 K. The percentage numbers above each column denote the relative population of each kind of island. The numbers under them denote the absolute number density.

Table 5. Average island height for ethylene and control experiments

Experiment		1-layer islands		2-layer islands		3-layer islands		Scanning bias, tip, V
		Range of height, nm	Average height, nm	Range of height, nm	Average height, nm	Range of height, nm	Average height, nm	
30 *L*, tube dosing, 120 K	Before ethylene exposure	0.20 - 0.27	0.24 ± 0.02	0.41 - 0.55	0.49 ± 0.05	0.74 - 0.77	0.76 ± 0.02	+3.0
	After ethylene exposure	0.25 - 0.28	0.26 ± 0.01	0.44 - 0.48	0.46 ± 0.01	0.72 - 0.73	0.73 ± 0.01	
	Annealing to 150 K	0.25 - 0.28	0.26 ± 0.01	0.44 - 0.50	0.47 ± 0.03	0.70 - 0.79	0.75 ± 0.04	
0 *L*, tube dosing, 120 K (control)	"Before ethylene exposure"	0.24 - 0.32	0.28 ± 0.03	0.55 - 0.59	0.57 ± 0.02	0.76 - 0.83	0.82 ± 0.05	+1.5
	"After ethylene exposure"	0.23 - 0.26	0.24 ± 0.02	0.45 - 0.48	0.46 ± 0.02	0.72 - 0.73	0.73 ± 0.01	+3.0
	Annealing to 150 K	n.a. due to double tip effect						
3 *L*, backfilling, 120 K	Before ethylene exposure	0.25 - 0.33	0.30 ± 0.03	0.57 - 0.64	0.61 ± 0.02	n.a.	n.a.	-3.0
	After ethylene exposure	0.26 - 0.34	0.32 ± 0.03	0.60 - 0.63	0.61 ± 0.01	n.a.	n.a.	
0 *L*, backfilling, 120 K (control)	"Before ethylene exposure"	0.29 - 0.34	0.32 ± 0.02	0.60 - 0.63	0.61 ± 0.01	n.a.	n.a.	-3.0
	"After ethylene exposure"	0.28 - 0.34	0.32 ± 0.02	0.59 - 0.63	0.61 ± 0.02	n.a.	n.a.	

After annealing to 150 K, presumably the temperature where ethylene desorbs from Ag single crystal surfaces [4,9,10,12], the relative population of the islands roughly remains constant, with a variation of only a few percent, for both the control experiment and ethylene experiment. So if it's assumed that ethylene also desorbs from heterogeneous Ag on Si(111)-7×7 at this temperature, then the assumption is consistent with the fact that island relative population is unperturbed at 150 K. However, there is always a possibility that ethylene does not exert a significant effect on island relative stability even when it's adsorbed on the surface, as indicated by the 120 K experiment.

Another ethylene experiment is also performed, but entirely at 120 K, with a lower exposure of ethylene (3 *L* via backfilling). The relative population of islands is shown in Fig. 6. For the initial surface, less Ag is deposited on the Si substrate than the previous experiment (0.58 ML), so the percentage of 1-layer islands is higher, ranging from 33% to 38%. The remainders of the islands are all 2-layer islands. There are no 3-layer islands.

After ethylene exposure, the main ranking of relative population is preserved (Fig. 6(c) and 6(d)). Ethylene thus has no significant effect on perturbing the relative population. However, there is a trend that 2-layer islands decay by 10% after ethylene exposure. The absolute density of 2-layer islands decreases by 647 nm^{-2}, accounting for 41% of the initial density. In the meantime, the density of 1-layer islands only decreases by 79 nm^{-2}, accounting for 10% of the initial density. There seems to be an effect of ethylene that preferentially promotes the coarsening of 2-layer islands in this experiment. However, such a drastic effect is not observed in the previous experiment where ethylene is dosed in a much higher exposure (30 *L*, tube-dosing). So why a low exposure of ethylene like this (3 *L*, backfilling)

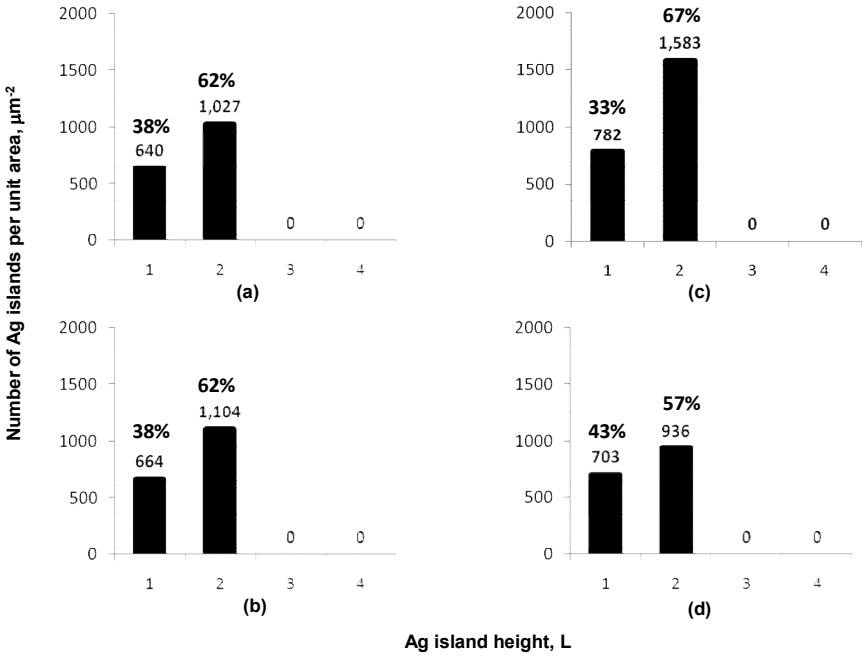

Fig. 6.

Island height distribution of another pair of ethylene experiments (control and ethylene, 120 K, 3 *L*, backfilling). No annealing available. The left panel (a, c) correspond to control experiment, and the right panel (b, d) corresponds to the experiment with ethylene exposure. Data in (a) is taken at similar lapse of time as in (c). Data in (b) is taken at similar lapse of time as in (d). (c) Initial island height distribution at 120 K, (e) after 3 *L* ethylene exposure (backfilling) at 120 K. The percentage numbers above each column denote the relative population of each kind of island. The numbers under them denote the absolute number density.

can produce such a significant effect while a much higher exposure of ethylene (30 *L*, tube dosing) cannot is still puzzling. And it might lead to the conclusion that ethylene may not be necessarily involved in this change of island height distribution. Perhaps when ethylene backfills the chamber, it can displace other molecules from chamber walls or react with chamber walls (including cryostat walls), depending on the history of the chamber. The

displaced or reacted molecules might then affect the surface. We note that this experiment is performed much, much earlier than the others reported in this chapter, so the chamber wall surfaces may have been in a different condition. In the meanwhile, the relative population of islands for the control experiment is very steadily maintained in this experiment, as in the others.

There are also experiments where the sample is only cooled down to 150 K and ethylene is dosed at this temperature. The distribution of islands is shown in Fig. 7 (25 *L* ethylene, backfilling) and Fig. 8 (2.5 *L* ethylene, backfilling). The Ag coverage is 0.88 ML and 0.91 ML, respectively. Both figures show that the island height distribution is essentially preserved throughout ethylene exposure. This could be mainly attributed to the two reasons that are mentioned previously, i.e. either ethylene cannot adsorb on the heterogeneous Ag surface at this temperature, or it has no significant effect on relative population of Ag islands anyway. And as mentioned before, although the results from other reference [4-12] make it more likely to be the first reason, it is still difficult to completely rule out the latter without further study.

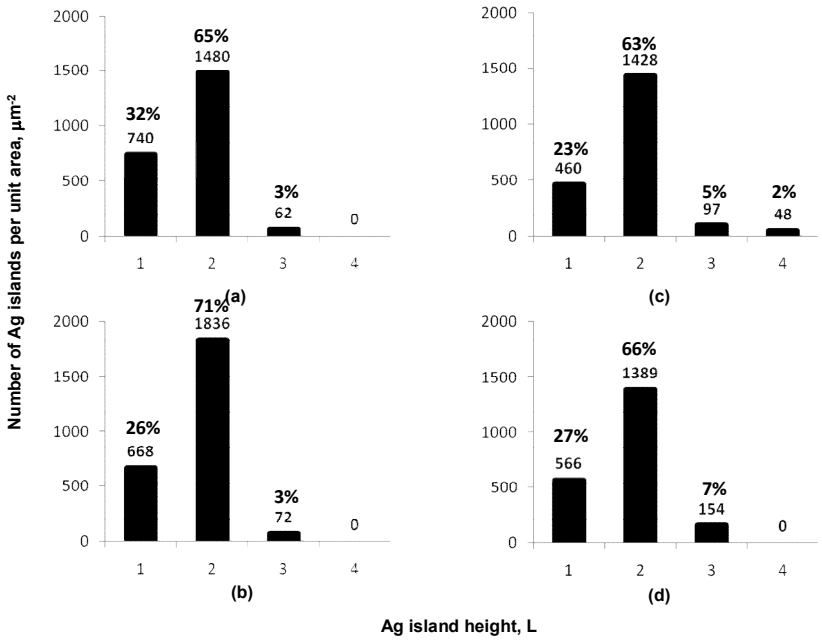

Fig. 7. Island height distribution of another pair of experiments with ethylene exposure (25 *L,* tube dosing) at 150 K. The left panel (a, c) correspond to control experiment, and the right panel (b, d) corresponds to the experiment with ethylene exposure. Data in (a) is taken at similar lapse of time as in (c). Data in (b) is taken at similar lapse of time as in (d). (c) Initial island height distribution at 120 K, (e) after 25*L* ethylene exposure (tube dosing) at 150 K. The percentage numbers above each column denote the relative population of each kind of island. The numbers under them denote the absolute number density.

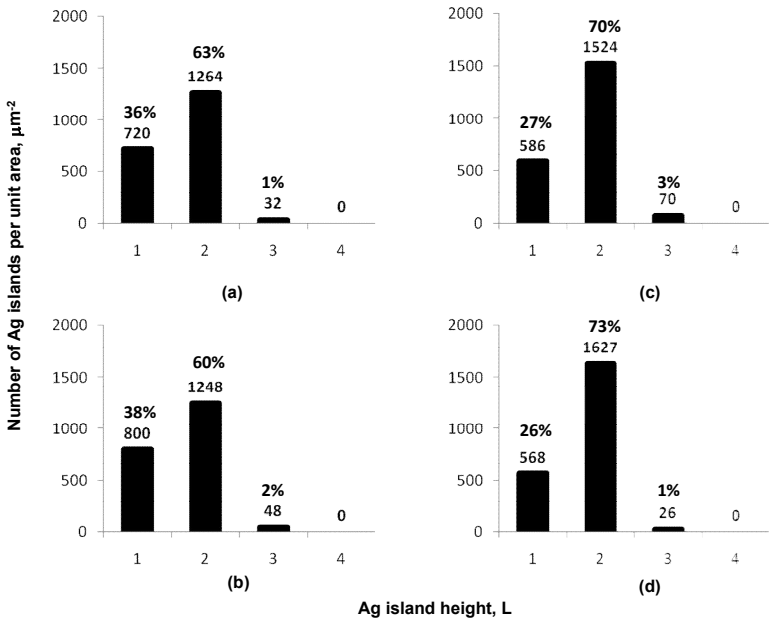

Fig. 8. Island height distribution of another pair of experiments with ethylene exposure (2.5 *L,* tube dosing) at 150 K. The left panel (a, c) correspond to the control experiment, and the right panel (b, d) corresponds to the experiment with ethylene exposure. Data in (a) is taken at similar lapse of time as in (c). Data in (b) is taken at similar lapse of time as in (d). (c) Initial island height distribution at 120 K, (e) after 2.5*L* ethylene exposure (tube dosing) at 150 K. The percentage numbers above each column denote the relative population of each kind of island. The numbers under them denote the absolute number density.

Root-mean-square (RMS) roughness of the wetting layer

The RMS roughness of the wetting layer can reveal whether the wetting layer is perturbed by foreign species. In the ethylene experiment, the change of roughness reflects possible adsorption of ethylene on the wetting layer. Studies show Ag cannot saturate the entire Si substrate, which leaves part of the Si substrate exposed during ethylene exposure [16,29]. So the interaction of Si with ethylene is possibly significant. In fact, ethylene adsorbs on Si(111)-7×7 with the lowest desorption temperature of 420 K [30], much higher than the one for ethylene on Ag surfaces [4,9,10,12]. Other studies show ethylene di-σ bonds with Si

(111)-7×7 [31,32], which is a stronger bonding than the π-bonding with Ag surfaces.

A detailed database of such information is listed in Table 6. The numbers are reported in the format "average value ± 1 standard deviation", in units of nm. The approach used for determining the RMS value is the same as in Section 4.2, Chapter 3 Oxygen Appendices. As mentioned in Chapter 3, roughness may vary as a function of the sampled area, and it usually approaches an asymptotic value when the area exceeds a critical value. This value is denoted as the critical sampling area. Such value is determined for roughness of each stage, as shown in Table 6. Figure 9 demonstrates an example of how the critical sampling area is determined. The critical value in this study is 45 nm^2. All the roughnesses reported below are taken from areas large enough that the variation with larger size is less than the accuracy of the measurement.

Table 6. RMS roughness of the wetting layer for ethylene and control experiments

Experiment		Critical sampling area, nm^2	RMS roughness of the wetting layer, nm	Scanning bias, V
30 *L*, tube dosing, 120 K	Before ethylene exposure	45	0.62 ± 0.04	+3.0
	After ethylene exposure	49	0.59 ± 0.03	
	Annealing to 150 K	360	0.54 ± 0.06	
0 *L*, tube dosing, 120 K (control)	"Before ethylene exposure"	208	0.40 ± 0.03	+3.0
	"After ethylene exposure"	63	0.28 ± 0.05	
	Annealing to 150 K	84	0.51 ± 0.11	
3 *L*, backfilling, 120 K	Before ethylene exposure	374	0.64 ± 0.01	-3.0
	After ethylene exposure	25	0.54 ± 0.05	
0 *L*, backfilling, 120 K (control)	"Before ethylene exposure"	310	0.52 ± 0.03	-3.0
	"After ethylene exposure"	239	0.64 ± 0.03	

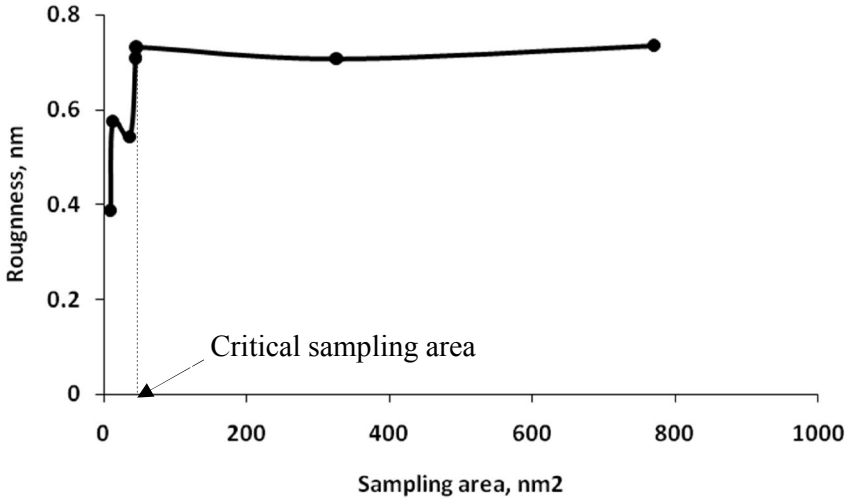

Fig. 9. An example of determining critical sampling area. 120 K, clean Ag/Si(111)-7×7 surface.

Fig. 10 and Fig. 11 show representative images of the wetting layer of 30 L (tube dosing) ethylene experiment and 3 L (backfilling) ethylene experiment, respectively.

4. Discussion

The bonding site of ethylene on Ag islands is not directly observed due to lack of atomic resolution of the Ag substrate. But experimental [27] and theoretical [13,14] studies have been dedicated to the similar issue for Ag surfaces based on bulk phase. There is no consensus so far. Theoretical studies [13,14] favor the argument that ethylene is most stable at on-top sites for Ag(110) and (100) surfaces, though Tang *et al* [27] postulate that ethylene favors four-fold hollow site on Ag(100), based on simulated near edge X-ray absorption fine structure (NEXAFS) spectra.

Most of the protrusions form pairs on Ag islands, as shown in Fig. 2(a). Most of the pairs line along the same direction, making them more likely to be a double-tip effect than real structure. Nonetheless, there is a chance that they represent pairs of molecules, and so it is worthwhile to analyze the separation between them. The average spacing between the two paired-up protrusions (peak-to-peak value, based on line profile scans) is 1.2 ± 0.1 nm. So even though we cannot directly image the binding site, this value may shed some light on it. The spacing is very close to that between two protrusions on the clean Ag islands as shown in Fig. 2(d) and (e), which is 1.1 nm, under similar tunneling conditions.

Due to different dosing methods, the actual ethylene exposure is probably quite different for the two experiments. For the one with dosing tube, the outlet of the doser is close to the sample, so there is probably a significant pressure gradient from sample to ionization gauge, where the pressure used in calculating exposure is measured. So the actual exposure is higher than the apparent exposure based on ionization gauge readings. Yet the density of protrusions on island centers for the two experiments is not significantly different, neither is there a significant difference between the morphology of decorated island edges. So it is very likely that 30 *L* exposure by backfilling has already saturated the surface. An experimental study [5] shows the saturation exposure is less than 10 *L* for Ag(111) on bulk phase. However, due to the inhomogeneity of the exposed wetting layer, it is not very accurate to directly compare Ag(111) with our sample, but this comparison probably provides at least an order-of-magnitude estimate of the saturation exposure. And also due to the complication of the wetting layer, it is difficult to measure the total coverage of ethylene at saturation.

5. Conclusions

The adsorption of ethylene on Si supported Ag islands is studied. Protrusions are observed on Ag islands by STM after ethylene exposure. Such protrusions disappear at 150 K. Island edges are also decorated after ethylene exposure. Protrusive rims are observed at the top edges of Ag islands. These rims also disappear at 150 K. Given the fact that 150 K is the temperature where ethylene desorbs from most low Miller-index Ag surfaces, it is very likely the protrusions and rims are formed by ethylene-related features. Island height distribution is studied for ethylene adsorption and no significant change is observed for relative population of islands of different layer thicknesses.

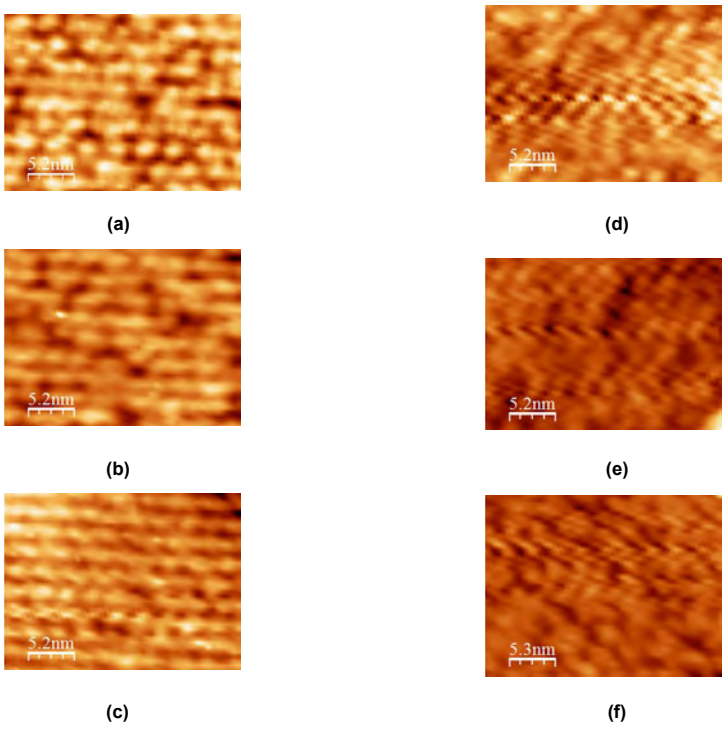

Fig. 10. Representative STM images of the wetting layer of the experiment with 30 *L* ethylene exposure (tube dosing, 120 K) (left panel) and its control experiment (right panel).

(a) initial surface, (b) after ethylene exposure, (c) after annealing, (d) the control experiment corresponding to (a), (e) the control experiment corresponding to (b), (f) the control experiment corresponding to (c). All image sizes are 26.5 × 20 nm^2, taken at +3.0 V tip bias, and 0.5 nA tunneling current.

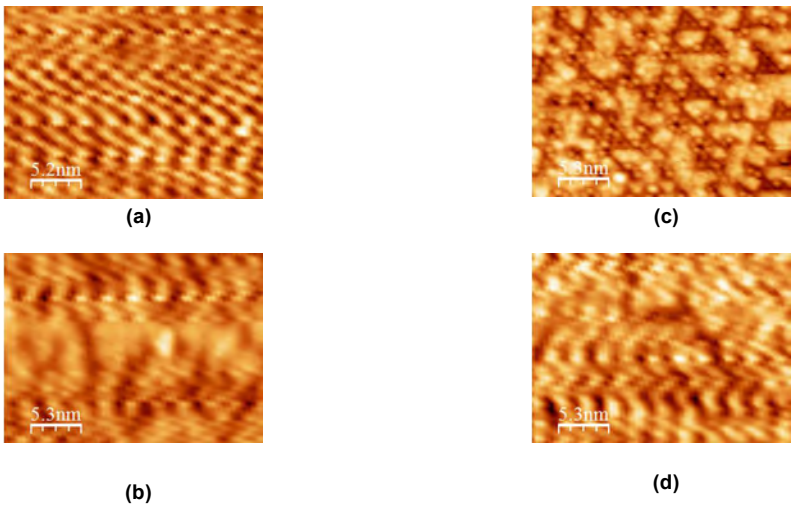

Fig. 11. Representative STM images of the wetting layer of the experiment with 3 *L* ethylene exposure (backfilling, 120 K) (left panel) and its control experiment (right panel). (a) initial surface, (b) after ethylene exposure, (c) the control experiment corresponding to (a), (d) the control experiment corresponding to (b). All image sizes are 26.5 × 20 nm^2, taken at -3.0 V tip bias and 0.5 nA tunneling current.

Acknowledgements

This work was supported by the Office of Science, Basic Energy Sciences, Material Sciences and Engineering Division of the U.S. Department of Energy (USDOE). This manuscript has been authorized by Iowa State University of Science and Technology under Contract No. DE-AC02-07CH11358 with the U.S. Department of Energy.

References

[1] M.O. Ozbek, R. A. van Santen, Catal. Lett.143 (2013), 131–141.

[2] P.A. Kilty, W.M.H. Sachtler, Catal. Rev. – Sci. and Engr. 10 (1974),1.

[3] H.H. Voge, C.R. Adams, Adv. Catal. 17 (1967), 151.

[4] D. Stacchiola, G. Wu, M. Kaltchev, and W.T. Tysoe, Surf. Sci.486 (2001), 9.

[5] T.E. Felter, W.H. Weinberg, P.A. Zhdan, and G.K. Boreskov, Surf. Sci. 97 (1980), L313.

[6] C. Backx, C.P.M. de Groot, and P. Biloen, Appl. Surf. Sci. 6(1980), 256.

[7] B. Kruger and C. Benndorf, Surf. Sci. 178 (1986), 704.

[8] D.A. Slater, P. Hollins, and M.A. Chesters, J.Electron.Spectrosc.Relat.Phenom.64/65 (1993), 95.

[9] C.T. Campbell and M.T. Paffett, Appl. Surf. Sci. 19(1984), 28.

[10] X.-L. Zhou and J. M. White, J. Phys. Chem, 96(1992), 7703.

[11] M. Akita, N. Osaka, S. Hiramoto, and K, Itoh, Surf. Sci. 427 (1999), 374.

[12] D. Arvantis, K. Baberschke, L. Wenzel, U. Dobler, Phys, Rev. Lett, 57 (1986), 3175.

[13] C.G.P.M. Bernardo, J.A.N.F. Gomes. J of Mol. Strctr. (Theochem). 582 (2002), 159.

[14] K. Itoh , T.Kiyohara , H. Shinohara, C.Ohe , Y. Kawamura, and H. Nakai, J. Phys.Chem. B.106 (2002), 10714.

[15] Y. Han, D.-J.Liu, Phys. Rev. B. 80 (2009), 155404.

[16] L. Gavioli, K.R. Kimberlin, M.C. Triniges, J.F. Wendelken, Z. Zhang. Phys. Rev. Lett.82 (1999), 129.

[17] B. Unal, A. Belianinov, P.A. thiel, M.C. Tringides, Phys. Rev. B. 81 (2010), 085411.

[18] D.K. Goswami, K. Bhattacharjee, B. Satpati, S. Roy, P.V. Satyam, B.M. Dev, Surf. Sci. 601 (2007), 603.

[19] D. Shao, X. Liu, N. Lu, C.-Z. Wang, K.-M. Ho, M.C. Tringides, P.A. Thiel, Surf. Sci. 606 (2012), 1871.

[20] I. Horcas, R. Fernández, J. M. Gómez-Rodríguez, J. Colchero, J. Gómez-Herrero, A. M. Baro. Rev. Sci. Instrum. 78 (2007), 013705.

[21] J.R. Hahn, W. Ho. Phys. Rev. B. 80 (2009), 165428.

[22] J. Buisset, H.-P.Rust, E.K. Schweizer, L. Cramer, A.M. Bradshaw. Phys. Rev. B. 54 (1996), 10373.

[23] T. Okada, Y. Kim, Y. Sainoo, T. Komeda, M. Trenary, M. Kawai, J. Phys. Chem. Lett. 2 (2011), 2263.

[24] M.-L. Bocquet, P. Sautet, J. Cerda, C. I. Carlisle, M. J. Webb, D. A. King, J. Am. Chem. Soc. 125 (2003), 3119.

[25] J.R. Hahn, W. Ho, J. Phys. Chem. B. 109 (2005), 20350.

[26] M.-L. Bocquet, P. Sautet. Surf. Sci. 415 (1998), 148.

[27] J.C. Tang, J.F. Shen, Y.B. Chen. Surf. Sci. Lett. 244 (1991), L125.

[28] A. Kokalj, A.D. Corso, S. de Gironcoli, S. Baroni. J. Phys. Chem. B. 110 (2006), 367.

[29] P. Sobotík, I. Ošt'ádal, J.Mysliveček, T.Jarolímek, F.Lavický, Surf. Sci. 482-485 (2001), 797.

[30] P. Klimesch, G. Meyer, H. Henzler, Surf. Sci. 137 (1984), 79.

[31] J. Yoshinobu, H. Tsuda, M. Onchi, M. Nishijima, Solid State Commun. 60 (1986), 801.

[32] J. Yoshinobu, D. Fukushi, M. Uda, E. Nomura, M. Aono, Phys. Rev. B. 46 (1992), 15.

CHAPTER 5
ANNEALING THE AG/SI(111)-7×7 SURFACE AFTER OXYGEN EXPOSURE

A paper to be submitted

Dahai Shao[1,2], and P.A. Thiel[1,2,3]

[1]Ames Laboratory, [2]Department of Chemistry, and [3]Department of Materials Science and Engineering

Iowa State University, Ames Iowa 50011 USA

Abstract

Annealing the Ag/Si(111)-7×7 surface after oxygen exposure is studied to further clarify the cause of the growth of 3-layer islands after oxygen exposure at 300 K. After mild annealing at 310-340 K, Ag islands grow into even higher islands (4-9 layers), indicating the adsorption of oxygen probably affects the growth by reducing kinetic barriers to forming 3-D islands. Similar annealing conditions are also performed on control experiments, where 2-layer islands are strongly promoted in terms of island density after annealing. For the control experiment, annealing also modifies island morphology by shaping islands more hexagonally. These changes suggest 2-layer islands are likely to be energetically favored at RT. A long annealing time (30 min) is shown to trigger conversion the Ag/Si(111)-7×7 surface to a Si(111)-(√3×√3)R30°-Ag-like structure, even at very mild annealing conditions (T=320-330 K). The survival of Ag islands after such annealing indicates that conversion is only partially complete.

1. Introduction

Thermal annealing is used in many surface science studies to overcome kinetic barriers

and thus expedite the approach to equilibrium. For example, it is widely used in metal sample cleaning after ion-sputtering [1]. Sputtering is effective in removing surface contaminants from atmosphere. In the meantime, however, sputtering also tends to bombard away the surface atoms/molecules of interest. So annealing is necessary in order for the sputtered surface to recover from sputtering damage and restore the stable structure again.

Ag growth on Si(111)-7×7 is affected by annealing. For deposition at 150 K followed by subsequent annealing to 300 K, the Ag islands show a uniform distribution with 2-layer islands being strongly favored [2]. This is different from the scenario of Ag growth directly at 300 K, where a significant portion of 3-layer islands also exist [3]. For Ag deposition above 300 K, the strong preference of 2-layer islands is entirely disrupted, and islands higher than 3 layers are observed under such deposition condition [14,15].

With oxygen adsorption on the Ag/Si(111)-7×7 surface, the island distribution is modified and 2-layer islands are not strongly favored over islands of other layer thicknesses [4]. After the adsorption of oxygen, a significant number of 3-layer islands are detected, with a small portion of 4-layer islands as well. The detailed results are shown in Chapter 2. However, it is still not clear that the growth of higher islands is energetically stable, or metastable due to kinetic effects. So it is highly desirable to anneal this system to further clarify the cause of this change.

2. Experimental details

For all experiments of Run 2, an annealing experiment is performed at the end. The annealing is achieved by directly passing a current through the sample to increase its temperature to a certain value for a certain amount of time. The temperature is calibrated by two thermocouples, as shown in Fig. 1. One thermocouple that directly measures the temperature of

the top plate of sample holder is labeled as Thermocouple I (W-5% Re). The other thermocouple that is embedded in the manipulator arm is denoted as Thermocouple II (Ni-Cr), and it measures the temperature of the manipulator arm, which connects with the sample holder via contact brushes and the bottom sample plate. The average temperature of the two thermocouples is taken as the estimate of the sample temperature, although it might be lower than the real sample temperature since there could be a temperature gradient from the sample to the two thermocouples, caused by the potential heat-conducting resistance between the sample and the sample holder. The relation of measured temperature and annealing power is plotted in Figure 2. Both thermocouple readings demonstrate linear relationship with annealing power. And both curves can be extrapolated to values close to 300 K (within ±7 K) when annealing power reaches zero. The two thermocouple readings are very close (with maximum difference of 3 K) for the same annealing power. The data used for constructing these temperature-power curves are listed in Table 1.

Table 2 shows an overview of annealing experiments performed in this work. And the detailed experimental conditions are listed in Table 3. Please note that for 2-layer experiments, there are two groups which have very close deposition conditions, denoted as 2-layer A, and 2-layer B, respectively. The annealing is not available for 1-layer oxygen experiment due to the electronics failure for that run.

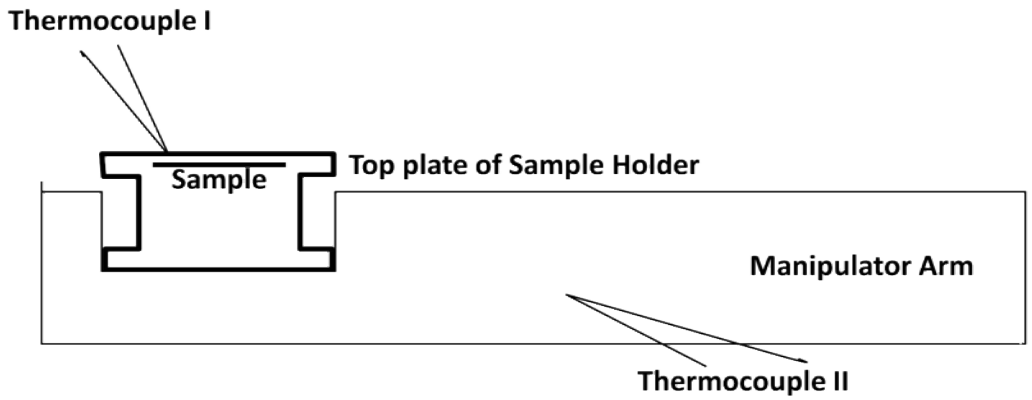

Fig. 1. Schematic diagram of temperature-measurement system.

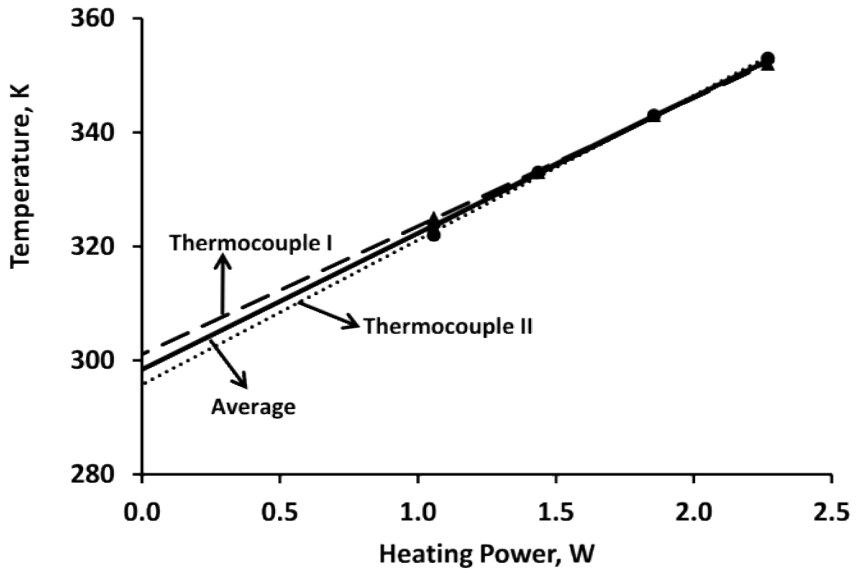

Fig. 2. Relation between measured temperature and annealing power. Measured temperature is plotted as a function of annealing power. The dashed line corresponds to the temperature measured by Thermocouple I, the dotted line corresponds to Thermocouple II, and the solid line corresponds to the average of the temperature measured by the two thermocouples. All these curves are extrapolated to intercept with y-axis.

Table 1. Data used for constructing temperature-power curves.

Step	Annealing Current, A	Annealing Voltage, V	Annealing Power, W	Temperature by Thermo-couple I, K	Temperature by Thermo-couple II, K	Annealing time, sec
1	0.20	5.289	1.06	322	325	600
2	0.25	5.743	1.44	333	333	900
3	0.30	6.185	1.86	343	343	900
4	0.35	6.481	2.27	353	352	1200

The methods of measuring island height and island density is the same as described in Section 4, Chapter 3. However, the data may not be statistically reliable due to the limited number of images available for analysis. Specifically, for island density, generally only one or two 250×250 nm^2 images are available for analysis. So all the available images are used for island density analysis. For island height, sometimes there are a limited number of islands available for a certain layer thickness, 2-layer islands of the 1-layer annealing experiment, for example. So all islands are used for height analysis in such case.

3. Experimental results and interpretation

3.1. Change of island morphology after annealing

Annealing is performed for clean Ag/Si(111)-7×7 surface at various Ag coverages ranging from 0.51 to 1.96 ML, as shown in Table 2.Detailed conditions of annealing are listed in Table 3. The annealing temperatures are about 310 to 340 K, only about 10 to 40 K higher than room temperature, indicating the annealing is quite mild.

Fig. 3 shows the STM images for clean Ag/Si(111)-7×7 experiments after annealing. For 1-layer experiments (θ=0.51 ML), the islands are too small to make visual inspection for possible

morphology change. For 1+2-layer experiment (θ=0.69 ML), the shape of islands becomes more hexagonal for most islands after annealing, as shown in Fig. 3(c) and 3(d). Since the equilibrium shape for (111) orientation of fcc metal is hexagonal, this change in morphology indicates the annealing condition used for these experiments, even very mild, is effective in expediting the approach to a more stable state. The annealing for 2-layer B experiment (θ=1.96 ML) is a two-step procedure. The annealing power of Step 1 is quite close to that of Steps 1-5 in 1+2-layer experiment, as shown in Table 2. After Step 2, islands also become more hexagonal than those before annealing, as shown in Fig. 3(e) and 3(g). Such change in morphology is an indication that the current annealing condition is effective in promoting island growth towards more stable states, even for a higher initial Ag coverage. It is not very reliable to determine to what extent the process has proceeded or whether it has gone close to completion by only performing the visual inspection of island geometries. However, it could demonstrate a general trend that the very mild annealing used in this study is effective in promoting islands to grow into a more stable shape.

The shape change is not very significant for those of 1-layer control experiment (Fig. 3(a) and 3(b)). This could be attributed to the fact that the island size is too small to make good visual inspection. Besides this, the island density is very low in this group (especially for the surface after annealing), rendering the inspection of island shape much less reliable statistically.

Table 2. Experimental conditions of annealing experiments.

Coverage (θ), ML	Initial island distribution	Annealing available for oxygen experiment?	Annealing setting for oxygen exposure	Annealing available for control?	Annealing setting for control
0.51	1 layer	No	n.a.	Yes	320 K, 45 s
0.69	1+2 layer	Yes	336 K, 240 s (final step)	Yes	336 K, 240 s
1.73	2 layer A	Yes	329 K, 1800 s	Yes	329 K, 1800 s
1.96	2 layer B	Yes	321 K, 90 s (final step)	Yes	324 K, 90 s (final step)

Table 3. Detailed annealing conditions of annealing experiment.

Experiment	Annealing Step	Annealing temperature, K	Cumulative annealing Time, s
1 layer control	1	320	45
1+2 layer	1	313	100
	2	313	160
	3	312	400
	4	309	760
	5	313	1360
	6	336	1600
1+2 layer control	1	336	240
2 layer A	1	320	1800
2 layer A control	1	329	1800
2 layer B	1	311	240
	2	321	330
2 layer B control	1	310	240
	2	324	330

For the Ag/Si(111)-7×7 surfaces after oxygen exposure, islands demonstrate a different trend of change in morphology after annealing. There is no annealing data for 1-layer experiment (θ=0.51 ML) due to electronics failure. For the 1+2-layer experiment (θ=0.69 ML), a series of annealing steps are used to investigate the surface, as shown in Table 3. STM images are shown for each step in Fig. 4. Unfortunately, starting from Fig. 4(g), the images are affected by distortion and a a multiple-tip effect to varying extents. From Fig. 4(a) to 4(l), which correspond to Step 0-5 (where 0 is denoted as "before annealing"), there is no evidence that the island shape becomes more hexagonal, although the distortion and a a multiple-tip effect make this inspection less reliable. For Step 6, where a much higher annealing temperature is reached, the islands show very different morphology, as shown in Fig. 4(m) and 4(n). Islands become much less dense (as will be shown next) and much larger in area.

For 2-layer B experiment (θ=1.96 ML), annealing is a two-step procedure, as mentioned previously. The annealing temperature of Step 1 (311 K) is very close to those of Steps 1-5 of 1+2-layer oxygen experiment (309 to 313 K). However, Step 2 is lower in annealing temperature (321 K) than Step 6 of 1+2-layer oxygen experiment (336 K). STM images of this experiment are shown in Fig. 5. No obvious change of island shape is observed. This probably indicates 2-layer islands are not energetically favored after oxygen exposure.

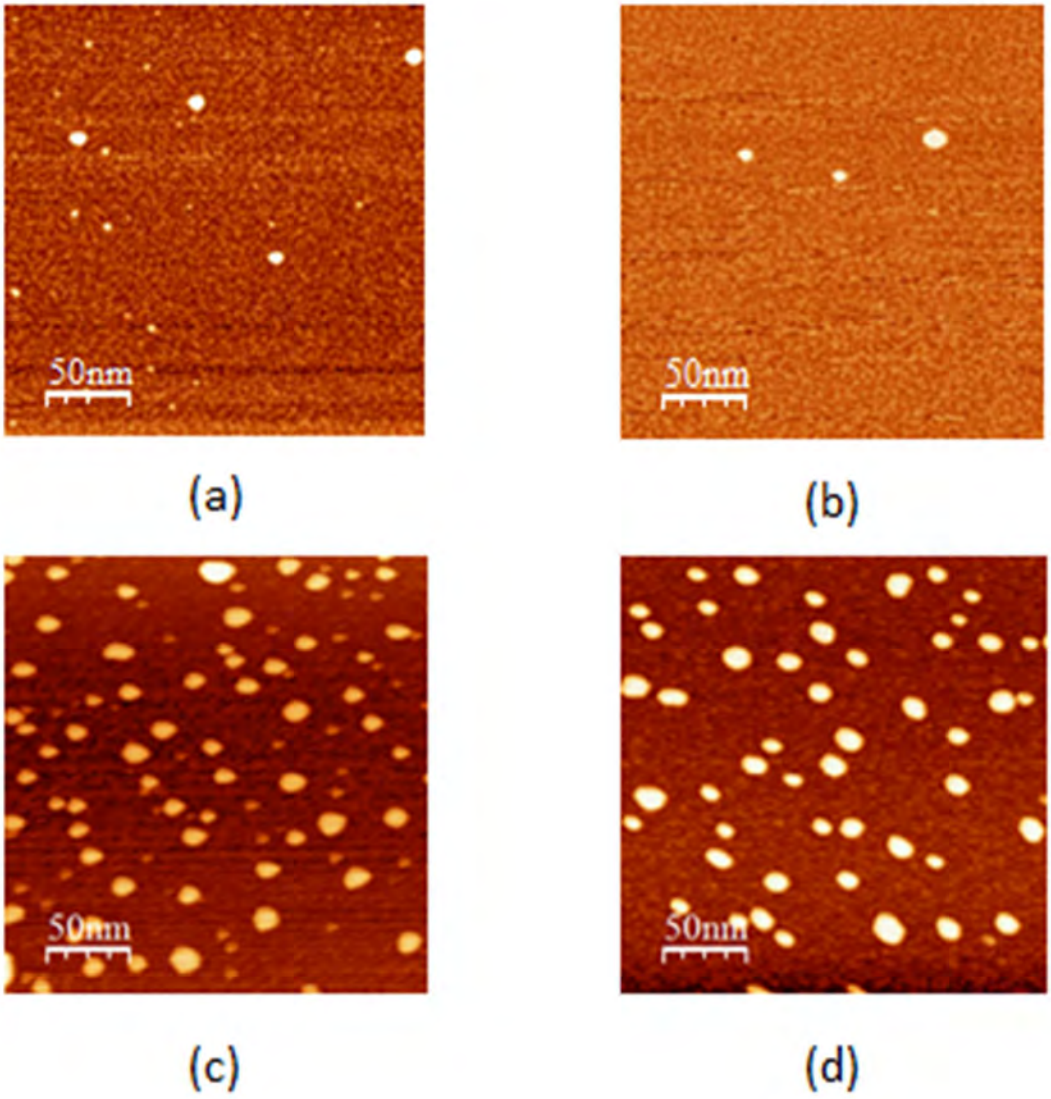

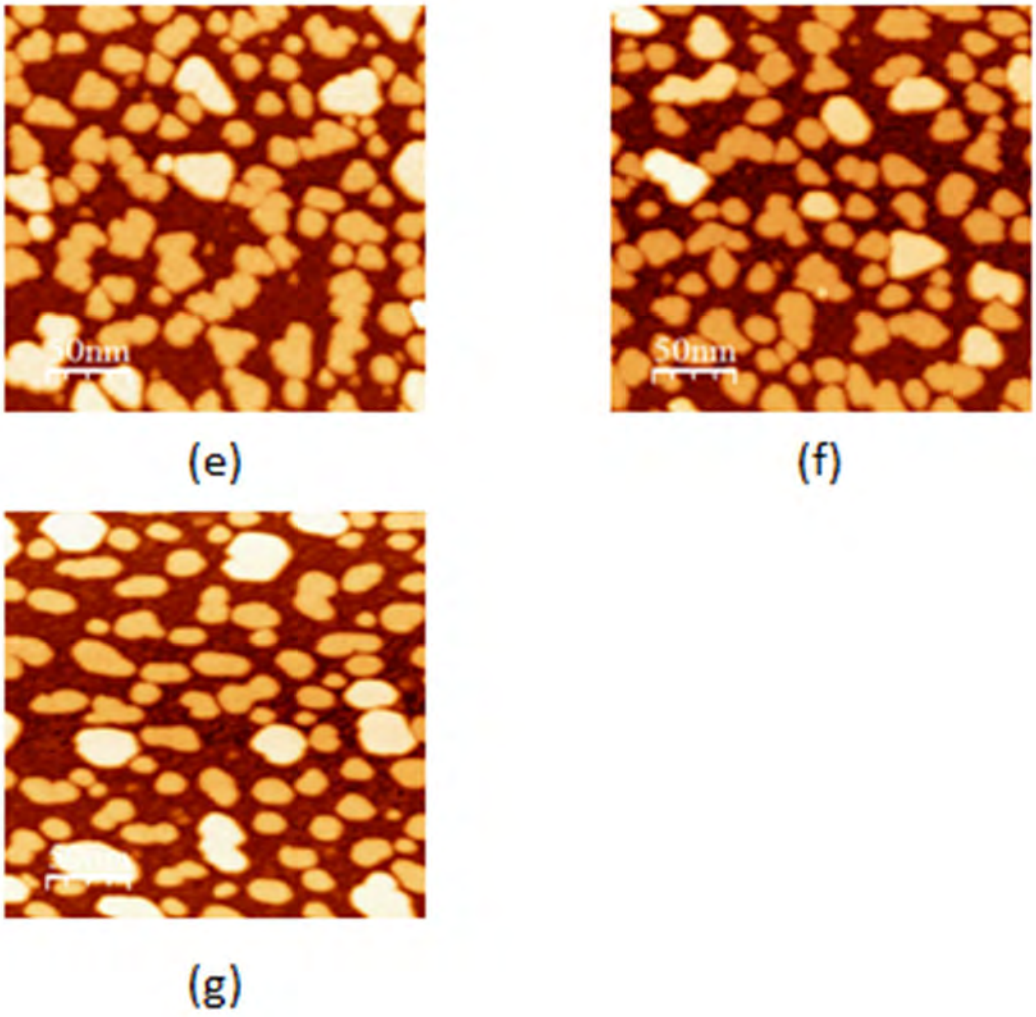

Fig. 3. STM images of clean Ag/Si(111)-7×7 surfaces after annealing. (a) 1-layer control experiment (θ=0.51 ML), before annealing, (b) 1-layer control experiment (θ=0.51 ML), after annealing, (c) 1+2-layer control experiment (θ=0.69 ML), before annealing, (d) 1+2-layer control experiment (θ=0.69 ML), after annealing, (e) 2-layer B control experiment (θ=1.96 ML), before annealing, (f) 2-layer B control experiment (θ=1.96 ML), after annealing Step 1, (g) 2-layer B control experiment (θ=1.96 ML), after annealing Step 2.

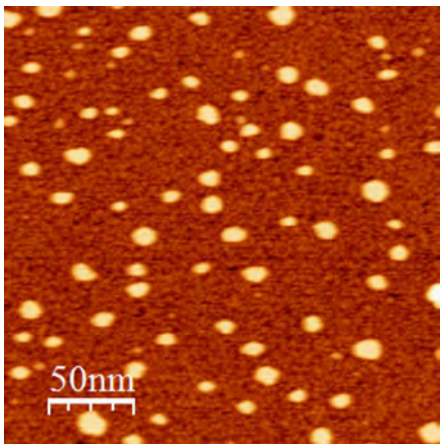

(a)

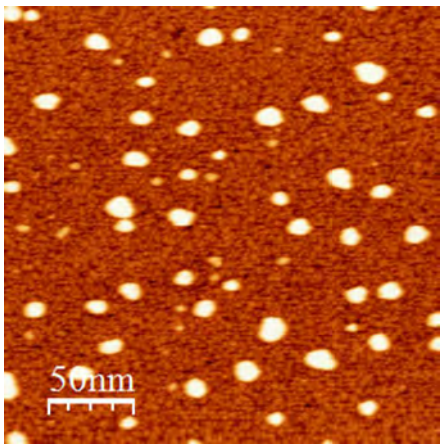

(b)

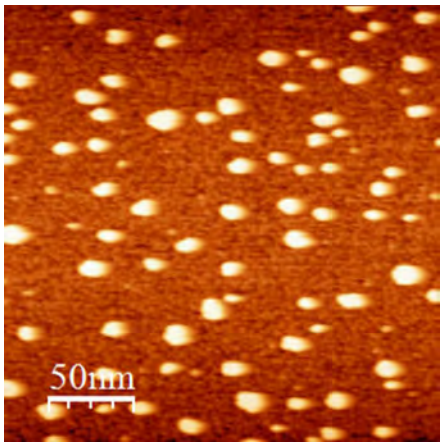

(c)

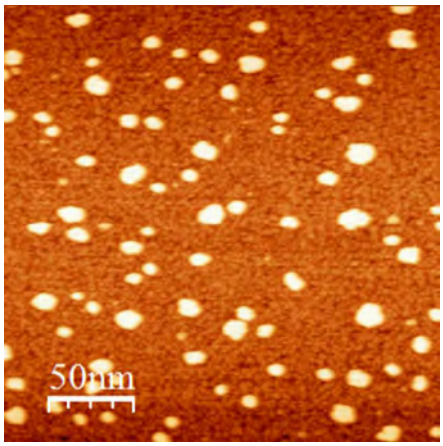

(d)

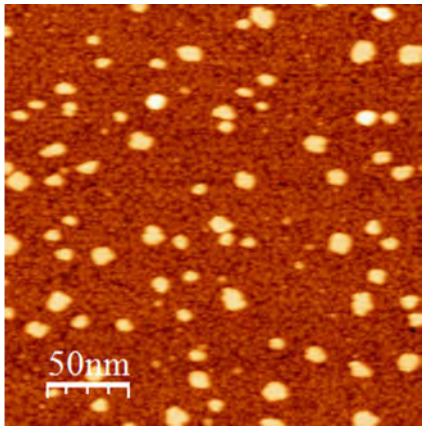

(e)

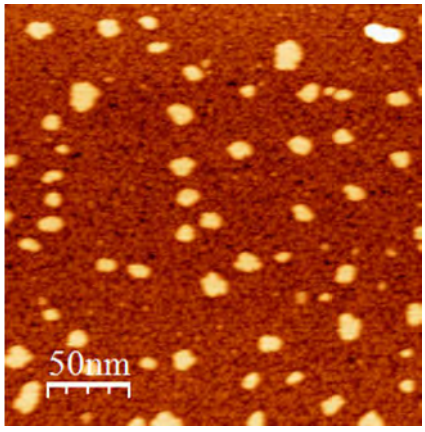

(f)

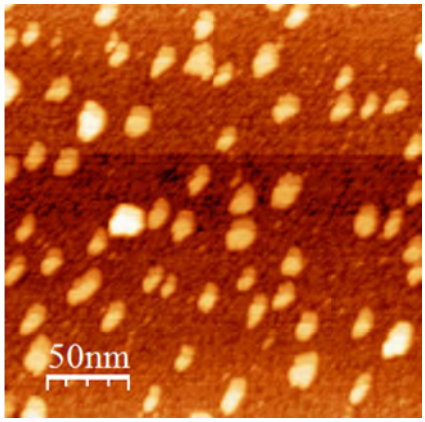

(g)

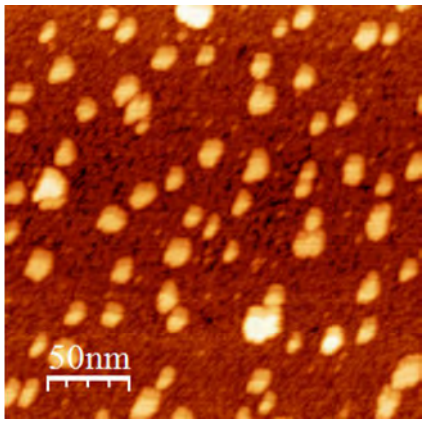

(h)

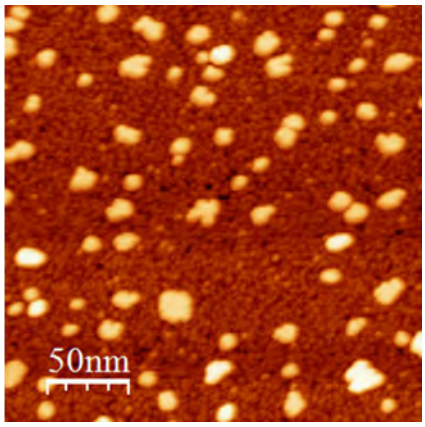

(i)

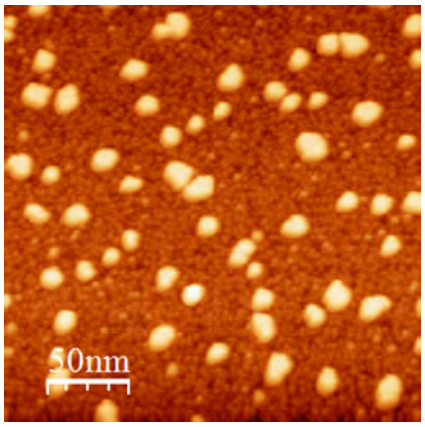

(j)

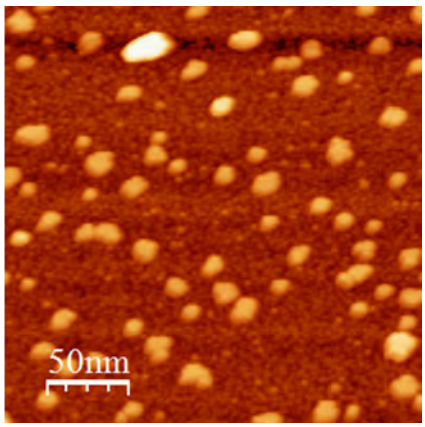

(k)

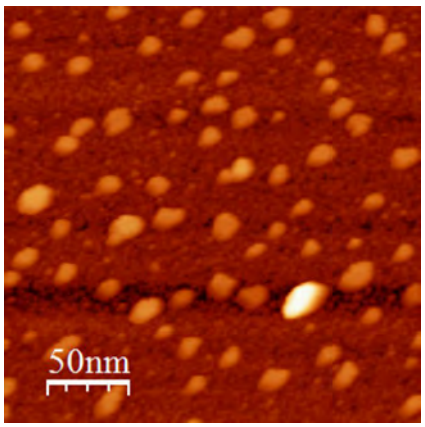

(l)

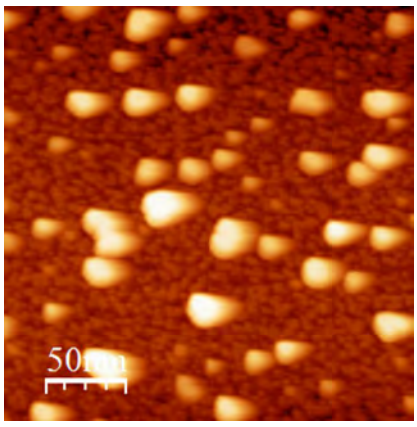

(m)

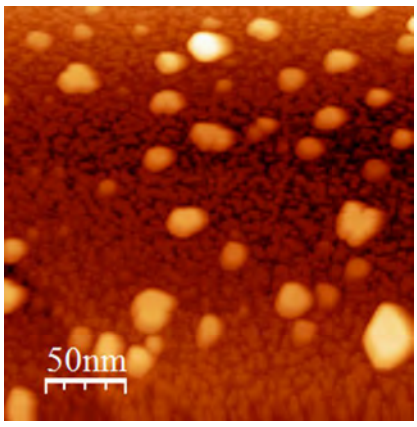

(n)

Fig. 4. STM images of Ag/Si(111)-7×7 surfaces after oxygen exposure and the subsequent annealing. 1+2-layer experiment (θ=0.69 ML), oxygen exposure is 100 *L*. (a, b) before annealing, (c, d) After Annealing Step 1, (e, f) After Annealing Step 2, (g, h) After Annealing Step 3, (i, j) After Annealing Step 4, (k, l) After Annealing Step 5, (m, n) After Annealing Step 6. Images are 250×250 nm^2, taken at -1.0 V tip bias, 0.5 nA tunneling current.

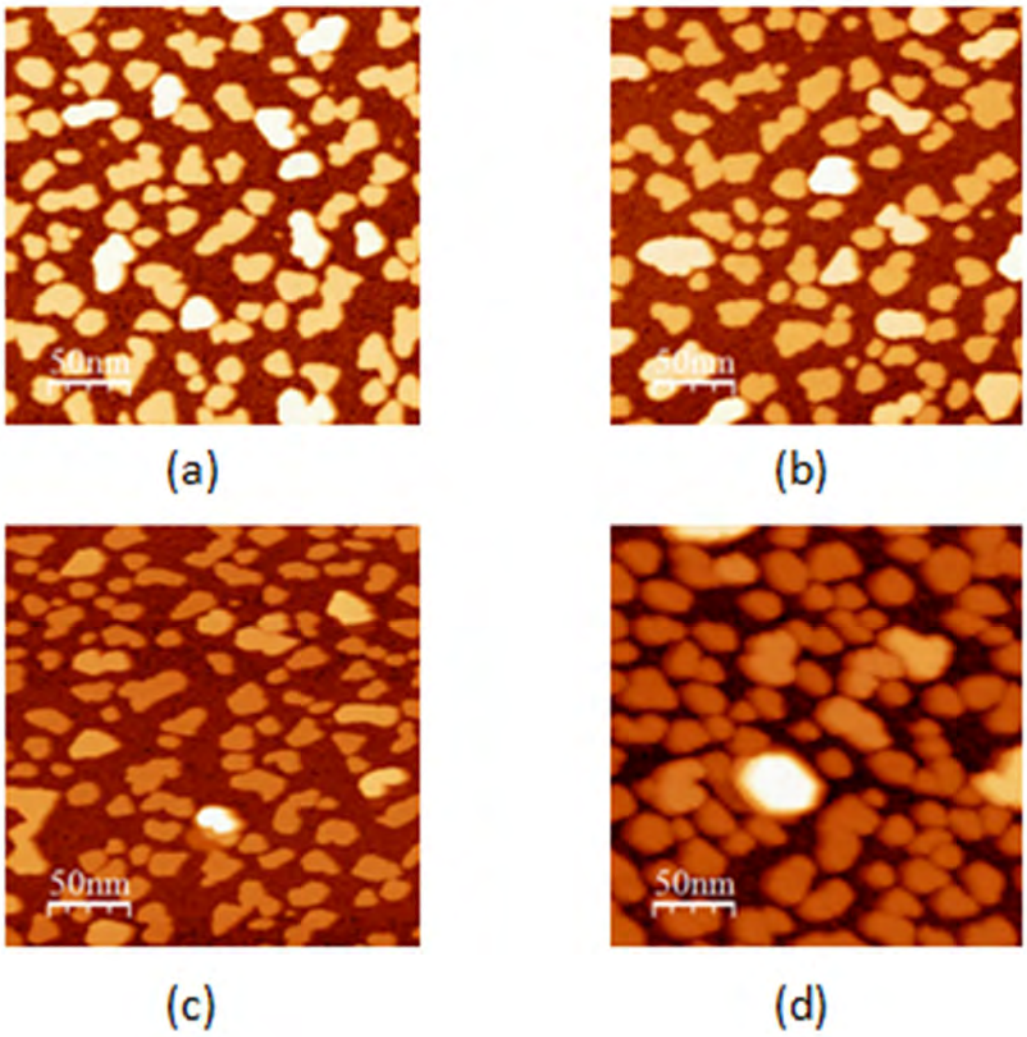

Fig. 5. STM images of Ag/Si(111)-7×7 surfaces after oxygen exposure and the subsequent annealing. 2-layer B experiment (θ=1.96 ML), oxygen exposure is 100 *L*. (a, b) before annealing, (c) After Annealing Step 1, (d) After Annealing Step 2. Images are 250×250 nm^2, taken at -1.0 V tip bias, 0.5 nA tunneling current.

3.2. Change of island height distribution after annealing

For clean Ag/Si(111)-7×7 surfaces, Fig. 6 - Fig. 8 show the island height distribution of these experiments before and after annealing. For 1-layer experiment, the distribution is greatly changed after annealing, as shown in Fig. 6. The relative population of 2-layer islands is increased from 15.2% to 80.0%, accompanied by a great decrease of that of 1-layer islands (from 84.8% to 20.0%).

A similar trend is also seen for 1+2-layer experiment (Fig. 7), where the relative population of 2-layer islands is increased from 60.0% to 91.5%, while that of 1-layer islands is decreased from 40.0% to 8.49%. This trend is consistent with other studies [2] that the 2-layer islands are energetically favored than islands of other layer thickness at 300 K.

For the 2-layer B experiment (Fig. 8), the trend that 2-layer islands are favored is still preserved, although the increase of relative population of 2-layer islands is not as significant as those of the other two experiments. A possible explanation could be that the initial distribution is already closer to the more energetically stable state than the other two experiments are, so not much room is left for the distribution to further approach that state. For the 2-layer B experiment, one feature in the data that cannot be overlooked is that the relative population of 3-layer islands does not change much after annealing (it decreases from 15.6% to 14.4%), as shown in Fig. 8. One might expect a more significant decrease. A plausible explanation may be that the conversion from 3-layer to 2-layer islands requires heavier annealing to overcome the kinetic barriers.

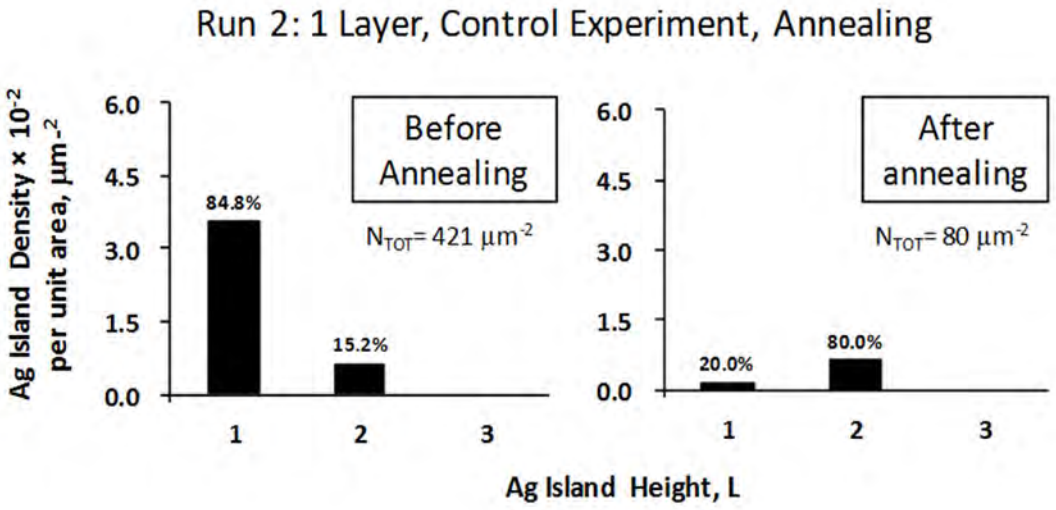

Fig. 6. Island height distribution before and after annealing for 1-layer (θ=0.51 ML), the control experiment. The percentage numbers above each column are the relative populations for an island of each layer thickness. N_{TOT} is denoted as the total island density of all islands, in units of μm^{-2}.

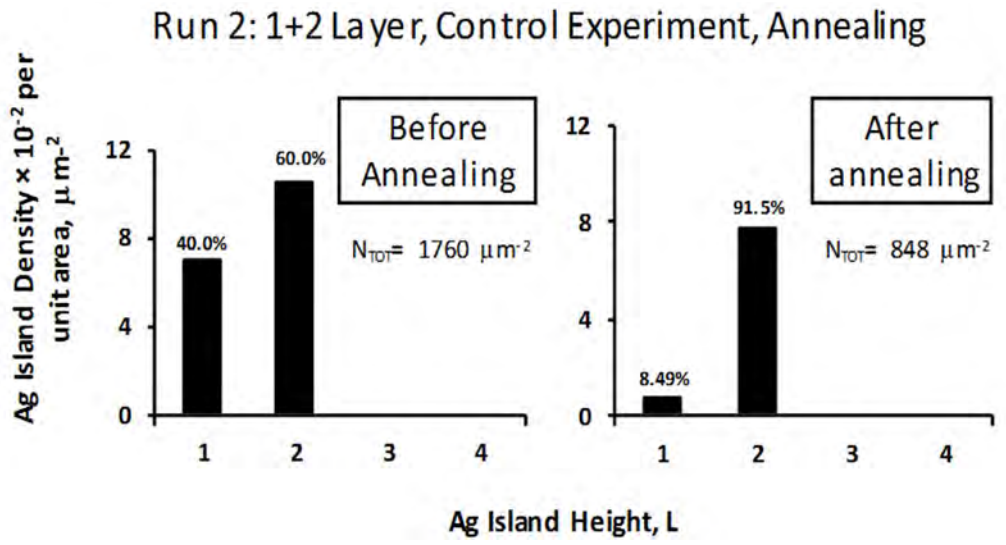

Fig. 7. Island height distribution before and after annealing for 1+2-layer (θ=0.69 ML), the control experiment. The percentage numbers above each column are the relative populations for an island of each layer thickness. N_{TOT} is denoted as the total island density of all islands, in units of μm^{-2}.

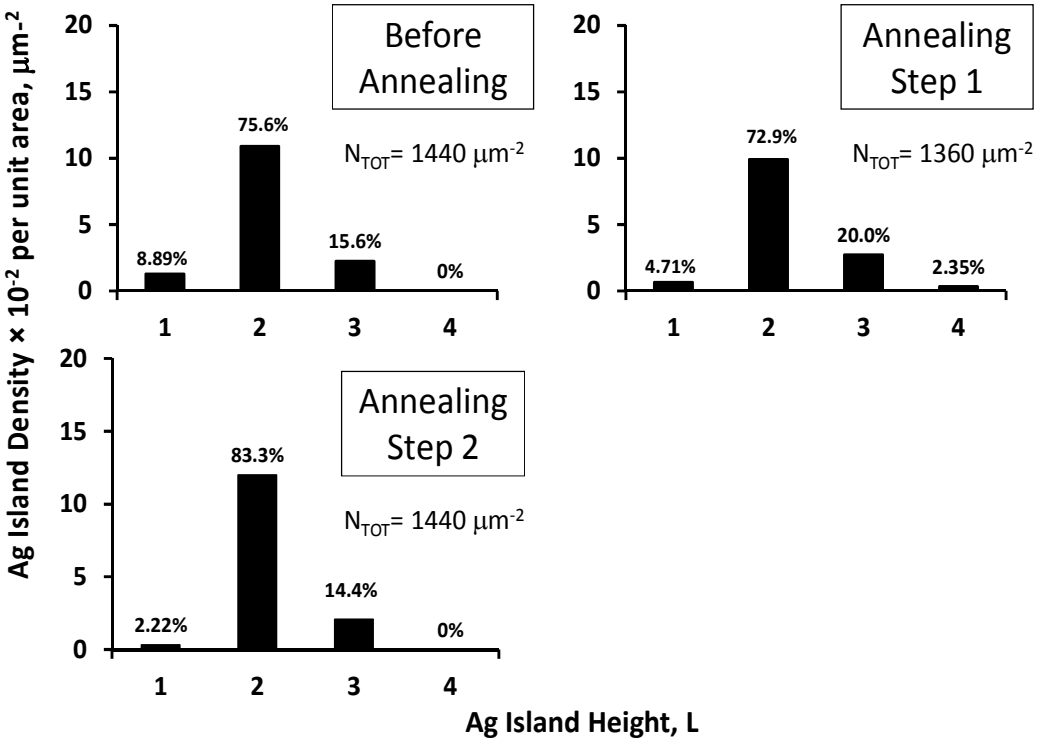

Fig. 8. Island height distribution before and after annealing for 2-layer (θ=1.96 ML), the control experiment. The percentage numbers above each column are the relative populations for an island of each layer thickness. N_{TOT} is denoted as the total island density of all islands, in units of μm^{-2}.

For the Ag/Si(111)-7×7 surfaces after oxygen exposure, islands demonstrate a different trend of change in island height distribution after annealing The analysis of island height distribution for 1-layer experiment (θ=0.51 ML) is not available due to electronics failure.

Fig. 9 shows the trend of relative island population after annealing for 1+2-layer experiment (θ=0.69 ML). Distribution of absolute island density is shown in Fig. 11. (Data from Step 3 are excluded due to severe distortion and a a multiple-tip effect). Step 0 is

denoted as the surface before annealing. From Step 0 to 5 (Step 6, where a more drastic annealing is used, will be mentioned separately later), there is no monotonic change over annealing steps for islands of any layer thickness. For 3-layer islands, however, there is a decreasing trend of relative population if the comparison is performed between Steps 0-2 and 4-5. For 1- and 2-layer islands, the relative population basically remains constant, except for Step 5, where 2-layer islands show a significant increase. These trends may indicate that annealing promotes the distribution moving to equilibrium similar to that of the clean surface even with oxygen present. And if this is the case, then the effect of oxygen (promoting the growth of 3-layer islands) could be most likely attributed to a kinetic-limited scenario. However, the fact that island shape does not become more hexagonal makes this argument less credible. The limited number of sample analyzed (only 1 or 2 images of 250 x 250 nm^2) may also seriously compromise the credibility of the analysis.

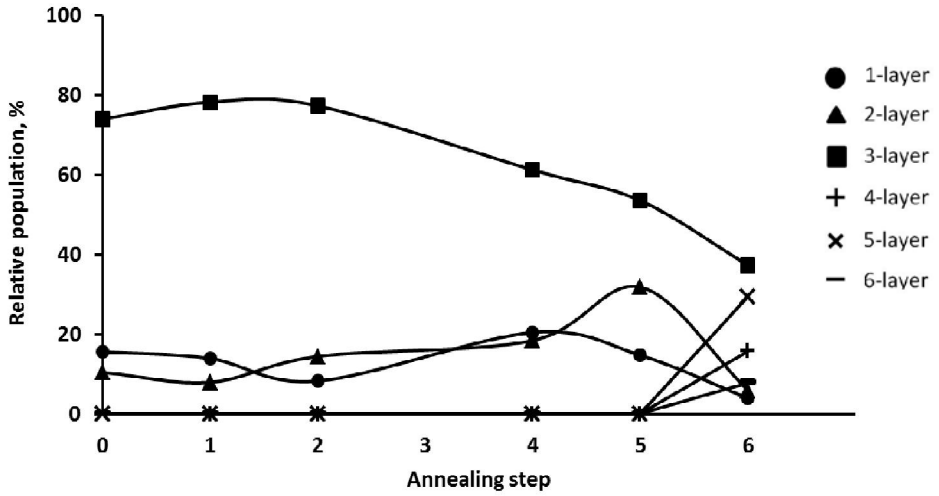

Fig. 9. Trends of relative island population over annealing steps, for an island of each layer thickness. Run 2: 1+2-layer experiment (θ=0.69 ML), 100 *L* oxygen exposure. Circles show 1-layer islands, triangles show 2-layer islands, squares show 3-layer islands, crosses show 4-layer islands, x's show 5-layer islands, and horizontal lines show 6-layer islands. For Step 3,

data are absent due to severe distortion and a a multiple-tip effect. Step 0 is denoted as "before annealing".

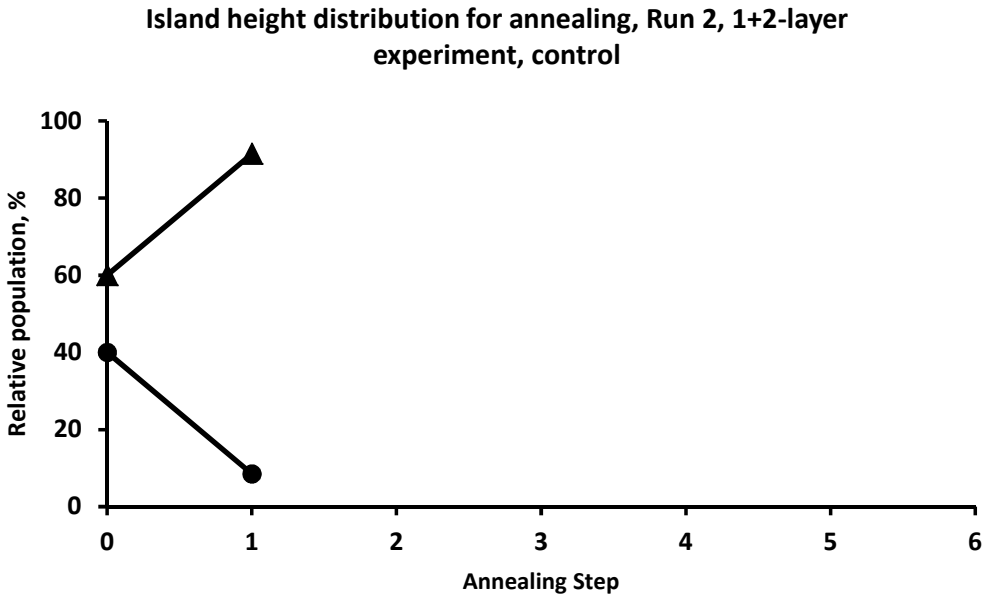

Fig. 10. Trends of relative island population over annealing steps, for an island of each layer thickness. Run 2: 1+2-layer experiment (θ=0.69 ML), the control experiment. Circles show 1-layer islands, triangles show 2-layer islands,. Step 0 is denoted as "before annealing".

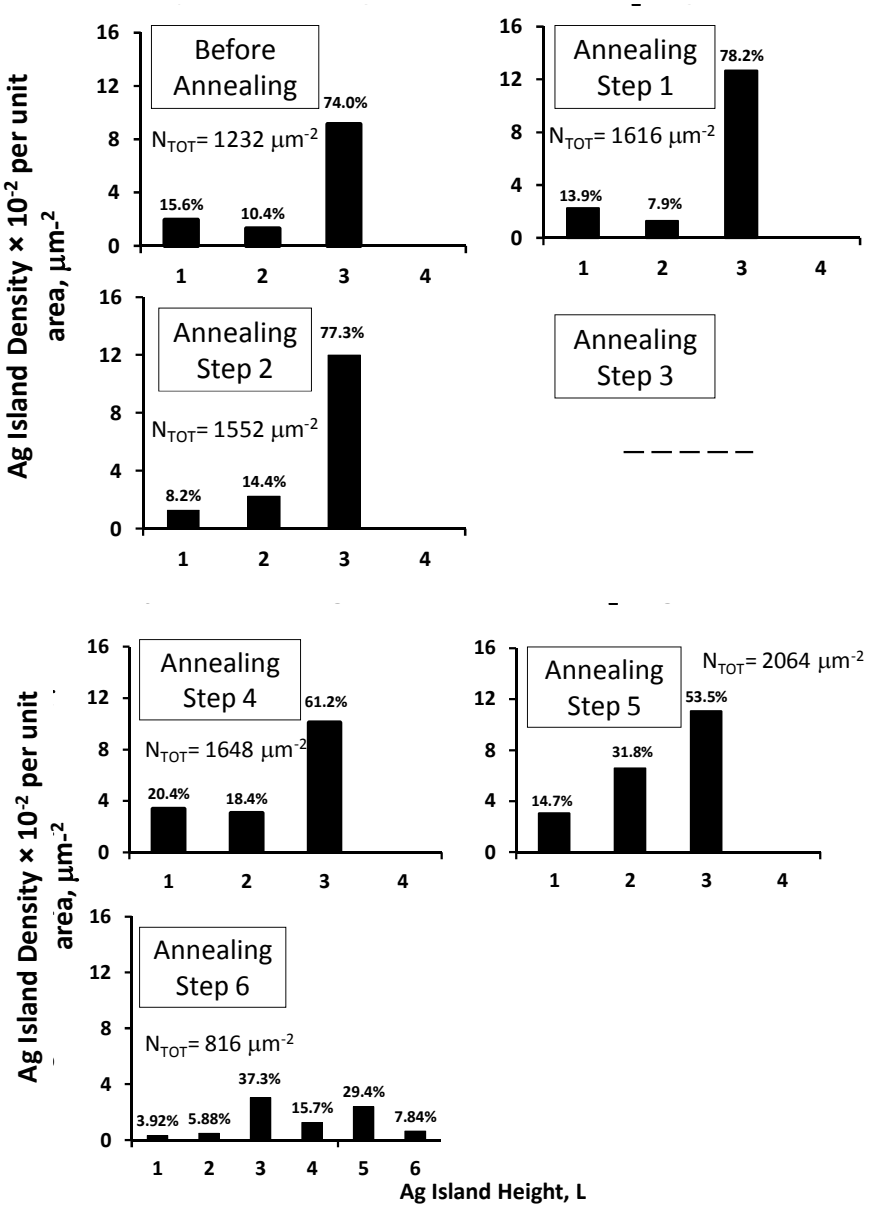

Fig. 11. Island height distribution before and after annealing for 1+2-layer (θ=0.69 ML), 100 *L* oxygen exposure. The percentage numbers above each column are the relative populations for an island of each layer thickness. N_{TOT} is denoted as the total island density of all islands, in units of μm^{-2}. Data from Step 3 is absent due to severe distortion and multiple tip effect.

For Step 6, where a much higher annealing temperature is measured (336 K compared with 309 – 313 K from Steps 1-5, shown in Table 3), the island distribution changes

significantly. The relative population of 1-, 2-, and 3-layer islands all decrease to varying extents. In the meanwhile, many higher islands are detected, including those of 4-, 5-, and even 6-layer high, as shown in Fig. 9. . This change, combined with the fact that oxygen adsorption promotes the growth of 3-layer islands before annealing, further confirms that oxygen adsorption probably modifies the island height distribution energetically, since if it is only a kinetic effect, then a stronger annealing would have further helped the surface return to the scenario where 2-layer islands dominate. This transition to higher islands occurs at 336 K, as determined via the calibration curve shown in Fig. 2. A similar transition for clean Ag/Si(111)-7×7 has also been reported, but at a much higher temperature (450 K)[2].

A similar graph of such trend for the control experiment is shown in Fig. 10, where there is a increase of relative population of 2-layer islands with the decrease of that of 1-layer islands. Such trend is consistent with other control experiments.

For the 2-layer B experiment, similar trend is also observed after annealing. After the Annealing Step 1 (311 K), no obvious change in island height distribution occurs, as shown in the images in the upper panel of Fig.12. However, after Annealing Step 2 (321 K), higher islands are found. Besides islands of 4- to 6-layers high, even higher islands such as 7-, 8-, and 9-layers high are observed (lower panel of Fig. 12).Such trend agrees with the 1+2-layer experiment after annealing. The temperature needed for this transition to occur is 321 K, which is 15 K lower than the one needed for such transition to occur for 1+2-layer experiment. A possible explanation is that with higher Ag coverage, the initial distribution is already closer to state that is energetically stable. So less energy is needed for the surface to approach that state.

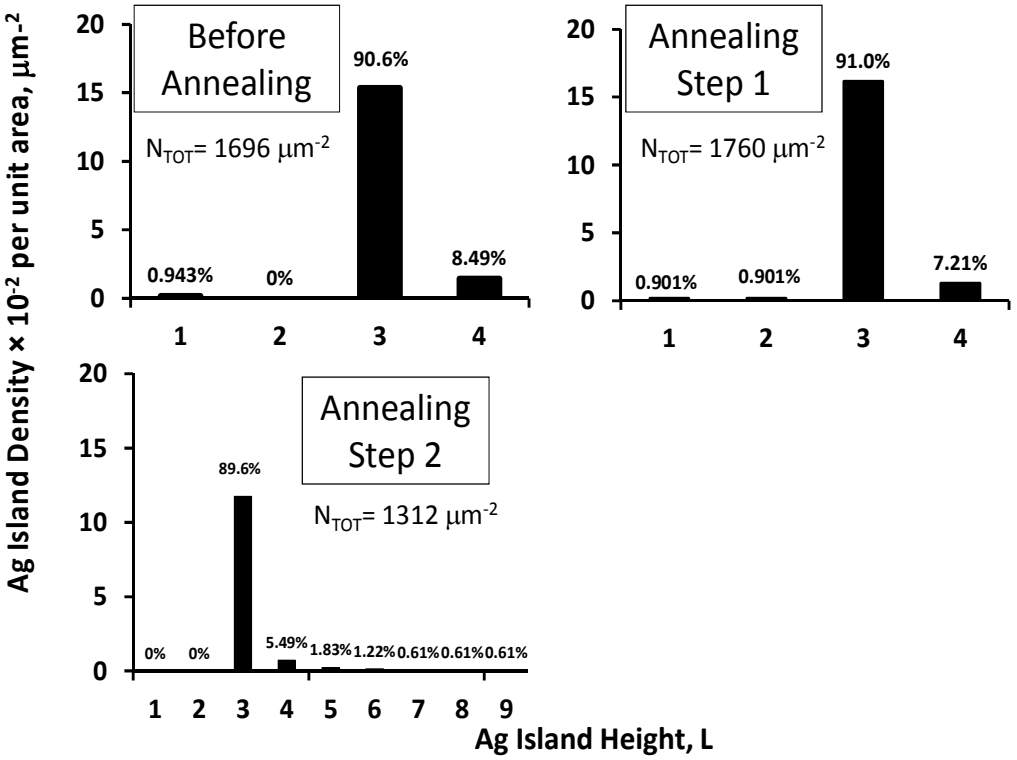

Fig. 12. Island height distribution before and after annealing for 2-layer B experiment (θ=1.96 ML), 100 *L* oxygen exposure. The percentage numbers above each column are the relative populations for an island of each layer thickness. N_{TOT} is denoted as the total island density of all islands, in units of μm^{-2}.

3.3. The conversion to Si(111)-(√3×√3)R30°-Ag-like structure

Si(111)-(√3×√3)R30°-Ag-called √3 herein-is a well studied system [5-9] . It is formed when Ag is deposited on Si(111)-7×7 and subsequently annealed to 500-900 K[5]. There has been much debate about the structure of √hat the atomic level. To date, the most accepted models are inequivalent triangle (IET) [6] and the honeycomb chain trimer (HCT) [7]. They are closely related to each other. When the conversion from Si(111)-7×7 to √3 is completed, the system shows an "island-hole" morphology to balance the Si mass, with holes denoted as 2-dimensional features lower than the Si(111)-7×7, and islands as those higher. It is generally

believed that the areal ratio of island to hole (R_{IH}) is close to 1 [8]. But this value is reported to be far from 1 and depends on preparation history √3 [9]. Based on this study [9], R_{IH} reaches up to 6 after Ag deposition at 500 K. And as the Ag deposition temperature increases, it gradually decreases. Eventually at 800 K Ag deposition, it falls down to 1. Such significant deviation of R_{IH} is ascribed to the accumulation of Ag-rich features at island rims. These Ag-rich features would contribute to holes at higher temperature. Such idea is supported by Ueno *et al* who report √3 island edges serve as reservoirs for adatom gas of Ag [13].

In this study, annealing for 30 min promotes similar conversion for the 2-layer A (θ=1.73 ML) experiment. But the annealing temperature is only in the range of 320-330 K. Such conversion occurs to both the control and oxygen experiments.STM images of the surface before and after conversion are shown in Fig. 13. Specifically, for Fig. 13(d), the height difference is so big that the substrate is not imaged in good resolution. To improve that, part of the substrate is extracted and is shown separately as an expansion of Fig. 13(d). For Fig. 13(b) (clean surface) and the expansion of Fig. 13(d) (after oxygen exposure), there are dark and bright features that resemble the holes and islands on the √d surface from published studies [9,10]. Atypical line profile is shown for both surfaces. The line profiles correspond to solid lines drawn in these images. To construct a statistical analysis for the dimensions of these features, 20 such line profiles are collected to determine the depth of holes and height of islands. The data are shown in Table 4. The level of the original Si(111)-7×7 surface is referred as level zero for the depths and heights.

Table 4. Depth of holes and height of islands of the surface after conversion to √3-like structure. The 2-layer A experiments. Each number is based on the average of 20 line profiles.

	Depth of holes, nm	Height of islands, nm
Clean Ag/Si surface	0.14 ± 0.03	0.19 ± 0.04
Ag/Si surface after oxygen exposure	0.18 ± 0.02	0.20 ± 0.03

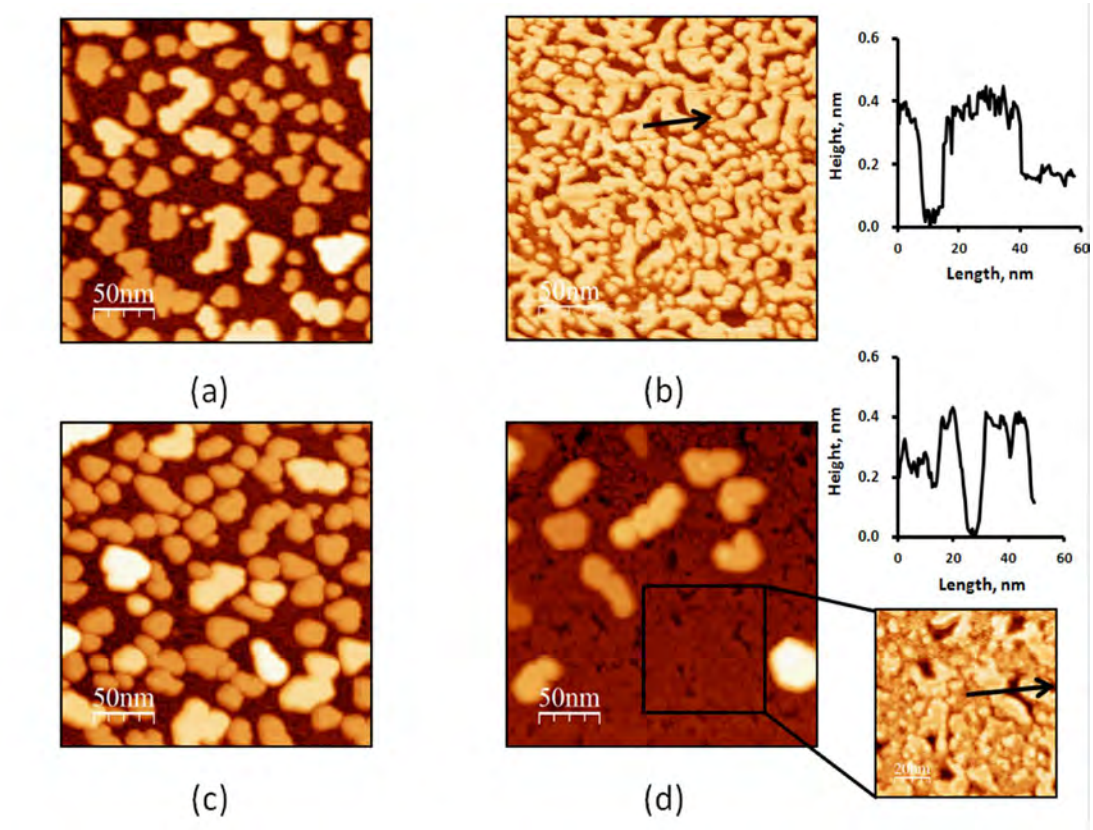

Fig. 13. Representative STM images of Ag/Si(111)-7×7 surface. A √3-like structure appears after 30 min annealing at 320-330 K. The 2-layer A experiment, 100 *L* oxygen exposure. (a) clean Ag/Si surface before annealing, (b) clean Ag/Si surface after annealing. The image to the right of (b) is a line profile corresponding to the solid line with an arrow in (b). The direction of the arrow corresponds to the direction of x+ in the line profile. (c) oxygen-covered surface before annealing, (d) oxygen-covered surface after annealing. The

smaller image to the right of (d) is an expansion of the boxed area in (d). The line profile above this image corresponds to the solid line drawn in it. The direction of the arrow corresponds to the direction of x+ in the line profile. Images (a)-(d) are 250×250 nm^2, the expansion image of (d) is 100×100 nm^2, all images are taken at -1.0 V tip bias, 0.5 nA tunneling current.

The temperature needed for converting to this structure is only about 320 K. This is much lower than 500 K, which is generally the minimum temperature reported for √h conversion [5]. So it is very likely that this is only a partially-converted √3 phase.

Both the clean experiment and oxygen experiment demonstrate √3 pattern after annealing**.** However, the adsorption of oxygen does make an important difference on island height distribution. As shown in Fig. 13(d), higher islands emerge after annealing (4- to 8-, and even 10- and 15-layer islands), while for clean surface, there are no such features.(Please note that the island height here is based on the Si(111)-7×7 surface instead of the wetting layer.)This also indicates that the √3 conversion is only partially finished since Ag islands would not survive the complete conversion to √3.

4. Discussion

The phenomena after annealing in all aforementioned experiments are shown in a schematic diagram in Fig. 14. For control experiments, annealing changes island shape to varying extents. In most of the scenarios islands become more hexagonal, indicating the islands are promoted to an energetically more stable state, since the hexagonal shape is more favorable than are other geometries on fcc (111) orientations. The change in island height distribution that favors 2-layer islands also indicates that annealing is effective in promoting the surface to an energetically more stable state, since 2-layer islands have been reported as the energetically-favored features on Ag/Si(111)-7×7 surface [2,3,11,12].

For the surface after oxygen exposure, the scenario is quite different. Islands do not become more hexagonal. And the island height distribution does not favor 2-layer islands anymore. These may indicate that the energetic preferences of Ag islands may be modified by oxygen adsorption. And this modification probably promotes growth of higher islands. So a likely scenario is that the kinetic barrier for islands to grow higher (>3 layer) is reduced by oxygen adsorption. On the other hand, Gavioli *et al* reports that higher islands emerge for clean Ag/Si(111)-7×7 surface as well, but at a much higher temperature (ca. 450 K) [2]. So there is a possibility that the adsorption of oxygen facilitates such change and makes it possible at a much lower temperature by reducing the kinetic barrier.

For experiments with different initial Ag coverages, the temperatures needed for any of the abovementioned changes to occur are quite different. As shown in Fig. 14, generally the temperatures needed for the 2-layer experiments are 10 to 15 K lower than those for the 1+2-layer experiments. A plausible explanation would be that the initial island distribution

of 2-layer experiments is closer to such stable state so they need less energy to reach there.

The conversion of Si(111)-7×7 to √3 is normally considered as a drastic phase change. Such conversion usually occurs at 500 to 900 K [5]. In this study, a similar conversion is observed, but at a much lower temperature (320 to 330 K). Therefore it is very likely that such conversion is only partially completed. Ag islands survive such conversion for the 2-layer A oxygen experiment, which also supports this idea. The conversion occurs to both the control and oxygen experiments, indicating oxygen is not crucially involved in such process. Instead, the annealing time may play an important role in it. The annealing time is 30 min for the experiments with such √3-like conversion, as shown in Table 3. Such annealing time is much longer than those of other experiments.

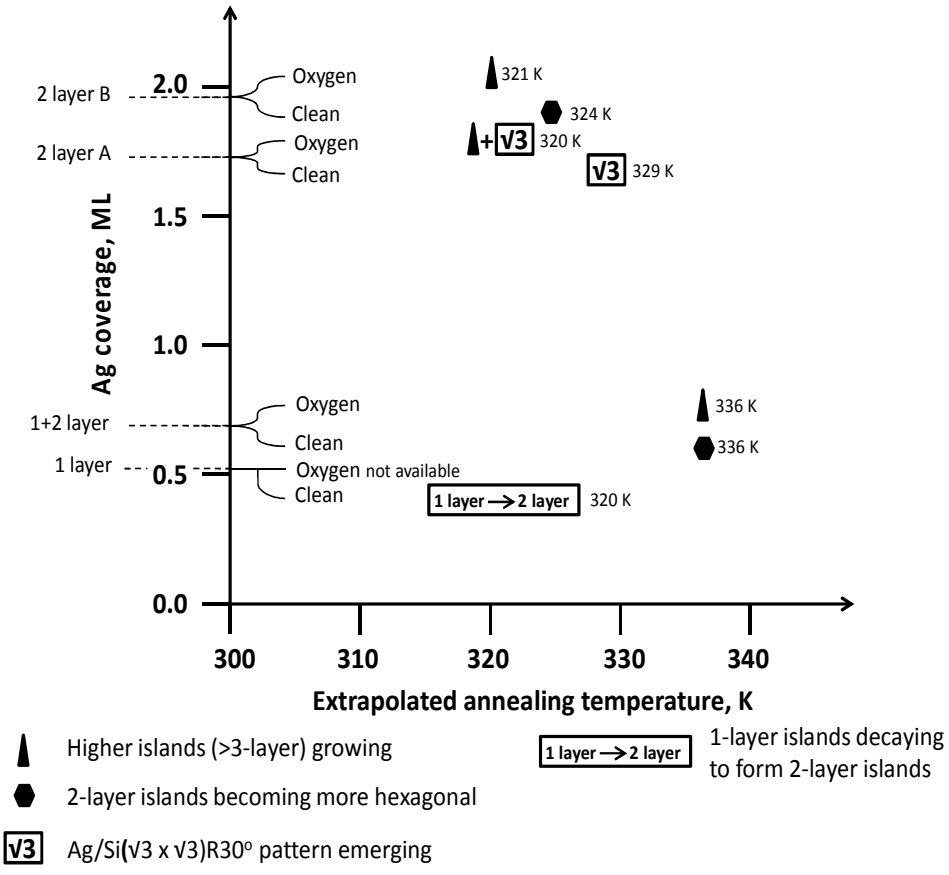

Fig. 14. A schematic diagram of annealing phenomena of all aforementioned experiments.

"Oxygen" represents the experiments with Ag deposition and oxygen exposure of 100 *L*, and "Clean" represents the control experiments.

5. Conclusions

Annealing of Ag/Si(111)-7×7 surface after oxygen exposure is studied. Ag grow into higher islands (> 3 layer) after mild annealings, indicating oxygen probably affect the growth by reducing kinetic barriers to forming 3-D islands. Similar annealings are also performed on control experiments, where 2-layer islands are strongly promoted in terms of island density after annealing. Annealing also modifies island morphology by shaping islands more hexagonally. These changes suggest 2-layer islands are likely to be energetically favored at RT. A long annealing (30 min) is shown to promote the Ag/Si(111)-7×7 surface to convert into a Si(111)-($\sqrt{3}\times\sqrt{3}$)R30°-Ag-like structure, even at very mild annealing conditions (T=320-330 K). The survival of Ag islands during such conversion indicates it is probably a partially converted phase.

Acknowledgements

This work was supported by the Office of Science, Basic Energy Sciences, Material Sciences and Engineering Division of the U.S. Department of Energy (USDOE). This manuscript has been authorized by Iowa State University of Science and Technology under Contract No. DE-AC02-07CH11358 with the U.S. Department of Energy.

References

[1] K. Oura, V. G. Lifshits, A. A. Saranin, A. Z. Zotov, M. Katayama. Surface Science: An introduction. Springer-Verlag, Berlin, Germany, 2003.

[2] L. Gavioli, K.R. Kimberlin, M.C. Triniges, J.F. Wendelken, Z. Zhang. Phys. Rev. Lett. 82 (1999), 129.

[3] B. Unal, A. Belianinov, P.A. Thiel, M.C. Tringides, Phys. Rev. B. 81 (2010), 085411.

[4] D. Shao, X. Liu, N. Lu, C.-Z. Wang, K.-M. Ho, M.C. Tringides, P.A. Thiel, Surf. Sci. 606 (2012), 1871.

[5] V.G. Lifshits, A.A. Saranin, A.V. Zotov, Surface Phases on Silicon: Preparation, Structures, and Properties. Wiley, WestSussex, England, 1994.

[6] H. Aizawa, M. Tsukada, N. Sato, S. Hasegawa, Sur. Sci. 429 (1999), L509.

[7] Y.G. Ding, C.T. Chan, and K.M. Ho, Phys. Rev. Lett. 67 (1991), 1454.

[8] A. Shibata, Y. Kimura, K. Takayanagi, Surf. Sci. 275 (1992), L697.

[9] A. Belianinov, B. Unal, N. Lu, M. Ji, K.-M. Ho, C.-Z. Wang, M.C. Tringides, P.A. Thiel, Phys. Rev. B. 82 (2010), 245413.

[10] D.W. McComb, D.J. Moffatt, P.A. Hackett, B.R. Williams, B.F. Mason, Phys. Rev. B. 49 (1994), 17139.

[11] D.K. Goswami, K. Bhattacharjee, B. Satpati, S. Roy, P.V. Satyam, B.N. Dev, Surf. Sci. 601 (2007), 603.

[12] L. Huang, S. Jay Chey, J.H. Weaver, Surf. Sci. 416 (1998), L1101.

[13] M. Ueno, I. Matsuda, C. Liu, and S. Hasegawa, Jpn. J. Appl. Phys. 42 (2003), 4894.

[14] P. Sobotík, I. Ošt'ádal, J. Mysliveček, T. Jarolímek, F. Lavický, Surf. Sci. 482 (2001), 797.

[15] A. Shibata, Y. Kiruma, K. Takayanagi, Surf. Sci. 303 (1994), 161.

CHAPTER 6

ADDITIONAL INFORMATION ABOUT

ANNEALING THE AG/SI(111)-7×7 AFTER OXYGEN EXPOSURE

1.Introduction

This chapter provides additional results of data analysis for Chapter 5. The results consist of island height information, representative line profiles of island height, and Root-Mean-Square (RMS) roughness of wetting layers. The following content is sorted by the initial island height distribution, i.e. 1-layer, 1+2-layer, and 2-layer (corresponding to the 2-layer B experiment mentioned in Chapter 5).

2. Results

2.1. 1-layer experiment

In this group, the annealing is performed for the control experiment, but unfortunately not for the oxygen-exposure experiment, due to an unstable connection in the heating circuit at the time of the experiment. This problem is resolved for later experiments. So the following analysis of this section is based only on clean Ag/Si(111)-7×7 surface.

2.1.1. Island height and representative line profiles

2.1.1.1 Oxygen Experiment

Annealing is not available due to electronic failure.

2.1.1.2 Control Experiment

After annealing, the average height of 2-layer islands is 0.57 nm, based on the only 4 islands imaged. The height of the only one 1-layer island is 0.30 nm. These numbers are consistent with the island heights before annealing, as shown in Table. 1. The data are reported in the format "average value +/- 1 standard deviation". One representative line profile of Ag an island of each layer thickness is shown in Fig. 1.

Table 1. 1-layer, the control experiment (for 100 *L* oxygen exposure), Average island height before and after annealing.

Annealing step	Island height, nm	
0 (Before annealing)	1-layer 0.30 ± 0.01	2-layer 0.58 ± 0.04
1	1-layer 0.30	2-layer 0.57 ± 0.04

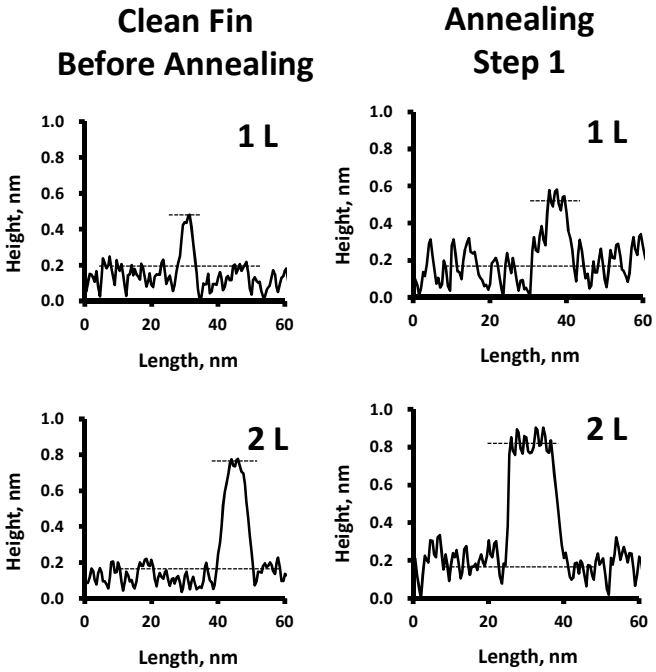

Fig. 1. Run 2: 1-layer, the control experiment (for 100 *L* oxygen exposure). One representative line profile for an island of each layer thickness

2.1.2. RMS roughness of the wetting layer

2.1.2.1 Oxygen Experiment

Annealing is not available due to electronics failure.

2.1.2.2 Control Experiment

The average RMS roughness of the wetting layer after annealing is 0.081±0.005 nm. Compared with the number before annealing (0.055 ± 0.003 nm), it is increased dramatically by 49%. This is quite uncommon in light of the fact that surface usually becomes smoother after annealing. Perhaps the noise level could contribute to this increase of roughness to some extent, since the noise is much more severe after annealing.

Table 2. Run 2: 1-layer, the control experiment (for 100 *L* oxygen exposure). Average RMS roughness of the wetting layer before and after annealing.

Annealing step	Average RMS roughness of the wetting layer, nm
0 (before annealing)	0.055 ± 0.003
1	0.081 ± 0.005

2.2. 1+2-layer experiments

2.2.1. Island height and representative line profiles

2.2.1.1 Oxygen experiment

The average height for an island of each layer thickness corresponding to different annealing steps is shown in Table 3.The data is in the format “average height +/- 1 standard deviation”. For islands of certain heights, only very limited number of islands is detected, so instead of using average value and standard deviation, all available island height data are listed for these islands.

One line profile for an island of each layer thickness before and after annealing is shown as in Fig. 2.

Table 3. Run 2: 1+2-layer, oxygen exposure experiment (100 *L*)..The average height for an island of each layer thickness corresponding to different annealing steps.

Annealing step	Island height, nm		
0(Before annealing)	1-layer 0.29 ± 0.03	2-layer 0.47 ± 0.02	3-layer 0.74 ± 0.01
1	1-layer 0.30 ± 0.02	2-layer 0.48 ± 0.03	3-layer 0.74 ± 0.01
2	1-layer 0.30 ± 0.03	2-layer 0.49 ±0.02	3-layer 0.75 ± 0.04
3	n.a. due to a a multiple-tip effect		
4	1-layer 0.28 ±0.04	2-layer 0.50 ±0.02	3-layer 0.75 ±0.02
5	1-layer 0.31 ± 0.03	2-layer 0.49 ± 0.04	3-layer 0.76 ±0.03
6	1-layer 0.29	2-layer 0.51, 0.50	3-layer 0.77 ± 0.03
	4-layer 1.02 ± 0.02	5-layer 1.24 ± 0.03	6-layer 1.46 ± 0.04

O

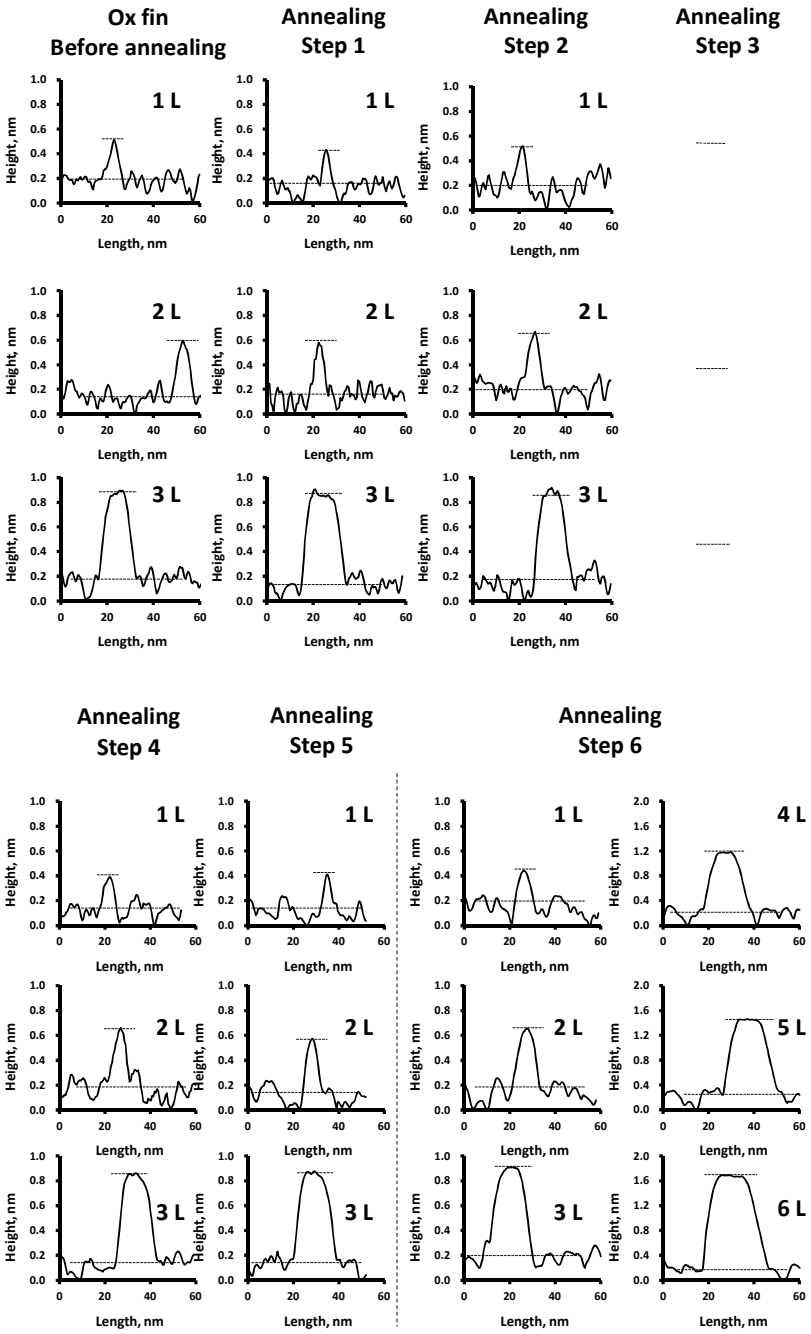

Fig. 2. Run 2: 1+2-layer, oxygen exposure experiment (100 *L*). Representative line profiles for an island of each layer thickness corresponding to each annealing step. Please be noted that for Annealing Step 6, higher y-scale is used for islands of 4-, 5-, and 6-layer. No line profiles are available for Step 3 due to severe a multiple-tip effect.

2.2.1.2 The control experiment

The average height for an island of each layer thickness is shown in Table 4. The data is in the format "average height +/- 1 standard deviation".

Table 4. Run 2: 1+2-layer, the control experiment (for 100 *L* oxygen exposure).

The average height for an island of each layer thickness before and after annealing.

Experiment	1-layer height, nm	2-layer height, nm	3-layer height, nm
Before annealing	0.31 ± 0.02	0.64 ± 0.02	n.a.
After annealing	0.32 ± 0.02	0.63 ± 0.01	n.a.

One line profile for an island of each layer thickness before and after annealing is shown as in Fig. 3.

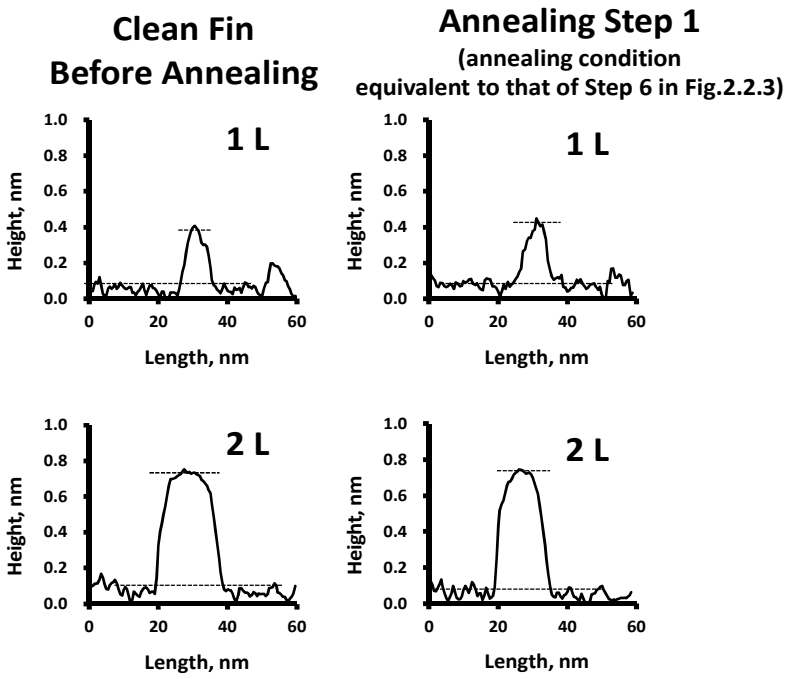

Fig. 3. Run 2: 1+2-layer, the control experiment (for 100 *L* oxygen exposure). Representative

line profiles for an island of each layer thickness before and after annealing.

2.2.2 RMS roughness of the wetting layer

2.2.2.1. Oxygen Experiment

The average RMS roughness of the wetting layer corresponding to each annealing step is listed in Table 5. As the annealing goes on from Step 1 to 6, there is no monotonic change of roughness.

Table 5. Run 2: 1+2-layer, oxygen exposure experiment (100 *L*).

Average RMS roughness of the wetting layer for each annealing step.

Annealing step	Average RMS roughness of the wetting layer, nm
0 (before annealing)	0.080 ± 0.002
1	0.068 ± 0.002
2	0.081 ± 0.003
3	n.a. due to a multiple-tip effect
4	0.059 ± 0.005
5	0.059 ± 0.003
6	0.078 ± 0.002

2.2.2.2. Control Experiment

The average RMS roughness of the wetting layer corresponding to each annealing step is listed in Table 6. After the annealing, the roughness decreases from 0.052 nm to 0.035 nm. This is consistent with the fact that annealing usually flattens sample surfaces.

Table 6. Run 2: 1+2-layer, the control experiment (for 100 *L* oxygen exposure).

Average RMS roughness of the wetting layer for each annealing step.

Annealing step	Average RMS roughness of the wetting layer, nm
0 (before annealing)	0.052 ± 0.002
1(annealing condition equivalent to that of Step 6 in Table 2.2.4)	0.035 ± 0.005

2.3. 2-layer experiment (corresponding to 2-layer B experiment in Chapter 5)

2.3.1. Island height and representative line profiles

2.3.1.1 Oxygen experiment

The average height of an island of each layer thickness corresponding to different annealing steps is shown in Table 7. The data is in the format "average height ± 1 standard deviation". For islands of certain heights, only a limited number of islands are detected, so instead of using average height and standard deviation, all available island height data are used.

Table 7. Run 2: 2-layer, oxygen exposure experiment (100 *L*). The average height for an island of each layer thickness corresponding to different annealing steps.

Annealing step	Island height, nm			
0 (Before annealing)	1-layer 0.29 ± 0.02	2-layer 0.49 ±0.03	3-layer 0.76 ±0.01	4-layer 1.00 ± 0.02
1	1-layer n.a.	2-layer 0.48	3-layer 0.76 ±0.02	4-layer 1.00 ± 0.03
2	1-layer n.a.	2-layer n.a.	3-layer 0.77 ± 0.03	4-layer 1.02 ± 0.02
	5-layer 1.24, 1.23	6-layer 1.53, 1.47	7-layer 1.74	8-layer 2.01
	9-layer 2.24			

One line profile for each kind of island corresponding to different annealing steps is shown as in Fig. 4.

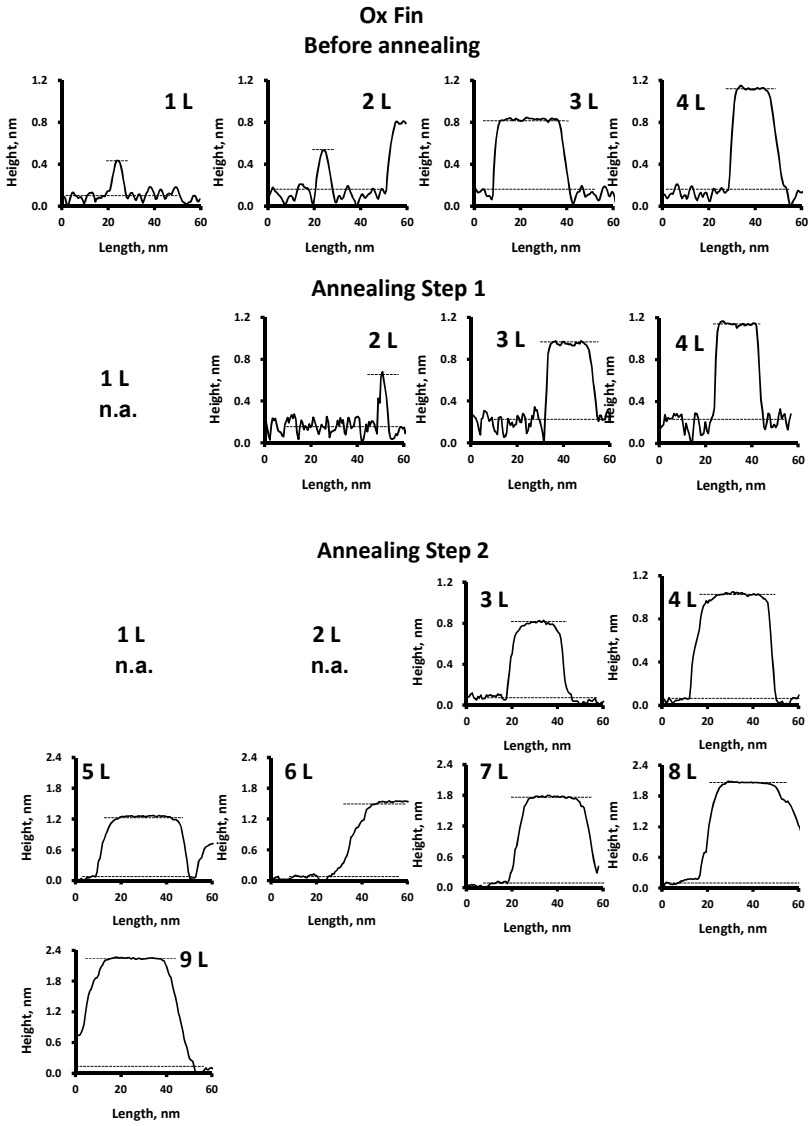

Fig. 4. Run 2: 2-layer B, oxygen exposure experiment (100 *L*). One representative line profile for an island of each layer thickness.

2.3.1.2 Control experiment

The average height of an island of each layer thickness is shown in Table 8. The date are reported in the format "average value +/- 1 standard deviation". Representative line profiles are shown in Fig. 5.

Table 8. Run 2: 2-layer B, the control experiment (for 100 *L* oxygen exposure). The average height for an island of each layer thickness corresponding to different annealing steps.

Annealing step	Island height, nm			
0(Before annealing)	1-layer 0.29 ± 0.02	2-layer 0.64±0.01	3-layer 0.85±0.01	4-layer n.a.
1	1-layer 0.30 ±0.02.	2-layer 0.63 ±0.03	3-layer 0.87±0.03	4-layer 1.14, 1.16
2	1-layer 0.28 ±0.02	2-layer 0.63 ±0.01	3-layer 0.88± 0.01	4-layer n.a.

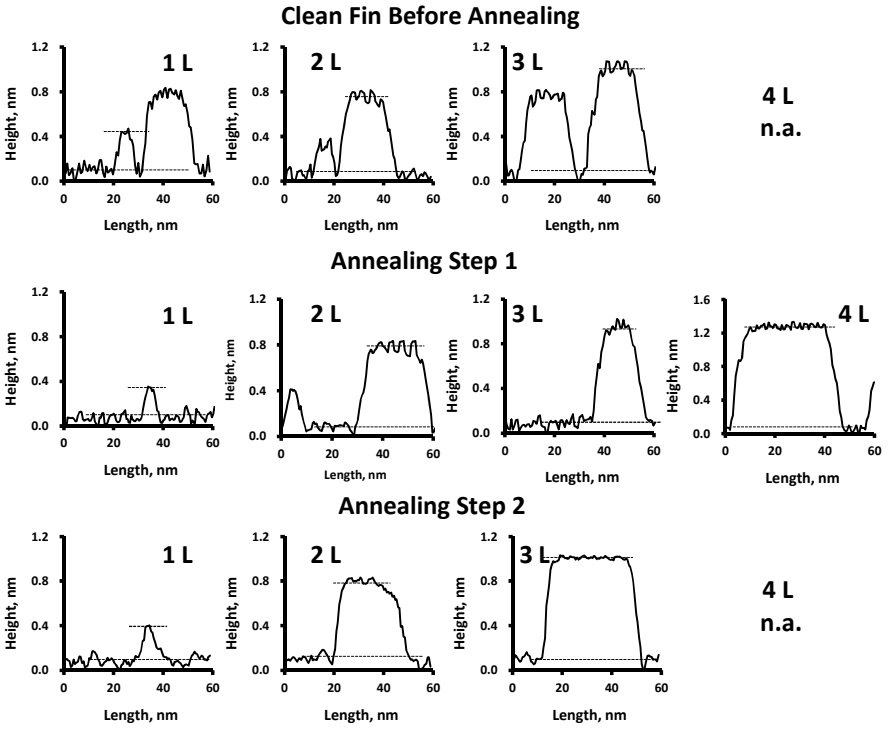

Fig. 5. Run 2: 2-layer B, the control experiment (for 100 *L* oxygen exposure). One representative line profile for an island of each layer thickness is shown.

2.3.2 RMS roughness of the wetting layer

2.3.2.1. Oxygen Experiment

The average RMS roughness of the wetting layer corresponding to each annealing step is listed in Table 9. The roughness remains quite constant until Step 2, where it drops to 0.035 nm, only 48% of the value of "before annealing" and "after Step 1".

Table 9. Run 2: 2-layer B, oxygen exposure experiment (100 *L*).

Average RMS roughness of the wetting layer for each annealing step.

Annealing step	Average RMS roughness of the wetting layer, nm
0 (before annealing)	0.073 ± 0.003
1	0.072 ± 0.003
2	0.035 ± 0.003

2.3.2.2. Control Experiment

The average RMS roughness of the wetting layer corresponding to each annealing step is listed in Table 10. The roughness generally remains constant through annealing.

Table 10. Run 2: 2-layer B, the control experiment (for 100 *L* oxygen exposure).

Average RMS roughness of the wetting layer for each annealing step.

Annealing step	Average RMS roughness of the wetting layer, nm
0 (before annealing)	0.040 ± 0.011
1	0.038± 0.004
2	0.042± 0.003

CHAPTER 7

ADSORPTION OF OXYGEN ON AG/NIAL(110)

A Paper to be submitted

Dahai Shao[1,2], Mark Wallingford[1,2,] Emma Kwolek[1,2], Allison White[1,2], and P.A. Thiel[1,2,3]

[1]Ames Laboratory, [2]Department of Chemistry, and [3]Department of Materials Science and Engineering

Iowa State University, Ames Iowa 50011 USA

Abstract

The morphology of Ag islands on NiAl(110) after oxygen exposure is studied. Ag forms highly-anisotropic islands with a strong height preference of even layers on clean NiAl(110) surface. After 1 *L* oxygen exposure at RT, small depressions appear on upper surface of 1st bilayer (BL) islands, while the 2nd BL islands remain unperturbed. The density of such depressions increases drastically as the cumulative oxygen exposure increases to 11 *L*. The edges of the 1st BL islands are etched and shrink to form indentations at such exposure. The change of morphology is probably attributed to a static form of adsorbed oxygen on Ag islands. In the meantime, the 2nd BL islands still remain unperturbed. A possible explanation is that oxygen may have a higher adsorption energy on 2nd BL islands and thus strongly disfavored. At oxygen exposure up to 111 *L*, 1st BL islands are entirely decomposed into amorphous clusters. Such drastic change may be ascribed to a preferential oxidation of Al and the subsequent formation of a phase of aluminum oxide. The formation of oxide layer may destroy the NiAl(110) surface where Ag islands grow on. 2nd BL islands surprisingly survive such process and remain intact. One possible explanation is that 2nd BL islands may somehow stabilize the surrounding

substrate and prevent it from being oxidized by oxygen. An alternating pattern of ripples are found on island upper surfaces for Ag islands on clean NiAl(110) surface. Such pattern disappear after oxygen exposure and transform into ripples with a uniform spacing.

1. Introduction

The epitaxial growth of nanometer-sized metal film on metal or semiconductor substrate has been studied extensively[1-13]. Among them, Ag growth on binary intermetallic compound NiAl(110) is especially intriguing[6,7,12,13] because of the almost perfect match of their in-plane lattice constant despite the dramatic difference of their bulk-phase crystal structure [6]. The crystal structure of NiAl resembles that of CsCl (bcc, Lattice Constant=0.289 nm) [6], while the crystal structure of Ag is fcc, with a lattice constant of 0.408 nm [14], much larger than the former. However, in the (110) direction, the in-plane lattice constant of the two are very close. For NiAl(110), Ni and Al form inter-penetrating rectangles with one metal at the four corners and the other in the center. The dimensions of these rectangles are 0.409×0.289 nm^2. For Ag(110), Ag atoms form rectangular unit cells with the dimensions of 0.408×0.289 nm^2.So if Ag adatoms adopt the atop sites of NiAl(110) substrate, then the growth of Ag on NiAl(110) would be more homoepitaxial-like due to the absence of a lateral mismatch strain.

An initial bilayer growth mode mediated by quantum size effect has been reported for Ag growth on NiAl(110) [6]. In this study, Ag prefers bilayer islands for the first two levels, showing an fcc Ag(110)-like lateral structure. DFT calculations based on quantum confinement of electrons also show oscillating patterns of surface energy with energy minima at even layers for the first few layers, which supports this experimental observation [6].

Oxygen is reported to have a significant effect on quantum-size-effect-mediated growth

of Ag on Si(111)-7×7 [15]. Specifically, the island height distribution and the wetting layer roughness are reported to be greatly changed by oxygen adsorption at 300 K. The present study shows oxygen adsorption also promotes a dramatic change of surface morphology of the Ag bilayer islands on NiAl(110).

2. Experimental details

The sample used for these studies was used previously in our group for studies that were conducted mainly by Dr. Chad Yuen. These studies concerned Au films on NiAl(110). The origin, growth, and preparation of the sample (external to UHV) is described elsewhere, along with the prior experimental results and some STM images of the clean surface[6].

Experiments were performed in an Omicron variable-temperature, ultrahigh-vacuum (UHV) chamber equipped with Auger electron spectroscopy (AES), X-ray photoelectron spectroscopy (XPS), LEED, and STM. The base pressure of the chamber was 1.2×10^{-8} Pa. The NiAl(110) single crystal sample was cleaned by repeated cycles of Ar^+ sputtering (10 min each sputter position, 3 positions in total, 1 keV, 300 K, $P_{Ar}=2.4 \times 10^{-4}$ Pa) followed by annealing to 1133 K for 20 min, until the surface was judged clean by AES and STM. An AES spectrum is shown in Fig. A-1 of Appendix.

STM images were processed using WSxM software [16].STM images revealed that the sample preparation procedure can produce a NiAl(110) surface with broad terraces. In the data presented in this study specifically, the terraces were up to 120 nm wide. These terraces were separated by steps and step bunches. 50 line scans across these steps demonstrated an average step height of 0.204 nm with a standard deviation of 0.003 nm, identical to the literature value of 0.204 nm estimated from the bulk phase lattice constant of NiAl [17]. This consistency indicated

the piezo-scanner of the STM was calibrated in the z-direction, which was crucial in determining the vertical dimension accurately.

Ag was evaporated at 300 K via a Mantis electron-beam evaporator. Pressure did not exceed 1.4×10^{-8} Pa during the evaporation. The flux was 9×10^{-4} bilayer (BL) s^{-1}. Flux was estimated as the coverage of Ag evaporant per unit time. The coverage used to estimate the flux was based on the area of Ag features, calculated by WSxM software [16].

The sample was exposed to oxygen, at 300 K, by back-filling the chamber through a leak valve. Oxygen pressures were in the range of 4×10^{-7} to 4×10^{-5} Pa. Exposures are given in Langmuirs (L), where 1 L = 1.3 x 10^{-4} Pa s. O_2 (Matheson, lecture bottle, 99.95%) was used without further purification, and its purity was checked against a mass spectrometer in the STM chamber.

The measurement of depth of depressions is based on line profiles. It is very similar to the method of measuring island height, mentioned in Section 4, Chapter 3. The only difference is that the depressions are treated as upside-down islands in such analysis. The approach used for measuring depression area also resembles that mentioned in Section 4, Chapter 3.

Ag coverage is determined with WSxM software and reported in units of monolayer (ML). Similar to the method shown in Section 4, Chapter 3, total coverage θ_{TOT} is determined by Equation 1.

$$\theta_{TOT}=2(\theta_1 + \theta_2) \quad (1)$$

Where θ_{TOT} is the total coverage, θ_1 is the fractional area of all features that are 1-BL high (including all 1-BL islands, and the first level of the 2-BL islands), and θ_2 is the fractional area of all features that are 2-BL high (including the second level of 2-BL islands). The coefficient 2 is introduced since all the fractional areas correspond to bilayer islands therefore it needs to be

converted to monolayer in terms of coverage. The discretion of dividing 2-BL islands into 2 levels simply results from the morphology of such features, where the 2nd level appears as being superimposed onto the 1st level and is usually much smaller in area than the latter. Therefore it can be easily separated from the latter when performing coverage determination, as shown in Fig. 2. Statistically, total coverage is measured based on 5 images with size 250×250 nm^2 each.

3. Experimental results

Fig.1 shows STM images of Ag islands deposited on NiAl(110) at 300 K. The coverage of Ag is 0.54 ML, measured from an extended region of terraces.

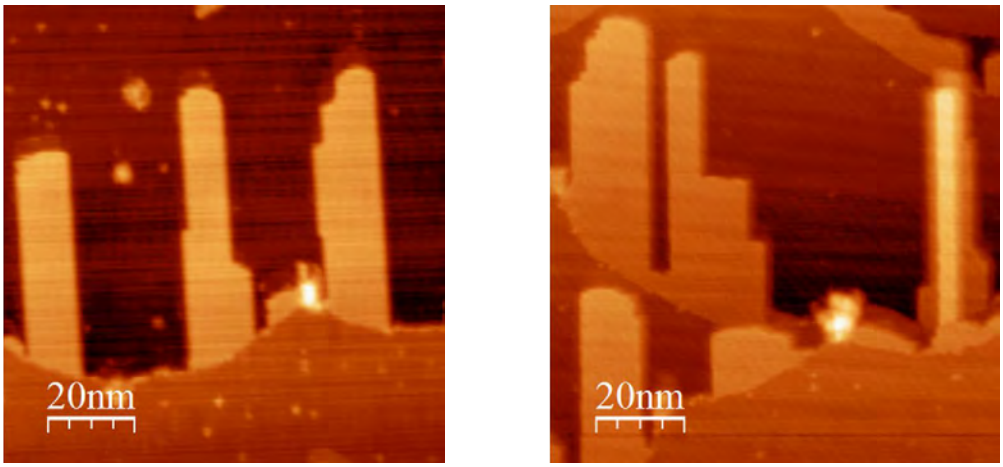

Fig. 1. STM data of Ag on NiAl(110) at 300 K. Image size 100 × 100 nm^2. +1.0 V tip bias, 0.5 nA tunneling current. (a) and (b) are taken from different areas of the surface and are both representative images of the surface.

Consistent with other reported studies [6,12], Ag forms two dimensional islands. These islands grow outward from step edges and form long, fingerlike, highly-anisotropic protrusions, as shown in Fig. 1(a) and 1(b). Analysis of pixel height histograms (taken over a number of 20 regions of islands and their surrounding terraces for islands of each kind indicates most of the islands are 0.32 nm high, with a standard deviation of 0.02 nm, which matches the value reported for the 1st bilayer (BL) islands 0.32 nm [6]. There are also a few features on top of these 1st BL islands, forming even narrower and more rectangular shapes, as shown in Fig. 1(b). Analysis of pixel height histograms indicate the average height of these features is 0.28 nm, with a standard deviation of 0.01 nm, identical to the value reported in literature for the 2nd BL [6].

Histograms are determined through WSxM with a function named “roughness analysis”. For an island of interest, it is cropped into an area along with and only with the surrounding terrace and planed subsequently, before the pixel height histogram is taken. For such area, a histogram is produced through showing mainly two peaks, one corresponding to the substrate terrace, and the other corresponding to the island grown on it, as shown in Fig. 3.The sampled areas usually include nearly equal amounts of island and terrace so the two peaks are comparable in number of pixels. The height of an island is determined from the difference between the two peaks in x-direction of the histogram.

For statistical purposes, 20 areas are sampled for islands of each kind. And the result is reported in the format “average height +/- 1 standard deviation”, in units of nm.

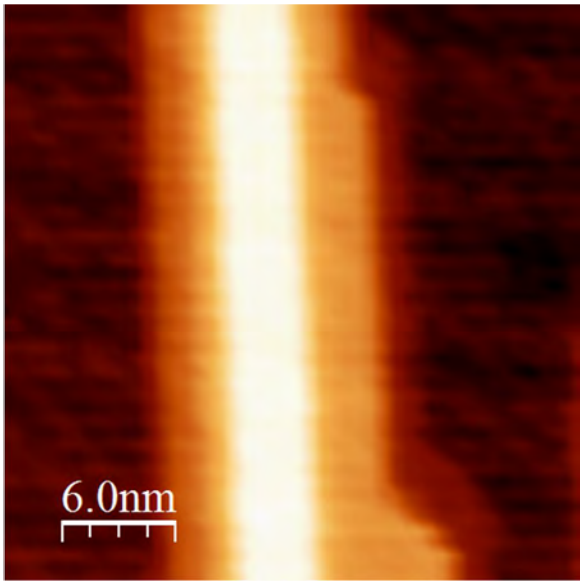

Fig. 2. An STM image of part of a 2nd BL Ag island on NiAl(110), the brightest rod-like feature is the 2nd BL of this island, the slightly darker feature which surrounds the 2nd BL is the 1st BL of

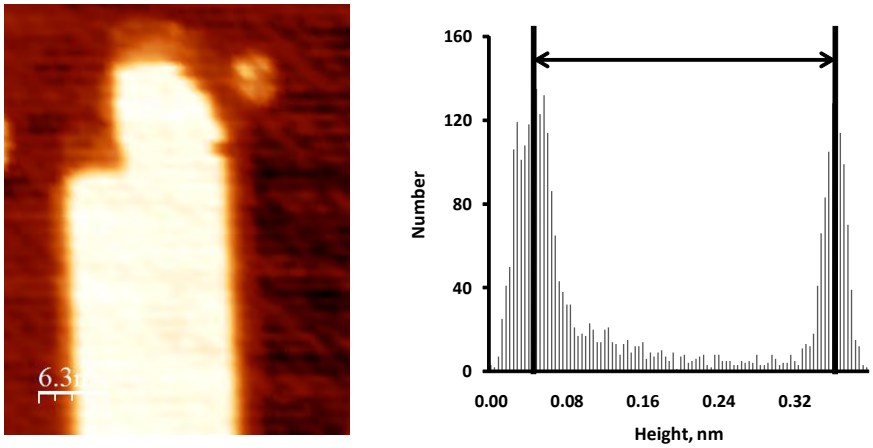

Fig. 3. (a) An STM image of part of a 1st BL Ag island on NiAl(110), 31 × 39 nm^2, -1.0 V tip bias, 0.5 nA tunneling current, (b) the pixel height histogram of the island. The line with arrows indicates the height estimated for this island.

FIG. A-2. (a) STM data for part of a 1st BL Ag island deposited on NiAl(110), 31x39 nm^2, -1.0 V tip bias, 0.5 nA tunneling current, (b) the pixel height histogram of this island. The line with arrows indicates the height estimated for this islands.

Fig.A-2

Ag/NiAl(110) after 1 *L* O_2 exposure

After O_2 exposure, the Ag islands do not show significant change. Fig. 4 shows Ag islands (a) before O_2 exposure, (b) after 1 *L* O_2 exposure, (c) after 11 *L* O_2, and (d) after 111 *L* O_2, respectively. As shown in Fig. 4(b), island edges are a little more ragged after 1 *L* O_2 exposure than before oxygen exposure. The rectangular shapes are however maintained. For some islands, small depressions emerge on top. Fig. 5 shows a closer view of these features for an island after 1 *L* O_2 exposure.

The average depth of the depressions is 0.07 ± 0.01 nm (in the format average value +/- 1 standard deviation, which is used all through this chapter) at the tip bias of +1.0 V. The measurement is based on line scans. The number only differs by 0.01 nm (0.06 ± 0.01 nm) at a tip bias of -1.0 V, indicating that this value is not insensitive to the tunneling bias of this experiment. The value is much lower than interlayer spacing of Ag films at any low index orientations. So perhaps one possible speculation might be that it is a static form of adsorbed oxygen (perhaps a Ag-O reconstruction) that has lower height then Ag atoms.

Measurement of the area of these depressions has also been performed, showing an average value of 1.3 nm^2 (at 1.0 V) or 1.7 nm^2 (at -1.0 V). Both numbers are accompanied by a large standard deviation, as shown in Table 1. This may result from the wide spread of the actual values, or the finiteness of the sample pool available for the analysis, since further analysis of density indicates the number of such depressions at this stage is very low.

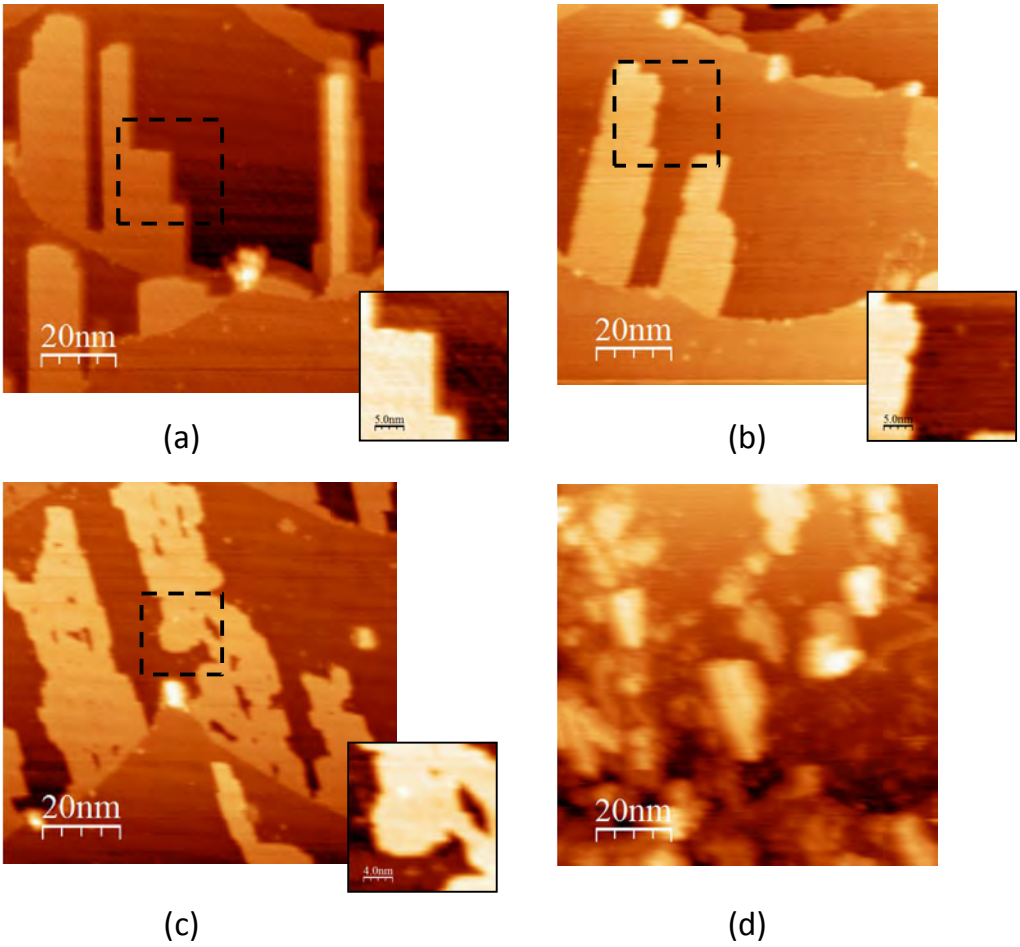

Fig. 4. Representative STM images of Ag islands (a) before O_2 exposure, the area enclosed by the dashed square is shown at higher magnification in a smaller image at the lower right corner of it, (b) after 1 *L* O_2 exposure, the area enclosed by the dashed square is shown at higher magnification in a smaller image at the lower right corner of it, (c) after 11 *L* O_2exposure, the area enclosed by the dashed square is shown at higher magnification in a smaller image at the lower right corner of it, and (d) after 111 *L* O_2 exposure. Images are of 100 × 100 nm^2, taken at +1.0 V tip bias, 0.5 nA tunneling current. The smaller images are of 25 × 25 nm^2.

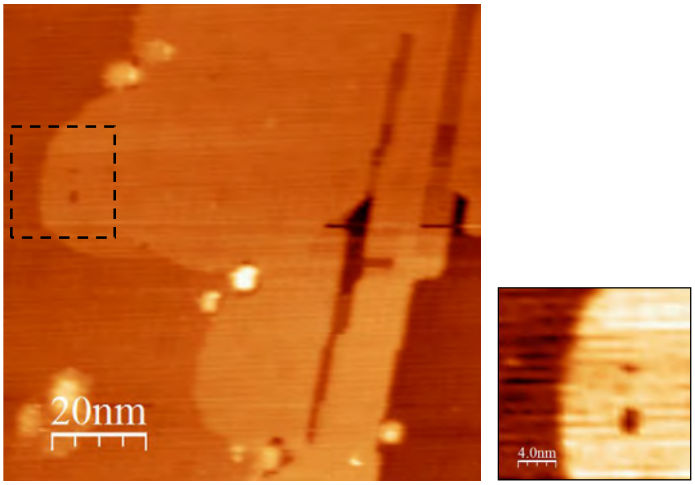

Fig. 5. STM images for Ag islands after 1 *L* O_2 exposure, 100 × 100 nm^2. taken at +1.0 V tip bias, 0.5 nA tunneling current. The area enclosed by the dashed square is shown at higher magnification in a smaller image right to it, 20 × 20 nm^2.

Ag/NiAl(110) after 11 *L* O_2 exposure

After 11 *L* O_2 exposure, the surface demonstrates a significant change in morphology, as shown in Fig. 4(c). Island edges are etched into crooked shapes. Some parts of the island edges even shrink inward forming deep indents, as shown in the small image of Fig. 4(c).The tops of islands also register depressions. It is apparent that the density of depressions is significantly larger than after 1 *L* O_2 exposure. This trend agrees with the fact that the cumulative oxygen exposure increases as the experiment progresses. That leads to the speculation that the number of depressions probably reflects the extent of Ag reacting with oxygen. A further, more quantitative analysis of the density shows the number at this stage is at least 1 to 2 orders of magnitude higher than at the previous stage, as shown in Table 1.

Table 1. Statistical analysis of depth, area, and density of depressions on Ag/NiAl(110) after oxygen exposure.

Cumulative oxygen exposure, *L*	Tip bias, V		Average depth of depressions, nm, (average value ± 1 standard deviation, based on line scans),	Average area of depressions, nm^2,(average value ± 1 standard deviation)	Number of depressions sampled for depth and area analysis	Density of depressions, nm^{-2}	Area sampled for density analysis, nm^2
1	+1.0		0.07 ± 0.01	1.3 ± 0.9	10*	5.0×10^{-5}	2.5×10^5
	-1.0		0.06 ± 0.01	1.7 ± 1.1	8*	1.3×10^{-4}	6.0×10^4
11	Deep depressions (>0.2 nm)	+1.0	0.28 ± 0.03	6.4 ± 4.1	23	6.7×10^{-4}	2.5×10^5
		-1.0	0.27 ± 0.05	4.5 ± 1.1	10*	1.0×10^{-3}	1.0×10^4
	Shallow depressions (≤ 0.2 nm)	+1.0	0.12 ± 0.04	2.2 ± 0.6	40	1.1×10^{-3}	2.5×10^5
		-1.0	0.11 ± 0.04	0.8 ± 0.2	33*	3.3×10^{-3}	1.0×10^5
111	+1.0		n.a.	n.a.	n.a.	n.a.	n.a.

The number with a superscript * indicates it's the maximum amount available for analysis.

A quantitative analysis of the depth of depressions show the numbers bifurcate into two groups, with each of them accompanied by a relative small standard deviation, as shown in Table 1.The average values of the two groups are, for the images at 1.0 V bias for example, 0.28 ± 0.03 nm and 0.12 ± 0.04 nm. Based on the difference of depth, the two groups are noted as deep depressions, and shallow depressions, respectively, in later text. It is shown in Table 1 that this bifurcation also holds for the images at -1.0 V bias (0.27 ± 0.05 nm and 0.11 ± 0.04 nm). For both of the groups, the average depth is not sensitive to reversing the tunneling polarity, since there is only a difference of 0.01 nm for the images at these two biases. A closer view of the bifurcation reveals that the depth of the deep depressions is close to the thickness of the 1st BL islands (0.32 nm). Considering the general reactivity of Ag with oxygen in likely situations, a very possible scenario is that oxygen etches off the two layer of Ag from island tops and leaves a vacancy in them. Although the possibility of forming static islands of Ag-O surface species cannot be excluded provided the Ag-O species are lower in height. A better lateral resolution would help illustrate the situation.

The average depth of the shallow depressions is 0.11 to 0.12 nm. This number is close to the interlayer spacing of Ag in (110) direction (0.14 nm). So a possible speculation is that only one layer of Ag is etched away from the islands in these depressions. The shallow depressions resemble those found after 1 *L* O_2 exposure, but the average depth is 0.05 nm higher than after 1 *L* O_2 exposure, as shown in Table 1. So it is hard to argue that these features are the same. And if they are not, there is a chance that the features after 1 *L* O_2 exposure survive the 11 *L* O_2 exposure and contribute to the statistical average of the latter.

Average island area is also determined, as shown in Table 1.For images taken at 1.0 V,

the average area for deep depressions and shallow depressions are 6.4 ± 4.1 nm^2 and 2.2 ± 0.6 nm^2, respectively. Although there is a significant different between the average values, the standard deviation is too high to manifest a reliable difference between them. However, for images at -1.0 V, the two averages are 4.5 ± 1.1 nm^2 and 0.8 ± 0.2 nm^2, which manifest a significant difference between the two groups of depressions.

For each group, the average area varies significantly as the tunneling gap changes, as shown in Table 1, and it is not clear why the area is affected by tunneling gap. Fig. 6 shows the same depressions under opposite tunneling biases. These protrusions look almost identical. So the difference is most likely attributed to statistical difference by insufficient sampling.

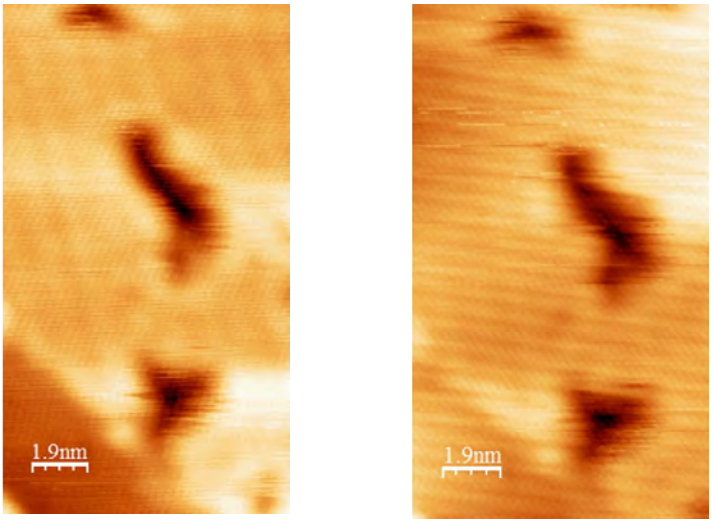

(a) (b)

Fig. 6. Same protrusions on ag/NiAl(110) under different tunneling conditions. (a), +1.0 V tip bias, (b) -1.0 V tip bias. Both are taken at 0.5 nA tunneling current. Images are both of 9.5 × 17 nm^2.

Ag/NiAl(110) after 111 *L* O_2 exposure

After 111 *L* O_2 exposure, most Ag islands turn into small clusters with irregular shapes. Most of the 1st BL islands are totally decomposed into small clusters. Most of the clusters are difficult to resolve and image. But for those that are relatively easy to resolve, height analysis shows an average value of 0.32 ± 0.03 nm, indicating these clusters are the remnants of 1st BL islands. This is probably because oxygen may preferentially oxidize aluminum at exposure of ~111 *L* and thus drastically modify the structure of NiAl(110) surface where Ag islands are grown on.

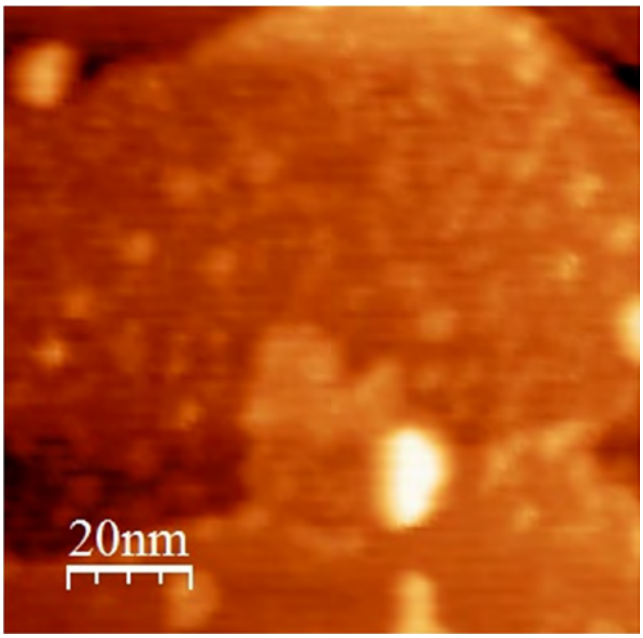

Fig. 7. An STM image of Ag islands on NiAl(110) after 111 *L* O_2 exposure, taken in the same experiment as in Fig. 4(d). 100 × 100 nm^2.taken at +1.0 V tip bias, 0.5 nA tunneling current..

At some regions on the terrace, even smaller clusters are detected, as shown in Fig. 7. The height analysis shows an average value of 0.15 ± 0.02 nm, a comparable height to the

single interlayer spacing of Ag(110). Therefore these features could probably correspond to single-layer-high Ag islands. Such single-layer Ag islands are formed probably because the NiAl(110) substrate has been destroyed by oxygen adsorption. Therefore the preference of bilayer growth mode no long exists.

On the other hand, 2nd BL islands respond to oxygen exposure quite differently than 1st BL islands, even though they only contribute to a small portion to the total island density. As shown in Fig. 8(a), 2nd BL islands remain un-etched after 11 *L* O_2 exposure, and they even survived 111 *L* O_2 exposure, as shown in Fig. 8(b). One possible explanation for this dramatic phenomenon is that the adsorption energy of oxygen on 2nd BL islands is much higher than that of the 1st BL islands. So oxygen is much less favored by 2nd BL islands.

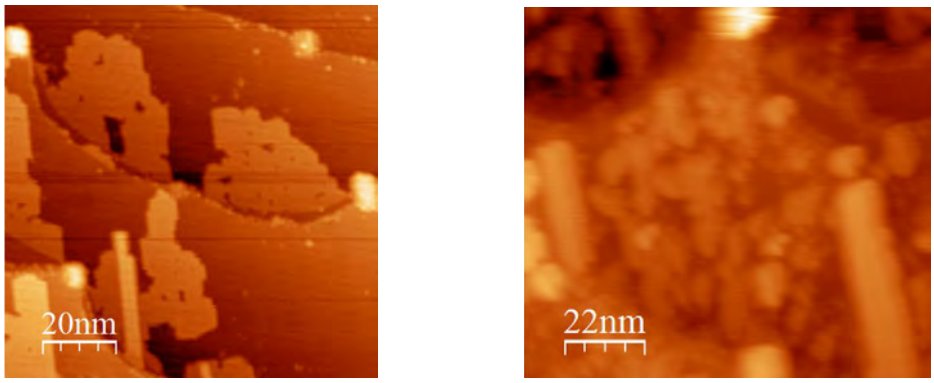

Fig. 8. STM images of Ag islands on NiAl(110) (a) after 11 *L* O_2, 100 × 100 nm^2, -1.0 V tip bias, 0.5 nA tunneling current, and (b) after 111 *L* O_2. 110×100 nm^2. +1.0 V tip bias, 0.5 nA tunneling current. The long bright rod-like features in both images are 2nd BL Ag islands. These images are taken in the same experiment as Fig. 4(d).

Analysis of area of Ag islands

Previous sections show different morphologies are observed on 1st BL and 2nd BL Ag islands with oxygen exposure. It is also of interest to study whether the island area responds to oxygen exposure differently for 1st and 2nd BL islands. Table 2 lists the percentage of area of these Ag islands per unit area of substrate. The relative populations of these numbers are listed as well. The approach used for measuring island area is described in Section 4, Chapter 3. The sampling area is usually equal to the sum of 4 to 5 images with the size of 250 × 250 nm^2, even if the number of available images is more than this. A typical line profile of these islands corresponding to each stage of this experiment is shown in Fig. 9.

The area percentage of 1st BL islands ranges from 26.4% to 32.8% throughout the experiment. At 111 *L* O_2 exposure, area percentage of 1st BL islands is 27.9%, only 1.5% higher than before oxygen exposure. So the influence of oxygen on the area of 1st BL islands is not quite significant. Such small variation is in contrast to the change in morphology where 1st BL islands are entirely decomposed into amorphous Ag clusters with the same height.

The area percentage of 2nd BL islands basically remains in the same level with O_2 exposure up to 11 *L*, as 1st BL islands. However, at 111 *L* O_2 exposure, the area percentage of 2nd BL islands increases to 6.2%. The relative population of these area percentages also reflects such trend. The relative population of 2nd BL islands basically remains at 4% to 5% with O_2 exposure up to 11 *L*, and it is increased greatly to 14% at 111 *L* O_2 exposure.

These changes indicate the 2nd BL islands are more favored after oxygen exposure, indicating the 2nd BL islands are probably more energetically stable after oxygen exposure. The increase of area percentage of 2nd BL islands at 111 *L* O_2 exposure is likely caused by the mass transport of Ag from 1st BL islands which are strongly disrupted by oxygen exposure.

Besides BL islands, there is also a significant portion of islands with an average height of 0.14 to 0.17 nm at 111 *L* O_2 exposure. Such height could probably correspond to islands of single layer high in (110) direction. There are also clusters with a lower height (~0.09 to 0.11 nm) after 111 *L* O_2 exposure. They are likely oxide-related features.

Ripples on the upper surface of Ag (110) islands on NiAl(110)

Previous studies show that ripple-like lateral structures are detected on top of Ag islands following its deposition on NiAl(110) substrate [6]. The structure of ripples varies as a function of island height. For islands of 1st BL high, they are imaged as dark lines, about 0.02 nm deep and either 0.08 or 0.12 nm apart [6]. Similar features have also been detected in this study, as shown in Fig. 8. For Ag islands before oxygen exposure, bright lines as protrusions are found on top of Ag islands, with an alternating spacing of 0.08 and 0.13 nm, as shown in Fig. 10(a). This resembles a previous study where similar features were found on Ag islands at 200 K [6]. After 1 *L* O_2 exposure, it seems this alternating spacing disappears. Instead, all the protrusions are of equal spacing (0.12 nm) apart, as shown in Fig. 10(b). It is noteworthy to mention that resolution at this stage is not ideal enough to completely substantiate this observation. After 11 *L* O_2 exposure (Fig. 10(c)), this trend becomes more pronounced, i.e. all protrusions are of equal spacing (0.12 nm) apart. The alternating pattern

Table 2. Analysis of island area for various oxygen exposures

Total oxygen exposure, *L*	Area of 1st level of ML's per unit area, %	Area of 1st level of BL's per unit area, %	Area of 2nd level of BL's per unit area, %	Relative percentage of 1st level of ML's, %	Relative percentage of 1st level of BL's, %	Relative percentage of 2nd level of BL's, %	Area sampled for analysis, nm^2
0	0	26.4	1.1	0	96	4	2.4×10^5
1	0	30.4	1.3	0	96	4	2.4×10^5
11	0	32.8	1.8	0	95	5	1.3×10^5
111	9.6	27.9	6.2	22	64	14	6.3×10^4

Relative percentage is defined as the area occupied by one type of islands relative to the area occupied by all types of islands.

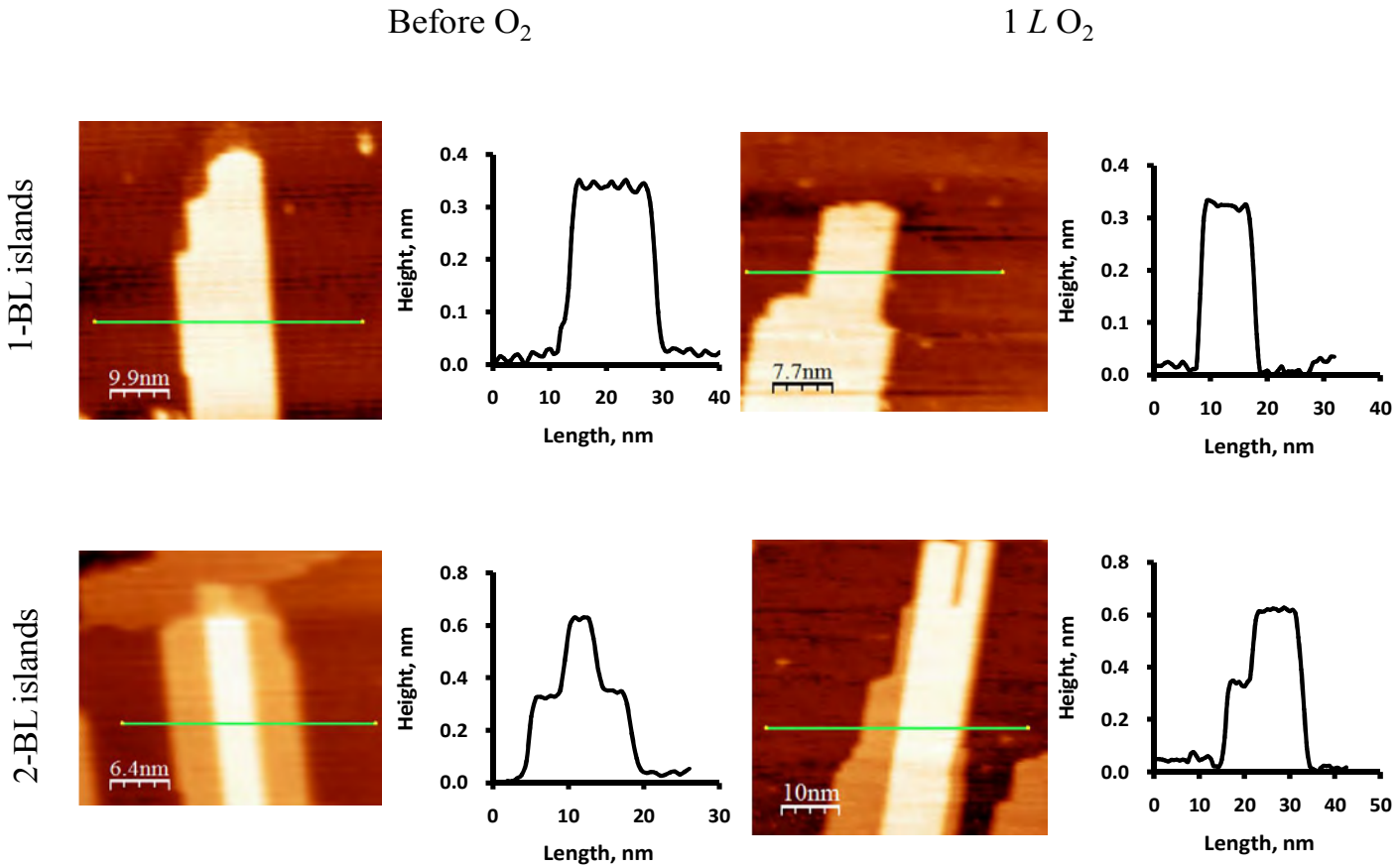

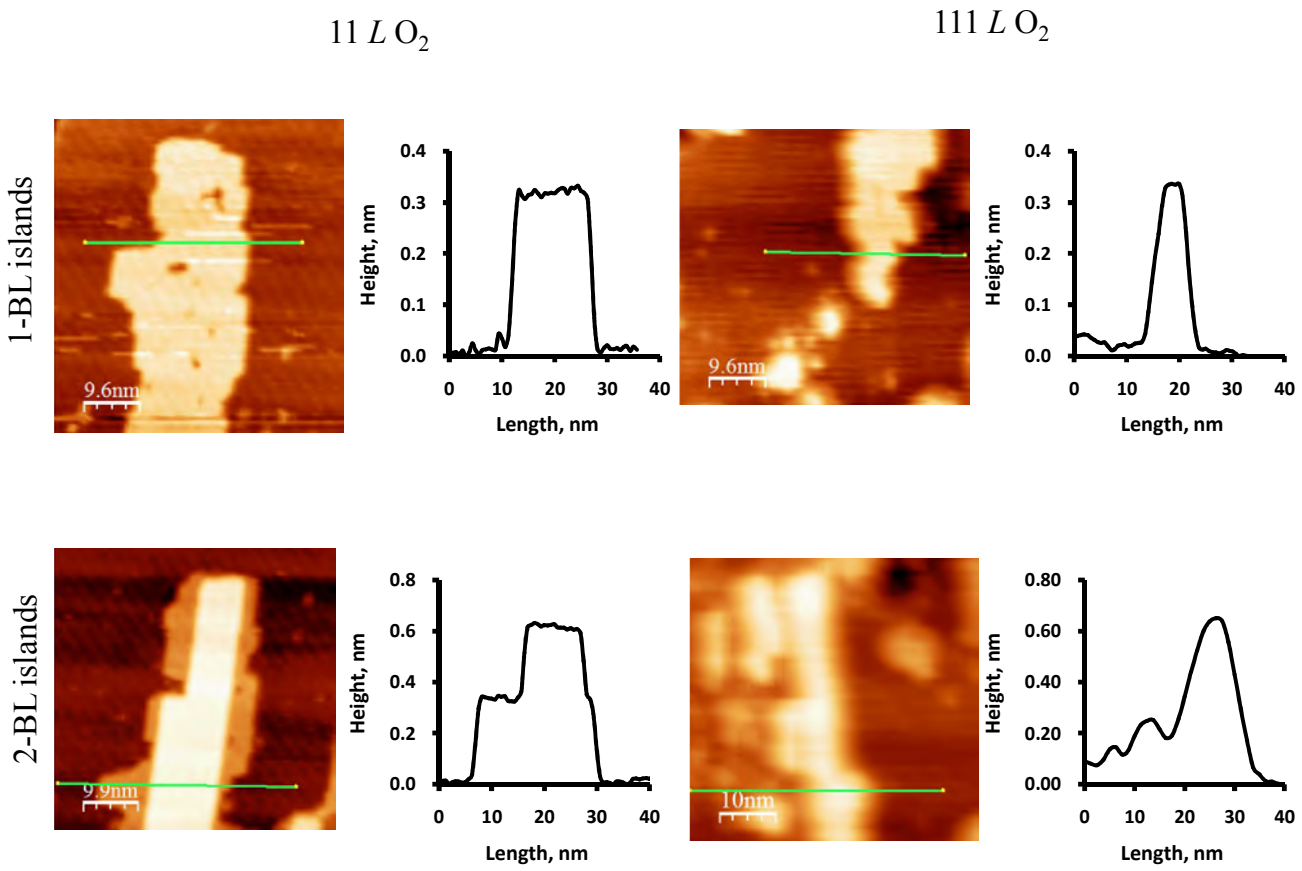

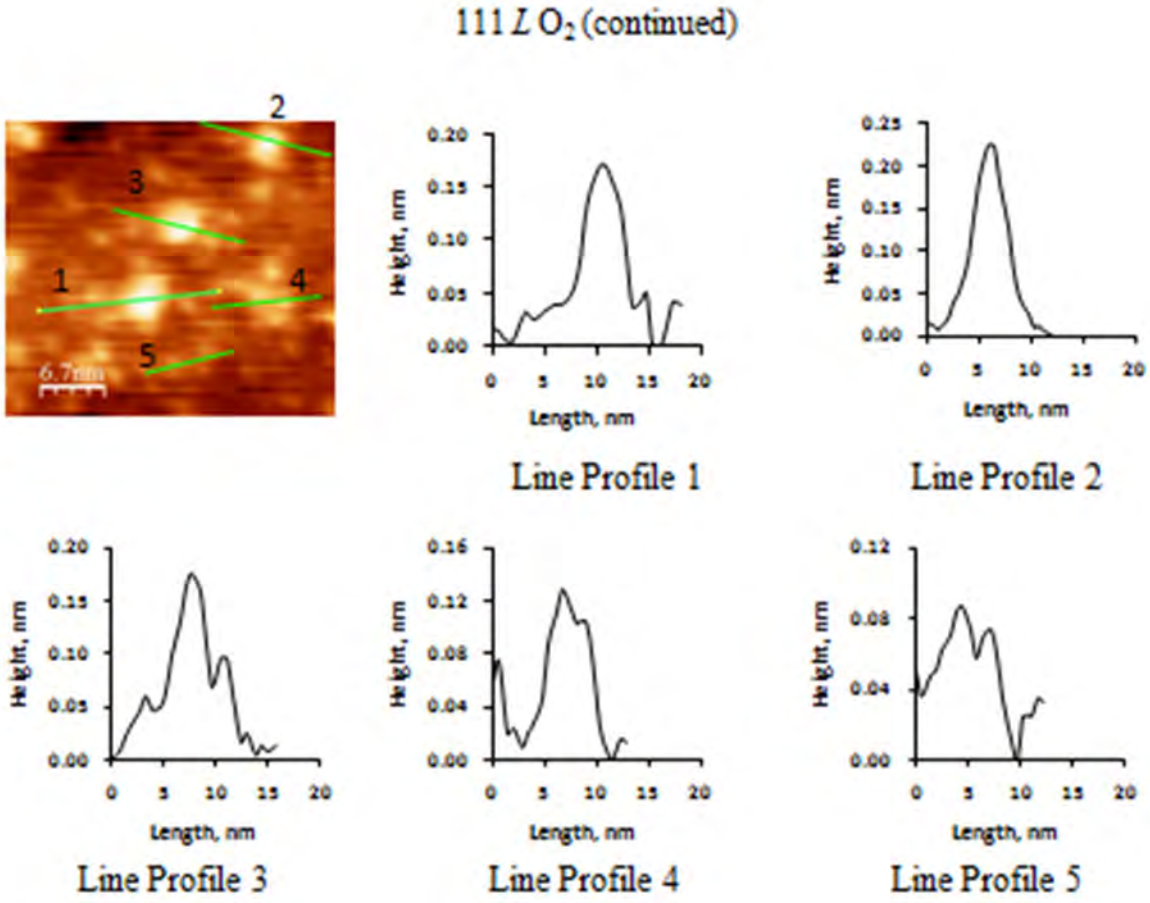

Fig. 9. Typical line profiles of Ag islands and corresponding STM images for various oxygen exposures.

of spacing cannot be observed anymore at this stage.

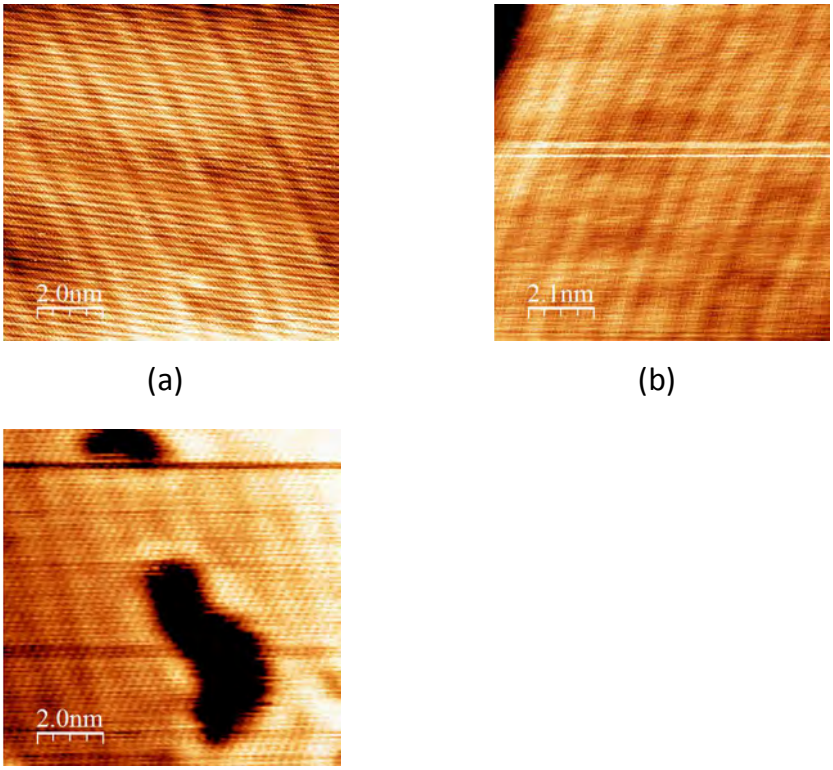

Fig. 10. STM images of ripple structures on Ag islands on NiAl(110) (a) before oxygen exposure, (b) after 1 *L* O_2, (c) after 11 *L* O_2. 10 ×10 nm^2, take at 1.0 V tip bias, 0.5 nA tunneling current.

4. Discussion

Shallow depressions at 11 *L* oxygen exposure probably correspond to single layer vacancies of Ag in (110) direction. Again, there is always a possibility that the depressions are formed by other features, without atomic resolution. But if this speculation is true, then the etching of Ag shows a layer-by-layer pattern. It is also possible that the process was

kinetically-limited. Perhaps given more time, probably hours or days, more deep depressions would be etched out of island tops. Unfortunately we do not have such time availability to observe such possible processes within a single experiment due to practical reasons.

Studies show oxygen exposure at ~ 100 *L* may induce the formation of a bulk-like aluminum oxide layer, which grows on top of the original NiAl(110) surface [18-20]. The formation of such oxide layer must play an important role in decomposing Ag islands. Preferential oxidation of Al in other Al-containing intermetallic compounds, such as 5-fold $Al_{70}Pd_{21}Mn_9$ has also been reported [21]. The chemisorbed oxygen promotes the formation of aluminum oxide and destroys the quasiperiodicity of the surface. On the other hand, the 2nd BL islands survive the high oxygen exposure, one possible explanation is 2nd BL islands might stabilize the NiAl(110) substrate and prevent it from being oxidized by oxygen. And if it's possible then the oxygen adsorption energy on the surrounding area of 2nd BL islands would also be higher than that of 1st BL islands.

5. Conclusions

The morphology of Ag islands on NiAl(110) after oxygen exposure is studied. Ag forms highly-anisotropic islands with a strong height preference of even layers on clean NiAl(110) surface. After 1 *L* oxygen exposure at RT, small depressions appear on upper surface of 1st BL islands, while the 2nd BL islands remain unperturbed. The density of such depressions increases drastically as the cumulative oxygen exposure increases to 11 *L*. The edges of the 1st BL islands are etched and shrink to form indentations at such exposure. The change of morphology is probably attributed to a static form of adsorbed oxygen on Ag

islands. In the meantime, the 2nd BL islands still remain unperturbed. A possible explanation is that oxygen may have a higher adsorption energy on 2nd BL islands and thus strongly disfavored. At oxygen exposure up to 111 *L*, 1st BL islands are entirely decomposed into amorphous clusters. Such drastic change may be ascribed to a preferential oxidation of Al and the subsequent formation of a phase of aluminum oxide. The formation of oxide layer may destroy the NiAl(110) surface where Ag islands grow on. 2nd BL islands surprisingly survive such process and remain intact. One possible explanation is that 2nd BL islands may somehow stabilize the surrounding substrate and prevent it from being oxidized by oxygen. An alternating pattern of ripples are found on island upper surfaces for Ag islands on clean NiAl(110) surface. Such pattern disappear after oxygen exposure and transform into ripples with a uniform spacing.

Acknowledgements

This work was supported by the Office of Science, Basic Energy Sciences, Material Sciences and Engineering Division of the U.S. Department of Energy (USDOE). This manuscript has been authorized by Iowa State University of Science and Technology under Contract No. DE-AC02-07CH11358 with the U.S. Department of Energy.

References

[1] L. Gavioli, K.R. Kimberlin, M.C. Triniges, J.F. Wendelken, Z. Zhang. Phys. Rev. Lett.82 (1999), 129.

[2] M. Miyazaki, H. Hirayama, Surf. Sci. 602 (2008), 276.

[3] K. Budde, E. Abram, V. Yeh, M.C. Tringides, Phys. Rev. B. 61 (2000), R10602.

[4] J. Braun, J.P. Toennies, Surf. Sci. 384 (1997), L858.

[5] D.A. Luh, T. Miller, J.J. Paggel, M.Y. Chou, T.C. Chiang, Science, 292 (2001), 1131.

[6] B. Unal, F. Qin, Y. Han, D.-J. Liu, D. Jing, A.R. Layson, C.J. Jenks, J.W. Evans, P.A. Thiel, Phys. Rev. B. 76 (2007), 195410.

[7] Y. Han, B.Unal, F. Qin, D. Jing, C.J. Jenks, D.-J.Liu, P.A. Thiel, J.W. Evans, Phys. Rev. Lett, 100 (2008), 116105.

[8] B. Unal, A. Belianinov, P.A. thiel, M.C. Tringides, Phys. Rev. B. 81 (2010), 085411.

[9] V. Fournee, H.R. Sharma, M. Shimoda, A.P. Tsai, B. Unal, A.R. Ross, T.A. Lograsso, P.A. Thiel, Phys. Rev. Lett. 95 (2005), 155504.

[10] M. Hupalo, V. Yeh, L. Berbil-Bautista, S. Kremmer, E. Abram, and M.C. Tringides' Phys. Rev. B. 64 (2001), 1556307.

[11] T.-C. Chiang, Surf. Sci. Rep. 39 (2000), 181.

[12] Y. Han, B. Unal, D. Jing, F. Qin, C.J. jenks, D.-J. Liu, P.A. Thiel, J.W. Evans, Phys. Rev. B. 81 (2010), 115462.

[13] T. Duguet, Y. Han, C. Yuen, D. Jing, B. Unal, J.W. Evans, P.A. Thiel, Proc. Natl. Acad. Sci. U.S.A. 108(2011), 989.

[14] E.R. Jette, F. Foote, J. Chem. Phys. 3 (1935), 605.

[15] D. Shao, X. Liu, N. Lu, C.-Z. Wang, K.-M. Ho, M.C. Tringides, P.A. Thiel, Surf. Sci. 606 (2012), 1871.

[16] I. Horcas, R. Fernández, J. M. Gómez-Rodríguez, J. Colchero, J. Gómez-Herrero, A. M. Baro. Rev. Sci. Instrum. 78 (2007), 013705.

[17] T. Hughes, E.P. Lautenschlager, J.B. Cohen, J.O. Brittain, J. Appl. Phys. 42 (1971),

3705.

[18] H. Isern, G.R. Castro, Surf. Sci. 211/212 (1989), 865.

[19] R.M. Jaeger, H. Kuhlenbeck, H.-J. Freund, M. Wuttig, W. Hofmann, R. Franchy, H. Ibach, Surf. Sci. 259 (1991), 235.

[20]A. Stierle, F. Renner, R. Streitel, H. Dosch, W. Drube, B.C.Cowie, Science 303 (2004), 1652.

[21] S.-L. Chang, W.B. Chin, C.-M. Zhang, C.J. Jenks, P.A. Thiel. Surf. Sci. 337 (1995), 135.

Appendix

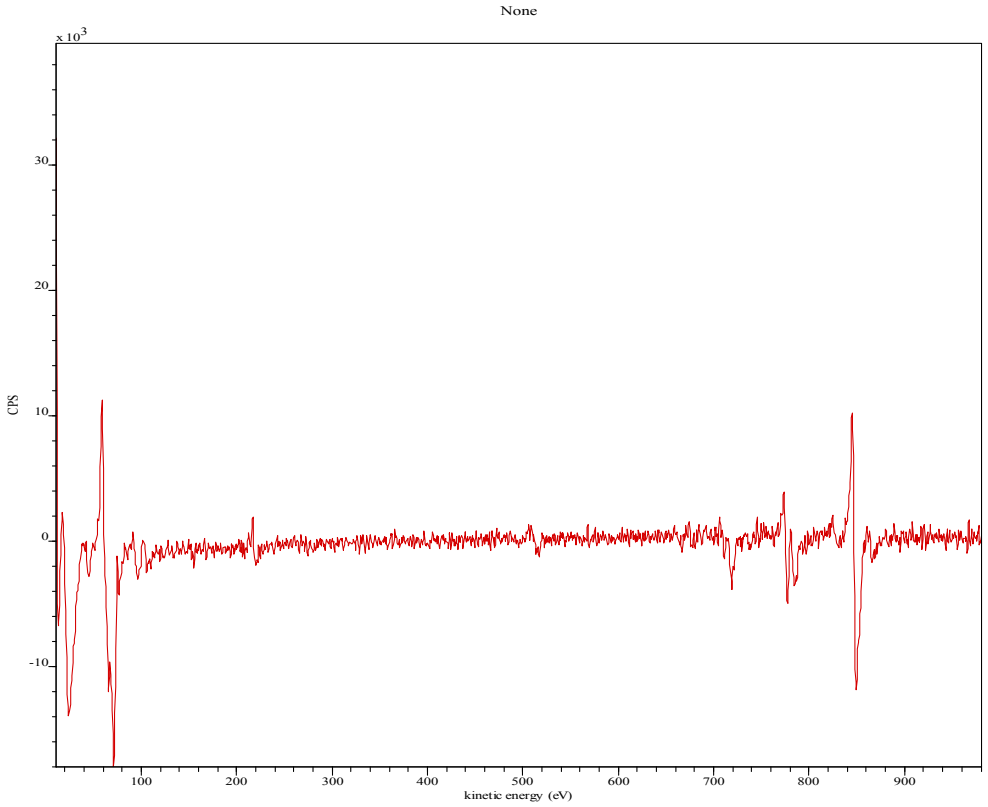

Fig.A-1. An AES spectrum of NiAl(110) surface after cleaning in derivative mode. The carbon, oxygen, and other impurities are under the detection limit.

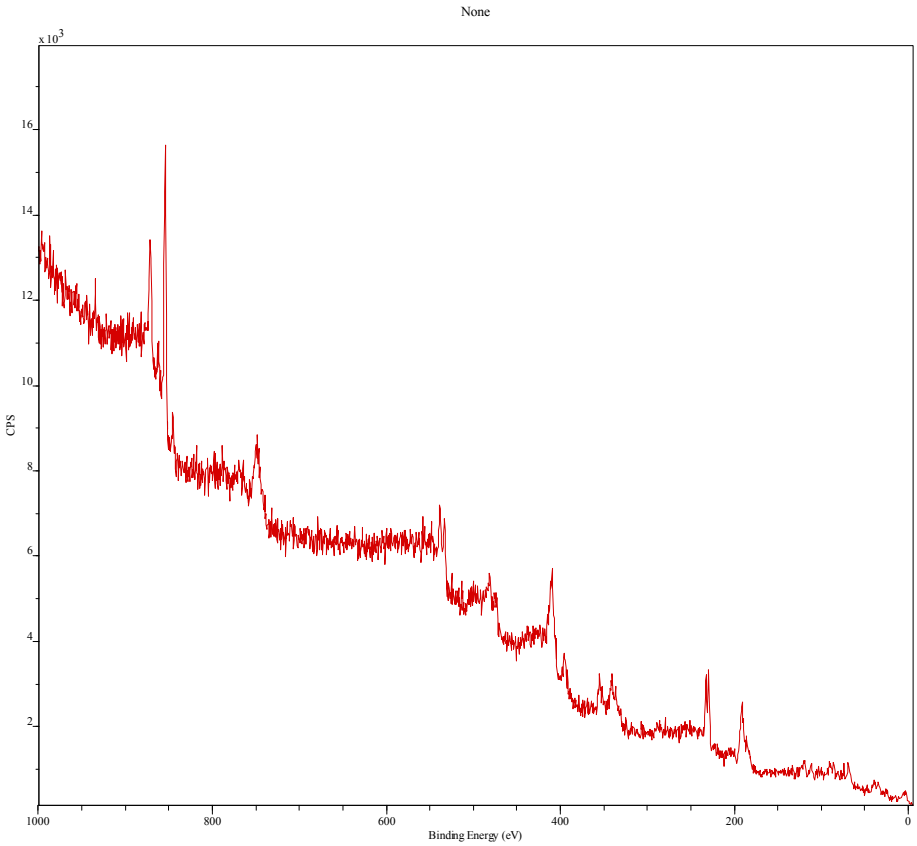

Fig.A-2. An XPS spectrum of NiAl(110) surface after cleaning. Mg cathode.

CHAPTER 8

CONCLUSIONS

Surface-supported Ag nanoparticles demonstrate quantum-size-effect (QSE) mediated growth behavior. 2-layer Ag islands are stabilized by QSE for Ag/Si(111)-7x7. O_2 exposure on such system changes the Ag island height distribution: promoting 3-layer island growth at the expense of 1-, and 2-layer islands. This is an indication that oxygen adsorption changes QSE of Ag/Si(111)-7x7. Mild annealing following O_2 exposure promotes growth of even higher islands (up to 9-layer high). Such trend indicates the instability of 3-layer islands with oxygen adsorption. Ethylene exposure on Ag/Si(111)-7x7 at 120 K leads to protrusions on Ag islands and protrusive rims on island edges. But ethylene does not affect QSE of Ag/Si(111)-7x7 significantly. O_2 exposure on Ag/NiAl(110) disrupts the relative stability of Ag bilayer (BL) islands stabilized by QSE. 1-BL island react with O_2 to form indentations and protrusions. However, these features do not occur on 2-BL Ag islands. A possible explanation is that the adsorption energy of oxygen is much higher on 2-BL islands than on 1-BL islands. At higher oxygen exposure (111 *L*), 1-BL islands are decomposed, probably due to a preferential oxidation of Al of NiAl substrate. 2-BL islands mostly remain intact. Such drastic difference is probably caused by the speculation that 2-BL islands stabilize the surrounding NiAl substrate and prevent them from being oxidized.

APPENDIX A.

CALIBRATION OF PIEZO-SCANNER OF STM

The STM piezo-scanner was calibrated on Jan. 4th, 2012, before taking experimental images. The calibration was based on comparing experimental dimensions of certain features of the Si(111)-7×7 surface with the corresponding literature values. These dimensions includedin-plane lattice constant and single step height.

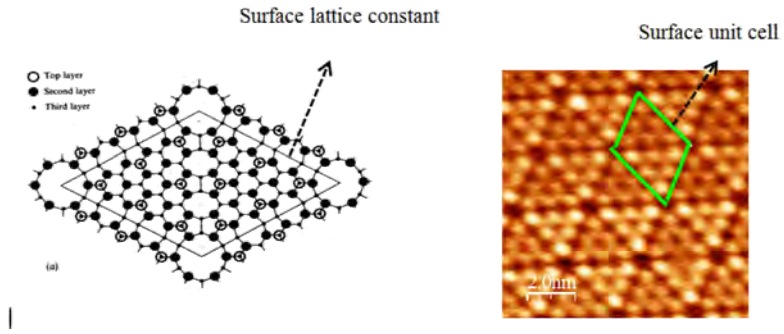

(a) (b)

Fig. 1. (a) Schematic diagram of Si(111)-7×7 unit cell and in-plane lattice constant [3]. (b) STM image of Si(111)-7×7 reconstructed surface from our work, solid line indicates the in-plane lattice constant, 10×10 nm^2, -1.0 V tip bias, 0.5 nA tunneling current.

For the in-plane calibration (x- and y-piezo calibration), the Si(111)-7×7 reconstructed surface is used. The unit cell is rhombic, so the length of any side of the unit cell can be measured as the in-plane lattice constant, as shown in Fig. 1(a). Unfortunately, most of our images are slightly skewed, as shown in Fig. 1(b). In order to compensate for such skewness, the lengths of all four sides of a unit cell are measured and the average value is taken as the

experimental value of in-plane lattice constant for that unit cell. The reported value shown in Table 1 is based on an average over 50 such experimental values. It is reported in the format "average value +/- 1 standard deviation". According to Table 1, this average value is 2.69 nm, identical to the literature value of 2.69 nm [1]. The standard deviation is 0.03 nm. The in-plane lattice constant is measured through WSxM software. For one side of a certain unit cell, a line is drawn between the two adjacent deepest depressions along the side, which defines the in-plane unit cell of the 7x7. And the length of this line is measured as one data point for calculating the average in-plane lattice constant by WSxM, as shown in Fig. 1(b).

Table 1. Piezocalibration based on in-plane lattice constant and single step height for Si(111)-7×7

	Experimental value, nm	Literature value, nm
In-plane lattice constant	2.69 +/- 0.03	2.69 [1]
Single step height	0.32 +/- 0.01	0.31 [2,4]

For step heights (z-piezo calibration), the average value is statistically based on 10 steps. For each step, the single step height is measured by randomly drawing a line across it in WSxM software. The height is measured through this line profile, based on the difference of the average heights of the two steps, as shown in Fig. 2. The experimental value of single step height is reported in the format "average value +/- 1 standard deviation", as shown in Table 1. The value is 0.32 +/- 0.01 nm, very close with the literature value 0.31 nm with a relative difference of only 3% [2,4]. Within the stated uncertainty, the experimental value agrees with the literature value.

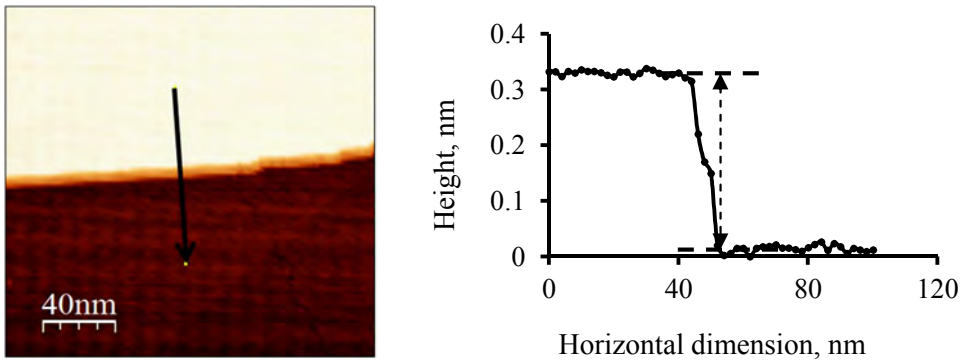

(a) (b)

Fig. 2. (a) An STM image of Si(111)-7×7 from our work that shows two adjacent steps and a line crossing them, 200×200 nm^2, -1.0 V tip bias, 0.5 nA tunneling current. (b) The corresponding line profile (solid line) and the schematic diagram (dotted lines) showing how the step height was measured.

The z-piezo calibration was also performed on NiAl(110) surface on Dec 2th, 2012. The step heights are measured and compared with the literature value to determine if the z-piezo is calibrated. The average value is statistically based on 50 steps. The approach used for measuring step height is the same as the one for Si(111)-7×7. A schematic diagram of a typical measurement is shown in Fig, 3. The experimental value is reported in the format "average value +/- 1 standard deviation", as shown in Table 2. The value is 0.204 +/- 0.003 nm, identical to the literature value 0.204nm [5]. Within the stated uncertainty, the experimental value agrees with the literature value.

Table 2. Piezocalibration based on and single step height for NiAl(110)

	Experimental value, nm	Literature value, nm
Single step height	0.204 +/- 0.003	0.204 [5]

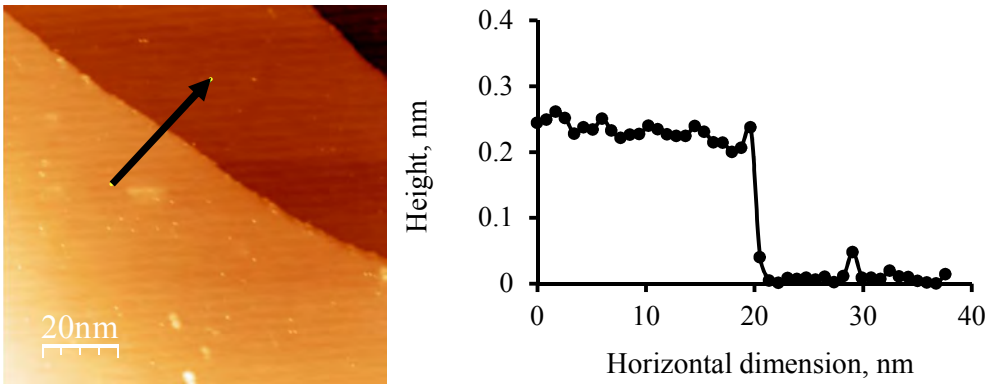

(a) (b)

Fig. 3. (a) An STM image of NiAl(110) from our work that shows three adjacent steps and a line crossing them, 100×100 nm^2, -1.0 V tip bias, 0.5 nA tunneling current. (b) The corresponding line profile showing how the step height was measured.

Both the in-plane lattice constant and step height show consistency with the literature values, indicating the piezo-scanner of STM is well calibrated.

References

[1] G. Binnig, H. Rohrer, Ch. Gerber, and E.Weibel, Phys. Rev. Lett. 50 (1983), 120.

[2] R. Wiesendanger, G. Tarrach, D. Bürgler, H.-J.Güntherodt.Europhys.Lett.12 (1990), 57.

[3] A. Zangwill. Physics at Surfaces. London: Cambridge University Press, 1988.

[4] V.G. Lifshites, A.A. Saranin, A.V. Zotov. Surface Phases on Silicon. Chichester: John Wiley and Sons, 1994.

[5] T. Hughes, E.P. Lautenschlager, J.B. Cohen, J.O. Brittain, J. Appl. Phys. 42 (1971), 3705.

APPENDIX B.

PROCEDURE OF FREEZE-PUMP-THAW CYCLE FOR PURIFYING LIQUIDS

These cycles are performed in order to evaporate liquid contaminants while the product of interest is frozen. So before running these cycles, please check what kind of contaminants there might be and see if they remain liquid when the product of interest is frozen. For example, if the product of interest is benzene,

(1) Before start, make sure the valve connecting the small turbo is closed, and the valve connecting roughing pump closed too.

(2) Freeze the vial containing benzene by liquid N_2,

(3) Open valve connecting the benzene vial,

(4) Open the valve connecting the roughing pump, pump down to 100mTorr from reading of Pirani gauge,

(5) Open the valve connecting the small turbo, pump down to 30 mTorr,

(6) Close all the valves above-mentioned, remove liquid N_2 to thaw benzene for about 15 to 20 min,

(7) After benzene is completely thawed, repeat the Step (1) to (5) twice more,

(8) Open the valve connecting to the individual gas line (each of these lines connects the main chamber through a leak valve), and open the valve connecting benzene vial for 10 min, then close it and pump down to 30 mTorr based on Step (3), and (4),

(9) Repeat Step (8) twice more,

(10) During the last cycle, before pumping down, close the valve connecting the individual gas line.

APPENDIX C.

EXPERIMENTAL DATABASE

Table Captions

Table 1 C_2H_4/Ag/Si(111)-7×7 Run 1

Table 2 O_2/Ag/Si(111)-7×7 Run 1

Table 3 O_2/Ag/Si(111)-7×7 Run 2

Table 4 C_2H_4/Ag/Si(111)-7×7 Run 2, O_2/Ag/Si(111)-7×7 Run 3

Table 5 O_2/Ag/NiAl(110) Run 1

Table 6 Au/NiAl(110) Run 1

Table 1. C_2H_4/Ag/Si(111)-7×7 , Run 1

Date	Sample of interest	Instr.	Purpose	Ag deposition temperature, K	Ethylene exposure temperature, K	Ethylene exposure, L	Page #	File Name	Notes
12/23/2010	Si(111)-7×7	STM	Check surface after sample preparation	-	-	-	60	2010-12-23	Rough surface, noisy
12/24/2010	Si(111)-7×7	STM	Check surface after sample preparation	-	-	-	61	2010-12-24	Rough surface, noisy
12/26/2010	Si(111)-7×7	STM	Clean Ag/Si surface, cool down to 120 K, check surface	120	-	0	61	2010-12-26	Rough surface, noisy
12/27/2010	Si(111)-7×7	STM	Clean Ag/Si surface, cool down to 120 K, check surface	120	-	0	62	2010-12-27	Very small and dense islands
01/05/2011	Si(111)-7×7	STM	Ethylene exposure	300	300	2.7	72	2011-01-05	Big terrace
01/06/2011	Si(111)-7×7	STM	Check surface after sample preparation	-	-	-	73	2011-01-06	
01/08/2011	Si(111)-7×7	STM	Ethylene exposure	300	120	2.5	74	2011-01-08	Noisy at 120 K

Table 1 (Continue)

Date	Sample of interest	Instr.	Purpose	Ag deposition temperature, K	Ethylene exposure temperature, K	Ethylene exposure, L	Page #	File Name	Notes
01/10/2011	Si(111)-7×7	STM	Coarsening, ethylene exposure	300	300	2.5	78	2011-01-10	
01/11/2011	Si(111)-7×7	STM	Check surface after sample preparation	-	-	-	79	2011-01-11	
01/12/2011	Si(111)-7×7	STM	Ethylene exposure	120	120	3.1	80	2011-01-12	Very small and dense islands
01/13/2011	Si(111)-7×7	STM	Clean Ag/Si surface, cooling-down to 120 K failed	300	-	0	81	2011-01-13	
01/14/2011	Si(111)-7×7	STM	Ethylene exposure	300	150	2.8	82	2011-01-14	
01/15/2011	Si(111)-7×7	STM	Clean Ag/Si surface, cool down to 120 K, check surface	300	-	0	83	2011-01-15	

Table 1 (Continue)

Date	Sample of interest	Instr.	Purpose	Ag deposition temperature, K	Ethylene exposure temperature, K	Ethylene exposure, L	Page #	File Name	Notes
01/17/2011	Si(111)-7×7	STM	Coarsening, ethylene exposure	300	150	25	83	2011-01-17	
01/20/2012	Si(111)-7×7	STM	Ethylene exposure	300	150	25	86	2011-01-20	
01/23/2012	Si(111)-7×7	STM	Ethylene exposure	300	300	25	88	2011-01-23	
01/25/2011	Si(111)-7×7	STM	Clean Ag/Si surface, cool down to 150 K, check surface	300	-	0	90	2011-01-25	
01/27/2011	Si(111)-7×7	STM	Ethylene exposure	300	120	25	90	2011-01-27	
01/28/2011	Si(111)-7×7	STM	Ethylene exposure	300	300	25	92	2011-01-28	

Table 2. O_2/Ag/Si(111)-7×7 Run 1

Date	Sample of interest	Instr.	Purpose	Ag deposition temperature, K	Oxygen exposure temperature, K	Oxygen exposure, L	Page #	File Name	Notes
02/03/2011	Si(111)-7×7	STM	Oxygen exposure	300	120	10	93	2011-02-03	
02/05/2011	Si(111)-7×7	STM	Check surface after sample preparation	-	-	-	95	2011-02-05	
02/09/2012	Si(111)-7×7	STM	Oxygen exposure	300	300	10	95	2011-02-09	
02/14/2011	Si(111)-7×7	STM	Check surface after sample preparation	-	-	-	97	2011-02-14	
02/15/2011	Si(111)-7×7	STM	Clean Ag/Si surface	300	-	0	97	2011-02-15	Control for 02/09/2011, and 02/21/2011
02/20/2011	Si(111)-7×7	STM	Check surface after sample preparation	-	-	-	98	2011-02-20	
02/21/2011	Si(111)-7×7	STM	Oxygen exposure	300	300	100	98	2011-02-21	

Table 3. O_2/Ag/Si(111)-7×7 Run 2

Date	Sample of interest	Instr.	Purpose	Ag deposition temperature, K	Oxygen exposure temperature, K	Oxygen exposure, L	Page #	File Name	Notes
05/20/2011	Si(111)-7×7	STM	Check surface after sample preparation	-	-	-	138	2011-05-20	
05/21/2011	Si(111)-7×7	STM	Check surface after sample preparation	-	-	-	139	2011-05-21	
05/24/2011	Si(111)-7×7	STM	Check surface after sample preparation	-	-	-	143	2011-05-24	
05/25/2011	Si(111)-7×7	STM	Calibrate Omicron evaporator	300	-	0	144	2011-05-25	failed
05/26/2011	Si(111)-7×7	STM	Calibrate Mantis evaporator	300	-	0	145	2011-05-26	failed
05/27/2011	Si(111)-7×7	STM	Calibrate Mantis evaporator	300	-	0	147	2011-05-27	
05/28/2011	Si(111)-7×7	STM	Clean Ag/Si	300	-	0	148	2011-05-28	

Table 3 (Continue)

Date	Sample of interest	Instr.	Purpose	Ag deposition temperature, K	Oxygen exposure temperature, K	Oxygen exposure, L	Page #	File Name	Notes
05/29/2011	Si(111)-7×7	STM	Clean Ag/Si	300	-	0	149	2011-05-29	With annealing
05/30/2011	Si(111)-7×7	STM	Oxygen exposure	300	300	100	151	2011-05-30	With annealing
05/31/2011	Si(111)-7×7	STM	Clean Ag/Si	300	-	0	154	2011-05-31	
06/01/2011	Si(111)-7×7	STM	Clean Ag/Si	300	-	0	155	2011-06-01	With annealing, control for 06/02/2011
06/02/2011	Si(111)-7×7	STM	Oxygen exposure	300	300	100	156	2011-06-02	With annealing
06/23/2011	Si(111)-7×7	STM	Check surface after sample preparation	-	-	-	172	2011-06-23	
06/24/2011	Si(111)-7×7	STM	Calibrate Ag evaporator	300	-	0	173	2011-06-24	

Table 3 (Continue)

Date	Sample of interest	Instr.	Purpose	Ag deposition temperature, K	Oxygen exposure temperature, K	Oxygen exposure, L	Page #	File Name	Notes
06/25/2011	Si(111)-7×7	STM	Oxygen exposure	300	300	100	175	2011-06-25	With annealing
06/28/2011	Si(111)-7×7	STM	Clean Ag/Si	300	-	0	178	2011-06-28	With annealing, control for 06/25/2011
06/29/2011	Si(111)-7×7	STM	Clean Ag/Si	300	-	0	180	2011-06-29	With annealing, control for 06/30/2011
06/30/2011	Si(111)-7×7	STM	Oxygen exposure	300	300	100	182	2011-06-30	With annealing

Table 4. C_2H_4/Ag/Si(111)-7×7 Run 2, O_2/Ag/Si(111)-7×7 Run 3

Date	Sample of interest	Instr.	Purpose	Ag deposition temperature, K	Ethylene exposure temperature, K	Ethylene exposure, L	Page #	File Name	Notes
12-29-2011	Si(111)-7×7	STM	Check surface after sample preparation	-	-	-	195	12-29-2011	
01-04-2012	Si(111)-7×7	STM	Calibrate Mantis Evaporator	300	-	-	198	01-04-2012	
01-05-2012	Si(111)-7×7	STM	Clean Ag/Si, cool down to 120 K, check surface	300	-	0	200	01-05-2012	
01-08-2012	Si(111)-7×7	STM	Ethylene exposure	300	120	3	203	01-08-2012	Failed to cool down, backfilling, old cylinder, maybe contaminated with acetylene
01-10-2012	Si(111)-7×7	STM	Ethylene exposure	300	120	3	206	01-10-2012	backfilling, old cylinder, maybe contaminated with acetylene
01-12-2012	Si(111)-7×7	STM	Ethylene exposure	300	300	3	208	01-12-2012	backfilling, old cylinder, maybe contaminated with acetylene
01-17-2012	Si(111)-7×7	STM	Ethylene exposure	300	120	3	212	01-17-2012	backfilling, old cylinder, maybe contaminated with acetylene

Table 4 (Continue)

Date	Sample of interest	Instr.	Purpose	Ag deposition temperature, K	Ethylene exposure temperature, K	Ethylene exposure, L	Page #	File Name	Notes
01-19-2012	Si(111)-7×7	STM	Calibrate piezo-scanner of STM	-	-	-	214	01-19-2012	
01-23-2012	Si(111)-7×7	STM	Oxygen and ethylene exposure,	300	120	3	215	01-23-2012	Subsequent oxygen exposure after Ag deposition at RT, 100 *L*, followed by ethylene exposure at 120 K (both backfilled), old ethylene cylinder, maybe contaminated with acetylene
01-31-2012	Si(111)-7×7	STM	Clean Ag/Si, cool down to 120 K , check surface	300	-	0	217	01-31-2012	
02-02-2012	Si(111)-7×7	STM	Clean Ag/Si, cool down to 150 K, check surface	300	-	0	219	02-02-2012	
02-03-2012	Si(111)-7×7	STM	Ethylene exposure, check surface at 120 K and 150 K	300	120	3	220	02-03-2012	Backfilling, new ethylene cylinder

Table 4 (Continue)

Date	Sample of interest	Instr.	Purpose	Ag deposition temperature, K	O_2 or C_2H_4 exposure temperature, K	O_2 or C_2H_4 exposure, L	Page #	File Name	Notes
02-06-2012	Si(111)-7×7	STM	Oxygen exposure	300	300 (O_2)	100 (O_2)	222	02-06-2012	
02-09-2012	Si(111)-7×7	STM	Ethylene exposure	300	120 (C_2H_4)	30 (C_2H_4)	224	02-09-2012	Ethylene backfilling, new ethylene cylinder, no annealing
02-12-2012	Si(111)-7×7	STM	Ethylene exposure	300	120 (C_2H_4)	30 (C_2H_4)	227	02-12-2012	Ethylene is tube dosed, new cylinder, annealed to 150 K at last
02-15-2012	Si(111)-7×7	STM	Clean Ag/Si, cool down to 120 K, check surface	300	-	0	229	02-15-2012	Annealed to 150 K at last
02-17-2012	Si(111)-7×7	STM	Ethylene exposure	300	120 (C_2H_4)	30 (C_2H_4)	227	02-12-2012	Ethylene is tube dosed, new cylinder, no annealing

Table 5. O_2/Ag/NiAl(110) Run 1

Date	Sample of interest	Instr.	Purpose	Ag deposition temperature, K	Oxygen exposure temperature, K	Oxygen exposure, L	Page #	File Name	Notes
11/19/2012	NiAl(110)	XPS	Search for manipulator position for XPS	-	-	-	239	20121109	
11/20/2012	NiAl(110)	XPS	Search for manipulator position for sputtering	-	-	-	240	2012112001-2012112009	
11/21/2012	NiAl(110)	XPS	Search for manipulator position for sputtering	-	-	-	245	2012112101 - 2012112104	
12/02/2012	NiAl(110)	STM	Check surface after sample preparation	-	-	-	252	20121202	
12/06/2012	NiAl(110)	STM	Check surface after sample preparation	-	-	-	255	20121206	
12/07/2012	NiAl(110)	XPS	Check surface after sample preparation	-	-	-	255	2012120701 – 2012120702	
12/08/2012	NiAl(110)	XPS and STM	Check surface after sample preparation	-	-	-	256	XPS: 2012120801 – 2012120805, STM: 20121208	Big terraces

Table 5 (Continue)

Date	Sample of interest	Instr.	Purpose	Ag deposition temperature, K	Oxygen exposure temperature, K	Oxygen exposure, L	Page #	File Name	Notes
12/09/2012	NiAl(110)	XPS	Check surface before experiment	-	-	-	257	2012120901	Annealing by PBN heater failed
12/13/2012	NiAl(110)	XPS	Check surface after sample preparation	-	-	-	258	2012121301 - 2012121302	
12/20/2012	NiAl(110)	XPS	Check surface after sample preparation	-	-	-	261	2012122101 - 2012122103	
01/02/2013	NiAl(110)	XPS	Search for manipulator position for XPS and sputtering	-	-	-	265	2013010201 - 2013010206	Good position for XPS and sputtering, single plate
01/03/2013	NiAl(110)	XPS	Check surface after sample preparation	-	-	-	266	2013010301	
01/04/2013	NiAl(110)	XPS	Check surface before experiment	-	-	-	267	2013010401	Following STM experiment failed, switched back to double decker
01/07/2013	NiAl(110)	XPS	Search for manipulator position for XPS and sputtering	-	-	-	268	2013010701 - 2013010702	Good position for XPS and sputtering, new double decker

Table 5 (Continue)

Date	Sample of interest	Instr.	Purpose	Ag deposition temperature, K	Oxygen exposure temperature, K	Oxygen exposure, L	Page #	File Name	Notes
01/08/2013	NiAl(110)	XPS and STM	Check surface after sample preparation	-	-	-	271	STM: 20130108, XPS: 2013010801	Sputter position off, needed adjustment
01/09/2013	NiAl(110)	XPS	Search for manipulator position for sputtering	-	-	-	272	2013010901 - 2013010925	Confirmed new sputter position
01/10/2013	NiAl(110)	STM	Check surface after sample preparation	-	-	-	275	20130110	
01/12/2013	NiAl(110)	STM	Search for manipulator position for XPS and sputtering	-	-	-	277	20130112	Surface improved, but many pinning sites
01/14/2013	NiAl(110)	XPS and STM	Check surface before experiment	-	-	-	278	STM: 20130114 XPS: 2013011401 - 2013011404	
01/15/2013	NiAl(110)	STM	Oxygen exposure	300	300	100	279	20130115	
01/16/2013	NiAl(110)	XPS and STM	Oxygen exposure	300	300	1, 10, 100	280	STM: 20130116 XPS: Folder 20130116	STM for checking initial surface

Table 5 (Continue)

Date	Sample of interest	Instr.	Purpose	Ag deposition temperature, K	Oxygen exposure temperature, K	Oxygen exposure, L	Page #	File Name	Notes
01/18/2013	NiAl(110)	STM	Check surface after sample preparation	-	-	-	283	20130118	
01/19/2013	NiAl(110)	XPS	Oxygen exposure	300	300	1, 10, 100	283	20130119	
01/21/2013	NiAl(110)	STM	Check surface after sample preparation	-	-	-	287	20130121	Surface rough, suspect that the sputtering position is off
01/22/2013	NiAl(110)	XPS	Search for manipulator position for sputtering	-	-	-	287	20130122	
01/24/2013	NiAl(110)	XPS	Search for manipulator position for sputtering	-	-	-	288	20130124	
01/25/2013	NiAl(110)	AES	Check surface cleanliness and sputtering position	-	-	-	290	20130125	
01/26/2013	NiAl(110)	AES and XPS	Study the temperature where oxide resurfaces	-	-	-	291	XPS: 20130126 AES: 20130126	

Table 5 (Continue)

Date	Sample of interest	Instr.	Purpose	Ag deposition temperature, K	Oxygen exposure temperature, K	Oxygen exposure, L	Page #	File Name	Notes
01/28/2013	NiAl(110)	STM	Check surface after sample preparation	-	-	-	293	20130128	
01/29/2013	NiAl(110)	LEED and STM	Check surface after sample preparation	-	-	-	293	LEED: Pic # 229-8611 – 229-8614 STM: 20130129	Rough surface

Table 6. Au/NiAl(110) Run 1

Date	Sample of interest	Instr.	Purpose	Au deposition temperature, K	Oxygen exposure temperature, K	Oxygen exposure, L	Page #	File Name	Notes
01/31/2013	NiAl(110)	STM	Calibrate Au Mantis evaporator	120	-	0	Book 2, 37	20130131	Annealing to 250 K failed
02/01/2013	NiAl(110)	XPS	Check surface after sample preparation	-	-	-	Book 2, 39	20130201	
02/04/2013	NiAl(110)	XPS and STM	Au/NiAl(110) deposition	300	-	0	Book 2, 39	STM: 20130204 XPS: 20130204	Poor image quality

ACKNOWLEDGEMENTS

This dissertation would not have been possible without the help of so many people in so many ways. First and foremost, I would like to express my sincere appreciation to Professor Patricia A. Thiel for her guidance, encouragement, advice, and support throughout my graduate studies. She has not only given me valuable guidance on my project, but has also been a great mentor for my professional career.

I would also like to thank all members, former and present, in Thiel research group, for their generous help and advice. I enjoyed the friendly and encouraging working environment very much.

I would like to express my gratitude to Professor James E. Evans, Dr. C.-J. Wang, Professor Kai-Ming Ho, Dr. Xiaojie Liu, and Dr. Ning Lu for their generous assistance for theoretical calculations. This dissertation would not have been complete without their help.

Finally, I wish to thank my family for their enduring love and support. I wouldn't have accomplished this far without them.

This work was performed at the Ames Laboratory under contract number DE-AC02-07CH11358 with the U.S. Department of Energy. The document number assigned to this thesis/dissertation is IS-T 3101.